Development and implementation of the Bio-electro-Fenton process : application to the removal of pharmaceuticals from water

Hélène Monteil

Thèse de doctorat de l'université Paris-Est

Spécialité : Science et technologie de l'environnement

Ecole doctorale Sciences, Ingénierie et Environnement

Thèse présentée par :

Hélène Monteil

Pour obtenir le grade de Docteur de l'université Paris-Est

Development and implementation of the bioelectro-Fenton process: application to the removal of pharmaceuticals from water

Thèse préparée au Laboratoire Géomatériaux et Environnement (LGE) sous la direction de Mehmet A. Oturan

Co-encadrants : Nihal Oturan et Yoan Péchaud

Reviewers:	
Prof. Karine Groenen-SERRANO	Professor at the university of Toulouse
Prof. Manuel A. RODRIGO	Professor at the university of Castilla-la-Mancha
Supervisor:	
Prof. Mehmet A. OTURAN	University of Paris-Est
Examiners:	
Dr. Emmanuel MOUSSET	University of Lorraine
Dr. Florence FOURCADE	University of Rennes 1
Dr. Yoan Péchaud	University of Paris-Est
Prof. Christine CACHER-VIVIER (présidente du jury)	University of Paris-Est

ACKNOWLEDGMENTS

First, I would like to thank Prof. Stéphanie Rossano for having given me the opportunity to work in her laboratory the LGE.

I also would like to acknowledge the director of this thesis Prof. Mehmet A. Oturan for his support during this project as well as for his scientific contributions and wise guidance during research works.

The contribution of Dr. Nihal Oturan during this thesis has also to be highlighted. I want to thank her for all the advice information and technical guidance which were always given as soon as possible.

A specific acknowledgment goes to Dr. Yoan Péchaud who spend a lot of time with me giving me very useful advice.

I wish to express my gratitude to the reviewers of this thesis, Prof. Manuel A. Rodrigo and Prof. Karine Groenen-Serrano for accepting to read and evaluate the present work as well as to the examiners, Prof. Christine Cacher-Vivier, Dr. Florence Fourcade, Dr. Emmanuel Mousset and again Dr. Yoan Péchaud.

I would like to thank the University Paris-Est and the doctoral school Sciences, Ingénierie, Environnement for funding conference fees and providing me financial support to perform this thesis work as well as ECOS-Sud who gave me the opportunity to go to Chili.

I want also to thank all the people from the LGE lab and especially Valentina, Douglas, Jules, Théo, Julie, Clément, Anne who make me spent a very nice time in this lab.

Je voudrais remercier ma famille et mes amis pour leur soutien tout au long de la thèse.

Enfin je terminerai par te remercier mon Loulou, tu as toujours été à mes côtés pendant ces 3 années dans les bons moments comme dans les moments de doute. Grâce à ton appui sans faille j'ai su trouver la motivation pour arriver au bout. Encore merci je t'aime.

ABSTRACT

Electrochemical advanced oxidation processes (EAOPs) constitute an efficient technology to treat the pharmaceuticals as they allow the formation of strong oxidants such as hydroxyl radicals able to remove nearly any type of organic contaminants thanks to their very high oxidation power. Among them the electro-Fenton and anodic oxidation processes are environmentally friendly methods as they use no chemical reagent (anodic oxidation) or only oxygen of air and iron ions as a catalyst (electro-Fenton).

In this thesis, four pharmaceuticals from different families and structures were selected based on their toxicity and their occurrence in environmental waters and their removal from water was performed by EAOPs. The objectives of this work were to determine the best operating conditions at lab scale (current and catalyst concentration), investigate the kinetic of degradation and mineralization and finally propose a mineralization pathway based on aromatic intermediates, carboxylic acids and ions released to the solution.

As these treatments were successfully applied, a lab scale pilot reactor composed alternately of BDD anodes and carbon felt cathodes with a bottom aeration system and working in the continuous mode was built to scale-up these processes in order to pre-industrialize them. Different configurations of electrodes were tested. The flow rate and the current were found to be more influent on the mineralization rate and on the energy consumption, respectively. To deeper understand the role of the flow rate and the configurations a hydrodynamic study was performed. The hydrodynamic results were gathered with a kinetic model for the mineralization to obtain a model predicting the percentage of mineralization at different position inside the reactor during the steady state. Thus, this model can help to optimize the operating conditions and to size future reactors depending on the mineralization objective of the treatment (high mineralization rate, combined treatment, high flow, …).

To reduce operating cost, the combination of an electrochemical process and a biological treatment was then investigated. In this frame, it was found that electrochemical treatment can (i) degrade the hydrochlorothiazide (ii) reduce significantly the concentration of its aromatic intermediates as they were shown to significantly inhibit the bacterial activity, (iii) promote the formation of biodegradable molecules such as carboxylic acids. The biodegradation of four carboxylic acids formed during the electro-Fenton treatment of the hydrochlorothiazide at lab scale was also studied. It was demonstrated that they were sequentially degraded with different lag phases and kinetics of degradation. Thus to mineralize them, a “plug flow” type reactor is recommended. The combination of treatment was then applied with an electrochemical treatment performed at low current with a BDD anode and a Platine anode. A mineralization degree of 38% and 50% were obtained by the biological treatment enabling to globally reach a mineralization rate of 66% and 85% with the BDD and the Platine anodes respectively. Thus this combined treatment was successful and open the way for the scale-up of these processes.

RESUME

Les procédés électrochimiques d'oxydation avancée constituent une technologie efficace pour traiter les produits pharmaceutiques car ils permettent la formation d'oxydants puissants tels que les radicaux hydroxyles capables d'éliminer presque tout type de contaminants organiques grâce à leur très haut pouvoir oxydant. Parmi eux, l'électro-Fenton et l'oxydation anodique sont des méthodes respectueuses de l'environnement car ils n'utilisent aucun réactif chimique (oxydation anodique) ou uniquement l'oxygène de l'air et des ions fer en tant que catalyseur (électro-Fenton).

Dans cette thèse, quatre produits pharmaceutiques appartenant à des familles différentes ont été sélectionnés en fonction de leur toxicité et de leur présence dans les eaux de l'environnement. Leur élimination de l'eau a été effectuée par électro-Fenton. Les objectifs de ce travail étaient de déterminer (i) les meilleures conditions opératoires à l'échelle du laboratoire (courant et concentration du catalyseur), (ii) la cinétique de dégradation et de minéralisation et enfin (iii) de proposer une voie de minéralisation basée sur des intermédiaires aromatiques, des acides carboxyliques et des ions libérés dans la solution.

Comme ces traitements ont été appliqués avec succès, un réacteur pilote composé alternativement d'anodes en BDD et de cathodes en feutre de carbone, doté d'un système d'aération et fonctionnant en mode continu a été construit pour évaluer la faisabilité d'un changement d'échelle et se diriger vers une pré-industrialisation du procédé. Différentes configurations d'électrodes ont été testées. Le débit et le courant se sont avérés être plus influents sur le taux de minéralisation et sur la consommation d'énergie, respectivement. Pour mieux comprendre le rôle du débit et des configurations, une étude hydrodynamique a été réalisée. Le modèle hydrodynamique a été associé à un modèle cinétique de minéralisation afin d'obtenir un modèle permettant de prédire le pourcentage de minéralisation à différentes positions à l'intérieur du réacteur en régime permanent. Ainsi, ce modèle peut aider à optimiser les conditions opératoires et à dimensionner les futurs réacteurs en fonction de l'objectif de minéralisation du traitement (taux de minéralisation élevé, traitement combiné, flux élevé,…).

Afin de réduire les coûts opératoires, la combinaison d'un procédé électrochimique et d'un traitement biologique a ensuite été étudiée. Afin d'obtenir un traitement combiné efficace, il a été constaté que le traitement électrochimique devait (i) dégrader l'hydrochlorothiazide (ii) réduire de manière significative la concentration de ses intermédiaires aromatiques car ils inhibent de manière significative l'activité bactérienne, (iii) favoriser la formation de molécules biodégradables telles que les acides carboxyliques. La biodégradation de quatre acides carboxyliques formés lors du traitement par électro-Fenton de l'hydrochlorothiazide a également été étudiée. Il a été démontré qu'ils étaient dégradés de manière séquentielle avec différentes phases de latence et cinétiques de dégradation. Ainsi, pour les minéraliser, un réacteur de type «piston» est recommandé. La combinaison de traitement a ensuite été appliquée à un traitement électrochimique effectué à faible courant avec une anode en BDD et une anode en Platine. Un degré de minéralisation de 38 et 50% a été obtenu par le traitement biologique permettant d'atteindre un taux de minéralisation global de 66 et 85% avec les anodes en BDD et Platine respectivement. Ainsi, cette combinaison de traitement a été un succès, un changement d'échelle du procédé peut alors être envisagé.

TABLE OF CONTENT

LIST OF TABLES

LIST OF FIGURES

ABBREVIATIONS:

ADE	Air diffusion electrode
AI	Aromatic intermediate
AO	Anodic oxidation
AOP	Advanced oxidation process
BA	Benzoic acid
BDD	Boron doped diamond
Bio-EF	Biological treatment combined with EF
BOD_{14}	Biological oxygen demand after 14 days
BOD_5	Biological oxygen demand after 5 days
BODu	Ultimate biological oxygen demand
CA	Carboxylic acid
CE	Current efficiency
CF	Carbon felt
COD	Chemical oxygen demand
CSTR	Continuously stirred tank reactor
CV	Cyclic voltammetry
DOC	Dissolved organic carbon
DOE	Design of experiment
DSA	Dimensionally stable anode
EAOP	Electrochemical advanced oxidation process
EC	Energy consumption
EF	Electro-Fenton
EF-B	EF first followed by a biological treatment
GC-MS	Gaz chromatography mass spectrum
GDE	Gas diffusion electrode
GF	Graphite felt
HCT	Hydrochlorothiazide
HPLC	High performance liquid chromatography
IC	Ionic chromatography
IOA	Index of agreement
k_{app}	Apparent rate constant
Kow	Octanol/water partition coefficient
LC-MS	Liquid chromatography mass spectrum

MCE	Mineralization current efficiency
MF	Micro fluidic
MR	Macro reactor
Nad	Nadolol
NSAID	Nonsteroidal anti-inflammatory drugs
NTU	Nephelometric Turbidity Unit
OFL	Ofloxacin
Pe	Peclet
Pt	Platinum
PTFE	Polytetrafluoroethylene
RPM	Rotation per minute
RTD	Retention time distribution
SBR	Sequence batch reactor
SEM	Scanning Electron Microcopy
SHE	Standard hydrogen electrode
TMD	Tramadol
TOC	Total organic carbon
UV	Ultraviolet
WWTP	Wastewater treatment plant

Introduction

Nowadays, the treatment of pharmaceuticals has become a hot topic as they are widely consumed all over the world. A strong increase in the consumption of pharmaceuticals has been observed during the last decades. In the US, IMS Health mentioned an increase of the sales from $152,8 to $280 billion which represents a 83% rise between 2000 and 2006 (Khetan and Collins 2007; Bouissou-Schurtz et al. 2014; Vergili et al. 2019). This increase can be explained by several factors such as: (i) population growth, (ii) population ageing, (iii) discovery of new properties of already existing drugs and (iv) decreasing price of drugs as patents expire (Daughton 2003).

As analytical chemistry techniques were improved during last years, especially in the limit of quantification, the presence of pharmaceutics was detected in natural water thus proving their non-effective elimination by wastewater treatment plants (WWTP), since concentrations ranging from ng L^{-1} to µg L^{-1} were usually found in natural water bodies (Lindsey et al. 2001; Bouissou-Schurtz et al. 2014). Indeed, in addition to the industrial and hospital effluents, these products are also released to urban wastewater whole or partly degraded after human and veterinary uses (Lindsey et al. 2001; Verlicchi et al. 2010). Pharmaceutical compounds are not efficiently eliminated by WWTP or by natural elimination processes in the environment (Laurencé et al. 2014). Several review papers provide a snapshot of the removal efficiency of some selected pharmaceutical molecules achieved in WWTPs (Miège et al., 2009; Gabet-Giraud et al., 2010; Luo et al., 2014).

Pharmaceuticals include lots of different compounds; they can be classified into groups aiming at doing the same action. The most important ones are the nonsteroidal anti-inflammatory drugs and analgesics, the antibiotics, the β-blockers and diuretics, the neuroactive compounds, the steroid hormones and the lipid regulators…

- Nonsteroidal anti-inflammatory drugs and analgesics: this group includes more than one hundred compounds (Feng et al. 2013). They are used as inflammatory reducer and analgesic; their high concentration in natural water can be explained by the fact that they do not need a prescription, allowing very great use.
- Antibiotics: their role is to kill bacteria or/and inhibit their multiplications. This group is composed of a huge number of molecules.
- Beta blockers: they are part of the most important prescription drugs all over the world and used in cardiovascular disease, which is a more and more common problem, and in relieving chest pain (Khetan and Collins, 2007) .
- Diuretic: they are used for anti-hypertensive medications.

Pharmaceuticals are ubiquitous in the environment

As pharmaceuticals have been detected in the environment, it is important to quantify their extent in environmental water. To estimate the concentration of pharmaceuticals in an effluent two main techniques are used: i) direct measure of the pollutant in the effluent (Table 2) and ii) use of PEC (Predicted Environment Concentration), a calculation to predict the concentration of a pollutant in an effluent based on approximations. The PEC is usually based on the fraction of active ingredient excreted in urine and feces but all the formulas are different and linked to their specific situations. For the different types of pharmaceuticals, it appears that for most of compounds, the PEC is higher than the concentration measured in the same condition, indicating that the PEC values are overestimated (Besse et al. 2008; Kümmerer 2009a; Escher et al. 2011; Sim et al. 2011; Bouissou-Schurtz et al. 2014; Gabet-Giraud et al. 2014; Mendoza et al. 2015; Al Qarni et al. 2016).

As can be seen in Table 2, β-blocker, NSAIDs and analgesics and antibiotics are present in

higher concentrations than diuretics both in surface water and in hospital wastewater. Among them, Atenolol and Metoprolol, Ibuprofen, Ciprofloxacin and Erythromycin have the highest concentrations. However, these results are very specific and cannot be expanded to other countries or even other regions.

Pharmaceuticals have harmful effect to living species

Besides measuring or predicting the concentration of pharmaceuticals, their toxicity is also an important characteristic. Two types of toxicity have to be distinguished: i) short term effect and/or exposure which is called acute toxicity and ii) long time effect and/or exposure, named as chronic toxicity. For persistent organic compounds (including the pharmaceutical), the chronic toxicity is more suitable, that is why European guidelines (EMEA 2006) recommend to use this term for the pharmaceuticals. However as the chronic toxicity data are often not available for pharmaceutical compounds (Crane et al. 2006) , acute toxicity data are in general used instead.

To measure those different toxicities several parameters are often used; the most important ones are LC_{50}, EC_{50}, NOEC and LOEC, defined in Table 1.

Table 1: Definition of the different toxicities

Abbrev.	Complete name	Definition
LC_{50}	Half Lethal Concentration	The concentration of a pollutant of the surrounding medium that will kill half of the sample population of a specific test species in a specified period of exposure
EC_{50}	Half Efficient Concentration	The concentration of a drug at which 50% of its maximum response is observed
NOEC	No Observed Effect Concentration	The highest concentration in which no effect is observed
LOEC	Low Observed Effect Concentration	The lowest concentration for which an effect is observed

Finally, another parameter called PNEC (Predicted No Effect Concentration) was introduced by the European guidelines (EMEA 2006). This value can be calculated based on the previous parameters described above (e.g. EC50. NOEC, ...). PNEC is obtained by dividing the given parameter by a safety factor (AF).

Among different class of pharmaceuticals defined above, the antibiotics seem to be the more toxic with PNEC < 1 µg L^{-1}, the more toxic being ciprofloxacin with a PNEC equal to 0.02 µg L^{-1} followed by ofloxacin, clarithromycin and erythromycin with 0.04 µg L^{-1} (Kümmerer 2003). The second more dangerous category of pharmaceuticals is the anti-inflammatories and analgesics with especially two compounds having a PNEC below 1 µg L^{-1}: ibuprofen (0.01 µg L^{-1}) and diclofenac (0.05 µg L^{-1}) (Mendoza et al. 2015). Among the β-blockers and the diuretics only one compound has been found as really hazardous: propranolol with a PNEC of 0.05 µg L^{-1} (Huggett et al. 2002).

PNEC is a good way to approximate the toxicity but it would be necessary to gather all information approved and to perform some others to have a unique PNEC based on chronic

toxicity for a larger number of species. Another point of limitation of this method is that it does not consider the potential effect of the presence of a cocktail of pharmaceuticals which was shown to have a different toxicity than that predicted by the PNEC values of the different pharmaceuticals taken separately. The synergetic effect can be whether antagonist or additive (Frédéric and Yves 2014). Tough a few studies were done on the additive effect, this phenomenon has been illustrated by Cleuvers (2005) and Brian et al. (2005). It is assumed that when different pharmaceuticals have the same action mode, their concentration can be considered as added in evaluating the toxicity of the solution (Escher et al. 2005; Fraysse and Garric 2005). In contrast, a study reported by Kümmerer (2009a) revealed that in presence of 5-fluorouracil, the thresholds effect of cephalosporine could be decreased significantly. As a consequence, to evaluate the real toxicity of effluents, the mixture toxicity must be used.

Even if the methods used for the evaluation of the toxicity of pharmaceuticals are still not very accurate, it clearly appears that these compounds represent a threat to the environment as most of them can be considered as persistent hazardous organic compounds.

Pharmaceuticals are among persistent organic pollutants:

The persistence of a pharmaceutical is its capacity to resist to physical, chemical and biological degradation processes and therefore to maintain a detectable concentration in water. As a consequence, persistent pollutants are not eliminated by a conventional WWTP or by natural elimination in the environment. The elimination processes occurring in a conventional WWTP are well-described by Margot et al. (2015). Pharmaceuticals can be eliminated from wastewater during the sewage treatment whether by being transferred to another phase or by being degraded. In the first case pharmaceuticals are sorbed onto sludge or onto particular compounds thanks to hydrophobic or electrostatic interactions or evaporated. Kümmerer underlines the fact

that very little has been done about the sorption of antibiotics and this needs to be studied as it is an important parameter (Kümmerer 2009b). For example, ciprofloxacin was found to sorb well onto activated sludge or sediments (Golet et al. 2002). Some pharmaceuticals can also be degraded, in the better case, reaching total mineralization of the mother molecule. This process can occur by biological transformation or by abiotic degradation which involves reactions such as photolysis or hydrolysis. Elimination can also happen during wastewater transportation, in this situation the process more likely to occur is photodegradation. This is well-explained in a relevant review article written by Khetan and Collins (2007). Thus, the percentage of removal is hardly ever equal to the degradation rate as some of the pollutants can adsorb themselves on the bacteria. This parameter is indirectly often evaluated thanks to the log(Kow), the octanol-water partition coefficient (Table 2).

Some pharmaceuticals, such as metoprolol, diclofenac and tramadol are hardly removed by sewage treatment plants with removal efficiency less than 40%. Other molecules such as atenolol, ketoprofen and trimethoprim are moderately removed (40-70%) whereas others (acetaminophen, naproxen, salicylic acid, etc.) are more efficiently removed (>70%) (Table 2). Therefore, according to this criterion: all the β-blockers and diuretics are of big concerns as well as diclofenac, mefenamic acid, naproxen, ketoprofen and tramadol (anti-inflammatories and analgesics) and azithromycin, clarithromycin, erythromycin, metronidazole, sulfamethoxazole and trimethoprim (antibiotics).

Table 2: Occurrence and typical removal of common pharmaceuticals in WWTP

Pharmaceutical family	Active Molecule	Chemical Structure	Occurrence in hospital effluent (µg L^{-1})	Occurrence in urban effluent (µg L^{-1})	Removal in a typical WWTP (%)	Log (Kow)	Refs.
β-blocker	Atenolol	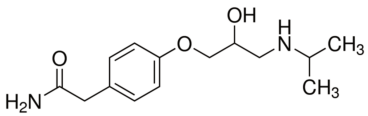	0.1-200	0.15-35* 2.405**: 0.99-8.38 0.1-33.1	8±5 63.4±24.4	0.16	(Miège et al. 2009; Gabet-Giraud et al. 2010; Verlicchi et al. 2010; Luo et al. 2014; Mendoza et al. 2015)
	Metoprolol	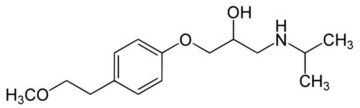	0.4-27	0.025-7 0.266:0.014-0.703 0.002-1.52	10±15 37.6±26.4	1.88	(Miège et al. 2009; Gabet-Giraud et al. 2010; Verlicchi et al. 2010; Luo et al. 2014)
	Nadolol	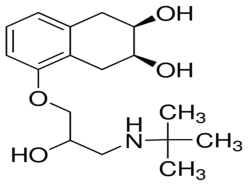		0.02142 0.0043		0.71	(Gabet-Giraud et al. 2010; Bouissou-Schurtz et al. 2014; Margot et al. 2015)

NSAIDs[a] and analgesics	Propranolol	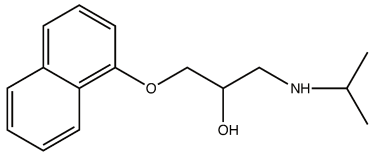	0.2-6	0.12-9 0.223:0.004-0.473	95	3.48	(Miège et al. 2009; Gabet-Giraud et al. 2010; Verlicchi et al. 2010)
	Sotalol	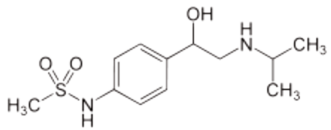		0.18-3.5 1.012:0.129-3.2		0.24	(Gabet-Giraud et al. 2010; Verlicchi et al. 2010)
	Diclofenac	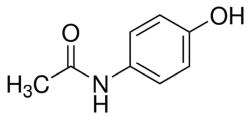		1.34:0.1-4.11 <0.001-94.2	36±18 35.8±23	4.51	(Miège et al. 2009; Luo et al. 2014)
	Ibuprofen	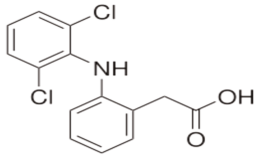	0.07-150	0.01-350 14.6:0.170-83.5 <0.004-8.56	75±30 91.4±8.1	3.97	(Miège et al. 2009; Verlicchi et al. 2010; Luo et al. 2014)
	Ketoprofen	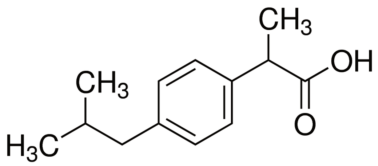		0.007-3 1.03: 0.08-5.7 <0.004-8.56	39±22 51.7±23.5	3.12	(Miège et al. 2009; Verlicchi et al. 2010; Luo et al. 2014)
	Mefenamic Acid	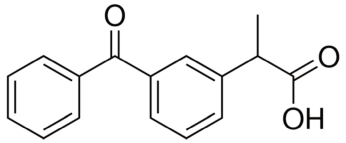		0.02-25 1.73:0.136-3.2 <0.017-1.27	30±20 36.00-34.2		(Miège et al. 2009; Verlicchi et al. 2010; Luo et al. 2014)

	Naproxen	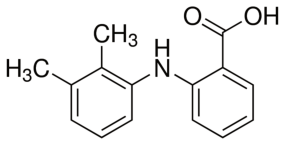	0.6-10[a]	0.018-27 26.4: 1.79-611 <0.002-52.9	77±17 75.5±18.5	3.18	(Miège et al. 2009; Verlicchi et al. 2010; Luo et al. 2014)
	Acetaminophen	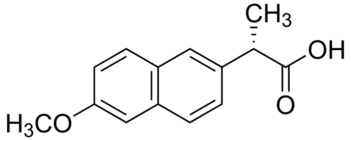		1.57-56.9	99.8±0.5	0.46	(Luo et al. 2014)
	Salicylic Acid	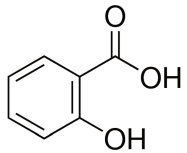		0.1-75 212: 16-606 0.58-63.7	98±1 96.6±4.1		(Miège et al. 2009; Verlicchi et al. 2010; Luo et al. 2014)
	Tramadol	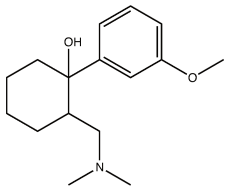	2.26	0.177	33	3.01	(Besse et al. 2008; Escher et al. 2011; Margot et al. 2015)
	Azithromycin	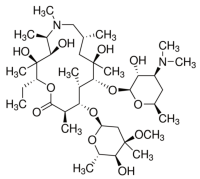		0.26	45		(Miège et al. 2009)
Antibiotics							
	Ciprofloxacin	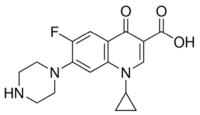	0.03-150	0.007-6 0.413: 0.18-0.571	73±30		(Miège et al. 2009; Verlicchi et al. 2010)

Clarithromycin	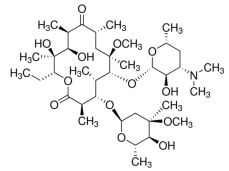		0.647	43	3.16	(Miège et al. 2009)
Erythromycin	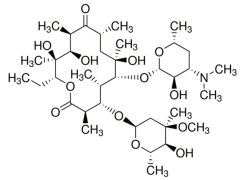	5-80	0.045-3 0.108:0.07-0.141 0.14-10	30.2±30.1		(Miège et al. 2009; Verlicchi et al. 2010; Luo et al. 2014)
Norfloxacin	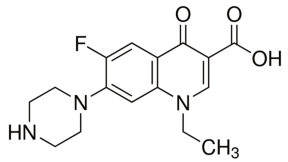	0.03-45	0.01-1 0.438: 0.343-0.515	83±3		(Miège et al. 2009; Verlicchi et al. 2010)
Ofloxacin	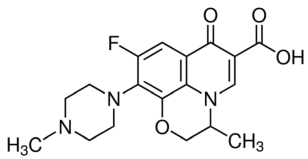	0.35-35	0.01-1		-0.39	(Verlicchi et al. 2010)
Roxythromycin	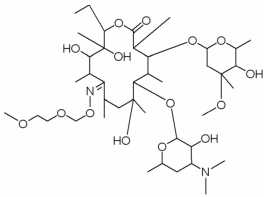		0.01-1 0.0620: 0.0250-0.11	37.5±7.5		(Miège et al. 2009; Verlicchi et al. 2010)
Sulfamethoxazole	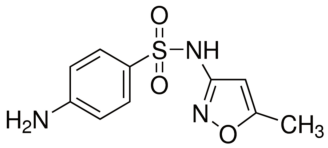		0.003-6 0.342: 0.02-1.25 <0.003-0.98	58±22 64.6±20.4		(Miège et al. 2009; Verlicchi et al. 2010; Luo et al. 2014)
Trimethoprim	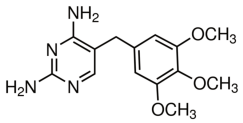		0.02-7 0.449: 0.08-13 0.06-6.80	46.8±26.3	0.91	(Miège et al. 2009; Verlicchi et

					al. 2010; Luo et al. 2014)
	Furosemide	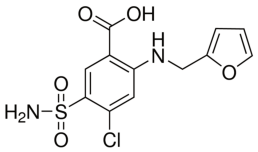	0.01473	2.03	(Mendoza et al. 2015)
Diuretic					
	Hydrochlorothiazide	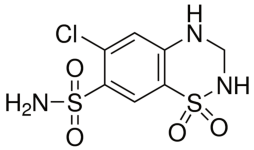	0.001735	-0.07	(Mendoza et al. 2015)

a: Non-steroidal anti-inflammatory drugs
*: minimum value-maximum value
**: mean value

Treatment of pharmaceutical wastewater: an issue to be addressed

To improve the removal rate in WWTPs, chlorination and UV irradiation are sometimes used after the biological treatment but the oxidizing power of both methods is not strong enough to degrade most of the pharmaceuticals, their metabolites or degradation products (Khetan and Collins 2007). Other physical and physicochemical methods such as coagulation-flocculation, activated carbon adsorption and membrane filtration can be used to remove pharmaceuticals from water (Luo et al. 2014). However, these treatments are separative methods, the pollutants are not destroyed but separated and transferred to another phase or produce concentrates that need to be further treated by other methods. In order to effectively degrade them, strong and non-selective oxidants are thus necessary.

Alternatively the so-called advanced oxidation processes (AOPs) have been developed to destroy efficiently toxic and/or persistent organic pollutants (Pignatello et al. 2006; Oturan and Aaron 2014). Most of the AOPs are aqueous phase oxidation processes based on the generation of highly strong oxidant like hydroxyl radicals, the second strongest oxidant after fluorine, which can destroy nearly any type of organic contaminants thanks to its very high oxidation power ($E° = 2.8$ V/SHE) (Brillas et al. 2009; Sirés and Brillas 2012; Oturan and Aaron 2014). Among different AOPs, electrochemical advanced oxidation processes (EAOPs) are of particular interest as they were shown to have a high removal efficiency and the capability to reach complete mineralization of the treated solutions (Rodrigo et al. 2014a; Sirés et al. 2014; Vasudevan and Oturan 2014). These processes are environmentally friendly and generate a great amount of hydroxyl radicals under specific operating conditions (Oturan et al. 2008a). The electro-Fenton (EF) process is one of the most popular EAOPs coupling the chemical Fenton's process to electrochemistry. It has been used successfully in the treatment of a lot of pharmaceutical active ingredients and real wastewaters (Isarain-Chávez et al. 2011a; Barros et al. 2014a; Feng et al. 2014; Panizza et al. 2014; Yahya et al. 2014; García-Montoya et al. 2015).

However EAOPs become generally expensive when the objective is the quasi-complete mineralization of treated solutions because this operation needs long electrolysis time leading to a significant amount of electrical energy consumption (Muñoz et al. 2005; Faouzi et al. 2006; Oturan et al. 2013). To reduce the operating cost and to make a cost-effective process, the combination of an EAOP with a biological treatment can be an appropriate solution to reduce the electrolysis time and to achieve the mineralization by a biological treatment (Scott and Ollis 1995; Olvera-Vargas et al. 2016a).

In this context, four pharmaceuticals belonging to different drug families (hydrochlorothiazide, ofloxacin, nadolol and tramadol) were selected to study their degradation and mineralization at lab scale by the EF process. The drug family and chemical structure of these molecules are provided in Table 3. They were chosen based on the following criteria: i) their occurrence in surface, hospital and industrial wastewaters, ii) their resistance to conventional treatment by WWTPs and iii) their toxicity. The objective was to find the best operating parameters to efficiently eliminate them and to study their degradation pathway. Then a pilot was built to scale-up the process from 230 mL to 1.7 L. The hydrodynamic and the efficiency of this reactor were studied. Finally, in the objective of decreasing the operating costs, a combination between the electrochemical process and a biological treatment was performed.

Table 3: Pharmaceuticals selected with their molecule structure

Name	Family	Molecular structure
Hydrochlorothiazide	diuretic	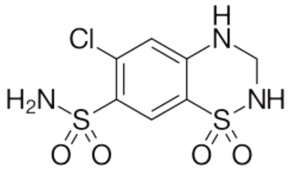
O-Floxacin	antibiotic	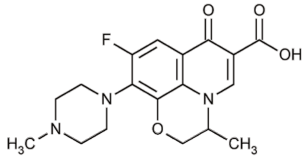
Nadolol	β-blocker	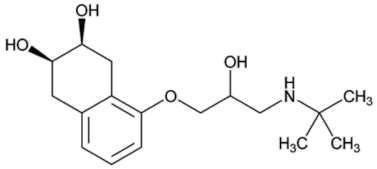
Tramadol	analgesic	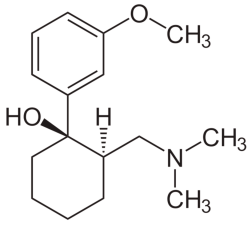

This thesis is organized in three main parts as described on the following scheme, the first part is demonstrating the efficiency of EF treatment at lab scale, the second one focuses on the pilot and the third part is considering the combined treatment. Those part are followed by recommendations and perspectives.

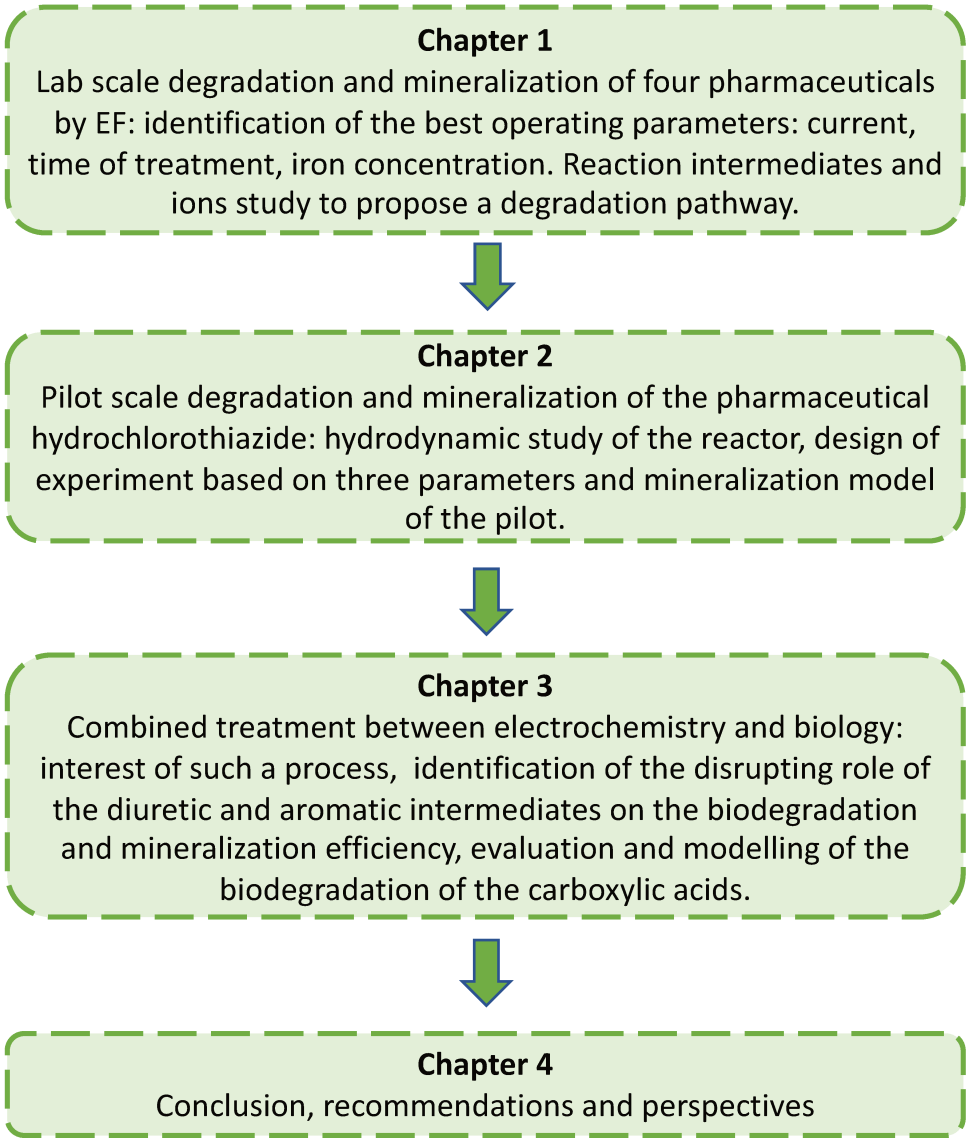

This thesis work aimed several novelty and originality

The treatment of persistent organic pharmaceuticals is a very challenging issue for the environment. This thesis project focuses for the first time on the treatment of the pharmaceuticals hydrochlorothiazide, the ofloxacin, the nadolol and the tramadol. It provides a detailed investigation on the oxidative degradation kinetics of the selected pharmaceuticals under the best operating parameters and proposes degradation pathways under action of hydroxyl radicals generated in EF process at batch reactor scale. Then a pilot scale reactor was engineered focusing on a long contact time between the compounds and the electrodes, a good

mixing and a good aeration. A design of experiment was also carried out on this pilot for the first time based on the liquid flow rate, the current density and the iron concentration and could evidence the main parameters for the mineralization efficiency and the energetic cost. An hydrodynamic study was performed as well as attempting to create a model to predict the percentage of mineralization in several locations of the reactor in the continuous mode. Those findings enable to give hints for further constructions of large scale reactors depending on the objective of the mineralization treatment. Finally, the combined bio-electro-Fenton process was also innovating as dealing with an already unworked molecule, the hydrochlorothiazide, and estimating the amount of energy that could be saved. It also highlights the specific conditions that should be applied in the electrochemical treatment to reach a good mineralization rate by explaining the role of the carboxylic acids, the aromatic intermediates and the pollutant in the biodegradation. A simple model is also presented to predict the inhibiting effects of the aromatic intermediates on the carboxylic acid biodegradation.

References:

Al Qarni H, Collier P, O'Keeffe J, Akunna J (2016) Investigating the removal of some pharmaceutical compounds in hospital wastewater treatment plants operating in Saudi Arabia. Environ Sci Pollut Res 23:13003–13014. doi: 10.1007/s11356-016-6389-7

Barros WRP, Borges MP, Reis RM, et al (2014) Degradation of dipyrone by the electro-fenton process in an electrochemical flow reactor with a modified gas diffusion electrode. J Braz Chem Soc 25:1673–1680. doi: 10.5935/0103-5053.20140160

Besse J-P, Kausch-Barreto C, Garric J (2008) Exposure assessment of pharmaceuticals and their metabolites in the aquatic environment: application to the French situation and preliminary prioritization. Hum Ecol Risk Assess An Int J 14:665–695. doi: 10.1080/10807030802235078

Bouissou-Schurtz C, Houeto P, Guerbet M, et al (2014) Ecological risk assessment of the presence of pharmaceutical residues in a French national water survey. Regul Toxicol Pharmacol 69:296–303. doi: 10.1016/j.yrtph.2014.04.006

Brian J V., Harris CA, Scholze M, et al (2005) Accurate prediction of the response of freshwater fish to a mixture of estrogenic chemicals. Environ Health Perspect 113:721–728. doi: 10.1289/ehp.7598

Brillas E, Sirés I, Oturan MA (2009) Electro-fenton process and related electrochemical technologies based on fenton's reaction chemistry. Chem Rev 109:6570–6631. doi: 10.1021/cr900136g

Cleuvers M (2005) Initial risk assessment for three b-blockers found in the aquatic environment. Chemosphere 59:199–205. doi: 10.1016/j.chemosphere.2004.11.090

Crane M, Watts C, Boucard T (2006) Chronic aquatic environmental risks from exposure to human pharmaceuticals. Sci Total Environ 367:23–41. doi: 10.1016/j.scitotenv.2006.04.010

Daughton CG (2003) Cradle-to-cradle stewardship of drugs for minimizing their environmental disposition while promoting human health. Environ Health Perspect 111:775–785. doi: 10.1289/ehp.5948

Escher BI, Baumgartner R, Koller M, et al (2011) Environmental toxicology and risk assessment of pharmaceuticals from hospital wastewater. Water Res 45:75–92. doi: 10.1016/j.watres.2010.08.019

Escher BI, Bramaz N, Eggen RIL, Richter M (2005) In vitro assessment of modes of toxic action of pharmaceuticals in aquatic life. Environ Sci Technol 39:3090–3100. doi: 10.1021/es048590e

Faouzi M, Cañizares P, Gadri A, et al (2006) Advanced oxidation processes for the treatment of wastes polluted with azoic dyes. Electrochim Acta 52:325–331. doi: http://dx.doi.org/10.1016/j.electacta.2006.05.011

Feng L, Oturan N, van Hullebusch ED, et al (2014) Degradation of anti-inflammatory drug ketoprofen by electro-oxidation: Comparison of electro-Fenton and anodic oxidation processes. Environ Sci Pollut Res 21:8406–8416. doi: 10.1007/s11356-014-2774-2

Feng L, van Hullebusch ED, Rodrigo MA, et al (2013) Removal of residual anti-inflammatory and analgesic pharmaceuticals from aqueous systems by electrochemical advanced oxidation processes. A review. Chem Eng J 228:944–964. doi: 10.1016/j.cej.2013.05.061

Fraysse B, Garric J (2005) Prediction and experimental validation of acute toxicity of beta-blockers in Ceriodaphnia dubia. Environ Toxicol Chem 24:2470–6.

Frédéric O, Yves P (2014) Pharmaceuticals in hospital wastewater: their ecotoxicity and contribution to the environmental hazard of the effluent. Chemosphere 115:31–39. doi: 10.1016/j.chemosphere.2014.01.016

Gabet-Giraud V, Miège C, Choubert JM, et al (2010) Occurrence and removal of estrogens and beta blockers by various processes in wastewater treatment plants. Sci Total Environ 408:4257–4269. doi: 10.1016/j.scitotenv.2010.05.023
Gabet-Giraud V, Miège C, Jacquet R, Coquery M (2014) Impact of wastewater treatment plants on receiving surface waters and a tentative risk evaluation: the case of estrogens and beta blockers. Environ Sci Pollut Res 21:1708–1722. doi: 10.1007/s11356-013-2037-7
García-Montoya MF, Gutiérrez-Granados S, Alatorre-Ordaz A, et al (2015) Application of electrochemical/BDD process for the treatment wastewater effluents containing pharmaceutical compounds. J Ind Eng Chem 31:238–243. doi: 10.1016/j.jiec.2015.06.030
Golet EM, Alder AC, Giger W (2002) Environmental exposure and risk assessment of fluoroquinolone antibacterial agents in wastewater and river water of the Glatt Valley watershed , Switzerland. Environ Sci Technol 36:3645–3651.
Huggett DB, Brooks BW, Peterson B, et al (2002) Toxicity of select beta adrenergic receptor-blocking pharmaceuticals (B-blockers) on aquatic organisms. Arch Environ Contam Toxicol 43:229–235. doi: 10.1007/s00244-002-1182-7
Isarain-Chávez E, Cabot PL, Centellas F, et al (2011) Electro-Fenton and photoelectro-Fenton degradations of the drug beta-blocker propranolol using a Pt anode: Identification and evolution of oxidation products. J Hazard Mater 185:1228–1235. doi: 10.1016/j.jhazmat.2010.10.035
Khetan KS, Collins JT (2007) Human pharmaceuticals in the aquatic environment : a challenge to green chemistry human pharmaceuticals in the aquatic environment : a challenge to green chemistry. Chem Rev 107:2319–2364. doi: 10.1021/cr020441w
Kümmerer K (2003) Promoting resistance by the emission of antibiotics from hospitals and households into effluent. Clin Microbiol Infect 9:1203–1214. doi: 10.1111/j.1469-0691.2003.00739.x
Kümmerer K (2009a) Antibiotics in the aquatic environment - a review - Part II. Chemosphere 75:435–441. doi: 10.1016/j.chemosphere.2008.12.006
Kümmerer K (2009b) The presence of pharmaceuticals in the environment due to human use - present knowledge and future challenges. J Environ Manage 90:2354–2366. doi: 10.1016/j.jenvman.2009.01.023
Laurencé C, Rivard M, Martens T, et al (2014) Anticipating the fate and impact of organic environmental contaminants: A new approach applied to the pharmaceutical furosemide. Chemosphere 113:193–199. doi: 10.1016/j.chemosphere.2014.05.036
Lindsey ME, Meyer M, Thurman EM (2001) Analysis of trace levels of sulfonamide and tetracycline antimicrobials in groundwater and surface water using solid-phase extraction and liquid chromatography/mass spectrometry. Anal Chem 73:4640–4646.
Luo Y, Guo W, Ngo HH, et al (2014) A review on the occurrence of micropollutants in the aquatic environment and their fate and removal during wastewater treatment. Sci Total Environ 473–474:619–641. doi: 10.1016/j.scitotenv.2013.12.065
Margot J, Rossi L, Barry DA, Holliger C (2015) A review of the fate of micropollutants in wastewater treatment plants. WIREs Water 2:457–487. doi: 10.1002/wat2.1090
Mendoza A, Aceña J, Pérez S, et al (2015) Pharmaceuticals and iodinated contrast media in a hospital wastewater: a case study to analyse their presence and characterise their environmental risk and hazard. Environ Res 140:225–241. doi: 10.1016/j.envres.2015.04.003
Miège C, Choubert JM, Ribeiro L, et al (2009) Fate of pharmaceuticals and personal care products in wastewater treatment plants--conception of a database and first results. Environ Pollut 157:1721–6. doi: 10.1016/j.envpol.2008.11.045

Muñoz I, Rieradevall J, Torrades F, et al (2005) Environmental assessment of different solar driven advanced oxidation processes. Sol Energy 79:369–375. doi: http://dx.doi.org/10.1016/j.solener.2005.02.014
Olvera-Vargas H, Cocerva T, Oturan N, et al (2016) Bioelectro-Fenton: a sustainable integrated process for removal of organic pollutants from water: application to mineralization of metoprolol. J Hazard Mater 319:13–23. doi: 10.1016/j.jhazmat.2015.12.010
Oturan MA, Aaron J-J (2014) Advanced oxidation processes in water/wastewater treatment: principles and applications. A Review. Crit Rev Environ Sci Technol 44:2577–2641. doi: 10.1080/10643389.2013.829765
Oturan MA, Guivarch E, Oturan N, Sirés I (2008) Oxidation pathways of malachite green by Fe3+-catalyzed electro-Fenton process. Appl Catal B Environ 82:244–254. doi: 10.1016/j.apcatb.2008.01.016
Oturan N, Wu J, Zhang H, et al (2013) Electrocatalytic destruction of the antibiotic tetracycline in aqueous medium by electrochemical advanced oxidation processes: Effect of electrode materials. Appl Catal B Environ 140–141:92–97. doi: 10.1016/j.apcatb.2013.03.035
Panizza M, Dirany A, Sirés I, et al (2014) Complete mineralization of the antibiotic amoxicillin by electro-Fenton with a BDD anode. J Appl Electrochem 44:1327–1335. doi: 10.1007/s10800-014-0740-9
Pignatello JJ, Oliveros E, MacKay A (2006) Advanced oxidation processes for organic contaminant destruction based on the Fenton reaction and related chemistry. Crit Rev Environ Sci Technol 36:1–84. doi: 10.1080/10643380500326564
Rodrigo MA, Oturan MA, Oturan N (2014) Electrochemically assisted remediation of pesticides in soils and water: A review. Chem Rev 114:8720–8745. doi: 10.1021/cr500077e
Scott JP, Ollis DF (1995) Integration of chemical and biological oxidation processes for water treatment: review and recommendations. Environ Prog 14:88–103. doi: 10.1002/ep.670140212
Sim WJ, Lee JW, Lee ES, et al (2011) Occurrence and distribution of pharmaceuticals in wastewater from households, livestock farms, hospitals and pharmaceutical manufactures. Chemosphere 82:179–186. doi: 10.1016/j.chemosphere.2010.10.026
Sirés I, Brillas E (2012) Remediation of water pollution caused by pharmaceutical residues based on electrochemical separation and degradation technologies: a review. Environ Int 40:212–229. doi: 10.1016/j.envint.2011.07.012
Sirés I, Brillas E, Oturan MA, et al (2014) Electrochemical advanced oxidation processes: today and tomorrow. A review. Environ Sci Pollut Res 21:8336–8367. doi: 10.1007/s11356-014-2783-1
Vasudevan S, Oturan MA (2014) Electrochemistry: as cause and cure in water pollution-an overview. Environ Chem Lett 12:97–108. doi: 10.1007/s10311-013-0434-2
Vergili I, Kaya Y, Gönder ZB, et al (2019) Occurence and prioritization of pharmaceutical active compounds in domestic / municipal wastewater treatment plants. Bull Environ Contam Toxicol 102:252–258. doi: 10.1007/s00128-019-02550-z
Verlicchi P, Galletti A, Petrovic M, BarcelÓ D (2010) Hospital effluents as a source of emerging pollutants: An overview of micropollutants and sustainable treatment options. J Hydrol 389:416–428. doi: 10.1016/j.jhydrol.2010.06.005
Yahya MS, Oturan N, El Kacemi K, et al (2014) Oxidative degradation study on antimicrobial agent ciprofloxacin by electro-fenton process: Kinetics and oxidation products. Chemosphere 117:447–454. doi: 10.1016/j.chemosphere.2014.08.016

CHAPTER 1

LITERATURE REVIEW

A review on Efficiency and Cost Effectiveness of Electro- and Bio-electro-Fenton processes: Application to the Treatment of Pharmaceutical Pollutants in Water

This chapter was adapted from the following review article(Monteil et al. 2018)(Monteil et al. 2018):

Monteil H, Péchaud Y, Oturan N, Oturan MA (2018). A review on efficiency and cost effectiveness of electro- and bio-electro-Fenton processes: application to the treatment of pharmaceutical pollutants in water. Chemical Engineering Journal (in press) doi:10.1016/j.cej.2018.07.179.

1. Introduction

The purpose of this review paper is first to give an overview of the newest knowledge concerning the EF process and the reactor configurations and then to provide an overview on its applications to the treatment of pharmaceutical compounds. Finally, the feasibility and the cost-effectiveness of the combined process bio-electro-Fenton (bio-EF) will be discussed and the whole literature about this topic will be provided.

2. Electrochemical advanced oxidation processes

2.1 Mechanisms involved in EAOPs

The most popular and commonly used electrochemical advanced oxidation processes (EAOPs) are anodic oxidation (AO), also called (electro-oxidation) and electro-Fenton (EF) processes. These processes are based on direct (AO) or indirect (EF) catalytic generation of hydroxyl radical ($^{\bullet}OH$) in the solution to be treated. Once generated in situ, these strong oxidizing agents will react on organic contaminants to oxidize them until their total or partial mineralization (Eqs. (1) and (2)).

Pollutants + $^{\bullet}OH \rightarrow$ intermediates (1)

Intermediates + $^{\bullet}OH \rightarrow \rightarrow \rightarrow CO_2 + H_2O$ + inorganic ions (2)

These types of processes have been well-described by several review papers (Brillas et al. 2009; Barrera-Dias et al. 2014; Oturan and Aaron 2014; Sirés et al. 2014; Pliego et al. 2015).

2.1.1 Direct oxidation (AO)

In this process the oxidation takes place at the surface of the anode. Heterogeneous hydroxyl radicals M($^{\bullet}OH$)) are formed at the anode surface from the oxidation of water according to the following reaction (Eq. (3)) (Marselli et al. 2003).

$$M + H_2O \rightarrow M(^{\bullet}OH) + H^+ + e^- \quad (3)$$

where M represents the anode material and M(•OH) is the hydroxyl radical adsorbed on the anode (M) surface.

For this kind of oxidation, two different types of transfer can limit the process: mass transfer or charge transfer. Mass transfer is done by migration (driven by the electrical field), by diffusion (driven by chemical potential gradient) and/or by convection processes. It can be expressed with the Nernst-Planck equation. As it is experimentally difficult to distinguish these three processes, the mass transfer process is generally approached in a semi-empirical way under specific conditions. These conditions are, i) the solution is conductive enough (use of a supporting electrolyte), ii) the solution is well-mixed and iii) the applied potential (or current) is high enough to oxidize efficiently the substrate.

Two different behaviors can occur depending on the anode material (Brillas et al. 2009). Active anodes promote the formation of higher states oxides or superoxides (MO) (Eq. (6)) (Simond et al. 1997).

$$M(^{\bullet}OH) \rightarrow MO + H^+ + e^- \quad (6)$$

This type of anodes form chemisorbed radicals which limit the reaction at the surface of the anode as there is a strong interaction between the radicals and the anode surface. The most common anodes of this type are Pt and mixed metal or DSA (dimensionally stable anode) anodes.

On the opposite, the non-active anodes enable the formation of physisorbed radicals with a quite weak interaction between hydroxyl radical (•OH) and the anode surface (M) (Eq. (2)). Hydroxyl radicals thus formed are able to react in the diffusion layer and can conduct to complete mineralization of organics. The most representative non-active anodes are BDD, tin or lead oxides and sub-stoichiometric titanium oxides.

AO process can also imply indirect (or mediated) oxidation occurring in the bulk of the solution thanks to the formation, at the electrode surface, of a mediator (an oxidizing species). Once migrated to the bulk solution, these oxidizing agents can participate in the oxidation of organic pollutants. Usually it concerns active chlorine species and peroxy anions. For instance, the relatively strong oxidants such as hypochlorous acid/hypochlorite anion (formed in chloride medium), peroxydisulfate anion (formed from sulfate medium) and peroxyphosphate anion (formed in phosphate medium) can be created (Barrera-Dias et al. 2014) at the anode surface and contribute to the oxidation process in the bulk solution.

2.1.2 Indirect electro-oxidation: Electro-Fenton (EF) process

EF process is an indirect EAOP since hydroxyl radicals are not generated directly from charge transfer at the electrode level but in the solution from the well-known Fenton's reaction (Eq. (8)) (Fenton 1894; Haber and Weiss 1934). In the Fenton's process, homogeneous hydroxyl radicals ($^{\bullet}OH$) are generated from Fenton's reagent, a mixture of H_2O_2 and Fe^{2+}, added externally to the solution to be treated. In contrast, for the EF process, the Fenton's reagent is electrochemically produced at the cathode. H_2O_2 is formed by a 2-electron reduction of dissolved O_2 (Eq. (9)) and Fe^{2+} by a single electron reduction of ferric cation (Eq. (10)). At the anode, water is oxidized to O_2 (Eq. (11)) and, depending on the anode material, adsorbed hydroxyl radicals can be formed (Eq. (3)).

$$Fe^{2+} + H_2O_2 \rightarrow Fe^{3+} + {}^{\bullet}OH + OH^- \quad (8)$$

$$O_2 + 2\ H^+ + 2\ e^- \rightarrow H_2O_2 \quad (9)$$

$$Fe^{3+} + e^- \rightarrow Fe^{2+} \quad (10)$$

$$2\ H_2O \rightarrow O_2 + 4\ H^+ + 4\ e^- \quad (11)$$

The Fenton's process was a major step forward as it is easy to implement and uses relatively

inexpensive and harmless chemicals (Bautista et al. 2008; Oturan and Aaron 2014). It was first applied in 1960 for the treatment of organic pollutants (Brown et al. 1964), since then a large application to the treatment of effluents was reported, such as the discoloring effluents of dye industries (Kuo 1992) or the treatment of different kind of wastewaters (Gogate and Pandit 2004).

Despite its interesting use in the treatment of effluents contaminated by organic pollutant, this process suffers from some drawbacks such as needing high amounts of Fenton's reagent to generate enough quantity of $^{\bullet}OH$. The introduction of a high amount of H_2O_2 and Fe^{2+} implies economic aspect and also the formation of ferric hydroxide sludge needing a supplementary processing. Moreover this situation favors the rate of wasting reactions (Eq. (12) and (13)) resulting in low efficiency.

$$^{\bullet}OH + H_2O_2 \rightarrow H_2O + HO_2^{\bullet} \quad (12)$$

$$^{\bullet}OH + Fe^{2+} \rightarrow Fe^{3+} + OH^{-} \quad (13)$$

The EF process, developed and popularized by Oturan's and Brillas' group at the beginning of the 21st century has been designed to avoid the disadvantages of the classical Fenton's process by coupling between electrochemistry and Fenton's chemistry (Brillas et al. 2000; Oturan 2000). Electrochemistry offers an amazing help in this respect (Vasudevan and Oturan 2014). Indeed, in contrast to the classical Fenton's process, in the EF process the Fenton's reagent is in situ generated (H_2O_2) or regenerated (Fe^{2+}): H_2O_2 is generated on a suitable cathode by a 2-electron reduction of dissolved O_2 (Eq. (9)) and regeneration of Fe^{2+} from Fe^{3+} formed in Fenton reaction (Eq. (10)). The electrocatalytic regeneration of ferrous iron allows the use of a catalytic amount of this ion as catalyst thus avoiding the ferric hydroxide sludge formation and also preventing the wasting of generated $^{\bullet}OH$ (Eq. (13)) (Brillas et al. 2009; Oturan and Aaron 2014). Therefore, the use of EF process instead of Fenton's process allows the following

advantages: (i) minimizing reagent cost by in situ generation of Fenton's reagent, (ii) avoiding risks related to transportation and storage of H_2O_2, (iii) avoiding (or minimizing) reactions wasting $^{\bullet}OH$ (Eqs. (12) and (13)) because H_2O_2 and Fe^{2+} concentrations are quite low since they are consumed as soon as they are formed, (iv) eliminating sludge formation and (v) generally providing high removal rate of organics due to the electrochemical regeneration of Fe^{2+} which catalyzes Fenton's reaction (Zhu et al. 2011; Rodrigo et al. 2014a; Sirés et al. 2014; Oturan and Oturan 2018).

The use of an appropriate cathode material is essential in the EF process; it should be able to generate efficiently H_2O_2 and have a low catalytic activity for its reduction. Moreover the cathode must have high overpotential for H_2 evolution since the process is optimal at acid medium (Oturan and Oturan 2018). These characteristics are generally satisfied by carbonaceous materials that are often used in EF process such as three-dimensional carbon materials (carbon felt, graphite felt, carbon sponge, activated carbon fiber) (Oturan et al. 2000; Wang et al. 2005; Özcan et al. 2008; Oturan et al. 2010; Panizza and Oturan 2011) and carbon-PTFE-O_2 gas diffusion cathode (Brillas et al. 1995). Other carbonaceous materials like graphite, reticulated vitreous carbon and carbon nanotubes have also been tested. More recently BDD and Ni foam have been also shown to be able to produce H_2O_2 (Oturan et al. 2010; Panizza and Oturan 2011; Saussereau et al. 2013; Bocos et al. 2016a).

On the other hand, the nature of the anode is also very important in EF process. In the case of the use of a non-active anode, M($^{\bullet}OH$) are produced on the anode surface (Panizza and Cerisola 2001). In this case EF process also includes AO process since homogeneous ($^{\bullet}OH$) and heterogeneous M($^{\bullet}OH$) are produced simultaneously in the bulk solution and on the anode surface, respectively, thus enhancing strongly the oxidation power of the process (Oturan et al. 2012). The best non-active anode material known is the BDD. However, its high cost can constitute an obstacle to its scale up for large-scale applications. Therefore, research is done on

the use of ceramic electrodes based on sub-stoichiometric titanium oxides (Ti_nO_{2n-1}) (Smith and Walsh 1998; Chaplin 2014). Recent studies have shown that this new anode material is able to provide results close to that of BDD in AO and EF processes (Ganiyu et al. 2017; Oturan et al. 2017).

During the EF treatment, numerous reactions are involved and the mass transfer constitutes an important parameter in the degradation of pollutant as some reactants have to reach the surface of the electrode (O_2, Fe^{3+}) when others have to reach the bulk from the electrode surface (H_2O_2, Fe^{2+}). For instance, the oxygen required for the formation of H_2O_2 (Eq. (9)) has to be transferred from the gas phase to the aqueous phase and then needs to be adsorbed onto the electrode surface before its reduction process (Brillas et al. 2009). The required dissolved oxygen concentration is reached usually by aeration. If oxygen is not provided at an adequate rate, it becomes a limiting factor, controlling H_2O_2 generation rate and consequently the EF process. As the diffusivity of oxygen in the gas phase is significantly higher than in the liquid phase, it is considered that the gas phase offers no transfer resistance. Thus, it can be suggested that the overall oxygen transfer rate (OTR) is controlled by the liquid phase, expressed as follows (Eq. (14)):

$$OTR = k_La\ (C^*_{bulk,\ O2} - C_{bulk,O2}) \quad (14)$$

where OTR is the oxygen mass transfer rate (mol m^{-3} s^{-1}), k_La is defined as the volumetric oxygen mass transfer coefficient (s^{-1}), $C^*_{bulk,\ O2}$ and $C_{bulk,O2}$ are the equilibrium concentration and the oxygen concentration in the bulk (mol m^{-3}), respectively.

It is worthy to note that the oxygen mass transfer has been well studied for water and wastewater treatment systems but not in EF process. The value of k_La depends mainly on the configuration of the reactors, on the air flow rate, on the airflow diffuser which will influence the bubbles size and on the hydrodynamics in the reactors.

The transfer from the bulk to the anode (pollutants) and the transfer from the cathode to the bulk (H_2O_2 and Fe^{2+}) are key points for the efficiency of the process. That is why, understanding the controlling parameter is important. As it was explained previously for the AO (Eqs. (4) – (6)), the expression of the current density in EF follows the same behavior. But, the system is more complex as for the EF, the oxidation of pollutants can occur on the anode surface (AO) and in the bulk (involving both homogenously generated $^{\bullet}OH$ from Fenton reaction and mediated oxidation from oxidants formed at the anode).

There are several operating parameters involved in EF process efficiency which have now long been studied (Brillas et al. 2009; Nidheesh and Gandhimathi 2012; Oturan and Aaron 2014; Martínez-Huitle et al. 2015). The principal parameters are: solution pH, applied current, catalyst nature and concentration, supporting electrolyte (nature and concentration), electrode gap, oxygen (or air) supply rate and temperature.

The pH is a very important parameter of this process, it is usually recommended to work at a pH around 3 (Boye et al. 2002). The acidic medium is required for the formation of H_2O_2 (Eq. (9)), however pH values lower than 2 lead to the transformation of H_2O_2 to peroxonium ($H_2O_3^+$) ion which is less reactive toward Fe^{2+} in the formation of $^{\bullet}OH$ via Fenton reaction and at higher pH this compound decomposes into water and oxygen (Wang and Lemley 2001; Feng et al. 2003; Wang et al. 2010b). Moreover, at pH above 4, Fe^{3+} precipitates as $Fe(OH)_3$ and at pH below 1, Fe^{2+} forms complexes with H_2O_2 (Pignatello 1992).

The current is another key factor in EF process since the rate of electrochemical reactions is promoting the generation of $^{\bullet}OH$ (Eqs. (9), (10) and consequently Eq. (8)) and M(OH) (Eq. (3)). Therefore this parameter influences significantly the oxidation and/or mineralization efficiency of the process (Narayanan and Rajendran 2003; Oturan and Aaron 2014). But a too high current promotes competitive reactions consuming electrical energy in side reactions

(reduction of water to H_2 or its oxidation to O_2) or wasting of $^{\bullet}OH$/M($^{\bullet}OH$) (recombination or oxidation reactions) in the electrolytic cell (Zhang et al. 2007; Brillas et al. 2009; Sirés et al. 2014). The current value determines also the type of limitation for the system whether by the mass transfer or by the charge transfer as explained previously. Usually this parameter is experimentally determined for each compound/equipment before treatment.

Another highly important parameter is the nature or concentration of the catalyst. Among different catalysts tested for EF process, it was evidenced that iron (Fe^{2+}/Fe^{3+}) is one of the best since it is not harmful, has low cost and requires low concentration (Brillas et al. 2009). With regard to the Fe^{2+} concentration, the optimal value depends on the cathode used; optimal values about 0.1 – 0.2 mM for carbon-felt cathode and 0.5 mM for gas diffusion cathode were reported many times in literature (Brillas et al. 2009; Oturan and Aaron 2014; Sirés et al. 2014). High Fe^{2+} concentration is generally avoided since it promotes the wasting reaction given in Eq. (13) (Panizza and Cerisola 2001; Oturan and Aaron 2014). This factor is also usually experimentally adjusted. Meanwhile the Cu^{2+}/Cu^{+} couple was also investigated as catalyst in the EF process and contradictory results have been published. For instance a recent study, demonstrated that copper could be more efficient and more cost-effective than iron with a higher TOC removal rate (Santana-martínez et al. 2016). But, other researchers highlighted that iron catalyst provides a better mineralization efficiency than cupper ions (Oturan and Oturan 2005).

Airflow and air diffuser are also important parameters that influence significantly both oxygen transfer and hydrodynamic conditions in the reactors. In the case of low oxygen flow rate the solution cannot be saturated in O_2 and oxygen transfer can become the limiting step affecting the efficiency of H_2O_2 production rate and accordingly $^{\bullet}OH$ generation rate through Fenton's reaction.

In addition, temperature is an influent parameter that impacts all the process. It affects the kinetics of chemical and electrochemical reactions and mass transfer parameters (diffusion

coefficient, etc.). In general, temperatures ranging between 20 and 30 °C are applied in the literature (Umar et al. 2010) since higher temperatures decrease O_2 solubility as well as promote H_2O_2 decomposition. For the nature of the electrolyte, good conductivity ions must be used. Indeed, Ghoneim et al. (Ghoneim et al. 2011) performed an experiment comparing the efficiency of the EF with three different electrolytes: Na_2SO_4, NaCl and KCl. The better efficiency of Na_2SO_4 have been explained by the higher conductivity of SO_4^{2-} compared to Cl^- (Gil et al. 2006). They also obtained a higher degradation rate using KCl than NaCl explained again with the greater conductivity of K^+ compared to Na^+. On the other hand, the degradation of methyl parathion by EF with sodium sulfate was slower than with $NaClO_4$ or $NaNO_3$ because of the formation of sulfato-complexes with iron (De Laat et al. 2004; Diagne et al. 2007). The electrolyte allows to increase the solution conductivity by avoiding an ohmic potential drop, responsible for a higher energetical consumption. Meanwhile it was demonstrated that a too high concentration of Na_2SO_4 can produce a great decrease in the TOC abatement which can be due to the side reaction of hydroxyl radicals with sulfate ions (Zhou et al. 2007; Gökkuş 2016).

2.2 Reactor configuration

Recent ways of enhancing efficiency and decreasing the costs in EAOPs consist in choosing a specific reactor configuration to enhance mass transfer and current efficiency. The reactor configuration is a key point for the efficiency of the pollutant degradation by electro-Fenton. Some review papers have given an overview of the different cell configurations used until 2012 (Brillas et al. 2009; Nidheesh and Gandhimathi 2012). Most of the studies have been performed at lab-scale with undivided cell reactors with volumes lower than 300 mL. Another system, quite similar to the previous one (undivided cell), is the use of divided cells with two or three electrodes. The undivided system has the advantage of lower operating costs due to the possible

use of a lower cell voltage in comparison with the divided cells. Moreover the latter has the advantage of avoiding H_2O_2 to reach the anode and to be oxidized there (Eq. (15)) thus preventing the following side reaction (Brillas et al. 2009).

$$H_2O_2 \rightarrow HO_2^{\bullet} + H^+ + e^- \quad (15)$$

Two other systems used to a lesser extent were the filter press reactors operating in batch and recirculation mode (Prabhakaran et al. 2009) and the bubble reactor operating in continuous mode (Rosales et al. 2009). However, in the last 5 years, new reactor configurations or enhanced configurations of formerly used reactors were developed that allows having a greater efficiency and/or lower costs (Martínez-Huitle et al. 2015). Therefore, the aim of this section is to give an overview of those new studies which are sum-up in Table 4. Some of these configurations are also illustrated in Fig. 1. The novelties include: i) the way of mixing in order to favor mass transport and transfer to the anode, ii) the manner in which the oxygen is transferred to the solution, iii) the shape and distance between electrodes and their number, iv) the shape and the volume of the cell and v) the type of out streaming.

2.2.1 Geometric parameters

Recent research has most specifically focused on geometric changes in electrodes. Among them, Su et al. (Su et al. 2013) studied the impact of using plate or rod electrodes for aniline removal (Fig. 1). The experimental conditions are described in Table 4. They found out that the plate electrodes have a better aniline degradation rate than the rod electrodes for added [H_2O_2] > 29 mM. This phenomenon is explained as the distance between the electrodes is lower (1.5 cm) for plate electrodes while it is significantly higher (5.5 cm) for rod electrodes. This allows the plate electrode system to have a lower electrical resistance and thus a better electrical efficiency. On the contrary, in the case of lower [H_2O_2] added to the solution, the rod electrode cell is more efficient at degrading the pollutant (Su et al. 2013). The area of the working

electrodes is 900 cm^2 and 600 cm^2 for the plate electrode reactor and 433 cm^2 and 36 cm^2 for the rod electrode reactor for the cathode and the anode respectively. Thus, the effect observed can also be partly explained by the difference on the surface of the electrodes.

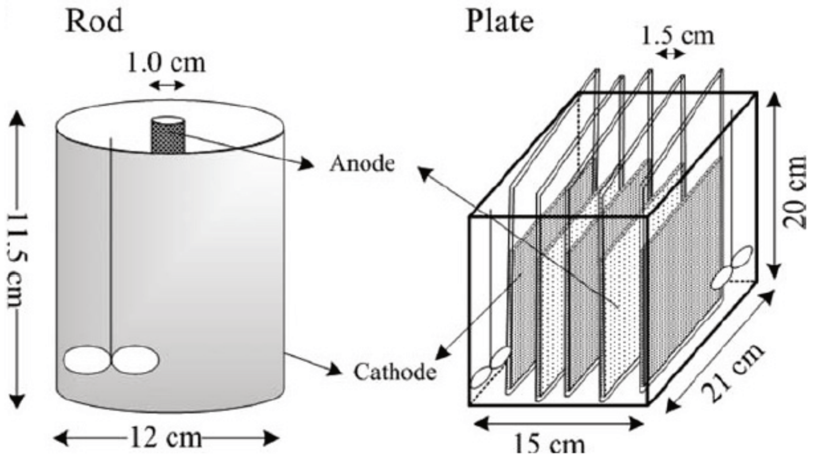

Fig. 1: Reactors with rod and plate electrodes. Reprinted with permission from ref (Su et al. 2013). Copyright 2012, American Institute of Chemical Engineers.

Another idea is to create a reactor composed of two gas diffusion electrodes (GDE): the two GDE cathodes placed in parallel, in the center of the cell, with two anodes, (Yu et al. 2015). This configuration enables a greater production of H_2O_2, and thus allows forming more hydroxyl radicals according to the Fenton's reaction (Eq. (8)). Authors compared this system (reactor 1) with the reactor composed of one anode and one cathode in the same position (reactor 2) and with the reactor composed of one anode and one cathode positioned vertically (reactor 3), the latter one being the mostly used configuration. As shown in Table 4, the reactor with two GDE cathodes is more efficient in terms of production of H_2O_2 and current efficiency compared to the other reactors. This reactor was also more cost-effective with a much lower energy consumption (Yu et al. 2015) with the same current intensity. The higher efficiency can be explained by the higher working area in this reactor as it is equipped with two more electrodes although the additional manufacturing costs are not taken into account in the cost

calculation. The parallel configuration of the electrodes in reactor 1 can explain the lower energy consumption. Indeed, this configuration reduces by two the current intensity which results in a lower voltage for the cell and thus in a lower energy consumption compared with reactor 2 where the current is not divided. The surfaces of the electrodes facing each other in reactor 3 are smaller causing a lower conductance and thus an increase of the cell voltage.

Another cell geometry has been proposed by Lei et al. (Lei et al. 2013): the trickle-bed reactor (Fig. 2) to enhance the efficiency of the electro-Fenton process. This system is made of several pieces which constitute the fixed part of the packed bed of the reactor using the downward movement of a liquid and the upward movement of gas. Details about the reactor configuration and the treatment conditions are given in Table 4. The air and the solution are both mixed before entering the cell. This configuration enables to dissolve the oxygen first in the liquid allowing the easy transfer of oxygen to the electrode surface and therefore enhancing the production of hydrogen peroxide. The authors found out that this system is as efficient as GDE reactor but avoids electrolyte leakage and gas bubbles which makes its application feasible at a larger scale (Lei et al. 2013).

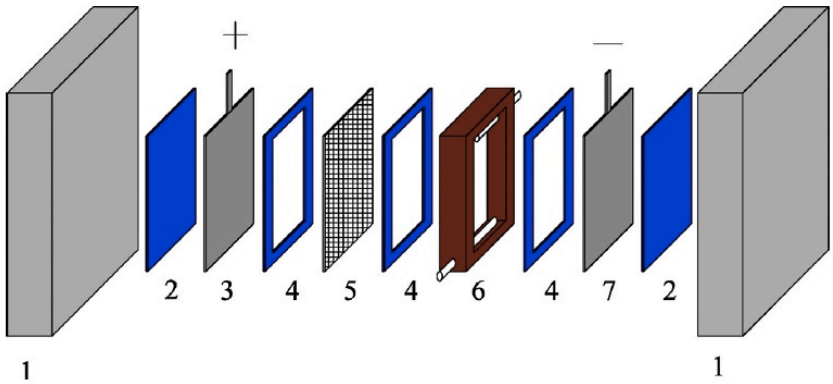

Fig. 2: Scheme of the trickle bed reactor. 1: Cell body, 2: Gasket, 3: Ti/PbO_2 anode, 4: Gasket ring, 5: Nylon diaphragm, 6: Cathode frame for loading graphite chips and 7: Nickel plate. Reprinted with permission from ref. (Lei et al. 2013). Copyright 2013, Elsevier

Finally, Xu et al. (Xu et al. 2016) suggested the use of tubular membranes for both anode and

cathode (Fig. 3).The electrodes and the experimental conditions used are detailed in Table 4. The reactor has the advantage of enhancing the mass transfer without needing any aeration. Using cyclic voltammetry (CV) analysis, the authors showed that the tubular anode exhibits better catalytic activity than the plate electrode. Indeed, the CV curves area for the tubular anode is 1.58-fold greater than that of plate anode. This greater catalytic activity can be explained by the presence of micro-porosity which provides a larger surface area for the tubular anode. The micro-porosity also enhances the dispersion and dissolution of oxygen present in the solution. In a plate electrode, the electrolyte flows along the electrode and some pollutant will bypass the electrode surface without undergoing degradation (Shukla et al. 2012). By flowing toward the electrode (and not along it), the mass-transfer to the electrode is enhanced. This is demonstrated with computational fluid dynamics (Wang et al. 2015) and by chronoamperometry measurements where the current density is greater for the tubular membrane; 1.71 and 3.43 mA cm^{-2} after a test time of 20 sec for the plate and porous electrode respectively (Zhang et al. 2016). Finally, the authors demonstrated that their system does not require aeration by measuring the amount of H_2O_2 and hydroxyl radicals produced with and without aeration (Table 4) (Xu et al. 2016).

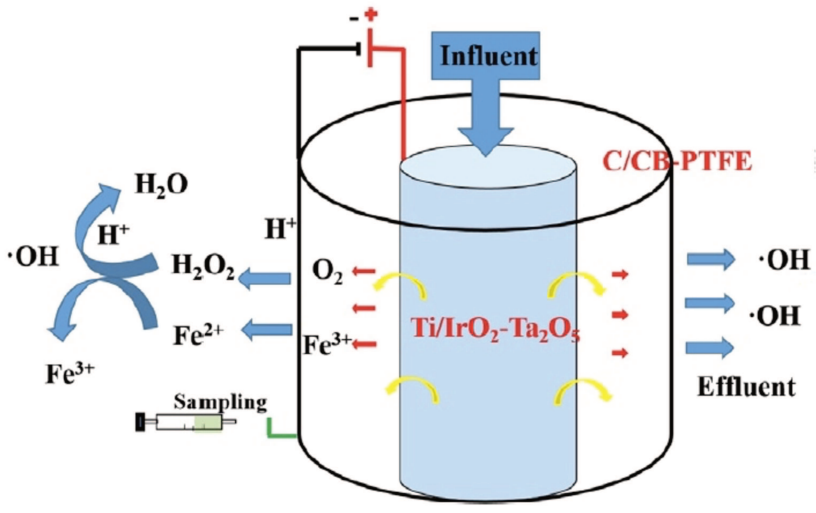

Fig. 3: Scheme of the dual tubular membranes EF reactor. Reprinted with permission from ref. (Xu et al. 2016). Copyright 2016, Elsevier.

Another tubular system was recently created. It is based on two driving forces: i) the transmembrane pressure and ii) the current. The authors demonstrated the efficiency of their system, described in Table 4 (tubular membrane A) by the higher H_2O_2 production of their system by finding optimums current and transmembrane pressure (Olvera-vargas et al. 2018).

2.2.2 Out streaming

As in the study on tubular membranes, research was done on the effect of the direction of the flow whether parallel to the electrodes (flow-by) or perpendicular to them (flow-through or vertical-flow). Two recent studies analyzed the degradation of methylene blue and tartrazine, respectively, under those different flowing conditions. The single compartment system working on methylene blue is composed of perforated DSA (dimensionally stable anode) electrode as the anode and a modified graphite felt as a cathode (Fig. 4) (Ma et al. 2016). The second multiple cell reactor, used to degrade tartrazine, is equipped with PbO_2 anodes and modified graphite felt mesh cathodes (Ren et al. 2016). Results obtained showed the superiority of the flow-through reactor over the flow-by reactor in the same conditions (Table 4). This result can be explained by the enhancement of the mass transport in the vertical-flow compared to the parallel flow (Santos et al. 2010; Liu and Vecitis 2012). The higher efficiency is related to the greater accumulation of H_2O_2 in the flow-through (57.8 mg L^{-1}) than in the flow-by system (51.9 mg L^{-1}) (Ma et al. 2016).

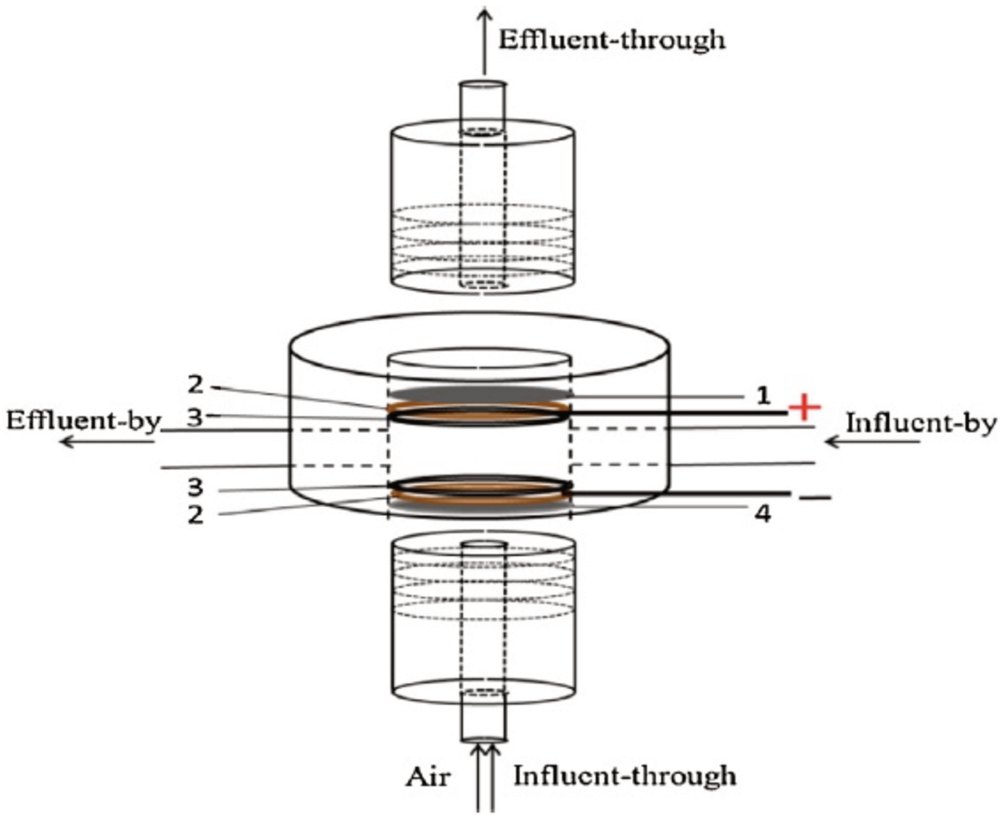

Fig. 4: Scheme of the flow-through reactor containing 1: a perforated DSA anode, 2: the titanium ring, 3: the insulating rubber ring and 4: the modified graphite felt cathode. Reprinted with permission from ref. (Ma et al. 2016). Copyright 2016, Elsevier.

Concerning the multiple flow through reactor (Fig. 5), made of maximum 10 compartments, both operating conditions were able to remove totally the 0.4 mM tartrazine from the aqueous solution; however the vertical flow was more efficient as can be seen from the TOC removal values (Table 4). By comparing the electrical energy consumption per kg TOC removed for a different number of compartments, the authors showed that the cost-efficient choice was the 8 compartments reactor (Ren et al. 2016). The higher mineralization efficiency and the lower energy consumption can be explained by the enhancement of the mass transfer of O_2 and pollutant thanks to the flow-through configuration. This better transfer provides a higher current efficiency and thus a lower energy consumption (Yang et al. 2009). Recently another stack electrode system was proposed by Hu et al. (2018) in which it was demonstrated that by putting

closer the electrodes, they could increase the COD abatement and decrease the energetical consumption. The specific energy consumption was of 50 and 30 kWh $(kgCOD)^{-1}$ for 1 pair of electrode separated by 10 and 2 mm, respectively, after 6 h electrolysis (Hu et al. 2018).

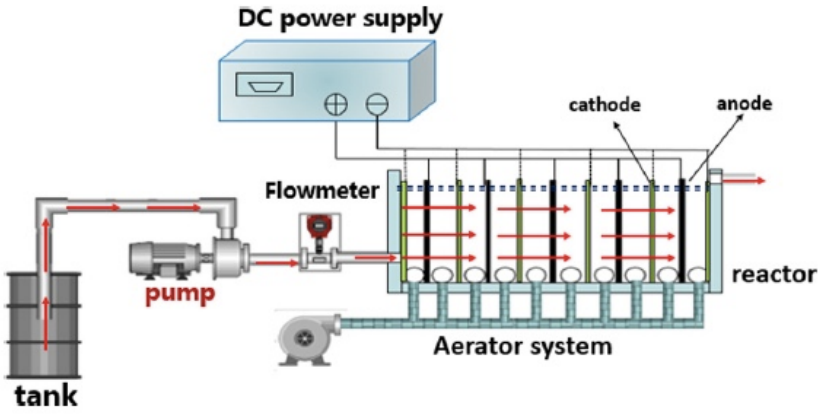

Fig. 5: Scheme of the 10-compartment reactor. Reprinted with permission from ref. (Ren et al. 2016). Copyright 2016, Elsevier.

2.2.3 Special way of supplying O_2

Recently an interesting idea appeared in numerous publications: a special way of providing oxygen to the system without supplying an air or oxygen flow rate. This system is based on the use of two parallel rotating cathodes with an anode in the middle (Fig. 6) (Yu et al. 2014). The operating parameters related to this reactor are described in Table 4. This system enables to bring oxygen without blowing air or O_2 in the solution making it more cost-effective and providing a good mass transfer between the solution and the electrode surface as demonstrated by comparing with the same electrodes but without rotating cathodes and providing O_2 (Table 4) (Yu et al. 2014).

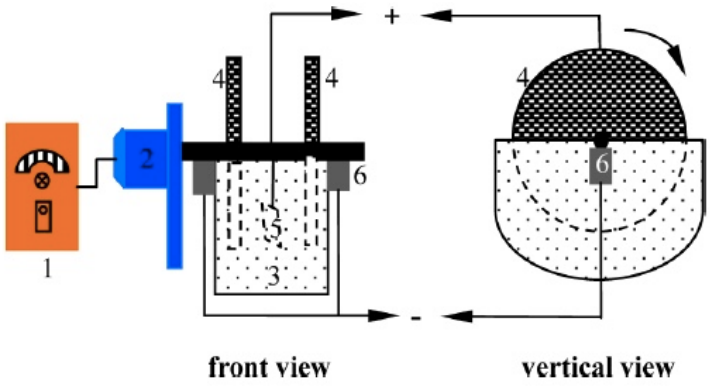

Fig. 6: Scheme of the reactor with two parallel rotating cathodes with 1: speed controller, 2: motor, 3: electrolytic cell, 4: rotating graphite felt disk cathode, 5: Pt anode and 6: carbon brush. Reprinted with permission from ref. (Yu et al. 2014). Copyright 2018, American Chemical Society.

Another two-compartment reactor avoiding the use of oxygen is based on the catalytic generation of H_2O_2 (Eq. (16)) thanks to Pd/C particles. The design of this novel reactor is based on the work reported by Liu et al. (Liu et al. 2007) reporting an electrolytic system able to generate different pH environment without adding any chemicals by using water electrolysis to create O_2 and H_2. A low pH was first used to produce H_2O_2 and then a high pH was employed to neutralize the treated solution before its release to the natural water stream (Liu et al. 2007). The characteristics of the reactor are described in Table 4. The first compartment enables the formation of H_2, O_2 and H^+ by water electrolysis, of H_2O_2 (Eq. (16)) by the catalytic reaction thanks to Pd/C and finally leading to hydroxyl radicals from the Fenton's reaction.

$$H_2 + O_2 \rightarrow H_2O_2 \qquad (16)$$

The second compartment accumulates OH^- which is utilized to neutralize the solution when needed. The main advantage of this system is to avoid chemicals to set the solution pH and to obtain a neutral solution after treatment that can be directed directly to a bioreactor. To illustrate the efficiency of their reactor, the authors compared the production of H_2O_2 and its accumulation to some values reported in the literature and concluded that it could produce more H_2O_2 than carbon fiber or carbon nanotubes cathodes but less than a GDE cathode. This reactor

presents some drawbacks such as a high voltage required due to the electrical resistance of the salt bridge and the high price of the catalyst; however it was shown to be reusable (Yuan et al. 2011). In order to overcome such drawbacks another system was created by Zhang et al. Their system produced O_2 and an acidic medium thanks to the use of a second anode where water is oxidized in O_2 and H^+. This system is promising by avoiding the use of O_2 and expensive material such as Pd (Zhang et al. 2017).

One of the latest study on a new way of providing O_2 was proposed by Perez et al., (Pérez et al. 2016) which consisted of a combination of a flow-through system and a Venturi-based jet aerator (Fig. 7) which allows an efficient production of H_2O_2 and a very good oxygen supply with low energy costs. This system is based on the Venturi effect as in the thinner part of the tube a depression is created which sucks the air into the system leading to a higher liquid velocity which enables to break the oxygen gas bubbles and thus helps their dissolution in water. This system is compared to a similar reactor using GDE cathode and a flow-by cell system. The reactor with Venture-based jet aerator can produce 960 mg H_2O_2 L^{-1} whereas the reactor with GDE cathode produces 700 mg H_2O_2 L^{-1} (Table 4). It is also showed that the efficiency of such aeration is higher than the same reactor without oxygen supply or with air sparging to the jet aerator. The concentration of H_2O_2 obtained at a current density of 75 mA cm^{-3} after 30 min, is very low for no oxygen supply and, 8 and 400 mgH_2O_2 L^{-1} for air sparging and jet aerator, respectively (Pérez et al. 2016).

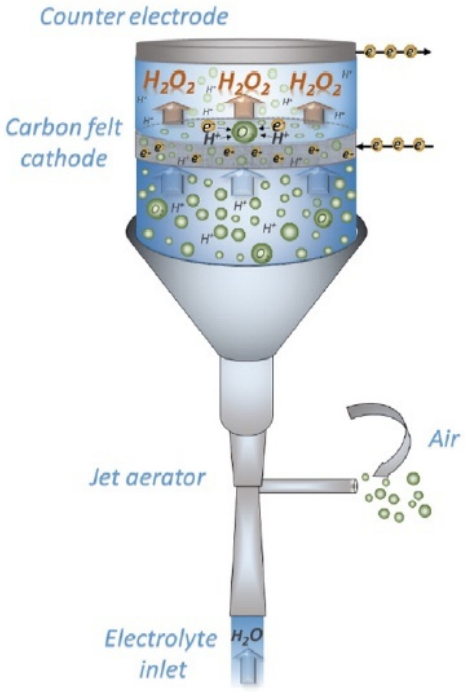

Fig. 7: Scheme of the jet-cell reactor. Reprinted with permission from ref. (Pérez et al. 2016). Copyright 2016, Elsevier.

2.2.4 Micro-fluidic

A different type of reactor was recently used for electro-Fenton processes: microfluidic reactors (Scialdone et al. 2013; Scialdone et al. 2014; Sabatino et al. 2016). It was first used by Scialdone et al. (2013) who studied the capacities of this type of reactor compared to a conventional undivided macro reactor. The two different reactors are described in Table 4. The micro-reactor had the following advantages: i) no use of electrolyte as there is a very small transfer resistance due to the very small interelectrode gap ii) no need of gaseous stream as oxygen is provided by water oxidation at the anode. The use of a graphite cathode provides a cheap and easy to handle system. The chemical oxygen demand (COD) is used as comparison parameter. As can be seen in Table 4, the abatement is more than two times higher for the microfluidic reactor compared to the macro reactor. The better efficiency of the micro reactor is explained by a comparison of H_2O_2 production which is 0.6 mM and 6 mM for the macro and microreactor, respectively. Besides, the calculated current efficiency (CE) values also highlight better performance of the

microreactor (8% for the macro-reactor against f 33% for the micro-reactor at 10 A m^{-2}). This fact can be explained by high solubility of O_2 in micro conditions: it is formed by water oxidation at the anode and dissolved close to its maximum solubility. As the system is small, the O_2 is present at a high concentration at the cathode (both electrodes being close to each other) and leads to the formation of a higher concentration of H_2O_2 (Scialdone et al. 2013). However, the very small size of the channels could be problematic since they can be plugged when real effluents with organic and mineral particles are treated. The group of Scialdone investigated also the performances of the different advanced oxidation processes for a microfluidic treatment and concluded that combining EF and electro-oxidation could significantly be enhanced by microfluidic (Scialdone et al. 2014). The last study on microfluidic system applied to EF dealt with the use of micro-reactor cells in series. The authors concluded that using three EF reactors in series was not useful compared to the use of one micro-reactor as the energy consumption value increases much more than the TOC abatement rate for the reactors in series (Sabatino et al. 2016).

2.2.5 Electrical energy consumption (EC)

In order to compare the cost effectiveness of different systems, their energetical treatment costs were estimated. For instance, the EC were of 0.5 and 20 kWh $(gTOC)^{-1}$ for the system with rotating cathodes (Yu et al. 2014) and for the system with the two cathodes in the center (Yu et al. 2015), respectively. This can suggest that the rotating cathode is a more cost-effective system. Meanwhile this treatment is done in batch so to well-evaluate the real cost of the treatment, experiments in continuous mode are required. In the case of flow-through reactors (Ma et al. 2016; Ren et al. 2016), the EC could be evaluated using a modified formula (Eq. (17)) in order to take into account the continuous mode.

$$\mathrm{EC} = \frac{E \times I}{(TOC_0 - TOC_t) \times D} \qquad (17)$$

with E, the cell voltage in Volt, I the current in Ampere, TOC_0, the initial TOC, TOC(t), the TOC at the steady state, D the flow rate in L h^{-1}.

Using this equation, it was found that the flow-through multiple system (Ren et al. 2016) is consuming 140 kWh (g TOC)$^{-1}$ whereas the flow-through single system (Ma et al. 2016) is consuming 4 kWh (g TOC)$^{-1}$ so 35 times less. Meanwhile an important point has to be underlined, the amount of treated pollutant was of 20 mg per h for the single system against 240 mg per h for the pilot (multiple system). So the gap is reduced by taking this point into account. Nevertheless the consumption is higher in the pilot which can be explained by the scale up of the treatment as the single system is done in 150 mL. However, it is at this step impossible to compare experiments done on the different reactor configurations (different pollutants, different initial TOC configuration, different flow mode, etc.). Much more researches are needed on this aspect and the EC should be estimated for each configuration under comparable conditions and considered as a key parameter.

Table 4: New cell configurations and the conditions of treatment

Name of the reactor	Volume	Distance between electrodes	Number of electrodes	Nature of the electrodes	Type of out streaming	Stirring	Active aeration	Efficiency	References
Trickle bed reactor Fig. 2	Active dimensions of the electrode: 42 cm^3		2 cathodes 1 anode	- Cathode frame for loading graphite chips - Ni cathode plate - Ti/PbO_2 anode	Recirculation flow or continuous mode	By the flow and aeration	Air flow rate of 0.1 m3 h^{-1}	Solution of X-3B 123 mg L^{-1} mineralized at 87% in 3 h at 4,5 V (10 mA cm^{-2})	(Lei et al. 2013)
Plate electrodes Fig. 1	5L (reactor)	1.5 cm	3 cathodes 2 anodes	- Cathodes: Ti coated with stainless steel - Anodes: Ti coated with IrO_2/RuO_2	Batch mode	Yes with a stirrer	No	At 58 mM of H_2O_2, 1.07 mM of Fe^{2+}, 22.5 mM of aniline initial concentration the percentage of removal of aniline were 87.2 and 77.2 % for plate and rod electrodes respectively after 1 h	(Su et al. 2013)
Flow through single system Fig. 4	150 mL (reactor)	0.8 cm	1 anode 1 cathode	Cathode: modified graphite felt Anode: perforated DSA	Continuous	By the flow and aeration	Pumped air at 50 mL min^{-1}	After 120 min of treatment, the TOC removal was 57.9% and 39.1% for the flow-through and flow-by system respectively with 50 mA, a pH of 3, a flow rate of 7 $mLmin^{-1}$, 0.3 mM of Fe^{2+} and an initial concentration of pollutant 50 mg L^{-1}	(Ma et al. 2016)
Flow through multiple system Fig. 5	2 L (reactor)	2 cm	4 anodes 5 cathodes (8 compartments)	Cathode: graphite felt mesh Anode: PbO_2/Ti mesh	Continuous	By the flow and aeration	Aeration rate: 80 mL min^{-1}	TOC removal vertical-flow system: 65%, the parallel-flow system 52% at pH 3, voltage 4.0 V, flow rate 40 mL min^{-1}, Fe^{2+} of 0.4 mM tartrazine.	(Ren et al. 2016)
Micro-fluidic (MF)	Height of the filter press 120 µm (MF)[a] 50 mL for the macro-reactor (MR)[b]	120 µm (MF) 1 cm (MR)	1 anode 1 cathode (MR) and a polytetrafluoroethylene spacer in addition for MF	Anode: Ti/$IrO_2Ta_2O_5$ Cathode: graphite (MF) Cathode: carbon felt (MR)	Flow mode with a single passage (MF) batch mode (MR)	No (MF) Yes, with a magnetic stirrer (MR)	No (MF) Yes, 0.35 L min^{-1} of compressed air (MR)	50 mL of 0.43 mM of Acid Orange 7 and 0.5 mM of $FeSO_4$, 0.035 M of Na_2SO_4 (only MR) at a pH of 3 in 500 min: COD abatement was of 75 % (MF) and of 30 % (MR) under 20 and 100 A/m^2 respectively for MF and MR.	(Scialdone et al. 2013)

Reactor with 2 cathodes in the center	200 mL (reactor)	1.5 cm	2 anodes 2 cathodes	Anode: DSA with IrO_2 Cathode: GDE (carbon black deposited on carbon fiber)	Batch mode	Yes, with a magnetic stirrer and aeration	Yes, air flow rate of 0.5 L min^{-1}	H_2O_2 was 566, 531 and 487 mg L^{-1}, the CE was 85.4, 75.8 and 70.2 % in 180 min and the energy consumption was 8.6, 14.7 and 24 kWh kg^{-1} H_2O_2 for reactor 1, 2 and 3 respectively under 0.05 M of Na_2SO_4, at a current intensity of 100 mA and at a pH of 7.	(Yu et al. 2015)
Venturi-based jet aerator Fig. 7	1 L (reactor)	1.8 cm	1 anode 1 cathode	Anode: Ti with IrO_2 Cathode: Modified Carbon felt	Flow mode	By the flow and aeration	Yes (jet aeration)	At 180 min and under 50 mA cm^{-3}, 0.05 M Na_2SO_4, 960 and 700 mg H_2O_2 dm^{-3} for the Venturi reactor and the flow-by cell with GDE.	(Pérez et al. 2016)
Tubular membrane Fig. 3	71 cm^3 (graphite electrode)	1.0 cm	1 anode 1 cathode	Anode: Ti/IrO_2-Ta_2O_5 Cathode: carbon black-polytetrafluoroethylene modified graphite	Batch mode	By the flow	No	A solution of 85 mg L^{-1} of tricyclazole(TCZ), with 0.05 M of Na_2SO_4, 1.0 mM of Fe^{3+}, pH of 3, membrane flux of 103 L m^{-2} h^{-1} and current density of 10 Am^{-2} have a TCZ degradation of around 80% in 30 min, a production of H_2O_2 of 1586 and 1494 mg m^{-2} h^{-1} and a $^{\cdot}OH$ concentration of 85.2 and 88.3 µM after 20 min with and without aeration respectively.	(Xu et al. 2016)
Tubular membrane (A)	1.5 L (reactor) 5 L whole system	1 cm	1 anode 1 cathode	Anode: Ti/Ti_4O_7 Cathode: graphite-based membrane	Batch mode	By the flow	Yes, air	A solution of 0.1 mM of paracetamol, 0.2 mM of Fe^{2+}, 0.05 M of Na_2SO_4 at pH 3, at 18 ºC, pressure of 2 bars and pumped at 3.0 L min^{-1} was mineralized at a rate of 44% under 100 mA in 8 hours.	(Olvera-vargas et al. 2018)
Two-compartment cell with Pd/C catalyst	2 reactors of 250 mL linked by a salt bridge		Compartment 1: 1 anode and 1 Cathode Compartment 2: 1 cathode	Pt flakes	Batch mode		No	Rhodamine B initial concentration (10 mg L^{-1}) decreased to 1.6 mg L^{-1} after 60 min, with 1 mM of Fe^{2+} using 50 mA for each cathode.	(Yuan et al. 2011)

Reactor with rotating cathodes Fig. 6	100 mL (reactor)	1.5 cm	1 anode 2 cathodes	Anode: Pt or DSA Cathodes: graphite felt	Batch mode	Rotation of the cathodes	No	A solution of 50 mg $L^{-1}$of methyl orange, 0.05 M Na_2SO_4, 0.2 mM Fe^{2+}, pH of 3, after 20 min the pollutant was degraded using 2.37 kWh m^{-3} for the rotating cathodes at 10 rpm and in 30 min using 3 kWh m^{-3} when using the rotation of the cathodes and providing 0.2 L min^{-1} of O_2.	(Yu et al. 2014)

a : MF, micro-fluidic reactor
b : MR, macro reactor

2.2.6 Hints for scale-up

The different parameters stated in this section are also very important in order to scale-up the process to treat real effluent at an industrial scale. The already published research and review articles gave some hints to scale-up the process concerning i) the size and organization of the electrodes, ii) the temperature, iii) the mixing, iv) the out streaming and v) the continuous mode. In order to treat larger volumes, the system must be larger. Regarding the electrodes, two options are possible; either using high surface electrodes or using a stack system. The use of bigger electrodes produces a non-uniform repartition of the current on the electrode surface which reduces the yield. By using stacking electrodes, the cost is higher so a compromise has to be reached. When stacking is used the electrode configuration is also important, the configuration will be either in monopolar or bipolar. In monopolar connection, all anodes and cathodes are directly connected to the power supply which provides a lower operating cost because of lower cell potential. In bipolar connection, only both border electrodes are connected to the current supplier which results in a higher cell voltage but this configuration provides a better depletion of organic pollutants (Martínez-Huitle et al. 2015). The parameter mixing is directly related to the mass transport and mass transfer phenomena. It can become a real problem during the scale-up and can decrease significantly the efficiency of the process. Martínez-Huitle et al. (2015) highlighted this fact, identifying a real lack of mass transport in big-sized mixed tank reactor compared to flow reactor. For example, dos Santos et al. (dos Santos et al. 2014) compared COD removal at a mixed cell and at a flow-pass cell, at 25 °C, with a current of 15 mA cm^{-2} and 20 mA cm^{-2} obtaining 50.3% and 76.2% of COD removal with a BDD anode for the mixed cell and flow cell, respectively. To improve the mass transport of mixed tank reactors, a recirculation can be added; this will not only improve mass transport efficiency but will also drag gas bubbles which otherwise would accumulate increasing the Ohmic resistance of the bulk and finally rising the energy consumption (Martínez-Huitle et al.

2015). The type of flow is also a key point for the scaling-up as it is directly related to the efficiency of the process, as seen before, the flow-through reactor provides better performance than the flow-by reactor. Radjenovic and Sedlak (2015) proposed the combination of this type of reactor with three-dimensional electrodes in order to obtain the better cell system for a large scale treatment. Computational fluid dynamics are recommended to optimize the flow system, especially at the entrance and at the exit of the cell where turbulences often happen. Nonetheless, only a few numbers of studies were reported on this tool (Frías-Ferrer et al. 2011; Cruz-Díaz et al. 2012; Rivero et al. 2012; Vázquez et al. 2013). Temperature belongs to the influent parameters in the reactor design, but it is often not studied as at bench scale there is no need to cool the system. However, at large scale applications, this parameter has to be taken into account and a cooling system can be involved.

For industrial applications level, the continuous mode has to be reached to enable the treatment of large amounts of wastewater. The stability of the electrodes is to be considered as this can directly pollute the solution or can decrease the efficiency of the process. Some studies evaluated the steady efficiency through several cycles (Rosales et al. 2012b; Bocos et al. 2016c; Plakas et al. 2016) or by inspecting the electrode surface thanks to Scanning Electron Microscopy (SEM) after the treatment (Iglesias et al. 2013). Most of the works describing a continuous electro-Fenton process are given in Table 5. Most of the experiments summarized in this table are carried out in heterogeneous system which avoids the formation of sludge and requires of a filtration post-treatment to eliminate or recover the catalyst (Brillas et al. 2009). Iron alginate gel beads are often used as solid catalysts aiming at degrading for example 81% of Lissamine Green B (Iglesias et al. 2013), 90% of Imidacloprid (Iglesias et al. 2014) and 99% of Azure B (Rosales et al. 2012b) (Table 5). The economic aspect of these reactors is often left aside, only a few studies considered it. With 20 A, 25.5 L of industrial effluent is degraded consuming 0.14 kWh $(g\ TOC)^{-1}$ (Casado and Fornaguera 2008), with 5 V, 0.15 L of Lissamine

Green B is partly mineralized (COD removal of 86%) costing 15.75 kWh (kg dye)$^{-1}$ (Bocos et al. 2016c), with 3.5 V, 3 L of Rhodamine B is treated reaching 98% of dye degradation consuming 50 Wh (g dye)$^{-1}$ (Nidheesh and Gandhimathi 2015) and with 0.14 A, 1 L of C.I. Acid red and blue are degraded using 0.024 kWh (g COD)$^{-1}$ (Pajootan et al. 2014) (Table 5). However, only a few articles reported the continuous mode; more work has to be done and especially treatments with real wastewaters need to be studied. Industrial water from a chemical firm and a pulp and paper company (Casado and Fornaguera 2008), landfill leachate (Zhang et al. 2012) and real wastewater from Mexico (Durán Moreno et al. 2004) are successfully degraded by EF in continuous mode. Thus the TOC removal is 80 and 60% for the effluents from chemical firm and the pulp and paper company, respectively, the COD removal was 60% for the landfill and 92.3% discoloration is obtained for the wastewater from Mexico (Table 5). In synthetic effluents, the concentration of pollutants is indeed higher than in real wastewaters, the interaction of different pollutants together and the effect of mineral ions as well as the effect of natural substances such as humic acids are not yet evaluated.

Table 5: EF applications by continuous reactors

EF system reactor configuration	Pollutants	Solution	Current / Voltage	Residence time	TOC removal	Pollutant degradation rate	COD removal	Energy consumption	Ref
Cylindrical plexiglas reactor, two electrodes placed at the center of the reactor separated by 10 mm Anode: graphite Cathode: modified graphite electrode using multi-walled carbon nanotubes with cationic surfactant	C.I. Acid Red 14 (a) C.I. Acid Blue 92 (b)	0.05 mM $Fe^{3+,}$ flow rate: 0.33 L h^{-1}*, pH: 3*, effective volume 1 L, aeration, 10 mg L^{-1}dye, NaCl: 1 g L^{-1}	0.14 A			91.22 % (a) 93.45% (b)	86.78% in 60 min	0.024 kWh $(gCOD)^{-1}$ at 1 h	(Pajootan et al. 2014)
System composed of 3 pairs of anode/cathode disc electrodes of 62 mm diameter Solution flows through the different porous electrodes Anodes: Carbon felt activated by ethanol treatment Cathodes: Carbon felt treated first by ethanol then by mixed valence iron $FeCl_2$ 4 H_20 and $FeCl_3$ 6 H_2O (0.4 mg Fe m^{-2} of cathode)	Diclofenac	Effective volume 49 mL, flow rate: 10 23°C, tap water, ~0.625 mg L^{-1} diclofenac, neutral pH, no addition of O_2	2 V* for each pair of cathode/anode	14.6 s	35%	85%			(Plakas et al. 2016)
Cell with two electrodes of 11 cm^2 separated by 6 cm Anode: BBD Cathode: graphite sheet	Imadacloprid	Air bubbling at 1 L min^{-1}, working volume 0.15 L, 100 mg L^{-1} 4.27g* Fe alginate gel beads (0.05 M Fe^{3+}), pH = 2*	5 V	4 h		90%			(Iglesias et al. 2014)

Undivided cell with two square electrodes of 100 cm^2 separated by 5 mm, flow-by effluent + a reservoir Anode: mesh of platinized titanium (a) or DSA (b) Cathode: thick carbon loaded with carbon black with PTFE	Industrial effluent from a chemical firm 37250 mg L^{-1} (a) pulp and paper company 328 mg L^{-1} (b)	Working volume 50 mL, O_2 diffusion through the cathode, 40°C, recirculation (ensure the good mass transfer) flow 900 Lh^{-1}, 0.05 M Na_2SO_4, 1 mM $FeSO_4$, pH = 3.2 (a), 3 (b), feeding flow calculated to obtain a TOC removal in steady state: 1.2 mL min^{-1} (a) 1 L h^{-1} (b)	20 A		80% (a) 60% (b)			Steady state 0.14 kWh $(gTOC)^{-1}$ (a) 0.38 kWh $(gTOC)^{-1}$ (b)	(Casado and Fornaguera 2008)
Stirred tank reactor of 12 cm * 10 cm * 16.5 cm with 5 electrodes of 15 cm * 10 cm vertical and with an alternating of anode/cathode separated by 2 cm* 2 Anodes: Ti/RuO_2-IrO_2-SnO_2-TiO_2 mesh 3 Cathodes: Ti mesh	Landfill leachate with pH = 8 (COD 2720 mg L^{-1})	800 mL working volume, magnetic stirring, initial pH = 3*, H_2O_2/Fe^{2+} molar ratio of 6*, H_2O_2 = 0.170 M*	1 A	40 min*			60% in 60 min		(Zhang et al. 2012)
Fluidized bed reactor composed of a glass column with intern dimeter 2 cm height 16 cm Anode: graphite sheet (14*0.7 cm^2) Cathode: Ni-Foam half coated with iron-chitosan (14 cm*0.7 cm) separated by 1 cm	Lissamine Green B	Initial pH = 2, mixed by continuous air flow at 0.15 vvm[a], 100 mg L^{-1} dye, 0.15 L working volume, 0.01 M Na_2SO_4	5 V	45 min and 90 min	75%	> 95%	86%	15.75 kWh kg^{-1} dye	(Bocos et al. 2016c)
Cylindrical glass reactor with two electrodes of 84.16 cm^2 separated by 10 cm, flow-by effluent Anode: graphite bar Cathode: graphite bar	Lissamine Green B (a) (30 mg L^{-1}) Reactive Black 5 (b) (100 mg L^{-1})	Catalyst 115 g Fe alginate gel beads made of Sodium alginate, $Bacl_2$, $Fe_2(SO_4)_3$ (2.68 mM iron), working volume 1.5 L, air bubbling near the cathode at 1.5 L min^{-1}, pH= 2*, 22°C	3 V*	6 h (a) 12.5 h (b)		81% (a) 87% (b)			(Iglesias et al. 2013)

Cylindrical glass reactor with two electrodes of 15 cm^2 separated by 4.3 cm, flow-by effluent Anode: graphite sheet Cathode: graphite sheet	Lissamine Green B (a) (8.5 mg L^{-1}) Azure B (b) (4.83 mg L^{-1})	Catalyst: 8.69 g Fe alginate gel beads made of Sodium alginate, $BaCl_2$, $FeCl_3$ (0.05 M Fe^{3+}), working volume 0.15 L, air bubbling near the cathode at 1 L min^{-1}, pH = 2*	14.19 V	30 min	93% (a) 89% (b)	99%			(Rosales et al. 2012a)
Bubble reactor made of a cylindrical glass with two bar electrodes Cathode: Graphite, 100 mm high and 6.35 mm diameter 30 mm of the bottom of the reactor Anode: Graphite 100 mm high and 6.35 mm diameter, 270 mm of the bottom of the reactor	Lissamine Green B (LGB), Methyl Orange (MO), Reactive Black 5 (RB5) Fuchsin Acid (FA)	8.5 mgL^{-1} (LGB), 1.5 mg L^{-1} (MO), 70 mgL^{-1} (RB5), 15 mg L^{-1} (FA), 0.04 M Na_2SO_4, 0.675 L working volume, bubbling compressed air at 1 L min^{-1}, pH = 2, 600 mg L^{-1} of iron dosage	15 V	21 h*	47%	43% (discoloration)			(Rosales et al. 2009)
An EF cell of 2 L with a hollow cylindrical iron anode (effective surface 289.4 cm^2), cylindrical solid graphite cathode (effective surface 35.8 cm^2) (a) This process follows by two sedimentations and a sand filtration (b) Air supplied at the bottom of the cell	Real wastewater from Mexico	Raw solution COD: 328.2 mg L^{-1}, turbidity: 39.3 NTU; pH adjusted to 3.5	1 A*	1 h*	-	92.3% discoloration	7.4% (2h) (a) 74.8% (b)	-	(Durán Moreno et al. 2004)
Bubble glass column reactor of diameter 10.4 cm and height 40 cm with two graphite cathodes of 100 cm^2 and one graphite anode in the middle of 80 cm^2. Air purged in the solution.	Rhodamine B (50 mg L^{-1})	3 L of electrolyte at 10 mL min^{-1}* composed of catalyst: $FeCl_3$ at 5* mg L^{-1} and at pH: 3*.	3.5 V*	8 h	-	98% dye removal	-	50 Wh $(g\ dye)^{-1}$ at 8 h	(Nidheesh and Gandhimathi 2015)

*: Best value for the parameter concerned

a: Vvm, volume of air under standard conditions per volume of liquid per minute

3. EF applied to the removal of pharmaceuticals from water

3.1 EF applied to β-blockers

Table 6 gives an overview of EF applied to β-blockers for the last few years. Only three β-blockers have been studied, atenolol, metoprolol and propranolol. They are always degraded in synthetic aqueous solution, with only one study evaluating the synergetic effect of using a solution composed of several β-blockers (Sirés et al. 2010). The concentration of the pollutants ranges from 26 mg L^{-1} to 150 mg L^{-1}. Most of these molecules require between 5 and 30 min to be completely oxidized but the mineralization of their solutions takes several hours of electrolysis. This difference of treatment time can be explained by involving several steps in the mineralization procedure while the oxidative degradation occurs in one step. Another reason can be the formation of intermediates products more difficult to oxidize than the initial pollutant, in the latter case.

The mineralization current efficiency (MCE) reported for these experiments is depending on the treatment time and is always less than 50%; it is partly due to side reactions occurring during the process. A link between the chemical structure and the apparent kinetic rate constant of degradation can be underlined thanks to Isarain-Chávez et al. (2011c) who performed the degradation of three beta-blockers under the same conditions. Atenolol has the higher degradation rate constant which is about 10 times greater than the value reported for metoprolol and propranolol. This difference can be explained by the chemical structure of atenolol containing an amide group which is more electrophilic than the groups contained in metoprolol and propranolol. One of the best pseudo first order kinetic constant is obtained for atenolol degradation with a value of 9.5 10^{-3} s^{-1} whereas the other constants are around 10^{-3} s^{-1} (Fig. 8). In spite of this high rate constant value, the electrical energy consumption is significantly higher (1.08 kWh $(g\ TOC)^{-1}$) than other b-blockers having a value of around 0.30 kWh $(g\ TOC)^{-1}$. This

can be related to the formation of hardly oxidizable intermediates in the former case. A compromise should then be reached between an efficient degradation and a cost-effective operating process. More studies taking into account the cost of the process are required in order to better evaluate the feasibility of this process.

Table 6: EF applied to β-blockers

Products	Electrodes Anode, Cathode, surface and O_2 feeding	Pollutant initial concentration	Solution	Current Voltage	Pollutant removing	Degradation efficiency	Pseudo first order kinetic constant (pollutant degradation)	MCE, Energy consumption	Ref
Atenolol	BDD/GDE (1) Pt/GDE - Pt/Carbon felt (2) BDD/GDE-BDD/Carbon felt (3) 3 cm^2 for each electrode *GDE fed with air at 20 mL/min*	158 mg L^{-1}	Batch, 0.05 M NA_2SO_4, pH = 3, Vsol = 100 mL, 35°C, magnetic bar for stirring (800 rpm), 0.5 mM Fe^{2+}	50 mA (1) 50 -12 mA (2) 50 -12 mA (3)	Total removal in: > 60 min (1) 25 min (2) 30 min (3)	in 360 min: 77% (1) 81% (2) 90% (3)	0.39 10^{-3} s^{-1} (1) 2.03 10^{-3} s^{-1} (2) 1.56 10^{-3} s^{-1} (3)	Between: 18 and 50% Δ (1) 22 and 35% Δ (2) 18 and 50% Δ (3)	(Isarain-Chávez et al. 2010a)
Atenolol	Platinized titanium (3*15 cm^2) Graphite* (6 cm^2) *With bubbling compressed air at 1L/min*	45 mg L^{-1}	Batch, 0.05* M NA_2SO_4, pH = 3*, Vsol = 250 mL, 20°C, magnetic bar for stirring (400 rpm), 5* mM Fe^{2+}	0.3* A	-	in 240 min, COD removal: 87%	1.58 10^{-4} s^{-1} (for COD removal)	After 4 h: 22.33% Δ 0.194 kWh $(kgCOD)^{-1}$	(El-Hanafi et al. 2014)
Atenolol	Pt mesh (4.5 cm^2) Carbon felt (14*5 cm^2) *With bubbling compressed air at 1L min^{-1}*	40 mg L^{-1}	Batch, 0.05 M NA_2SO_4, pH = 3, Vsol = 220 mL, room temperature, magnetic bar for stirring, 0.2 mM Fe^{3+}	300 mA	Total removal in 6 min	in 360 min 97%	9.5 10^{-3} s^{-1}	Between: 3 and 15% Δ 1.08 kWh $(gTOC)^{-1}$	(Sirés et al. 2010)
Atenolol		40 mg L^{-1}			-	in 480 min 100%	-	0.42 kWh $(gTOC)^{-1}$	
Metoprolol		52 mg L^{-1}							
Propranolol		52 mg L^{-1}							

Metoprolol	BDD onto Si / ADE	0.246 mM 66 mg L^{-1}	Batch, 0.05 M NA_2SO_4, pH = 3, Vsol = 100 mL, magnetic bar for stirring (800 rpm), 0.5 mM* Fe^{2+} 0.1 mM Cu^{2+}, 35 °C	120 mA	Total removal in 31 min	in 6h 85%	2.0 10^{-3} s^{-1}	Between 15 and 25% Δ	(Isarain-Chávez et al. 2011b)
	BDD onto Si /ADE – Pt/Carbon felt each electrode has a surface of 3 cm^2 *ADE is fed with air at 20 mL/min*			120 - 12 mA	17 min	95%	3.7 10^{-3} s^{-1}	15 and 47% Δ	
Atenolol (1) Metoprolol (2) Propranolol (3)	BDD/ADE	100 mg L^{-1}TOC for each compound	Batch recirculation, 0.1 M NA_2SO_4, pH = 3, Vsol = 10 L, 35°C, 0.5 mM Fe^{2+}, Flow rate 250 L h^{-1}	3 A	-	in 360 min: (1) 54% (2) 54% (3) 56%	(1) 2.24 10^{-3} s^{-1} (2) 0.22 10^{-3} s^{-1} (3) 0.13 10^{-3} s^{-1}	Between: (1) 10 and 20%, 0.412 kWh $(gTOC)^{-1}$ Δ (2) 5 and 15%, 0.421 kWh $(gTOC)^{-1}$ Δ (3) 20 and 40%, 0.405 kWh $(gTOC)^{-1}$ Δ	(Isarain-Chávez et al. 2011c)
	Pt/ADE-Pt/CF			3-0.4 A	-	(1) 26% (2) 22% (3) 35%	(1) 0.36 10^{-3} s^{-1} (2) 0.18 10^{-3} s^{-1} (3) 0.15 10^{-3} s^{-1}	(1) 20 and 45%, 0.280 kWh $(gTOC)^{-1}$ Δ (2) 10 and 40%, 0.291 kWh $(gTOC)^{-1}$ Δ (3) 30 and 50%, 0.224 kWh $(gTOC)^{-1}$ Δ	
	BDD/ADE-Pt/CF Each electrode: 10cm*10cm *Compressed air flow rate: 150 mL/min*			3-0.4 A	-	(1) 61% (2) 66% (3) 65%	(1) 2.43 10^{-3} s^{-1} (2) 0.74 10^{-3} s^{-1} (3) 0.91 10^{-3} s^{-1}	(1) 20 and 45%, 0.386 kWh $(gTOC)^{-1}$ Δ (2) 5 and 30%, 0.359 kWh $(gTOC)^{-1}$ Δ (3) 20 and 35%, 0.354 kWh $(gTOC)^{-1}$ Δ	

Propranolol	BDD onto Si /Carbon-PTFE 3 cm^2 each electrode *fed with air at 20mL min^{-1}*	154 mg L^{-1}	Batch, 0.05 M NA_2SO_4, pH = 3, Vsol = 100 mL, 35°C, magnetic bar for stirring (800 rpm), 0.5 mM Fe^{2+}	10 mA cm^{-2}	-	78 % in 420 min	-	Between 20 and 78% Δ	(Isarain-Chávez et al. 2010b)
				40 mA cm^{-2}	Total removal in 29 min	85% in 420 min		10 and 22% Δ	
				80 mA cm^{-2}	-	91 % in 420 min		2 and 10% Δ	
Propranolol	monopolar connection: Pt/ADE -Pt/CF of 3 cm^2 each, *ADE fed with 20 mL min^{-1} air*	154 mg L^{-1}	Batch, 0.05 M NA_2SO_4, pH = 3, Vsol = 100 mL, 35 °C, magnetic bar for stirring (800 rpm), 0.5 mM Fe^{2+}	120-12 mA	Total removal in 12 min	70 % in 420 min	4.0 10^{-3} s^{-1}	8 and 32 % Δ	(Isarain-Chávez et al. 2011a)
Propranolol	Ti_4O_7 (4 * 6 cm^2) Carbon-felt (14 * 5 cm^2) *Bubbling of compressed air at 1 L min^{-1}*	26 mg L^{-1}	Batch, Vsol = 230 mL, 0.05 M NA_2SO_4, pH = 3, 23 °C, magnetic bar for stirring, 0.1 mM Fe^{2+}	120 mA	Total removal in 10 min	96 % in 480 min	12.9 10^{-3} s^{-1}	6 and 18 % Δ	(Ganiyu et al. 2017)

*: best value for the parameter
(1), (2), (3): letters to identify different conditions of treatment
Δ: MCE between x% and y%: x and y are the two extremum values during the EF treatment

3.2 EF applied to anti-inflammatories and analgesics

Seven anti-inflammatories and analgesics are studied by the EF process. Table 7 gives some details about these experiments and their treatment efficiency. The efficiency of the treatment measured by the TOC removal degree varies significantly as it was 57% in 8 h for salicylic acid with graphite plates as electrodes whereas it reached 95% in 1.5 h for ketoprofen using BDD and carbon felt as anode and cathode, respectively. Concerning the pseudo first order kinetics, the apparent rate constant (k_{app}) values range from 10^{-4} to 10^{-3} s^{-1} (Fig. 8). Finally, as for beta-blockers, the best way to identify the usefulness of the process is the energetic consumption which is available for only five studies, the more cost-effective among them appears to be dipyrone with the DSA-Cl_2/GDE system with 0.049 kWh (g TOC)$^{-1}$ and with a k_{app} of 1.2 10^{-3} s^{-1} aiming at a TOC removal of 63% in 90 min.

Table 7: EF applied to treatment of anti-inflammatories and analgesics

Products	Electrodes Anode, Cathode, surface and *O_2 feeding*	Pollutant initial concentration	Solution	Current Voltage	Pollutant degradation	TOC removal	Pseudo first order kinetic constant (pollutant degradation)	MCE, Energy consumption	Ref
Diclofenac	BDD onto Nb (64 cm^2) Stainless steel (64 cm^2*) with compressed air bubbled* separated by 2 cm	50 mg L^{-1} 100 mg L^{-1}	Batch recirculation, 0.05 M Na_2SO_4, pH=3, Vsol = 4L, room temperature, 0.5 mM Fe^{2+}, flow rate 2 L min^{-1}	1.56 mA cm^{-2} 6.25 mA cm^{-2} 1.56 mA cm^{-2} 6.25 mA cm^{-2}	-	in 180 min: 62% 84% 69% 79%	-	0.27 kWh $(gTOC)^{-1}$ 0.78 kWh $(gTOC)^{-1}$ 0.41 kWh $(gTOC)^{-1}$ 0.68 kWh $(gTOC)^{-1}$	(García-Montoya et al. 2015)
Dipyrone	DSA-Cl_2 20 cm^2 GDE containing CoPc and PTFE (20 cm^2) *fed with O_2* pseudo reference electrode Pt//Ag/AgCl/KCl	50 mg L^{-1}	Batch recirculation, 0.1 M H_2SO_4 0.1 M K_2SO_4, pH = 3, Vsol = 1.5 L, 20°C, 1 mM Fe^{2+}, flow rate 50 L h^{-1}	-2.1 V	90 % removal in 30 min	in 90 min 62.8 %	1.2 10^{-3} s^{-1}	0.049 kWh $(gTOC)^{-1}$	(Barros et al. 2014a)
Dipyrone	DSA-Cl_2 20 cm^2 GDE containing CoPc and PTFE (20 cm^2) *fed with O_2* pseudo reference electrode Pt//Ag/AgCl/KCl	50 mg L^{-1}	Batch, 0.1 M H_2SO_4 0.1 M K_2SO_4, pH = 3, Vsol = 400 mL, 1 mM Fe^{2+}	-0.9* V	96 % removal in 90 min	in 90 min 54.4%	6.7 10^{-3} s^{-1}	0.27 kWh $(gTOC)^{-1}$	(Barros et al. 2014b)
Ibuprofen	BDD onto Si (3cm^2) Carbon-PTFE (3cm^2) *fed with 20mL min^{-1} of O_2*	41 mg L^{-1}	Batch, 0.05 M NA_2SO_4, pH = 3, Vsol = 100 mL, 25°C, magnetic bar for stirring, 0.5 mM Fe^{2+}	33.3 mA cm^{-2}	Total removal of Ibuprofen 30 min	81 % (DOC removal) in 6h	4.9 10^{-4} s^{-1}	Between 5 and 8% Δ	(Skoumal et al. 2009)

Ibuprofen	BDD onto Nb (25cm^2) 3D Carbon felt (14*5 cm^2) *with bubbling compressed air at 1L min^{-1}*	41 mg L^{-1}	Batch, 20% acetonitrile, 0.05 M NA_2SO_4, pH = 3, Vsol = 230 mL, 23°C, magnetic bar for stirring, 0.2 mM Fe^{3+}	50 mA 500 mA	Total removal in 240 min 50 min	- -	0.3 10^{-3} s^{-1} 1.23 10^{-3} s^{-1}	- -	(Loaiza-Ambuludi et al. 2013)
Ketoprofen	BDD onto Nb (24 cm^2) Carbon felt (18*6 cm^2) *with air at 1L min^{-1}*	50 mg L^{-1}	Batch, 0.05 M NA_2SO_4 in tap water pH = 3, Vsol = 250 mL, magnetic bar for stirring (800 rpm), 0.1 mM* Fe^{2+}	100 mA 750 mA 2000 mA	Total removal in 40min 20 min 15 min	in 1h30, 60 % 95% 95%	2.3 10^{-3} s^{-1} 3.8 10^{-3} s^{-1} 6.4 10^{-3} s^{-1}	Between 15 and 50% Δ 4 and 15 % Δ 4 and 9% Δ	(Feng et al. 2014)
Naproxen	- DSA-O_2 (IrO_2) Carbon-PTFE - BDD Carbon-PTFE Each electrode 20 cm^2 *fed with atmospheric air at an overpressure of 8.6 kPa* separated by 1.2 cm	40 mg L^{-1}	Batch recirculation, 0.05 M $NaClO_4$, pH = 3, Vsol = 2.5 L, 35 °C, 0.5 mM Fe^{2+}, flow rate 180 L h^{-1}	50 mA cm^{-2}	- Total removal in 12 min	in 6h, 50 % 45%	- 5.2 10^{-3} s^{-1}	Between 5 and 27 % Δ, 1.2 kWh (gTOC)$^{-1}$ (average) 5 and 35 % Δ, 2.25 kWh (gTOC)$^{-1}$ (average)	(Coria et al. 2016)
Paracetamol	Pt (3 cm^2) Oxygen diffusion cathode (3 cm^2)	157 mg L^{-1}	Batch, 0.05 M NA_2SO_4 pH = 3, Vsol = 100 mL, magnetic bar for stirring ,1 mM* Fe^{2+} + 0.25 mM Cu^{2+}, 35°C	100 mA	Total removal in 24 min	in 360 min 70%	-	-	(Sirés et al. 2004)

Paracetamol	Pt foils Porous carbon prepared with a N_2 O_2 gas flow (2 cm^2) separated by 3 cm *O_2 bubbling*	15 mg L^{-1}	Batch, 0.05 M NA_2SO_4, pH = 3, Vsol = 30 mL, magnetic bar for stirring (800 rpm), 0.2 mM* Fe^{2+}	-20 mA cm^{-2}	-	in 10 h 95%	-	-	(Le et al. 2016a)
Salicylic acid	BDD onto Si (3 cm^2) Carbon PTFE (3 cm^2) *fed with 12mL min^{-1} O_2*	164 mg L^{-1}	Batch, 0.05 M NA_2SO_4, pH = 3, Vsol = 100 mL, 35°C, 0.5 mM Fe^{2+}, magnetic bar for stirring	33 mA cm^{-2} 100 mA cm^{-2} (17.1V cell) 150 mA cm^{-2} (21V cell)	Total removal in 30 min - -	in 180 min 73% 85% 90%	$1.8*10^{-3}$ s^{-1} - -	at 180 min: 22% 8.4%, 308 kWh m^{-3} 6.0%, 472 kWh m^{-3}	(Guinea et al. 2008)
Salicylic acid	Graphite plates of 25 cm^2 separated by 3 cm, *bubbling compressed air near the cathode*	100 mg L^{-1}	Batch, 5 mg L^{-1}* $NaHCO_3$, pH = 2.5* , Vsol = 750 mL, 20 mg L^{-1}* Fe^{2+}	8V	75% removal in 8h	in 8h 57%	-	-	(George et al. 2014)

*: best value for the parameter (average): the average between the maximum and minimum value for the energy consumption.
Δ: MCE between x% and y%: x and y are the two extremum values during the EF treatment

3.3 EF applied to antibiotics and diuretics

More studies were done on antibiotics as they are a large group of pharmaceuticals widely used all over the world. The k_{app} values are in the same range for beta-blockers and anti-inflammatories which demonstrates the ability of this process to treat pharmaceuticals (Fig. 8). The better value (26 10^{-3} s^{-1}) is obtained for flumequine degradation using a BDD/carbon felt cell. 17 different pharmaceuticals were degraded through an EF process (Table 8). The treatment time for complete oxidative degradation of pollutant is quite different from one system to another; it can be of 4.5 h for cefalexin or of 3 min for flumequine; it is around 30 min for most cases. The TOC or the DOC (dissolved organic carbon) removal is around 6 h for most of the experiments. Concerning the MCE, for almost all the experiments the values are around 15%, only in one study, this value reached up to 55% for chloramphenicol, due probably to the very high initial pollutant concentration (245 mg L^{-1}). The energy consumption is also in the same range as for the other pharmaceuticals being around 1 kWh (g TOC)$^{-1}$ or 1 kWh (g DOC)$^{-1}$.

To sum up, the EF is a clearly efficient process able to degrade lots of different groups of pharmaceuticals. Some points have yet to be studied more deeply. First in order to apply this process at the industrial scale, pilot studies are required to treat issues that have been explained previously like, for instance, mass transfer. Our group is actually working on a pilot in order to evaluate the scaling-up of the EF. To prepare the transition to industrial scale, the EF needs to be studied in continuous mode; this has only been done a few times (Table 5). The concentration of the pollutant ranges from around 50 mg L^{-1} to 150 mg L^{-1} which is significantly higher than the concentration in wastewater as discussed in the introduction section. In order to simulate the efficiency of the process better and in a more similar context of real wastewater treatment, smaller concentrations should be involved or real effluent should be used which has only been done a few times (Durán Moreno et al. 2004; Casado and Fornaguera 2008). Indeed, in a real

effluent, due to the presence of several pharmaceuticals, some interactions between them can slow down the process. As the cost remains generally high for mineralization process, combining this process with a biological treatment could decrease significantly the operating costs. Therefore the cost of the process is to be considered more deeply. The bio-treatment being more cost-effective than the EF, a comparison of their efficiency was done by analyzing their apparent kinetic constant for the same pharmaceuticals (Fig. 8). For all the data given in Fig. 8, the EF is significantly more efficient. However, the scale of the process is not the same as for the bio-treatment an industrial scale is used whereas for the electro-Fenton the volume is around 300 mL. But, for the biological degradation, the limiting parameter is the degradation kinetic, this implies that the scale-up is not impacting too much on the process; this enables the comparison between both processes. Because of this difference of efficiency, the solution to degrade efficiently and at a lower cost can be to combine both processes.

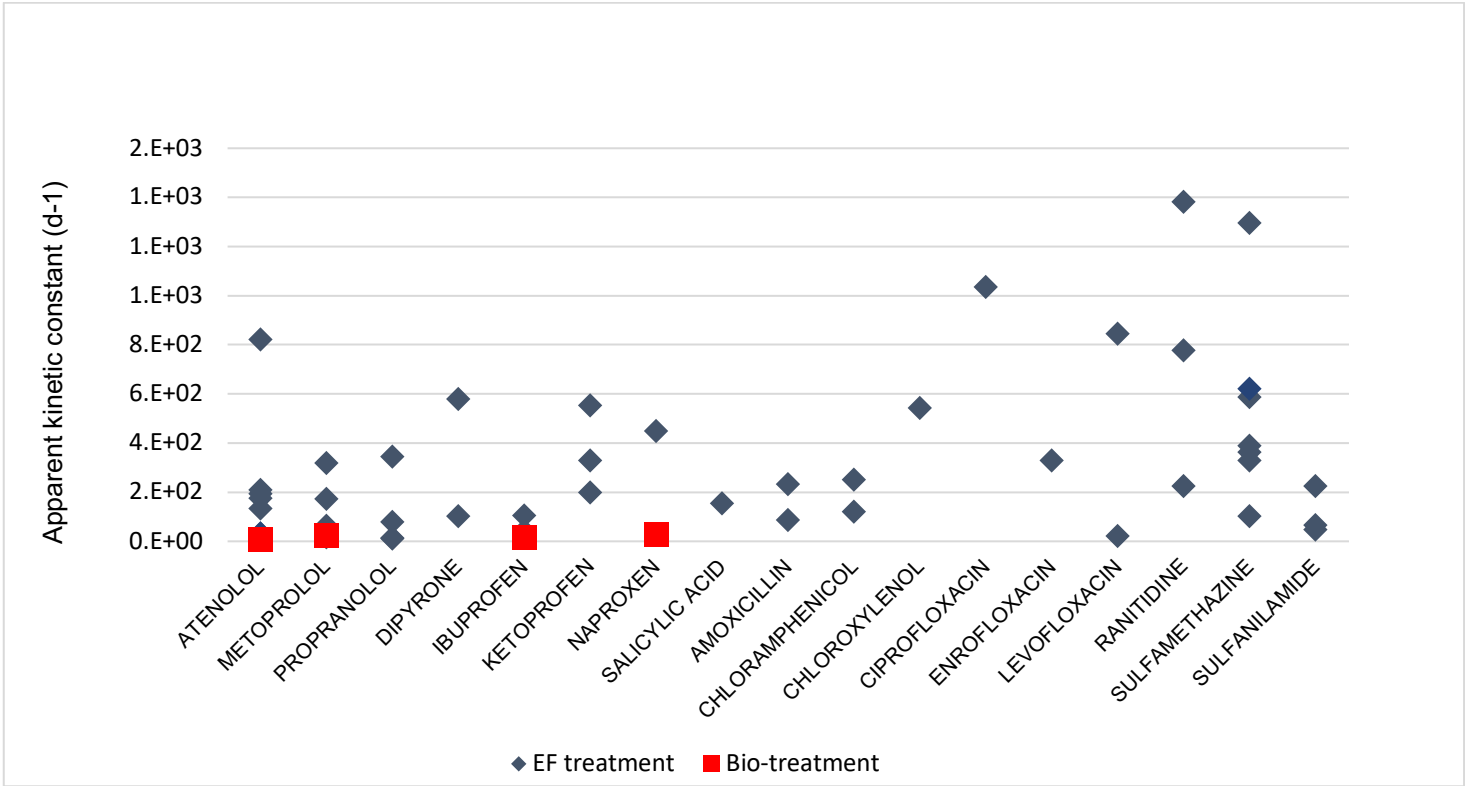

Fig. 8: Apparent kinetic constants for different pharmaceuticals treated by EF process or by a bio-treatment

Table 8: EF applied to antibiotics and diuretics

Products	Electrodes Anode, Cathode, surface and O_2 feeding	Pollutant initial concentration	Solution	Current Voltage	Pollutant degradation	TOC removal	Pseudo first order kinetic constant (pollutant degradation)	MCE, Energy consumption	Ref
Amoxicillin	BDD (4.5cm^2) Carbon felt (77 cm^2) *With compressed air*	48 mg L^{-1}	Batch, 0.05 M NA_2SO_4, pH = 3, Vsol = 250 mL, magnetic bar for stirring, 0.2 mM Fe^{2+}	60 mA 300 mA	Total removal in 20 min 10 min	In 10 h: 80 % > 90 %	2.7 10^{-3} s^{-1} 1.0 10^{-3} s^{-1}	Between 10 and 30 % Δ 3 and 11 % Δ	(Panizza et al. 2014)
Amoxicillin	Ti_4O_7 (4 * 6 cm^2) Carbon-felt (14 * 5 cm^2) *Bubbling of compressed air at 1 L min^{-1}*	20 mg L^{-1}	Batch, Vsol = 230 mL, 0.05 M NA_2SO_4, pH = 3, 23 °C, magnetic bar for stirring, 0.1 mM Fe^{2+}	120 mA	Total removal in 5 min	In 6h 90 %	10.3 10^{-3} s^{-1}	Between 10 and 25 % Δ 0.2 and 0.7 kWh gTOC^{-1}	(Oturan et al. 2017)
Cefalexin	RuO_2/Ti mesh 54 cm^2 Activated carbon felt (54 cm^2) *with pure oxygen at 0.1L min^{-1}*	200 mg L^{-1}*	Batch, 0.05 M NA_2SO_4, pH = 3*, Vsol = 500 mL, room temperature, magnetic bar for stirring, 1 mM* Fe^{2+}	6.66* mA cm^{-2}	Total removal in 4.5 h	In 8 h 60%	-	Between 7.5 and 22% Δ	(Ledezma Estrada et al. 2012)
Chlorophene	BDD onto Si (3 cm^2) Carbon-PTFE (3 cm^2) *fed with 20mL min^{-1} of O_2* (1) BDD onto Si (3 cm^2) Carbon felt (70 cm^2) *bubbling compressed air 1 L min^{-1}* (2)	84 mg L^{-1}	Batch, 0.05 M NA_2SO_4, pH = 3, Vsol = 200 mL, 20°C, magnetic bar for stirring, 4 mM Fe^{3+} (1) or 0.2 mM Fe^{3+} (2)	60 mA 300 mA	Total removal in 90 min (1)	In 6 h 67 % (1) (1) 25% (2) 100%	-	Between 7 and 27% (1) Δ 4 and 12% (1) 4 and 22% (2) Δ	(Sirés et al. 2007a)

Chloramphenicol	BDD (3 cm^2) Carbon-PTFE (3 cm^2) *fed with 300 mL/min of air (1)* Pt (3 cm^2) air diffusion filter press (2)	245 mg L^{-1}	0.05 M NA_2SO_4, pH = 3, Vsol = 100 mL (1), 35°C, magnetic bar for stirring (800 rpm), 0.5 mM Fe^{2+} (2) 10 L at a flow rate of 200L h^{-1}	33.3 mA cm^{-2} (1) 100 mA cm^{-2} (2)	Total removal in 27 min (1) 60 min (2)	DOC removal 81 % after 6 h (1) DOC removal 40% after 6h (2)	2.9 10^{-3} s^{-1} (1) 1.4 10^{-3} s^{-1} (2)	Between 18 and 55% (1) Δ 2 and 18 % Δ 1.1 kWh $(gDOC)^{-1}$ (2) (average)	(Garcia-Segura et al. 2014)
Chloroxylenol	BDD onto Si (3 cm^2) Carbon-PTFE (3 cm^2) *fed with 20mL min^{-1} of O_2*	100 mg L^{-1}	Batch, 0.05 M NA_2SO_4, pH= 3, Vsol= 100 mL, 25°C, magnetic bar for stirring, 1 mM Fe^{2+}	33 mA cm^{-2}	Total removal in 20 min	82 % in 6 h	6.3 10^{-3} s^{-1}	Between 10 and 25% Δ	(Skoumal et al. 2008)
Ciprofloxacin	Pt mesh height 5 cm i.d. 3 cm Carbon felt 14 cm *5 cm	50 mg L^{-1}	Batch, 0.05 M NA_2SO_4, pH = 3, Vsol = 230 mL, 23°C, magnetic bar for stirring, 0.1* mM Fe^{2+}	400* mA	Total removal in 8 min	in 6 h 94.62%	12 10^{-3} s^{-1}	Between 2.5 and 7% Δ	(Yahya et al. 2014)
Enrofloxacin	BDD onto Si (3 cm^2) Carbon-PTFE (3 cm^2) fed with 12 mL min^{-1} of O_2	158 mg L^{-1}	Batch, 0.05 M NA_2SO_4, pH = 3, Vsol = 100 mL, 35°C, magnetic bar for stirring (700 rpm), 0.5 mM Fe^{2+}	33 mA cm^{-2}	Total removal in 20 min	78 % in 6 h	3.8 10^{-3} s^{-1}	Between 15 and 28% Δ 0.47 kWh $(gTOC)^{-1}$ (0.2 mM Fe^{2+})	(Guinea et al. 2010)
Flumequine	BDD (3 cm^2) Carbon PTFE air diffusion electrode (3 cm^2) *fed with pumped air at 300 mL min^{-1}* separated by 1 cm	62 mg L^{-1}	Batch, 0.05 M NA_2SO_4, pH = 3, Vsol = 100 mL, 35°C, magnetic bar for stirring (800 rpm), 2 mM* Fe^{2+}	50 mA 300 mA	Total removal in 25 min 3 min	in 6 h 70 % 87%	3.2 $10^{-3}s^{-1}$ 26 10^{-3} s^{-1}	Between 10 and 22% Δ 2.5 and 10% Δ	(Garcia-Segura et al. 2012)
Furosemide	BDD (25 cm^2) Carbon felt piece *with bubbling compressed air*	33 mg L^{-1}	Batch, 0.05 M NA_2SO_4, pH = 3, Vsol = 230 mL, room temperature, magnetic bar for stirring, 0.1 mM* Fe^{2+}	100 mA 300 mA 500 mA	- Total removal in 7 min 5 min	in 4 h 80% 90% 95%	- 17 10^{-3} s^{-1} 20 10^{-3} s^{-1}	Between 6 and 18% Δ 2 and 9% Δ -	(Olvera-Vargas et al. 2015b)

Levofloxacin	BDD (6 cm^2) Carbon felt (60 cm^2) *with compressed air bubbled at 1L min^{-1}*	83 mg L^{-1}	Batch, 0.05 M NA_2SO_4, pH = 3, Vsol = 200 mL, magnetic bar for stirring, pyrite 1g L^{-1}* (0.2 mM Fe^{2+}), 25°C	100 mA (a) 300 mA (b)	Total removal in 210 min -	- in 8 h 98 %	0.25 10^{-3} s^{-1} -	Between 3 and 6.5% Δ 2.5 kWh $(gTOC)^{-1}$ (average)	(Barhoumi et al. 2015)
Levofloxacin	Pt (5 cm^2) three-dimensional carbon felt (10 cm * 8 cm) *with air bubbling*	54 mg L^{-1}	Batch, 0,05 M NA_2SO_4 pH = 3, Vsol = 200 mL, room temperature, 0.1* mM* Fe^{2+}	400* mA	Total removal in 10 min	COD removal in 6 h 91.2%	9.8 10^{-3} s^{-1}	Instantaneous current efficiency: between 5 and 17 %	(Yahya et al. 2016)
Ranitidine	BDD onto Nb (25 cm^2) Carbon felt (15*4 cm^2) *with bubbling compressed air at 1L min^{-1}*	31 mg L^{-1}	Batch, 0.05 M NA_2SO_4, pH = 3, Vsol = 230 mL, room temperature, magnetic bar for stirring, 0.1 mM Fe^{2+}	100 mA 500 mA	90 % removal 30 min Total removal in 10 min	in 6 h 70 % 95%	9.0 10^{-3} s^{-1} 16 10^{-3} s^{-1}	Between 6 and 18% Δ 2 and 5% Δ	(Olvera-Vargas et al. 2014)
Ranitidine	Filter-press Pt (20 cm^2) Carbon PTFE (20 cm^2) *fed with air at an overpressure of 8.6 kPa*	33.8 mg L^{-1} (1) 112.6 mg L^{-1} (2)	Batch recirculation, 0.05 M NA_2SO_4, pH = 3, Vsol = 2.5 L, 35 °C, 0.5 mM Fe^{2+}, flow rate 200 L h^{-1}	25 mA cm^{-2} 100 mA cm^{-2}	- Total removal in 30 min (2)	in 6 h: 24% (2) 60% (1) 44% (2)	1.1 10^{-3} s^{-1} (2) 2.6 10^{-3} s^{-1} (2)	between 10 and 25% Δ, 0.8 kWh $(gTOC)^{-1}$ (2) (average) 5 and 22% Δ, 2.1 kWh $(gTOC)^{-1}$ (2) (average) 3 and 11% Δ, 4.8 kWh $(gTOC)^{-1}$ (average) (1)	(Olvera-Vargas et al. 2015c)
Sulfachloropyridazine	BDD onto Nb (25 cm^2) Carbon felt (14,2*4,3 cm^2) *with bubbling compressed air*	59 mg L^{-1}	Batch, 0.05 M NA_2SO_4, pH = 3, Vsol = 220 mL, room temperature, 0.2 mM Fe^{2+}, magnetic bar for stirring	60 mA (a) 300 mA (b)	Total removal in 40 min 20 min	in 10 h 72% in 4h 34% in 10 h > 95% in 4 h 79%	1.9 10^{-3} s^{-1} 10 10^{-3} s^{-1}	-	(Dirany et al. 2012)

Sulfamethazine	BDD onto Si (3 cm^2) Carbon-PTFE (3 cm^2) *fed with 300mL min^{-1} of air*	193 mg L^{-1}	0.05 M NA_2SO_4, pH = 3, Vsol = 100 mL, 35°C, magnetic bar for stirring (800 rpm), 0.5 mM Fe^{2+}	33.3 mA cm^{-2}	Total removal in 20 min	DOC removal in 7 h: 81%	3.8 10^{-3} s^{-1}	Between 10 and 20 % Δ	(El-Ghenymy et al. 2013b)
				66.7 mA cm^{-2}	15 min	90%	6.8 10^{-3} s^{-1}		
				100 mA cm^{-2}	10 min	94%	15 10^{-3} s^{-1}		
Sulfamethazine	BDD/GF (1) DSA/GF (2) GF/GF (3) GF (graphite felt) cathode: 17.5 cm * 5 cm anode 24 cm^2	56 mg L^{-1}	Batch, 0.05 M NA_2SO_4, pH = 3, Vsol = 300 mL, room temperature, magnetic bar for stirring (800 rpm), 0.2 mM Fe^{2+}	20.83 mA cm^{-2}	Total removal in 20 min (1) (2) 15 min (3)	in 8 h: (2) 75% (1) 95%	in s^{-1} 4.2*10^{-3} (1) 4.5 10^{-3} (2) 7.2 10^{-3} (3)	-	(Sopaj et al. 2016)
				2.08 mA cm^{-2}	60 min (1) (2) 30 min (3)	(3) 73%	1.2 10^{-3} (1) 1.0 10^{-3} (2) 3.7 10^{-3} (3)	-	
Sulfamethazine	BDD (25 cm^2) Carbon felt (15 cm * 4 cm) *with compressed air bubbling 1L min^{-1}*	56 mg L^{-1}	Batch, 0.05 M NA_2SO_4, Vsol = 200 mL, room temperature, magnetic bar for stirring, (1) 0.2 mM Fe^{2+} pH= 3 (2) 2 g L^{-1} Pyrite and pH= 6.1	300 mA	Total removal in 40 min (2)	in 8 h: 92% (1) 94% (2)	1.710^{-3} s^{-1} (2)	Between: 3 and 11% (1) 3 and 12% (2) Δ	(Barhoumi et al. 2016)
Sulfamethoxa-zole	BDD onto Nb (25cm^2) Carbon felt (14 cm * 5 cm), *air flow rate = 1 L min^{-1}*	53 mg L^{-1}	Batch, 0.05 M NA_2SO_4, pH = 3, Vsol = 220 mL, 23 °C, magnetic bar for stirring, 0.2 mM Fe^{2+}	30 mA cm^{-2}	Total removal in -	in 10 h: 86%	-	-	(Dirany et al. 2010)
				100 mA cm^{-2}	20 min	94%	-		
				300 mA cm^{-2}	15 min	98%	4.3 10^{-3} s^{-1}		
Sulfanilamide	Filter-press with Pt/Carbon PTFE Electrodes surface: 20 cm^2 *fed with air at an overpressure of 8.6 kPa*	239 mg L^{-1}	Batch recirculation, 0.05 M NA_2SO_4, pH = 3, Vsol = 2.5 L, 35°C, 0.5 mM Fe^{2+}, flow rate 200 L h^{-1}	50 mA cm^{-2}	Total removal in 100 min	DOC removal in4 h: 25%	5.7*10^{-4} s^{-1}	Between: 18 and 20% Δ, 0.75 kWh $(gDOC)^{-1}$ (average)	(El-Ghenymy et al. 2013a)
				150 mA cm^{-2}	50 min	50%	7.7 10^{-4} s^{-1}	5 and 10% Δ, 1.8 kWh $(gDOC)^{-1}$ (average)	

Sulfanilamide	BDD (25 cm^2) Carbon felt (15 cm * 4 cm) *with compressed air bubbling 1L min*$^{-1}$	103 mg L^{-1}	Batch, 0.05 M NA_2SO_4, pH = 3, Vsol = 230 mL, room temperature, magnetic bar for stirring, 0.2 mM Fe^{2+}	100 mA 300 mA 1000 mA	Total removal in: - 30 min -	80% in 6 h 98% in 6 h 100% in 6 h	- 2.6 10^{-3} s^{-1} -	Between: 17 and 23% 6 and 14% Δ 4 and 11% Δ	(El-Ghenymy et al. 2014)
Tetracycline	BDD onto NB (24 cm^2) Carbon felt (14 cm*5 cm) (1) DSA (24 cm^2) Carbon felt (2) Pt (24 cm^2)/ Carbon felt (3) *with compressed air bubbling 1L min*$^{-1}$	100 mg L^{-1}	Batch, 0.05 M NA_2SO_4, pH = 3, Vsol = 220 mL, 23°C, magnetic bar for stirring, 0.1 mM Fe^{3+}	500 mA 200 mA	Total removal, - 30 min (1) 50 min (2) 40 min (3)	after 6 h, 99% (1) 22% (2) 81% (3) -	- 3.0 10^{-3} s^{-1} (1) 2.0 10^{-3} s^{-1} (2) 2.3 10^{-3} s^{-1} (3)	After 6 h in kWh $(gTOC)^{-1}$: 1.30 (1); 3.20 (2); 1.10 (3) -	(Oturan et al. 2013)
Triclosan Triclocarban	BDD onto Si (3 cm^2) Carbon-PTFE (17 cm * 4.1 cm) *fed with 12 mL min*$^{-1}$ *of* O_2	Triclosan: 50 mg L^{-1} (1) Triclocarban: 5 mg L^{-1} (2)	Batch, 0.05 M NA_2SO_4, pH = 3, Vsol = 200 mL, 20°C, magnetic bar for stirring, 0.2 mM Fe^{3+}	60 mA 300 mA	Total removal 120 min (1) (2) 90 min (2)	- -	- -	- -	(Sirés et al. 2007b)

(average): the average between the maximum and minimum value for the energy consumption.
Δ: MCE between x% and y%: x and y are the two extremum values during the EF treatment
*: best value for the parameter
(1), (2), (3): letters to identify different conditions of treatment

4. Bioelectro-Fenton: A combined process for application to treat pharmaceuticals

Conventional biological processes in WWTP do not always provide satisfactory results in terms of pharmaceuticals removal (Miège et al. 2009; Luo et al. 2014; Margot et al. 2015), since many of these organic substances are toxic or resistant to microorganisms. Therefore, one feasible option to remove the persistent organic compounds is to combine biological treatment with EAOPs such as EF. This attractive potential alternative is a solution to reduce the global cost which increases with treatment time in EF.

4.1 AOPs as a pretreatment for biodegradability improvement

Two properties of the solution are considered in the literature to assess the feasibility of a biological treatment: biodegradability and toxicity.

Biodegradability of the solution is a parameter of great importance when combined treatments are considered. It is often defined thanks to the ratio of BOD_5/COD, with BOD_5 the biochemical oxygen demand at 5 d. Usually, when this ratio is greater than 0.4, the solution is considered as biodegradable (Pulgarin et al. 1999). Less commonly, one can also find the ratio of BOD_{14}/COD in the literature, BOD_{14} being the biochemical oxygen demand at 14 d. The limitation of the BOD test is mainly due to the fact that micro-organisms used as inoculum in the BOD tests may not be initially adapted to transform the organic compounds present. Thus, a lag phase is often observed during the first days in the BOD curve that can lead to very low values of the BOD after 5 d. However, after this lag phase, degradation of the organic compounds can occur leading to a strong increase in the BOD curve. On the contrary, this value can also be under estimated when they are different compounds with different biodegradability levels. So, to overcome this potential underestimation of the biodegradability of the solution, the ultimate

BOD (BODu) can be used (Trellu et al. 2016a). Another bias of the use of BOD test is that in many papers, the concentration used in the BOD test is not the same as in the EF process. Thus, as the rate of biodegradation appears to vary with concentration, the inhibiting effect of the organic compounds can be underestimated. For these two main reasons, results of BOD tests should be interpreted with caution.

Another way to indirectly measure the biodegradability of organic effluents which was used in the most recent studies is the ratio between COD and TOC. Indeed, a decrease in COD (including oxidation of the pollutant) can promote the decrease of the solution toxicity. A decrease of the ratio COD/TOC is a favorable trend for biological treatment as there are fewer oxidative products (pollutant) and the amount of organic carbon is sufficient to feed bacteria (Chebli et al. 2010; Annabi et al. 2016). From these two parameters, the AOS (average oxidation state) can be estimated which is given in Eq. 18. This parameter enables to approximate the degree of oxidation of a solution. The lowest value is -4 for CH_4 and 4 for CO_2 (Scott and Ollis 1995).

$$AOS = \frac{4\,(TOC - COD)}{TOC} \tag{18}$$

with TOC in mg C L^{-1} and COD in mg O_2 L^{-1}.

Measuring the toxicity can also be interesting. However, there are usually errors in the interpretation of results. Several methods are used to measure the toxicity of solutions electrochemically pre-treated. In general, ecotoxicological bioassays standards are used. The most commonly used is the bacterial assay Microtox® which is based on natural or provided ability of bioluminescence of a bacterial strain. However, as it is a marine strain, doubts are arising due to its application as a reference when a combined treatment is considered. It should be highlighted that the toxicity measured is not representative of the toxicity of adapted consortia that are usually employed when biological treatments are considered. Thus with this

method, a high toxicity value does not mean that all the micro-organisms from a consortia will be inhibited or killed by the solution.

The choice of the relevance of the combined process and the order in which to apply it, whether the biological treatment first and the AOP after or the contrary, are in general based on the biodegradability and toxicity of the solution to be treated. A first methodology was proposed by Scott and Ollis (1995) who divided the wastewaters into four types. The first group gathers large-size molecules that are not biodegradable (polymers, pesticides, herbicides, emulsifying agents,…). In this case, a chemical treatment is advised first to hydrolyze the big molecules into smaller biodegradable molecules to allow their biodegradation. Mantzavinos and Psillakis (2004) and Annabi et al. (2016) explained this phenomenon: bigger molecules are less likely to be degraded by a biological treatment as their size prevents them from permeating cell walls. The second group is formed of molecules with a high biodegradability rate but also containing a small amount of non-biodegradable molecules which will require a post-chemical treatment to eliminate the resistant pollutants. Here it is cost-effective to start with a biological treatment and then use an AOP. The third group is composed of molecules with a toxic activity. In this case, an AOP pre-treatment could be preferred. Finally, the fourth group is made of solutions that contain molecules that are biologically transformed into dead-end intermediates compounds that cannot be further biologically degraded and can lead to strong inhibition of the biological activity. Thus, an additional AOP treatment should be performed in order to degrade these intermediate molecules (Scott and Ollis 1995).

This classification was completed by Comninellis et al. (2008) who added the notion of TOC to classify the pollutants. They defined 4 groups, one with biodegradable compounds which correspond to the second group of Scott and Ollis and three groups with non-biodegradable compounds: (i) wastewaters with a high TOC (> 100 mg L^{-1}) requiring a pre-treatment with an AOP before a biological treatment; (ii) wastewaters with a low TOC (< 100 mg L^{-1}) but with a

high toxicity; in this case a suitable AOP is necessary to degrade the toxic compounds but a biological treatment is not recommended as wastewaters have little metabolic value for the bacteria; (iii) wastewaters containing non-biodegradable molecules at low TOC and toxicity but with a characteristic which prevents their release, such as colored wastewaters. Here only an AOP is advised.

As it was seen with both classifications, most of the time an AOP is performed first followed or not by a biological treatment as illustrated by Mantzavinos and Psillakis as most of the already published works showed a rise in biodegradability and/or a decrease in toxicity with an AOP pre-treatment. But sometimes that is not the case (Mantzavinos and Psillakis 2004; Oller et al. 2011) for several reasons: (i) stable intermediates formed may be less degradable than the parent compound; (ii) AOPs are not specific, so the biodegradable molecules can be degraded before persistent ones; (iii) finding the good conditions for the pre-treatment is needed: if too short, the solution will not change enough to be treated by activated sludge and if too long the process will not be cost-effective; (iv) the compounds used during the AOP can be toxic for the biological treatment, for example, O_3 or H_2O_2: if they are not eliminated the second treatment will not be efficient and (v) if a high concentration of halides is used, the AOP process could form toxic organic halogens which increase the toxicity of the solution (Fang et al. 2016).

In short, even if some guidelines have been found to classify wastewaters, performing each treatment separately and studying the synergetic effect as well as measuring the toxicity and the biodegradability during each treatment are necessary in order to find the best combination with the highest efficiency and the lowest cost.

4.2 Effects of EF on effluents characteristics

4.2.1 Enhancement of biodegradability

Table 9 gives an overview of the recent studies in which biodegradability of pharmaceutical solutions is investigated, except for the combination of EF with a biological treatment, which will be more detailed in sub-section 4.3. According to this Table, among the twelve studies, only three studies were performed with both treatments: in two works, an EF treatment is followed by a biological degradation step and in the third one, the treatment is performed in the opposite order. In four cases, an EF treatment followed by a biological treatment was found quite inappropriate as only in one case the solution obtained was very toxic (L) (Mousset et al. 2014), in two studies the final solution have a BOD_5/COD lower than 0.3 after EF treatment (G,H) (Elias et al. 2011; Fourcade et al. 2013) and only in one study the biodegradability level was over the limit but the time of treatment was 24 h which made the process too expensive (B) (Ledezma Estrada et al. 2012). Meanwhile for those four experiments (B,G,H,L) the biodegradability was improved. It is only by performing the biological treatment that it will be possible to confirm if this treatment is actually useless. For the others experiments the efficiency of combining both processes should work and for some of them it can be really interesting in order to reduce the operating costs as the EF treatment allows to have a biodegradable solution in a short treatment time (C,D,E,F) (Mansour et al. 2012; Chu et al. 2013; Annabi et al. 2016; Tian et al. 2016).

Table 9: Biodegradability studies with EF and biological treatments

Raw Solution	Biological treatment	Treatment EF	Order of treatment	Efficiency of EF	Efficiency of biological treatment	Effect of both treatment	Evolution of toxicity	Evolution of biodegradability	Ref
(A): Lurgi coal gasification wastewater collected after a treatment plant with COD: 140-190 mg L^{-1}, BOD_5/COD: 0.05-0.09, TOC: 90-125 mg L^{-1}	Sludge deserved activated carbon from sewage	Undivided 1 L cell with Ti/SnO_2 as anode and Active carbon fiber as cathode (20 cm^2) for 1h at 10 mA cm^{-2}, raw pH	B-EF-B	TOC removal (1h) 42%, COD removal (1h): 50 %	COD removal: 45.82%, Color removal: 46.28% in 8 hours	COD removal: 82.72%, Color removal: 95.26%, TOC removal: 84%	-	0.45 after 1h	(Hou et al. 2015)
(B): Synthetic solution of cefelaxin at 200 mg L^{-1} (COD= 325 mg L^{-1}), solution non-biodegradable	-	Undivided cell with as anode: RuO_2/Ti (54 cm^2) as cathode: activated carbon felt (54 cm^2), 500 mL of Na_2SO_4 at 0.05 M, pH: 3*, 1 mM* Fe^{2+}, 6.66* mA cm^{-2}, O_2 at 0,1 L min^{-1}, 8h*	EF	COD removal (8h): 72%, Total removal of Cefelaxin (4 h)	-	-	-	At 2h BOD_5/COD: 0.05 and BOD_{14}/COD: 0.08 at 4.5 h: BOD_5/COD: 0.1 and BOD_{14}/COD: 0.2 at 8 h: BOD_5/COD: 0.26 and BOD_{14}/COD: 0.43 at 24 h: BOD_5/COD: 0.71 and BOD_{14}/COD: 1.0	(Ledezma Estrada et al. 2012)

(C): Synthetic solution of Sulfamethazine at 0,2 mM (COD= 88 mgO_2 L^{-1}), solution non-biodegradable	-	Undivided recirculation cell with as anode: Pt (10 cm^2) as cathode: carbon felt (208 cm^2), 1 L of Na_2SO_4 at 0.05 M, pH: 3*, 0,1 mM* Fe^{2+}, compressed air at 450 mL min^{-1}, solution flow rate: 2 L min^{-1}, 18°C	EF	COD removal at 60 min (500mA) : 38%, at 120 min (500 mA): 60%, at 120 min (300 mA): 56%	-	-	-	BOD_5/COD: at 60 min (500 mA): 0.5, at 120 min (500 mA): 0.8, at 120 min (300 mA): 0.97	(Mansour et al. 2012)
(D): Synthetic solution of Enoxacin at 50 mg L^{-1} (COD/TOC= 2.4, BOD_5/COD=0) solution non-biodegradable	-	Undivided cell with as anode: Pt (34.6 cm^2) as cathode: carbon felt (45 cm^2), 250 mL of Na_2SO_4 at 0.05 M, pH: 3, 0.2 mM* Fe^{2+}, 300* mA compressed air, 18°C, 3h	EF	COD/COD_0 (3 h): 42% TOC/TOC_0 (3 h): 30%, total removal of Sulfamethazine: 50 min	-	-	-	BOD_5/COD at 60 min: 0.25, at 180 min: 0.51 at 360 min: 0.30 and TOC/COD: at 60 min 1,62 at 360 min: 1,51	(Annabi et al. 2016)
(E): Synthetic solution of Rhodamine B at 50 mg L^{-1} (0,1 M, BOD_5/COD=0.049) solution non-biodegradable	-	Undivided cell with as anode: Pt (6 mm^2) as cathode: GDE modified with polytetrafluoroethylene-carbon black (25 cm^2), 500 mL of Na_2SO_4 at 0.05 M, pH: 3, 0.5 mM* Fe^{2+}, 5* mA cm^{-2}, compressed air at 1L min^{-1}, 25°C, 1 h 30*	EF	Total removal of Rhodamine B in 20 min, TOC removal (1 h 30): 87%	-	-	-	BOD_5/COD at 1h30: 0.331	(Tian et al. 2016)
(F): Synthetic solution of m-cresol at 200 mg L^{-1} (EF) 250 mg L^{-1} (Biological treatment)	Aerobic treatment with activated sludge	Undivided cell with as anode: Ti/SnO_2-Sb_2O_5-IrO_2 (38 cm^2) as cathode: CNT (32 cm^2) fed with air at 25 mL s^{-1}, 200 mL of Na_2SO_4 at 0.1 M, pH: 3, 0.4 mM Fe^{2+}, -1V (cathodic potential), 25°C	EF-B or B	TOC removal (1h) 12.5%	TOC removal in 240 min: 7.5% (250 mg L^{-1} m-cresol)	TOC removal in 240 min: (140 mg L^{-1} TOC) 43%	-	Evaluated by the experiments using an aerobic treatment	(Chu et al. 2013)

(G): Synthetic solution of whether Orange II (OR) (COD: 142 $mgO_2\ L^{-1}$) or Methyl Red (MR) (COD: 144 $mgO_2\ L^{-1}$), Biebrich Scarlet (BS) (COD: 106 $mgO_2\ L^{-1}$); for all the solution BOD_5/COD: 0	-	Undivided cell with as anode: Pt (31.4 cm^2) as cathode: graphite felt (74.5 cm^2), saturated calomel electrode as reference electrode with compressed air, 400 mL, pH: 1*, 0.1* mM Fe^{3+}, -0.5V*, 30°C*	EF	COD 45 min: OR: 144 $mgO_2\ L^{-1}$, MR: 140 $mgO_2\ L^{-1}$, BS: 104 $mgO_2\ L^{-1}$, 28h: OR: 29 $mgO_2\ L^{-1}$, MR: 90 $mgO_2\ L^{-1}$ 22h: BS: 26 $mgO_2\ L^{-1}$	-	-	-	BOD_5/COD 45 min: OR: 0, MR: 0.23, BS: 0, 28 h: OR: 0.81, MR: 0.14, 22 h: BS: 0.1	(Fourcade et al. 2013)
(H): Synthetic solution of Methyl Red (MR) (DOC: 61.3 mg L^{-1}, COD: 192 $mgO_2\ L^{-1}$), the solution BOD_5/COD: 0, high toxicity: EC_{50}: 3%, AOS: -0.7	-	Two-compartment cell: first one contains the azo dye, graphite felt as cathode (378 cm^2) and Saturated calomel electrode as reference electrode -0.5V applied with compressed air 0.1* mM Fe^{3+}, pH: 3, the second one contains Pt as anode (31.4 cm^2) pH: 1*, 30°C	EF	COD (24 h): 116 $mgO_2\ L^{-1}$ (48h) 82 $mgO_2\ L^{-1}$, DOC (24 h): 54. $mgO_2\ L^{-1}$ (48h) 47.7 mg L^{-1}	-	-	Low toxicity EC_{50}: 165% on *vibrio ficheri*	AOS (24h): 0.8 (48 h) 1.42 BOD_5/COD (48 h): 0.24	(Elias et al. 2011)
(I): Synthetic solution of Levofloxacin at 200 mg L^{-1}, BOD_5/COD: 0	-	Undivided cell with as anode: RuO_2/Ti mesh (57 cm^2) as cathode: activated carbon fiber felt (54 cm^2), with O_2 at 100* mL min^{-1}, 500 mL solution, Na_2SO_4 at 0,05 M pH: 3*, 1.0* mM Fe^{3+}, room temperature, 6.67* mA cm^{-2}	EF	TOC removal (6h) 61%, COD removal (6h): 54%, total removal of Levofloxacin in 120 min	-	-	-	BOD_5/COD: (6 h) 0.24, (10 h): 0.41	(Gong et al. 2016)

(J): Winnery wastewater from a Port wine company in the northeast of Portugal, DOC: 4298 mg L^{-1}, COD: 12,000 mgO_2 L^{-1}, BOD_5/COD = 0.7	Aerobic treatment with activated sludge	Flow plant recirculation containing a filter press with as anode: BDD (10 cm^2) and as cathode carbon-PTFE air diffusion (10 cm^2), 25 °C, pH: 2.8, 1.3 L treated, 35 mg L^{-1}, Fe^{2+}, 25 mA cm^{-2}	B-EF	DOC removal in 240 min: 54%	COD removal: 97% (residual content: 380 mgO_2 L^{-1}, DOC removal: 97% (residual content: 130 mg L^{-1}) in 10 d	DOC: 59 mg L^{-1}, DOC removal: 98,6%	-	BOD_5/COD: 0.4 (after biological treatment)	(Moreira et al. 2015)
(K): ynthetic solution of Acid Red 14 at 200 mg L^{-1}, BOD_5/COD: 0, AOS: -0.24	-	Undivided cell with as anode: RuO2/Ti mesh (57 cm^2) as cathode: activated carbon fiber felt (20 cm^2), with O_2 at 100* mL min^{-1}, 500 mL solution, Na_2SO_4 at 0,05 M pH: 3, 1.0* mM Fe^{2+}, 0.36 A	EF	TOC removal: 70% (6h)	-	-	-	BOD_5/COD (1 h 30): 0.05, (3h): 0.075, (6h): 0.4, AOS (1 h 30): -0.05, (6 h): 0.12	(Wang et al. 2010a)
(L): Synthetic solution of Phenanthrene 0,09 mM	-	Undivided cell with as anode: BDD (20 cm^2) as cathode: carbon felt (150 cm^2), with compressed air at 0.25 L min^{-1}, 400 mL, pH: 3, 0.2 mM Fe^{2+}, 22 °C, 0.150 M Na_2SO_4	EF	Mineralization: 25% (7 h)	-	-	Toxicity (% inhibition) 96% (7 h)	BOD_5/COD (7 h): 0.33	(Mousset et al. 2014)

B: biological treatment
*best value for the parameter
(A)…(L): identification of the article in the text

4.2.2 Toxicity assessment

With biodegradability, toxicity is the second very important parameter for a biological treatment. A dozen studies reported the toxicity assessment of solutions during EF treatments. Most of them used the Microtox® test. This was applied to herbicides such as mesotrione and diuron, to azo dyes such as acid orange 7 or to pharmaceuticals such as sulfamethoxazole, sulfamethazine and sulfanilamide. For all those studies an increase of the toxicity was observed at the beginning of the EF treatment, this was due to the formation of intermediate compounds more toxic than the parent pollutant. This increase in solution toxicity was usually attributed to cyclic/aromatic by-products which are formed after a few minutes of electrolysis. As an example, one of these intermediates can be hydroquinone, obtained both in the degradation of phenol (Pimentel et al. 2008) and chlorophenol (Yuan and Lu 2005). Then after reaching a plateau in the percentage of inhibition, solution toxicity decreases due to the progressive destruction of aromatic/cyclic intermediates and formation of carboxylic acids (which are much less toxic) and to the progress in the mineralization of the solution. Depending on the starting pollutant, the complete removal of toxicity (0% of inhibition) can be achieved in 2 h as for the sulfamethazine or after 8.33 h for the mesotrione. Indeed, as for the efficiency of the EF process, the decrease of toxicity is also different when using, for example, different anode materials (mainly BDD or Pt) or different operating parameters such as current intensity or initial concentration of pollutant (Oturan et al. 2008c; Dirany et al. 2011; El-Ghenymy et al. 2014; Murati et al. 2014; Barhoumi et al. 2016; Le et al. 2016b). In the study concerning the degradation of the herbicide diuron, the authors performed the toxicity assessment both on *Vibrio Fischeri* (Microtox®) and *green algae* and found a really different behavior for these two different tests. For the algae, toxicity decreases rapidly whereas for the bacteria the toxicity rises because of the intermediates formed and then decreases. These results highlight that the toxicity observed depends on the organism used in the test. To give an overall information on

the toxicity and thus to be more reliable, tests need to be done on several different species or methods (Oturan et al. 2008c). Other toxicity assessments were done by using other species. Coledam et al. (2016) studied the degradation of the antibiotic norfloxacin and measured the evolution of toxicity using the bacteria *E. Coli* showing that the toxicity remained very high during the first two hours of EF treatment before starting to decrease. By identifying reaction intermediates, they attributed the toxicity of the solution to fluoroquinolone, a cyclic compound that remained in the medium during two h before being degraded. This test was also performed on *Daphnia magna*, a freshwater crustacean, for the degradation of the azo dye orange II. The same scheme appeared, a rise in toxicity after 5 min of treatment and then a decrease of this toxicity until no inhibition after one hour of treatment (Lin et al. 2014). Among all those studies, one assessed the cytotoxicity during the degradation of the herbicide sulfentrazone on sheep corneal epithelial cells and no toxicity was found for both the parent compound and the by-products (Lima et al. 2010).

Toxicity was also measured by the oxidative stress which is a pathophysiological mechanism coming from the imbalance of the production of reactive species and organism defenses that can lead from molecular damage to the cell death. In a study on the degradation of Yellow 9 performed by EF, the activity of catalase was measured in order to evaluate the oxidative stress. Indeed, the enzyme catalase is involved in protecting the cell from oxidative stress. Thus a high concentration of catalase means that the cell is fighting against this process. It was found that only Yellow 9 induced toxicity as the catalase activity decreased with the time of electrolysis (Kourdali et al. 2014). Another study looked at toxicogenomics and evaluated in addition the type of stress. Three well-known molecules were studied: bisphenol A, triclosan and ibuprofen; they were chosen because their degradation pathway is quite reliable. For bisphenol A, a large range of stress response was found whereas for its by-products the stress was concentrated on DNA and membrane. For triclosan, an oxidative stress was evaluated for the parent compound

and for the intermediates; an anomalous production of proteins and an alteration of the cell membrane was assessed. Finally, for ibuprofen, the parent compound alters the cell transport function and induces a high membrane stress. The by-products, as far as they are concerned, promote membrane, protein and DNA stress (Gou et al. 2014). This type of study is really interesting to understand better how the toxicity operates and then it is easier to work with and to know when a bio-treatment could be useful.

In the five last years, only two studies were found dealing with both biodegradability and toxicity (H-L) (Elias et al. 2011; Mousset et al. 2014). In order to perform the combination of both EF and biological treatment more studies are in fact needed.

4.3 Combined process applied to pharmaceuticals removal

4.3.1 Anodic oxidation as pre-treatment for a post-biodegradation process

A few studies reported the experiment of a combined process using an AOP and a biological treatment applied to pharmaceutical wastewater. To the best of our knowledge, the first attempt of an hybrid process combining bio-treatment and an electrochemical process was done by Carvalho et al. (2007). Biotic degradation products formed during biological treatment of a synthetic solution of dye Acid Orange 7 was carried out by anodic oxidation using BDD anode obtaining a COD removal of 90% and a TOC removal of 30% after 8 h treatment. Then, some works on the combination between biodegradation and AO process were carried out (Khoufi et al. 2009; Ganzenko et al. 2014; Olvera-Vargas et al. 2015a; Olvera-Vargas et al. 2016b). During the combined process, AO was used as a pre-treatment step followed by an anaerobic digestion and an ultrafiltration to reach 88% of COD removal, 72.5% of color removal and 90% of total suspended solids removal with a residence time of 4 h in the EF reactor. The use of an aerobic treatment was also investigated (Khoufi et al. 2009).

Yahiaoui et al. (2013) used an anodic oxidation process as AOP as a pre-treatment step for a biological treatment to degrade the antibiotic tetracycline. The optimal operating conditions were evaluated on a synthetic solution using a central composite design with an electrolytic cell equipped with Pb/PbO_2 anode and Pt cathode. In order to keep enough organic carbon to perform a biological treatment, the solution was electrolyzed through the following conditions: 40 °C, 275 mA, and 100 mg L^{-1} initial concentration until the complete disappearance of tetracycline. Biodegradability was also assessed along the electrolysis and reached a value of 0.41 after 5 h of treatment. At this point, 36.7% of the initial DOC remained in the medium. The aerobic treatment using activated sludge confirmed the beneficial effect of the biological treatment as the combined process reaching 76% DOC removal.

4.3.2 Coupling between EF and bio-treatment

The combination between EF and biological treatment called bio-electro-Fenton (Bio-EF) has been performed by Oturan's group (Olvera-Vargas et al. 2016a; Ganzenko et al. 2017; Olvera-Vargas et al. 2018) performing EF step as pre-treatment or post-treatment for coupling with a biological treatment applied to the removal of pharmaceuticals such as metoprolol (beta-blocker), furosemide (diuretic), ranitidine (antihistaminic H2) and real pharmaceutical wastewater (Table 10). In particular, the study reported by Olvera-Vargas et al. (Olvera-Vargas et al. 2016a) constitutes a complete and systematic research including toxicity assessment by Microtox method as well as MCE and EC data in addition to the evaluation of the biodegradability (BOD_5/COD) during EF treatment (Fig. 9). The biodegradability ratio of 0.4 was reached only after 1 h EF treatment at 500 mA constant current with 47% TOC removal of a solution of the beta-blocker metoprolol. A mineralization rate of 90% is attained after 6 d of biological treatment (Fig. 10). The shortness of the EF step allowed the reduction of a significant energy consumption (6 times) compared to EF alone. The evolution of solution

toxicity was also monitored by using Microtox® assay (Fig. 11).

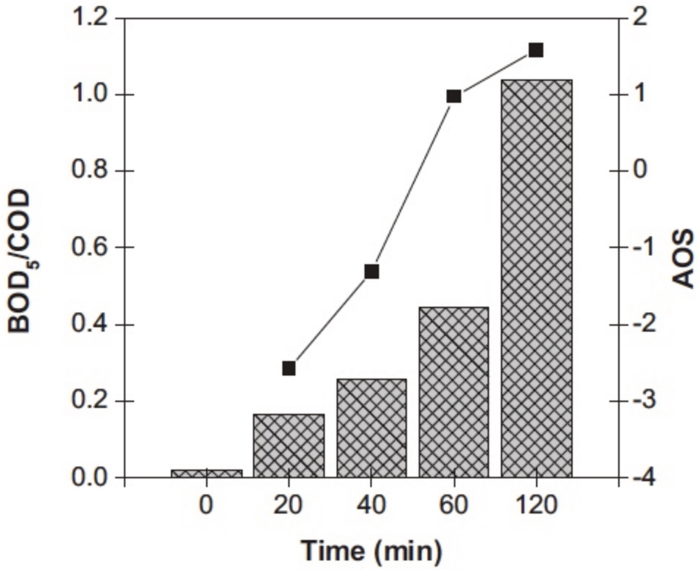

Fig. 9: BOD_5/COD ration (▨) and AOS (■) evolution as a function of time for the EF of 0.22 L of 0.1 mM of metoprolol solution in 0.05 M Na_2SO_4 and 0.1 mM Fe^{2+} at pH 3 using BDD anode at 300 mA and room temperature. Reprinted with permission from ref. (Olvera-Vargas et al. 2016a). Copyright Elsevier, 2016.

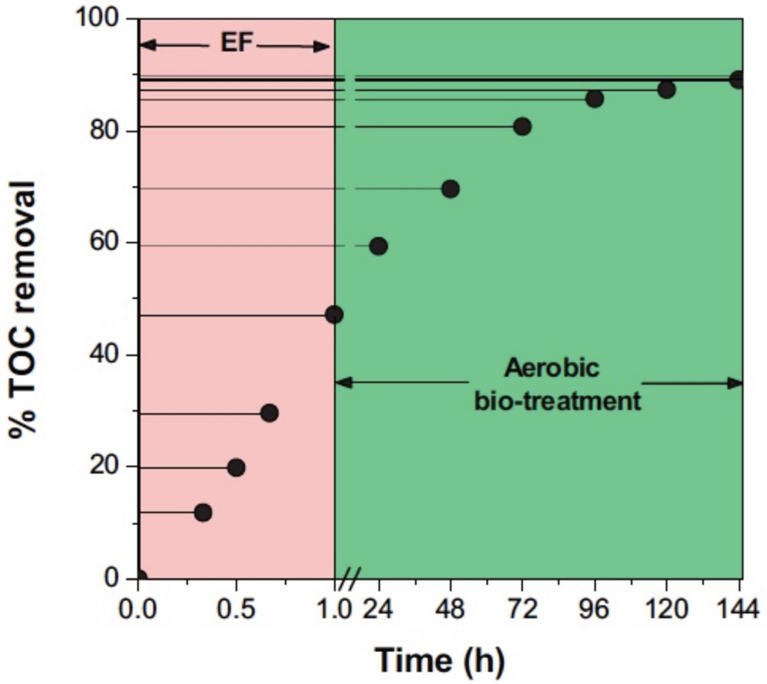

Fig. 10: TOC removal during the combine treatment of a 26.74 mg L^{-1} of metoprolol solution. The EF treatment was conducted in the condition of Fig. 9 and the biological treatment used 12 pure cultures of microorganisms under aerobic conditions. Reprinted with permission from ref. (Olvera-Vargas et al. 2016a). Copyright Elsevier, 2016.

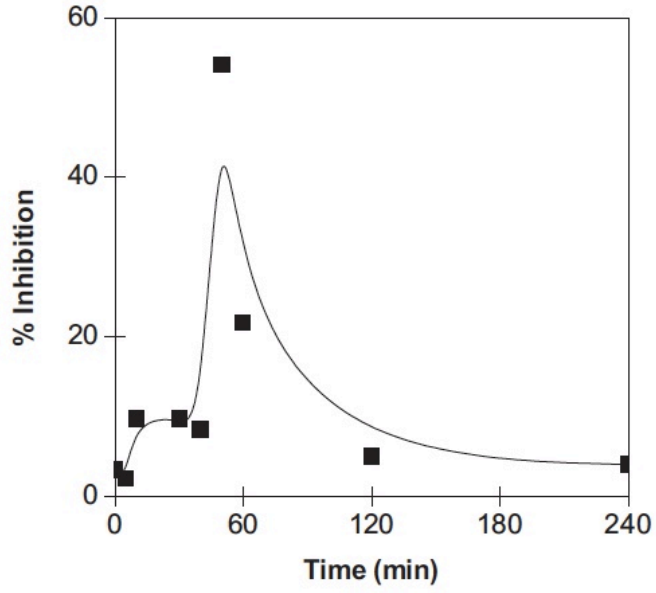

Fig. 11: % of inhibition of bioluminescence of *V. fischeri* bacteria after 15 min for the EF treatment of 0.22 L of 0.1 mM of metoprolol solution in 0.05 M Na_2SO_4 and 0.1 mM Fe^{2+} at pH 3 using BDD anode at 300 mA and room temperature. Reprinted with permission from ref. (Olvera-Vargas et al. 2016a). Copyright Elsevier, 2016.

For furosemide and ranitidine, some economic considerations were done using the French industrial price for electricity: 0.08 € $(kWh)^{-1}$. For 1 h electrolysis the energy cost was of 7.66 and 9.33 € $(kg\ TOC)^{-1}$ for furosemide and ranitidine, respectively, whereas for 8 h electrolysis to achieve nearly total mineralization the cost attained 43.03 and 46.77€ $(kg\ TOC)^{-1}$ for furosemide and ranitidine respectively with EF alone (Olvera-Vargas et al. 2016b). This clearly justifies the use of the combined process. For all the combined processes applied to pharmaceutical, the EF was used as a pre-treatment, except the report of Ganzenko et al. (2017) in which pre- and –post-EF scenarios have been performed, usually due to the toxicity of the compounds and the low biodegradability of the solution. In the latter work Ganzenko et al. (2017), compared the degradation and mineralization of a pharmaceutical effluent spiked with caffeine and 5-fluorouracil with two different orders of treatment (EF-Bio or Bio-EF) (Table 10). The results demonstrated a quite similar mineralization (more than 90% of COD removal)

for both orders but using the EF as pre-treatment appeared to be cost saving. Indeed, the best condition for EF-Bio was 2 h at 200 mA whereas for Bio-EF it required 4 h at 500 mA (Ganzenko et al. 2017).

The combination of EF treatment with a biological treatment to treat pharmaceuticals was also carried out by Ferrag-Siagh et al. (2013) in which they showed the efficiency of combining electro-Fenton process with a biological treatment for the degradation of the antibiotic tetracycline. They evaluated different parameters to find the best conditions for the EF (see Table 10). The treatment of tetracycline by biological treatment attained a TOC removal of 10% which clearly showed the inadequacy of this process due to the low biodegradability rate (BOD_5/COD) = 0.02) of the initial drug solution. To obtain a biodegradable solution, EF pre-treatment was applied to reach 46% and 72% TOC removal and, 0.33 and 0.44 BOD_5/COD ratio at 2 and 4 h treatment, respectively. Then the activated sludge treatment was performed during 25 d for the two electrolyzed solutions, obtaining an improvement of 23% and 14% in TOC removal for 2 h and 4 h EF pre-treated solutions, respectively (Ferrag-Siagh et al. 2013). The same group also investigated the degradation of tylosin, sulfamethazine and trimethoprim using the combined process obtaining a biodegradable solution (BOD_5/COD ratio ≥ 0.4) after EF pre-treatment step before biological treatment. The coupled process was then successfully applied to the treatment of a real effluent coming from a pharmaceutical industry (Ferrag-Siagh et al. 2014; Mansour et al. 2014; Mansour et al. 2015a; Mansour et al. 2015b).

The efficiency of the combination of both treatment is demonstrated in terms of TOC or COD removal but hardly ever the biodegradability or the toxicity of the solution resulting is taken into consideration. This point is of major interest as this treatment aims at delivering a clean water in the environment. One study performed toxicity tests on the treated solution (Roshini et al. 2017). Phytotoxicity tests on *Vigna radiada* seeds and microbial toxicity tests on *Pseudomonas aeruginosa* and *Bacillus sp.* were performed in order to demonstrate the

efficiency of their combined process for the degradation of textile wastewater. Both tests showed a decrease in toxicity. No such test could be found concerning the pharmaceutical effluent witch is upsetting.

In all the experiments performed on synthetic solutions as well as on real wastewaters; the cost-effectiveness and the efficiency of the coupling between EF and bio-treatment was proved. However, it should be noticed that as mentioned in section 2.3.5, the electrical consumption may be significantly different at pilot and full scale. It is also very important to underline one of the major drawbacks; the solution pH which is adjusted around 3 in EF step should be raised around 7 for the bio-treatment

.

Table 10: Combined process applied to pharmaceuticals

Raw Solution	Biological treatment	Treatment EF	Order of treatment	Efficiency of EF alone	Efficiency of biological treatment alone	Effect of both treatment	Evolution of biodegradability	Refs
100 mg/L tetracycline BOD_5/COD: 0.02, COD: 128 mgO_2/L	Activated sludge at 25°C, during 21 to 25 days in 500 mL with a cellulose cap to ensure the oxygenation by batch	Undivided Cell 1 L with a carbon felt cathode (194 cm^2) and a cylindrical platinum anode (5 cm * 1 cm) under agitation and O_2 flow, 800 mL of solution containing 0.1* mmol Fe^{2+} pH: 3*, 0.05* mol/L Na_2SO_4, at 300* mA current	EF-B	COD removal at 2 h: 66% 4 h: 86% 6 h: 93% TOC removal at 2 h: 46% 4 h: 72%	TOC removal after 25 days: 10%	TOC removal after 2 h of EF: 69%, after 4 h of EF: 86%	BOD_5/COD at 2h: 0.33, at 4h 0.44, at 6h 0.56	(Ferrag-Siagh et al. 2013)
100 mg/L Tylosin BOD_5/COD: 0, COD: 136 mgO_2/L AOS: 0.52	Activated sludge under aerobic conditions at 25°C, during 25 days in 500 mL by batch	Divided Cell of 1 L with a carbon felt cathode (194 cm^2) and a cylindrical platinum anode (5 cm * 1 cm) under agitation and O_2 flow, 800 mL of solution containing 0.1* mM Fe^{2+} pH: 3*, 0.05* mol/L Na_2SO_4, at 300* mA current	EF-B	TOC removal after 2h: 45%, 4h: 62%, 6h: 88%	TOC removal 0%	TOC removal after 2 h of EF: 77%, after 4 h of EF: 88%	BOD_5/COD at 2h: 0.3, at 4h 0.5 AOS at 2h: 1.87 4h: 1.95	(Ferrag-Siagh et al. 2014)
0.2 mM of Sulfamethazine	Fresh activated sludge at 25°C under continuous stirring by batch	Undivided Cell 1 L with a carbon felt cathode (208 cm^2) and a cylindrical platinum anode (5 cm * 2 cm) under agitation and O_2 flow rate of 450 mL/min, the electrolyte containing: 0.5 mM Fe^{2+}, pH: 3, 0.05 M Na_2SO_4, at 500 mA and 18°C	EF-B	TOC removal after 6h: 6.5% (with 0.1 mM pollutant 0.1 mM Fe^{2+} and at 200 mA)	TOC removal 0%	TOC removal after 0.5 h of EF: 61.4%, after 1 h of EF: 78.8% after 4 h: 93.9%	BOD_5/COD at 0.5h: <0.4, at 1h 0.5	(Mansour et al. 2014)
Wastewater from a pharmaceutical industry from Tunisia, 0.2 g/L Sulfamethazine, TOC: 188.7 mg/L, BOD_5/COD: 0.17	Fresh activated sludge at 25°C under continuous stirring by batch	Undivided Cell 1 L with a carbon felt cathode (208 cm^2) and a cylindrical platinum anode (5 cm * 2 cm) under agitation and O_2 flow rate of 450 mL/min, the electrolyte containing: 0.5* mM Fe^{2+}, pH: 3, 0.05 M Na_2SO_4, at 500* mA and 18°C*	EF-B	TOC removal after 100 min: 7.5%	-	TOC removal after 100 min EF: 81.4%	BOD_5/COD after 100 min: 0.35	(Mansour et al. 2015b)

Industrial pharmaceutical effluent containing 0.2 mM of Trimethoprim BOD_5/COD: 0.14	Activated sludge treatment during 15 days at 25°C by batch	Undivided Cell 1 L with a carbon felt cathode (208 cm^2) and a cylindrical platinum anode (5 cm * 2 cm) under agitation and O_2 flow rate of 450 mL/min, the electrolyte containing: 0.69* mM Fe^{2+}, pH: 3, 0.05 M Na_2SO_4, at 466* mA and 18°C*	EF-B	TOC removal at 3h: 14% at 5h: 16%	TOC removal 50%	TOC removal after 3h EF: 80% after 5h EF: 89%	BOD_5/COD at 3h: 0.45, at 5h: 0.47	(Mansour et al. 2015a)
Synthetic solution of 0.1 mM of Metoprolol BOD_5/COD: 0.02	Aerobic biological treatment at 30°C during 7 days by batch	Undivided Cell 300 mL with a carbon felt cathode and a BDD anode (25 cm^2) under agitation and compressed air bubbling, the 220 mL electrolyte containing: 0.1 mM Fe^{2+}, pH: 3, 0.05 M Na_2SO_4, at 300 mA	EF-B	TOC removal (1h): 47%	Very low TOC removal	TOC removal after 1h EF: 90%	BOD_5/COD at 1h: 0.44, AOS at 1h: 1.0	(Olvera-Vargas et al. 2016a)
Synthetic solution of 0.1 mM of Furosemide	Aerobic biological treatment at 30°C during 7 days by batch	Undivided Cell 300 mL with a carbon felt cathode and a BDD anode (24 cm^2) under agitation and compressed air bubbling, the 230 mL electrolyte containing: 0.1 mM Fe^{2+}, pH: 3, 0.05 M Na_2SO_4, at 500 mA	EF-B	TOC removal (1h): 64%	-	TOC removal after 1h EF: 93%	BOD_5/COD at 1h: 0.41	(Olvera-Vargas et al. 2016b)
Synthetic solution of 0.1 mM Ranitidine	Aerobic biological treatment at 30°C during 7 days by batch	Undivided Cell 300 mL with a carbon felt cathode and a BDD anode (24 cm^2) under agitation and compressed air bubbling, the 230 mL electrolyte containing: 0.1 mM Fe^{2+}, pH: 3, 0.05 M Na_2SO_4, at 500 mA	EF-B	TOC removal (1h): 59%	-	TOC removal after 1h EF: 94%	BOD_5/COD at 1h: 0.37	(Olvera-Vargas et al. 2016b)
Industrial pharmaceutical effluent spiked with 0.1 mM of Caffeine and 0.1 mM of 5-fluorouracil BOD_5/COD: 0.03	Pre-treatment: Activated sludge treatment during 24 h in batch Post-treatment:	Undivided Cell 1.4 L with a carbon felt cathode (475 cm^2) and a BDD anode (193 cm^2) under agitation and aeration, the 230 mL electrolyte containing: 0.2 mM Fe^{2+}, pH: 2.9, 0.05 M Na_2SO_4, at 200 or 500 mA	EF-B and B-EF	EF-B: 90% of removal of caffeine and 5-fluorouracil and COD removal of 60% in 2h at 200 mA	B-EF: 3% of caffeine, 38% of 5-fluorouracil and 43% of COD were removed in 24h	EF-B: more than 90% of COD removal in 3 d of bio-treatment B-EF: 99% of COD removal after 4h of EF at 500 mA	BOD_5/COD at 2h: 0.61	(Ganzenko et al. 2017)

5. Conclusions and perspectives

Wastewaters from hospitals and pharmaceutical industries contain relatively high concentrations of pollutants as they have not already been mixed with other effluents. As highlighted in different publications, the EF process is faster, more efficient and more cost-effective on concentrated solutions of pharmaceuticals. Thus the best approach to treat these wastewater with EF seems to be the treatment of the wastewaters directly at the exit of hospitals or pharmaceutical production plants.

A major advantage of EF compared to the non-AOP treatments is that this process is able to destroy quite every type of pollutants thanks to the non-selectivity of the hydroxyl radicals and to reach almost complete mineralization of treated solutions.

One major problem concerning the EF is its relatively high treatment cost when using longer treatment times, required to reach high mineralization degree to destroy resistant intermediates formed during the process. Research was done to reduce this treatment cost or enhance the efficiency of the EF treatment. These studies were based on the improvements of geometrical parameters or flowing characteristics in order to improve mass transfer and to limit electrical resistance that are in general the limiting steps, on avoiding the addition of external O_2 or on using micro-fluidic. Several reactor configurations were proposed and their advantages and drawbacks as well as the best configurations depend on the objectives, on the nature of the wastewater (organic pollutants, presence of solid particles, etc.). In order to reach the industrial scale with the EF process, more research is needed to assess the feasibility: (i) to operate in continuous mode, (ii) to treat real wastewaters, (iii) to decrease the cost associated to catalyst by testing recoverable solid catalyst catalysts at pilot scale. In terms of engineering, a better characterization of the hydrodynamic of the reactors at pilot scale is required to develop models coupling mass transfer phenomena, hydrodynamic behavior, electrochemical reactions, etc. in order to predict the efficiency of the reactors and helping to resolve a number of design aspects

required for a mid-term pre-industrialization. In addition, more studies at pilot scale are required to get more information about the energetical consumption of each configuration. Only few studies gathered part of these parameters; this is why it is an important research focus.

EF process has demonstrated its efficiency but the treatment cost is still relatively high (at least 0.39 kWh (g TOC)$^{-1}$) and a good way for saving energy in order to industrialize it, is its combination with a biological treatment. In the case of the treatment of pharmaceutical wastewaters, EF process as a pre-treatment followed by a biological treatment proved its accuracy. However, all the experiments were performed at laboratory scale and under batch conditions. Therefore, for a pre-industrialization of the combined treatment, experiments must be conducted at pilot scale and the feasibility of conducting continuous or semi-continuous reactors must be assessed. The extent of conditioning of the active biomass used for the biological treatment to the parent compound, to the reaction intermediates, or to the compound mixtures also needs to be addressed. In addition, more work is needed to determine the monitoring parameters to control the reactor's operation.

Thus to answer some of the previous points, a lab-scale pilot was built for this thesis and it was tested to treat different solutions of pharmaceuticals on its one or combined with a biological treatment. This will be developed in the next chapters.

References:

Annabi C, Fourcade F, Soutrel I, et al (2016) Degradation of enoxacin antibiotic by the electro-Fenton process: optimization, biodegradability improvement and degradation mechanism. J Environ Manage 165:96–105. doi: 10.1016/j.jenvman.2015.09.018

Barhoumi N, Labiadh L, Oturan MA, et al (2015) Electrochemical mineralization of the antibiotic levofloxacin by electro-Fenton-pyrite process. Chemosphere 141:250–257. doi: 10.1016/j.chemosphere.2015.08.003

Barhoumi N, Oturan N, Olvera-Vargas H, et al (2016) Pyrite as a sustainable catalyst in electro-Fenton process for improving oxidation of sulfamethazine. Kinetics, mechanism and toxicity assessment. Water Res 94:52–61. doi: 10.1016/j.watres.2016.02.042

Barrera-Dias C, Cañizares P, Fernández FJ, et al (2014) Electrochemical advanced oxidation processes : an overview of the current applications to actual industrial effluents. J Mex Chem Soc 58:256–275.

Barros WRP, Borges MP, Reis RM, et al (2014a) Degradation of dipyrone by the electro-fenton process in an electrochemical flow reactor with a modified gas diffusion electrode. J Braz Chem Soc 25:1673–1680. doi: 10.5935/0103-5053.20140160

Barros WRP, Borges MP, Steter JR, et al (2014b) Degradation of dipyrone by electrogenerated H2O2 combined with Fe2+ using a modified gas diffusion electrode. J Electrochem Soc 161:H867–H873. doi: 10.1149/2.0091414jes

Bautista P, Mohedano AF, Casas J a., et al (2008) An overview of the application of Fenton oxidation to industrial wastewaters treatment. J Chem Technol Biotechnol 82:1323–1338. doi: 10.1002

Bocos E, Iglesias O, Pazos M, ??ngeles Sanrom??n M (2016a) Nickel foam a suitable alternative to increase the generation of Fenton's reagents. Process Saf Environ Prot 101:34–44. doi: 10.1016/j.psep.2015.04.011

Bocos E, Pérez-Álvarez D, Pazos M, et al (2016b) Coated nickel foam electrode for the implementation of continuous electro-Fenton treatment. J Chem Technol Biotechnol 91:685–692. doi: 10.1002/jctb.4626

Boye B, Dieng MM, Brillas E (2002) Degradation of herbicide 4-chlorophenoxyacetic acid by advanced electrochemical oxidation methods. Environ Sci Technol 36:3030–3035. doi: 10.1021/es0103391

Brillas E, Bastida RM, Llosa E, Casado J (1995) Electrochemical destruction of aniline and 4-chloroaniline for wastewater treatment using a carbon-PTFE-O2-fed cathode. J Electrochem Soc 142:1733–1741. doi: 10.1149/1.2044186

Brillas E, Calpe JC, Casado J (2000) Mineralization of 2,4-D by advanced electrochemical oxidation processes. Water Res 34:2253–2262. doi: 10.1016/S0043-1354(99)00396-6

Brillas E, Sirés I, Oturan MA (2009) Electro-fenton process and related electrochemical technologies based on fenton's reaction chemistry. Chem Rev 109:6570–6631. doi: 10.1021/cr900136g

Brown RF, Jamison SE, Pandit UK, et al (1964) The reaction of Fenton's reagent with phenoxyacetic acid and some halogen-substituted phenoxyacetic acids. J Org Chem 29:146–153. doi: 10.1021/jo01024a034

Carvalho C, Fernandes A, Lopes A, et al (2007) Electrochemical degradation applied to the metabolites of Acid Orange 7 anaerobic biotreatment. Chemosphere 67:1316–1324. doi: 10.1016/j.chemosphere.2006.10.062

Casado J, Fornaguera J (2008) Pilot-scale degradation of organic contaminants in a continuous-flow reactor by the helielectro-Fenton method. Clean - Soil, Air, Water 36:53–58. doi: 10.1002/clen.200700091

Chaplin BP (2014) Critical review of electrochemical advanced oxidation processes for water

treatment applications. Environ Sci Process Impacts 16:1182–1203. doi: 10.1039/C3EM00679D
Chebli D, Fourcade F, Brosillon S, et al (2010) Supported photocatalysis as a pre-treatment prior to biological degradation for the removal of some dyes from aqueous solutions; acid red 183, Biebrich Scarlet, methyl red sodium salt, orange II. J Chem Technol Biotechnol 85:555–563. doi: 10.1002/jctb.2342
Chu Y, Zhang D, Liu L, et al (2013) Electrochemical degradation of m-cresol using porous carbon-nanotube-containing cathode and Ti/SnO2-Sb2O5-IrO2 anode: Kinetics, byproducts and biodegradability. J Hazard Mater 252–253:306–312. doi: 10.1016/j.jhazmat.2013.03.018
Coledam DAC, Aquino JM, Silva BF, et al (2016) Electrochemical mineralization of norfloxacin using distinct boron-doped diamond anodes in a filter-press reactor, with investigations of toxicity and oxidation by-products. Electrochim Acta 213:856–864. doi: 10.1016/j.electacta.2016.08.003
Comninellis C, Kapalka A, Malato S, et al (2008) Advanced oxidation processes for water treatment: advances and trends for R&D. J Chem Technol Biotechnol 83:769–776. doi: 10.1002/jctb
Coria G, Sirés I, Brillas E, Nava JL (2016) Influence of the anode material on the degradation of naproxen by Fenton-based electrochemical processes. Chem Eng J 304:817–825. doi: 10.1016/j.cej.2016.07.012
Cruz-Díaz M, Rivera FF, Rivero EP, González I (2012) The FM01-LC reactor modeling using axial dispersion model with a reaction term coupled with a continuous stirred tank (CST). Electrochim Acta 63:47–54. doi: 10.1016/j.electacta.2011.12.038
De Laat J, Truong Le G, Legube B (2004) A comparative study of the effects of chloride, sulfate and nitrate ions on the rates of decomposition of H2O2and organic compounds by Fe(II)/H2O2and Fe(III)/H2O2. Chemosphere 55:715–723. doi: 10.1016/j.chemosphere.2003.11.021
Diagne M, Oturan N, Oturan MA (2007) Removal of methyl parathion from water by electrochemically generated Fenton's reagent. Chemosphere 66:841–848. doi: 10.1016/j.chemosphere.2006.06.033
Dirany A, Efremova Aaron S, Oturan N, et al (2011) Study of the toxicity of sulfamethoxazole and its degradation products in water by a bioluminescence method during application of the electro-Fenton treatment. Anal Bioanal Chem 400:353–360. doi: 10.1007/s00216-010-4441-x
Dirany A, Sirés I, Oturan N, et al (2012) Electrochemical treatment of the antibiotic sulfachloropyridazine: kinetics, reaction pathways, and toxicity evolution. Environ Sci Technol 46:4074–4082. doi: 10.1021/es204621q
Dirany A, Sirés I, Oturan N, Oturan MA (2010) Electrochemical abatement of the antibiotic sulfamethoxazole from water. Chemosphere 81:594–602. doi: 10.1016/j.chemosphere.2010.08.032
dos Santos EV, Sena SFM, da Silva DR, et al (2014) Scale-up of electrochemical oxidation system for treatment of produced water generated by Brazilian petrochemical industry. Environ Sci Pollut Res 21:8466–8475. doi: 10.1007/s11356-014-2779-x
Durán Moreno A, Frontana-Uribe BA, Ramírez Zamora RM (2004) Electro-Fenton as a feasible advanced treatment process to produce reclaimed water. Water Sci Technol 50:83–90.
El-Ghenymy A, Cabot PL, Centellas F, et al (2013a) Mineralization of sulfanilamide by electro-Fenton and solar photoelectro-Fenton in a pre-pilot plant with a Pt/air-diffusion cell. Chemosphere 91:1324–1331. doi: 10.1016/j.chemosphere.2013.03.005
El-Ghenymy A, Rodríguez RM, Arias C, et al (2013b) Electro-Fenton and photoelectro-

Fenton degradation of the antimicrobial sulfamethazine using a boron-doped diamond anode and an air-diffusion cathode. J Electroanal Chem 701:7–13. doi: 10.1016/j.jelechem.2013.04.027
El-Ghenymy A, Rodríguez RM, Brillas E, et al (2014) Electro-Fenton degradation of the antibiotic sulfanilamide with Pt/carbon-felt and BDD/carbon-felt cells. Kinetics, reaction intermediates, and toxicity assessment. Environ Sci Pollut Res 21:8368–8378. doi: 10.1007/s11356-014-2773-3
El-Hanafi N, Mehibel L, Li HZ, et al (2014) Mineralization of the pharmaceutical β-Blocker atenolol by means of indirect electrochemical advanced oxidation process: parametric and kinetic study. Sep Sci Technol 49:2942–2950. doi: 10.1080/01496395.2014.943771
Elias B, Guihard L, Nicolas S, et al (2011) Effect of electro-Fenton application on azo dyes biodegradability. Environ Prog Sustain Energy 30:160–167. doi: 10.1002/ep
Fang C, Xiao D, Liu W, et al (2016) Enhanced AOX accumulation and aquatic toxicity during 2,4,6-trichlorophenol degradation in a Co(II)/peroxymonosulfate/Cl− system. Chemosphere 144:2415–2420. doi: 10.1016/j.chemosphere.2015.11.030
Feng J, Hu X, Yue PL, et al (2003) Degradation of azo-dye orange II by a photoassisted Fenton reaction using a novel Composite of Iron Oxide and Silicate nanoparticles as a catalyst. Ind Eng Chem Res 42:2058–2066. doi: 10.1021/ie0207010
Feng L, Oturan N, van Hullebusch ED, et al (2014) Degradation of anti-inflammatory drug ketoprofen by electro-oxidation: Comparison of electro-Fenton and anodic oxidation processes. Environ Sci Pollut Res 21:8406–8416. doi: 10.1007/s11356-014-2774-2
Fenton HJH (1894) LXXIII.-Oxidation of tartaric acid in presence of iron. J Chem Soc{,} Trans 65:899–910. doi: 10.1039/CT8946500899
Ferrag-Siagh F, Fourcade F, Soutrel I, et al (2013) Tetracycline degradation and mineralization by the coupling of an electro-Fenton pretreatment and a biological process. J Chem Technol Biotechnol 88:1380–1386. doi: 10.1002/jctb.3990
Ferrag-Siagh F, Fourcade F, Soutrel I, et al (2014) Electro-Fenton pretreatment for the improvement of tylosin biodegradability. Environ Sci Pollut Res 21:8534–8542. doi: 10.1007/s11356-014-2771-5
Fourcade F, Delawarde M, Guihard L, et al (2013) Electrochemical reduction prior to electro-Fenton oxidation of AZO dyes: impact of the pretreatment on biodegradability. Water Air Soil Pollut. doi: 10.1007/s11270-012-1385-0
Frías-Ferrer Á, Tudela I, Louisnard O, et al (2011) Optimized design of an electrochemical filter-press reactor using CFD methods. Chem Eng J 169:270–281. doi: 10.1016/j.cej.2011.02.053
Ganiyu SO, Oturan N, Raffy S, et al (2017) Use of Sub-stoichiometric Titanium Oxide as a Ceramic Electrode in Anodic Oxidation and Electro-Fenton Degradation of the Beta-blocker Propranolol: Degradation Kinetics and Mineralization Pathway. Electrochim Acta 242:344–354. doi: 10.1016/j.electacta.2017.05.047
Ganzenko O, Huguenot D, van Hullebusch ED, et al (2014) Electrochemical advanced oxidation and biological processes for wastewater treatment: a review of the combined approaches. Environ Sci Pollut Res 21:8493–8524. doi: 10.1007/s11356-014-2770-6
Ganzenko O, Trellu C, Papirio S, et al (2017) Bioelectro-Fenton: evaluation of a combined biological—advanced oxidation treatment for pharmaceutical wastewater. Environ Sci Pollut Res 1–10. doi: 10.1007/s11356-017-8450-6
García-Montoya MF, Gutiérrez-Granados S, Alatorre-Ordaz A, et al (2015) Application of electrochemical/BDD process for the treatment wastewater effluents containing pharmaceutical compounds. J Ind Eng Chem 31:238–243. doi: 10.1016/j.jiec.2015.06.030
Garcia-Segura S, Cavalcanti EB, Brillas E (2014) Mineralization of the antibiotic

chloramphenicol by solar photoelectro-Fenton. From stirred tank reactor to solar pre-pilot plant. Appl Catal B Environ 144:588–598. doi: 10.1016/j.apcatb.2013.07.071
Garcia-Segura S, Garrido JA, Rodríguez RM, et al (2012) Mineralization of flumequine in acidic medium by electro-Fenton and photoelectro-Fenton processes. Water Res 46:2067–2076. doi: 10.1016/j.watres.2012.01.019
George SJ, Gandhimathi R, Nidheesh PV, Ramesh ST (2014) Electro-fenton oxidation of salicylic acid from aqueous solution: Batch studies and degradation pathway. Clean - Soil, Air, Water 42:1701–1711. doi: 10.1002/clen.201300453
Ghoneim MM, El-Desoky HS, Zidan NM (2011) Electro-Fenton oxidation of Sunset Yellow FCF azo-dye in aqueous solutions. Desalination 274:22–30. doi: 10.1016/j.desal.2011.01.062
Gil L, Garcia-Breijo E, Ibañez J, et al (2006) Electronic tongue for qualitative analysis of aqueous solutions of salts using thick-film technology and metal electrodes. Sensors 6:1128–1138. doi: 10.3390/s6091128
Gogate PR, Pandit AB (2004) A review of imperative technologies for wastewater treatment I: Oxidation technologies at ambient conditions. Adv Environ Res 8:501–551. doi: 10.1016/S1093-0191(03)00032-7
Gökkuş Ö (2016) Oxidative degradation of basic black 3 by electro-generated Fenton's reagent using carbon fiber cathode. Clean Technol Environ Policy 18:1525–1534. doi: 10.1007/s10098-016-1134-y
Gong Y, Li J, Zhang Y, et al (2016) Partial degradation of levofloxacin for biodegradability improvement by electro-Fenton process using an activated carbon fiber felt cathode. J Hazard Mater 304:320–328. doi: 10.1016/j.jhazmat.2015.10.064
Gou N, Yuan S, Lan J, et al (2014) A quantitative toxicogenomics assay reveals the evolution and nature of toxicity during the transformation of environmental pollutants. Environ Sci Technol 48:8855–8863. doi: 10.1021/es501222t
Guinea E, Arias C, Cabot PL, et al (2008) Mineralization of salicylic acid in acidic aqueous medium by electrochemical advanced oxidation processes using platinum and boron-doped diamond as anode and cathodically generated hydrogen peroxide. Water Res 42:499–511. doi: 10.1016/j.watres.2007.07.046
Guinea E, Garrido JA, Rodríguez RM, et al (2010) Degradation of the fluoroquinolone enrofloxacin by electrochemical advanced oxidation processes based on hydrogen peroxide electrogeneration. Electrochim Acta 55:2101–2115. doi: 10.1016/j.electacta.2009.11.040
Haber F, Weiss J (1934) The Catalytic Decomposition of Hydrogen Peroxide by Iron Salts. Math Phys Sci 147:332–351. doi: 193.50.159.59
Hou B, Han H, Zhuang H, et al (2015) A novel integration of three-dimensional electro-Fenton and biological activated carbon and its application in the advanced treatment of biologically pretreated Lurgi coal gasification wastewater. Bioresour Technol 196:721–725. doi: 10.1016/j.biortech.2015.07.068
Hu Y, Lu Y, Liu G, et al (2018) Effect of the structure of stacked electro-Fenton reactor on treating nano filtration concentrate of landfill leachate. Chemosphere 202:191–197. doi: 10.1016/j.chemosphere.2018.03.103
Iglesias O, Gómez J, Pazos M, Sanromán MÁ (2014) Electro-Fenton oxidation of imidacloprid by Fe alginate gel beads. Appl Catal B Environ 144:416–424. doi: 10.1016/j.apcatb.2013.07.046
Iglesias O, Rosales E, Pazos M, Sanromán MA (2013) Electro-Fenton decolourisation of dyes in an airlift continuous reactor using iron alginate beads. Environ Sci Pollut Res 20:2252–2261. doi: 10.1007/s11356-012-1100-0
Isarain-Chávez E, Arias C, Cabot PL, et al (2010a) Mineralization of the drug β-blocker

atenolol by electro-Fenton and photoelectro-Fenton using an air-diffusion cathode for H2O2 electrogeneration combined with a carbon-felt cathode for Fe2+ regeneration. Appl Catal B Environ 96:361–369. doi: 10.1016/j.apcatb.2010.02.033
Isarain-Chávez E, Cabot PL, Centellas F, et al (2011a) Electro-Fenton and photoelectro-Fenton degradations of the drug beta-blocker propranolol using a Pt anode: Identification and evolution of oxidation products. J Hazard Mater 185:1228–1235. doi: 10.1016/j.jhazmat.2010.10.035
Isarain-Chávez E, Garrido JA, Rodríguez RM, et al (2011b) Mineralization of metoprolol by electro-fenton and photoelectro-fenton processes. J Phys Chem A 115:1234–1242. doi: 10.1021/jp110753r
Isarain-Chávez E, Rodríguez RM, Cabot PL, et al (2011c) Degradation of pharmaceutical beta-blockers by electrochemical advanced oxidation processes using a flow plant with a solar compound parabolic collector. Water Res 45:4119–4130. doi: 10.1016/j.watres.2011.05.026
Isarain-Chávez E, Rodríguez RM, Garrido JA, et al (2010b) Degradation of the beta-blocker propranolol by electrochemical advanced oxidation processes based on Fenton's reaction chemistry using a boron-doped diamond anode. Electrochim Acta 56:215–221. doi: 10.1016/j.electacta.2010.08.097
Khoufi S, Aloui F, Sayadi S (2009) Pilot scale hybrid process for olive mill wastewater treatment and reuse. Chem Eng Process Process Intensif 48:643–650. doi: 10.1016/j.cep.2008.07.007
Kourdali S, Badis A, Boucherit A (2014) Degradation of direct yellow 9 by electro-Fenton: process study and optimization and, monitoring of treated water toxicity using catalase. Ecotoxicol Environ Saf 110:110–120. doi: 10.1016/j.ecoenv.2014.08.023
Kuo WG (1992) Decolorizing dye wastewater with Fenton's reagent. Water Res 26:881–886. doi: 10.1016/0043-1354(92)90192-7
Le TXH, Charmette C, Bechelany M, Cretin M (2016a) Facile preparation of porous carbon cathode to eliminate paracetamol in aqueous medium using electro-Fenton system. Electrochim Acta 188:378–384. doi: 10.1016/j.electacta.2015.12.005
Le TXH, Nguyen T Van, Yacouba ZA, et al (2016b) Toxicity removal assessments related to degradation pathways of azo dyes: toward an optimization of electro-Fenton treatment. Chemosphere 161:308–318. doi: 10.1016/j.chemosphere.2016.06.108
Ledezma Estrada A, Li YY, Wang A (2012) Biodegradability enhancement of wastewater containing cefalexin by means of the electro-Fenton oxidation process. J Hazard Mater 227–228:41–48. doi: 10.1016/j.jhazmat.2012.04.079
Lei Y, Liu H, Shen Z, Wang W (2013) Development of a trickle bed reactor of electro-Fenton process for wastewater treatment. J Hazard Mater 261:570–576. doi: 10.1016/j.jhazmat.2013.08.010
Lima AC de A, Melo AM dos S, Pires EV, et al (2010) Electroanalytical studies of sulfentrazone in protic medium, its degradation by the electro-Fenton process, and toxicity assessment using ss-DNA. Chemosphere 81:884–889. doi: 10.1016/j.chemosphere.2010.08.003
Lin H, Zhang H, Wang X, et al (2014) Electro-fenton removal of orange II in a divided cell: reaction mechanism, degradation pathway and toxicity evolution. Sep Purif Technol 122:533–540. doi: 10.1016/j.seppur.2013.12.010
Liu H, Vecitis CD (2012) Reactive transport mechanism for organic oxidation during electrochemical filtration: Mass-transfer, physical adsorption, and electron-transfer. J Phys Chem C 116:374–383. doi: 10.1021/jp209390b
Liu H, Wang C, Li X, et al (2007) A novel electro-Fenton process for water treatment : reaction-controlled pH adjustment and performance assessment. Environ Sci Technol

41:2937–2942. doi: 10.1021/ES0622195
Loaiza-Ambuludi S, Panizza M, Oturan N, et al (2013) Electro-Fenton degradation of anti-inflammatory drug ibuprofen in hydroorganic medium. J Electroanal Chem 702:31–36. doi: 10.1016/j.jelechem.2013.05.006
Luo Y, Guo W, Ngo HH, et al (2014) A review on the occurrence of micropollutants in the aquatic environment and their fate and removal during wastewater treatment. Sci Total Environ 473–474:619–641. doi: 10.1016/j.scitotenv.2013.12.065
Ma L, Zhou M, Ren G, et al (2016) A highly energy-efficient flow-through electro-Fenton process for organic pollutants degradation. Electrochim Acta 200:222–230. doi: 10.1016/j.electacta.2016.03.181
Mansour D, Fourcade F, Bellakhal N, et al (2012) Biodegradability improvement of sulfamethazine solutions by means of an electro-Fenton process. Water Air Soil Pollut 223:2023–2034. doi: 10.1007/s11270-011-1002-7
Mansour D, Fourcade F, Huguet S, et al (2014) Improvement of the activated sludge treatment by its combination with electro Fenton for the mineralization of sulfamethazine. Int Biodeterior Biodegrad 88:29–36. doi: 10.1016/j.ibiod.2013.11.016
Mansour D, Fourcade F, Soutrel I, et al (2015a) Mineralization of synthetic and industrial pharmaceutical effluent containing trimethoprim by combining electro-Fenton and activated sludge treatment. J Taiwan Inst Chem Eng 53:58–67. doi: 10.1016/j.jtice.2015.02.022
Mansour D, Fourcade F, Soutrel I, et al (2015b) Relevance of a combined process coupling electro-Fenton and biological treatment for the remediation of sulfamethazine solutions - Application to an industrial pharmaceutical effluent. Comptes Rendus Chim 18:39–44. doi: 10.1016/j.crci.2014.05.005
Mantzavinos D, Psillakis E (2004) Enhancement of biodegradability of industrial wastewaters by chemical oxidation pre-treatment. J Chem Technol Biotechnol 79:431–454. doi: 10.1002/jctb.1020
Margot J, Rossi L, Barry DA, Holliger C (2015) A review of the fate of micropollutants in wastewater treatment plants. WIREs Water 2:457–487. doi: 10.1002/wat2.1090
Marselli B, Garcia-Gomez J, Michaud P-A, et al (2003) Electrogeneration of hydroxyl radicals on boron-doped diamond electrodes. J Electrochem Soc 150:D79–D83. doi: 10.1149/1.1553790
Martínez-Huitle CA, Rodrigo MA, Sirés I, Scialdone O (2015) Single and coupled electrochemical processes and reactors for the abatement of organic water pollutants: a critical review. Chem Rev 115:13362–13407. doi: 10.1021/acs.chemrev.5b00361
Miège C, Choubert JM, Ribeiro L, et al (2009) Fate of pharmaceuticals and personal care products in wastewater treatment plants--conception of a database and first results. Environ Pollut 157:1721–6. doi: 10.1016/j.envpol.2008.11.045
Moreira FC, Boaventura RAR, Brillas E, Vilar VJP (2015) Remediation of a winery wastewater combining aerobic biological oxidation and electrochemical advanced oxidation processes. Water Res 75:95–108. doi: 10.1016/j.watres.2015.02.029
Mousset E, Oturan N, van Hullebusch ED, et al (2014) Treatment of synthetic soil washing solutions containing phenanthrene and cyclodextrin by electro-oxidation. Influence of anode materials on toxicity removal and biodegradability enhancement. Appl Catal B Environ 160–161:666–675. doi: 10.1016/j.apcatb.2014.06.018
Murati M, Oturan N, Zdravkovski Z, et al (2014) Application of the Electro-Fenton process to mesotrione aqueous solutions, kinetics, degradation, pathways, mineralization and evolution of toxicity. Maced J Chem Chem Eng 33:121–137.
Narayanan TSNS, Rajendran GMN (2003) Degradation of o-chlorophenol from aqueous solution by electro-Fenton process. Fresenius Environ Bull 12:776–780.

Nidheesh PV, Gandhimathi R (2015) Electro Fenton oxidation for the removal of Rhodamine B from aqueous solution in a bubble column reactor under continuous mode. Desalin Water Treat 55:263–271. doi: 10.1080/19443994.2014.913266
Nidheesh P V., Gandhimathi R (2012) Trends in electro-Fenton process for water and wastewater treatment: an overview. Desalination 299:1–15. doi: 10.1016/j.desal.2012.05.011
Oller I, Malato S, Sánchez-Pérez JA (2011) Combination of Advanced Oxidation Processes and biological treatments for wastewater decontamination: a review. Sci Total Environ 409:4141–4166. doi: 10.1016/j.scitotenv.2010.08.061
Olvera-Vargas H, Cocerva T, Oturan N, et al (2015a) Bioelectro-Fenton: a sustainable integrated process for removal of organic pollutants from water: application to mineralization of metoprolol. J Hazard Mater 319:13–23. doi: 10.1016/j.jhazmat.2015.12.010
Olvera-Vargas H, Cocerva T, Oturan N, et al (2016a) Bioelectro-Fenton: a sustainable integrated process for removal of organic pollutants from water: application to mineralization of metoprolol. J Hazard Mater 319:13–23. doi: 10.1016/j.jhazmat.2015.12.010
Olvera-Vargas H, Oturan N, Brillas E, et al (2014) Electrochemical advanced oxidation for cold incineration of the pharmaceutical ranitidine: Mineralization pathway and toxicity evolution. Chemosphere 117:644–651. doi: 10.1016/j.chemosphere.2014.09.084
Olvera-Vargas H, Oturan N, Buisson D, et al (2015b) Electro-oxidation of the pharmaceutical furosemide: kinetics, mechanism, and by-products. Clean - Soil, Air, Water 43:1455–1463. doi: 10.1002/clen.201400656
Olvera-Vargas H, Oturan N, Buisson D, Oturan MA (2016b) A coupled bio-EF process for mineralization of the pharmaceuticals furosemide and ranitidine: feasibility assessment. Chemosphere 155:606–613. doi: 10.1016/j.chemosphere.2016.04.091
Olvera-Vargas H, Oturan N, Oturan MA, Brillas E (2015c) Electro-Fenton and solar photoelectro-Fenton treatments of the pharmaceutical ranitidine in pre-pilot flow plant scale. Sep Purif Technol 146:127–135. doi: 10.1016/j.seppur.2015.03.046
Olvera-vargas H, Rouch J, Coetsier C, et al (2018) Dynamic cross-flow electro-Fenton process coupled to anodic oxidation for wastewater treatment : Application to the degradation of acetaminophen. Sep Purif Technol 203:143–151. doi: 10.1016/j.seppur.2018.03.063
Olvera-Vargas H, Trellu C, Oturan N, Oturan MA (2018) Bio-electro-Fenton: A New Combined Process – Principles and Applications BT - Electro-Fenton Process: New Trends and Scale-Up. In: Zhou M, Oturan MA, Sirés I (eds). Springer Singapore, Singapore, pp 29–56
Oturan MA (2000) An ecologically effective water treatment technique using electrochemically generated hydroxyl radicals for in situ destruction of organic pollutants: Application to herbicide 2,4-D. J Appl Electrochem 30:475–482. doi: 10.1023/A:1003994428571
Oturan MA, Aaron J-J (2014) Advanced oxidation processes in water/wastewater treatment: principles and applications. A Review. Crit Rev Environ Sci Technol 44:2577–2641. doi: 10.1080/10643389.2013.829765
Oturan MA, Peiroten J, Chartrin P, Acher AJ (2000) Complete destruction of p-Nitrophenol in aqueous medium by electro-fenton method. Environ Sci Technol 34:3474–3479. doi: 10.1021/es990901b
Oturan N, Brillas E, Oturan MA (2012) Unprecedented total mineralization of atrazine and cyanuric acid by anodic oxidation and electro-Fenton with a boron-doped diamond anode. Environ Chem Lett 10:165–170. doi: 10.1007/s10311-011-0337-z

Oturan N, Ganiyu SO, Raffy S, Oturan MA (2017) Sub-stoichiometric titanium oxide as a new anode material for electro-Fenton process: Application to electrocatalytic destruction of antibiotic amoxicillin. Appl Catal B Environ 217:214–223. doi: 10.1016/j.apcatb.2017.05.062
Oturan N, Oturan MA (2005) Degradation of three pesticides used in viticulture by electrogenerated Fenton's reagent. Agron Sustain Dev. doi: 10.1051/agro
Oturan N, Oturan MA (2018) Electro-Fenton process : background , new developments and applications. In: Martínez-Huitle CA, Rodrigo MA, Scialdone O (eds) Electrochemical Water Treatment Methods. Elsevier, pp 1–32
Oturan N, Trajkovska S, Oturan MA, et al (2008) Study of the toxicity of diuron and its metabolites formed in aqueous medium during application of the electrochemical advanced oxidation process "electro-Fenton." Chemosphere 73:1550–1556. doi: 10.1016/j.chemosphere.2008.07.082
Oturan N, Wu J, Zhang H, et al (2013) Electrocatalytic destruction of the antibiotic tetracycline in aqueous medium by electrochemical advanced oxidation processes: Effect of electrode materials. Appl Catal B Environ 140–141:92–97. doi: 10.1016/j.apcatb.2013.03.035
Oturan N, Zhou M, Oturan MA (2010) Metomyl degradation by electro-Fenton and electro-Fenton-like processes: a kinetics study of the effect of the nature and concentration of some transition metal ions as catalyst. J Phys Chem A 114:10605–10611. doi: 10.1021/jp1062836
Özcan A, Şahin Y, Savaş Koparal A, Oturan MA (2008) Carbon sponge as a new cathode material for the electro-Fenton process: Comparison with carbon felt cathode and application to degradation of synthetic dye basic blue 3 in aqueous medium. J Electroanal Chem 616:71–78. doi: 10.1016/j.jelechem.2008.01.002
Pajootan E, Arami M, Rahimdokht M (2014) Discoloration of wastewater in a continuous electro-Fenton process using modified graphite electrode with multi-walled carbon nanotubes/surfactant. Sep Purif Technol 130:34–44. doi: 10.1016/j.seppur.2014.04.025
Panizza M, Cerisola G (2001) Removal of organic pollutants from industrial wastewater by electrogenerated Fenton's reagent. Water Res 35:3987–3992. doi: 10.1016/S0043-1354(01)00135-X
Panizza M, Dirany A, Sirés I, et al (2014) Complete mineralization of the antibiotic amoxicillin by electro-Fenton with a BDD anode. J Appl Electrochem 44:1327–1335. doi: 10.1007/s10800-014-0740-9
Panizza M, Michaud P a., Cerisola G, Comninellis C (2001) Anodic oxidation of 2-naphthol at boron-doped diamond electrodes. J Electroanal Chem 507:206–214. doi: 10.1016/S0022-0728(01)00398-9
Panizza M, Oturan MA (2011) Degradation of Alizarin Red by electro-Fenton process using a graphite-felt cathode. Electrochim Acta 56:7084–7087. doi: 10.1016/j.electacta.2011.05.105
Pérez JF, Llanos J, Sáez C, et al (2016) Electrochemical jet-cell for the in-situ generation of hydrogen peroxide. Electrochem commun 71:65–68. doi: 10.1016/j.elecom.2016.08.007
Pignatello JJ (1992) Dark and photoassisted iron(3+)-catalyzed degradation of chlorophenoxy herbicides by hydrogen peroxide. Environ Sci Technol 26:944–951. doi: 10.1021/es00029a012
Pimentel M, Oturan N, Dezotti M, Oturan MA (2008) Phenol degradation by advanced electrochemical oxidation process electro-Fenton using a carbon felt cathode. Appl Catal B Environ 83:140–149. doi: 10.1016/j.apcatb.2008.02.011
Plakas K V., Sklari SD, Yiankakis DA, et al (2016) Removal of organic micropollutants from drinking water by a novel electro-Fenton filter: Pilot-scale studies. Water Res 91:183–

194. doi: 10.1016/j.watres.2016.01.013
Pliego G, Zazo J a., Garcia-Muñoz P, et al (2015) Trends in the intensification of the Fenton process for wastewater treatment: an overview. Crit Rev Environ Sci Technol 45:2611–2692. doi: 10.1080/10643389.2015.1025646
Prabhakaran D, Kannadasan T, Basha CA (2009) Treatability of resin effluents by electrochemical oxidation using batch recirculation reactor. Int J Environ Sci Tech 6:491–498. doi: 10.1007/BF03326088
Pulgarin C, Invernizzi M, Parra S, et al (1999) Strategy for the coupling of photochemical and biological flow reactors useful in mineralization of biorecalcitrant industrial pollutants. Catal Today 54:341–352. doi: 10.1016/S0920-5861(99)00195-9
Radjenovic J, Sedlak DL (2015) Challenges and opportunities for electrochemical processes as next-generation technologies for the treatment of contaminated water. Environ Sci Technol 49:11292–11302. doi: 10.1021/acs.est.5b02414
Ren G, Zhou M, Liu M, et al (2016) A novel vertical-flow electro-Fenton reactor for organic wastewater treatment. Chem Eng J 298:55–67. doi: 10.1016/j.cej.2016.04.011
Rivero EP, Rivera FF, Cruz-Díaz MR, et al (2012) Numerical simulation of mass transport in a filter press type electrochemical reactor FM01-LC: Comparison of predicted and experimental mass transfer coefficient. Chem Eng Res Des 90:1969–1978. doi: 10.1016/j.cherd.2012.04.010
Rodrigo MA, Oturan MA, Oturan N (2014) Electrochemically assisted remediation of pesticides in soils and water: A review. Chem Rev 114:8720–8745. doi: 10.1021/cr500077e
Rosales E, Iglesias O, Pazos M, Sanromán MA (2012a) Decolourisation of dyes under electro-Fenton process using Fe alginate gel beads. J Hazard Mater 213–214:369–377. doi: 10.1016/j.jhazmat.2012.02.005
Rosales E, Iglesias O, Pazos M, Sanromán MAÁ (2012b) Decolourisation of dyes under electro-Fenton process using Fe alginate gel beads. J Hazard Mater 213–214:369–377. doi: 10.1016/j.watres.2016.01.013
Rosales E, Pazos M, Longo MA, Sanromán MA (2009) Electro-Fenton decoloration of dyes in a continuous reactor: a promising technology in colored wastewater treatment. Chem Eng J 155:62–67. doi: 10.1016/j.cej.2009.06.028
Roshini PS, Gandhimathi R, Ramesh ST, Nidheesh P V (2017) Combined electro-Fenton and biological processes for the treatment of industrial textile effluent : mineralization and toxicity analysis. J Hazard Toxic Radioact Waste. doi: 10.1061/(ASCE)HZ.2153-5515.0000370.
Sabatino S, Galia A, Scialdone O (2016) Electrochemical abatement of organic pollutants in continuous-reaction systems through the assembly of microfluidic cells in series. 83–90. doi: 10.1002/celc.201500409
Santana-martínez G, Roa-morales G, Martin E, et al (2016) Electro-Fenton and electro-Fenton-like with in situ electrogeneration of H2O2 and catalyst applied to 4-chlorophenol mineralization. Electrochim Acta 195:246–256. doi: 10.1016/j.electacta.2016.02.093
Santos JLC, Geraldes V, Velizarov S, Crespo JG (2010) Characterization of fluid dynamics and mass-transfer in an electrochemical oxidation cell by experimental and CFD studies. Chem Eng J 157:379–392. doi: 10.1016/j.cej.2009.11.021
Saussereau E, Lacroix C, Guerbet M, et al (2013) Determination of levels of current drugs in hospital and urban wastewater. Bull Environ Contam Toxicol 91:171–176. doi: 10.1007/s00128-013-1030-7
Scialdone O, Galia A, Gattuso C, et al (2013) Electro-generation of H2O2 and abatement of organic pollutant in water by an electro-Fenton process in a microfluidic reactor.

Electrochem commun 26:45–47. doi: 10.1016/j.electacta.2015.09.109
Scialdone O, Galia A, Sabatino S (2014) Abatement of acid orange 7 in macro and micro reactors. Effect of the electrocatalytic route. Appl Catal B Environ 148–149:473–483. doi: 10.1016/j.apcatb.2013.11.005
Scott JP, Ollis DF (1995) Integration of chemical and biological oxidation processes for water treatment: review and recommendations. Environ Prog 14:88–103. doi: 10.1002/ep.670140212
Shukla P, Singh KK, Gupta PK, Ghosh SK (2012) Numerical simulation of flow electrolysers : effect of various geometric parameters.
Simond O, Schaller V, Comninellis C (1997) Theoretical model for the anodic oxidation of organics on metal oxide electrodes. Electrochim Acta 42:2009–2012. doi: 10.1016/S0013-4686(97)85475-8
Sirés I, Arias C, Cabot PL, et al (2004) Paracetamol mineralization by advanced electrochemical oxidation processes for wastewater treatment. Environ Chem 1:26–28. doi: 10.1071/EN04018
Sirés I, Brillas E, Oturan MA, et al (2014) Electrochemical advanced oxidation processes: today and tomorrow. A review. Environ Sci Pollut Res 21:8336–8367. doi: 10.1007/s11356-014-2783-1
Sirés I, Garrido JA, Rodríguez RM, et al (2007a) Catalytic behavior of the Fe3+/Fe2+ system in the electro-Fenton degradation of the antimicrobial chlorophene. Appl Catal B Environ 72:382–394. doi: 10.1016/j.apcatb.2006.11.016
Sirés I, Oturan N, Oturan MA (2010) Electrochemical degradation of beta-blockers. Studies on single and multicomponent synthetic aqueous solutions. Water Res 44:3109–3120. doi: 10.1016/j.watres.2010.03.005
Sirés I, Oturan N, Oturan MA, et al (2007b) Electro-Fenton degradation of antimicrobials triclosan and triclocarban. Electrochim Acta 52:5493–5503. doi: 10.1016/j.electacta.2007.03.011
Skoumal M, Arias C, Cabot PL, et al (2008) Mineralization of the biocide chloroxylenol by electrochemical advanced oxidation processes. Chemosphere 71:1718–1729. doi: 10.1016/j.chemosphere.2007.12.029
Skoumal M, Rodríguez RM, Cabot PL, et al (2009) Electro-Fenton, UVA photoelectro-Fenton and solar photoelectro-Fenton degradation of the drug ibuprofen in acid aqueous medium using platinum and boron-doped diamond anodes. Electrochim Acta 54:2077–2085. doi: 10.1016/j.electacta.2008.07.014
Smith JR, Walsh FC (1998) Reviews in applied electrochemistry. Number 50 - Electrodes based on Magneli phase titanium oxides: the properties and applications of Ebonex (R) materials. J Appl Electrochem 28:1021–1033. doi: 10.1023/A:1003469427858
Sopaj F, Oturan N, Pinson J, et al (2016) Effect of the anode materials on the efficiency of the electro-Fenton process for the mineralization of the antibiotic sulfamethazine. Appl Catal B Environ 199:331–341. doi: 10.1016/j.apcatb.2016.06.035
Su C-C, Pagaling E., Peralta GL, Lu MC (2013) Comparison of aniline degradation by Fenton and electro-Fenton reactors using plate and rod electrodes. Environ Prog Sustain Energy 32:1111–1117. doi: 10.1002/ep
Tian J, Olajuyin AM, Mu T, et al (2016) Efficient degradation of rhodamine B using modified graphite felt gas diffusion electrode by electro-Fenton process. Environ Sci Pollut Res 23:11574–11583. doi: 10.1007/s11356-016-6360-7
Trellu C, Ganzenko O, Papirio S, et al (2016) Combination of anodic oxidation and biological treatment for the removal of phenanthrene and Tween 80 from soil washing solution. Chem Eng J 306:588–596. doi: 10.1016/j.cej.2016.07.108
Umar M, Aziz HA, Yusoff MS (2010) Trends in the use of Fenton, electro-Fenton and photo-

Fenton for the treatment of landfill leachate. Waste Manag 30:2113–2121. doi: 10.1016/j.wasman.2010.07.003
Vasudevan S, Oturan MA (2014) Electrochemistry: as cause and cure in water pollution-an overview. Environ Chem Lett 12:97–108. doi: 10.1007/s10311-013-0434-2
Vázquez L, Alvarez-Gallegos A, Sierra FZ, et al (2013) CFD evaluation of internal manifold effects on mass transport distribution in a laboratory filter-press flow cell. J Appl Electrochem 43:453–465. doi: 10.1007/s10800-013-0530-9
Wang A, Li YY, Ru J (2010a) The mechanism and application of the electro-Fenton process for azo dye Acid Red 14 degradation using an activated carbon fibre felt cathode. J Chem Technol Biotechnol 85:1463–1470. doi: 10.1002/jctb.2450
Wang A, Qu J, Ru J, et al (2005) Mineralization of an azo dye Acid Red 14 by electro-Fenton's reagent using an activated carbon fiber cathode. Dye Pigment 65:227–233. doi: 10.1016/j.dyepig.2004.07.019
Wang CT, Chou WL, Chung MH, Kuo YM (2010b) COD removal from real dyeing wastewater by electro-Fenton technology using an activated carbon fiber cathode. Desalination 253:129–134. doi: 10.1016/j.desal.2009.11.020
Wang J, Li T, Zhou M, et al (2015) Characterization of hydrodynamics and mass transfer in two types of tubular electrochemical reactors. Electrochim Acta 173:698–704. doi: 10.1016/j.electacta.2015.05.135
Wang Q, Lemley AT (2001) Kinetic model and optimization of 2,4-D degradation by Anodic Fenton treatment. Environ Sci Technol 35:4509–4514. doi: 10.1021/es0109693
Xu A, Han W, Li J, et al (2016) Electrogeneration of hydrogen peroxide using Ti/IrO2-Ta2O5 anode in dual tubular membranes Electro-Fenton reactor for the degradation of tricyclazole without aeration. Chem Eng J 295:152–159. doi: 10.1016/j.cej.2016.03.001
Yahiaoui I, Aissani-Benissad F, Fourcade F, Amrane A (2013) Removal of tetracycline hydrochloride from water based on direct anodic oxidation (Pb/PbO2 electrode) coupled to activated sludge culture. Chem Eng J 221:418–425. doi: 10.1016/j.cej.2013.01.091
Yahya MS, El Karbane M, Oturan N, et al (2016) Mineralization of the antibiotic levofloxacin in aqueous medium by electro-Fenton process: kinetics and intermediate products analysis. Environ Technol 37:1276–1287. doi: 10.1080/09593330.2015.1111427
Yahya MS, Oturan N, El Kacemi K, et al (2014) Oxidative degradation study on antimicrobial agent ciprofloxacin by electro-fenton process: Kinetics and oxidation products. Chemosphere 117:447–454. doi: 10.1016/j.chemosphere.2014.08.016
Yang JI, Wang JUN, Jia J (2009) Improvement of electrochemical wastewater treatment through mass transfer in a seepage carbon nanotube electrode reactor. 43:3796–3802.
Yu F, Zhou M, Zhou L, Peng R (2014) A novel electro-Fenton process with H2O2 generation in a rotating disk reactor for organic pollutant degradation. Environ Sci Technol Lett 1:320–324. doi: 10.1021/ez500178p
Yu X, Zhou M, Ren G, Ma L (2015) A novel dual gas diffusion electrodes system for efficient hydrogen peroxide generation used in electro-Fenton. Chem Eng J 263:92–100. doi: 10.1016/j.cej.2014.11.053
Yuan S, Fan Y, Zhang Y, et al (2011) Pd-catalytic in situ generation of H2O2 from H2 and O2 produced by water electrolysis for the efficient electro-fenton degradation of rhodamine B. Environ Sci Technol 45:8514–20. doi: 10.1021/es2022939
Yuan SH, Lu XH (2005) Comparison treatment of various chlorophenols by electro-Fenton method: Relationship between chlorine content and degradation. J Hazard Mater 118:85–92. doi: 10.1016/j.jhazmat.2004.08.025
Zhang H, Fei C, Zhang D, Tang F (2007) Degradation of 4-nitrophenol in aqueous medium by electro-Fenton method. J Hazard Mater 145:227–232. doi:

10.1016/j.jhazmat.2006.11.016
Zhang H, Ran X, Wu X (2012) Electro-Fenton treatment of mature landfill leachate in a continuous flow reactor. J Hazard Mater 241–242:259–266. doi: 10.1016/j.jhazmat.2012.09.040
Zhang H, Wan X, Li G, Zhang F (2017) A three-electrode electro-Fenton system supplied by self-generated oxygen with automatic pH-regulation for groundwater remediation. Electrochim Acta 250:42–48. doi: 10.1016/j.electacta.2017.08.040
Zhang Y, Wei K, Han W, et al (2016) Improved electrochemical oxidation of tricyclazole from aqueous solution by enhancing mass transfer in a tubular porous electrode electrocatalytic reactor. Electrochim Acta 189:1–8. doi: 10.1016/j.electacta.2015.10.119
Zhou M, Yu Q, Lei L, Barton G (2007) Electro-Fenton method for the removal of methyl red in an efficient electrochemical system. Sep Purif Technol 57:380–387. doi: 10.1016/j.seppur.2007.04.021
Zhu X, Tian J, Liu R, Chen L (2011) Optimization of Fenton and electro-Fenton oxidation of biologically treated coking wastewater using response surface methodology. Sep Purif Technol 81:444–450. doi: 10.1016/j.seppur.2011.08.023

CHAPTER 2

Electro-Fenton treatment of different pharmaceuticals under study: Kinetic study, energy consumption, mineralization pathway

This chapter was adapted from published or submitted articles:

- **Efficient removal of diuretic hydrochlorothiazide from water by electro-Fenton process using BDD anode: a kinetic and degradation pathway study**
- **Electro-Fenton treatment of the widely used analgesic tramadol using BDD anode: a kinetic, energetic and degradation pathway study**
- **Complete study of the mineralization and degradation of the b-blocker Nadolol by electro-Fenton, comparison of different anodes**

1. Introduction

Nowadays, the elimination of pharmaceuticals from wastewaters has become a hot topic as these products are widely consumed all over the world. As an example, in western Europe around 300 mg of active substances are consumed every day per inhabitant (Khetan and Collins 2007; Bouissou-Schurtz et al. 2014; Luo et al. 2014; Vergili et al. 2019) and are hardly removed by wastewater treatment plants (WWTP). Indeed, between 60 and 90% of them remain in the environment. A study monitored around 50 pharmaceuticals after their treatment in WWTP in Europe and the United States; the average % of elimination was less than 50% (Jones et al. 2005; Margot et al. 2015). Once used, pharmaceuticals are eliminated in whole or in part by the human or animal bodies and then enter into the wastewaters of hospitals or municipalities. Wastewaters from pharmaceutical industries constitute another main source of drugs in natural water (Lindsey et al. 2001; Kabdasli et al. 2019). As these molecules are highly active, they can be harmful toward the environment (Boxall 2004; Küster and Adler 2014). Therefore, their elimination from wastewater using an efficient treatment process constitutes an important issue.

The diuretic hydrochlorothiazide (HCT) used for anti-hypertensive medications, is of particular interest as it was recently found both in hospital effluent (Mendoza et al. 2015) and in surface water (Bouissou-Schurtz et al. 2014). Indeed, this molecule was shown to have an average removal rate of 30% from typical WWTP (Margot et al. 2015). In addition, this molecule was reported to be hazardous toward the environment (Fernández et al. 2010) and therefore needs to be efficiently destroyed before being released into natural water body.

Nadolol (Nad) belongs to the β-blockers, it was chosen as it was detected in wastewaters since it is not completely removed by wastewater treatment plants (Gabet-Giraud et al. 2010). Additionally, it is harmful toward the environment (Khetan and Collins 2007).

Tramadol (TMD) is a centrally acting analgesic used in case of moderate to severe pain (Ghalwa et al. 2014; Antonopoulou and Konstantinou 2016). This medicine is widely used, as an

example in 2012 around 24 tons of TMD was prescribed in Germany (Lütke Eversloh et al. 2015). It was not efficiently removed by WWTPs as it was detected in effluents from households and hospitals even after treatment and in surface waters (Hummel et al. 2006; Rúa-Gómez and Püttmann 2012; Rúa-Gómez and Püttmann 2013).

Ofloxacin (OFL) belongs to the antibiotic family which is particularly toxic to micro-organisms. This molecule was found both in hospital effluents and surface water (Table 2) (Verlicchi et al. 2010). The presence of antibiotics in the environment leads to chronic toxicity and to the development of antibiotic resistant bacteria, this is why the substances have to be removed from wastewaters (Pulicharla et al. 2015; Changotra et al. 2017; Yu et al. 2019).

To eliminate persistent pharmaceuticals, the use of highly strong oxidants is thus compulsory. Hydroxyl radicals (•OH) seem to be a promising tool as being the second strongest oxidant after fluorine. They can degrade nearly any type of contaminants thanks to their very high oxidation potential ($E°_{(•OH/H_2O)}$ = 2.8 V vs SHE in acidic medium) (Sirés and Brillas 2012). The advanced oxidation processes (AOPs) (Oturan and Aaron 2014) and particularly electrochemical AOPs (EAOPs) (Brillas et al. 2009; Panizza and Cerisola 2009; Sirés et al. 2014; Nidheesh et al., 2018) are interesting processes for removal of organic pollutants from water as they have shown their ability in high oxidation rate and quasi-complete mineralization yield (Bellakhal et al. 2006; Faouzi et al. 2006; Dirany et al. 2012; Özcan et al. 2013; Mousset et al. 2016). The electro-Fenton (EF) is one of most popular EAOPs being an environmentally friendly and effective process to destroy organic pollutants (Oturan et al. 2000; Ganiyu et al. 2018; Monteil et al. 2019). That is why this process was chosen to treat the pharmaceutical solutions.

This process is based on the generation of •OH through Fenton's reaction (Eq. 19) in which Fenton's reagent (H_2O_2 + Fe^{2+}) is in situ electrochemically generated (H_2O_2, Eq. 20) or regenerated (Fe^{2+}, Eq. 21) from Fe^{3+} produced in Fenton's reaction (Oturan 2000; Brillas et al.

2009).

$$Fe^{2+} + H_2O_2 \rightarrow Fe^{3+} + OH + {}^{\bullet}OH^{-} \quad (19)$$

$$O_2 + 2\,H^{+} + 2\,e^{-} \rightarrow H_2O_2 \quad (20)$$

$$Fe^{3+} + e^{-} \rightarrow Fe^{2+} \quad (21)$$

The process is electrocatalytic since the catalyst (Fe^{2+}) is continuously electro-generated at the cathode. Comparing with classical Fenton's process, the EF process presents several advantages (Nidheesh and Gandhimathi 2012; Oturan and Aaron 2014) such as i) the in situ production of H_2O_2 avoiding the reagent cost and risks related to its transport and storage, ii) avoiding the precipitation of iron ion (catalyst) under ($Fe(OH)_3$ form because of its very low concentration and thus the formation of process sludge, iii) avoiding or decreasing significantly the rate of wasting reactions consuming $^{\bullet}OH$ because of very low concentration of Fenton's reagent in the system.

When using an appropriate anode such as BDD, the process becomes even more efficient (Oturan et al. 2012; Sopaj et al. 2016) due to the formation of heterogeneous hydroxyl radicals M($^{\bullet}OH$) on the anode surface from electrochemical oxidation of water (Eq. 22). The M($^{\bullet}OH$) thus formed are physically adsorbed on anode (M) in the case of non-active anodes like BDD, and are available for oxidation of organics (Panizza and Cerisola 2005; Rodrigo et al. 2010; Nidheesh et al., 2019).

$$M + H_2O \rightarrow M({}^{\bullet}OH) + H^{+} + 2\,e^{-} \quad (22)$$

Therefore, this study presents, for the first time, a detailed investigation of oxidative degradation (including kinetics data) and mineralization of the four pharmaceuticals from different families by the EF process with a BDD anode. The comparison with a Pt anode was performed for the HCT. The electrical energy consumed for almost complete mineralization was also considered. Preliminary experiments were carried out to find optimal operating

conditions. The oxidation reaction intermediates and carboxylic acids as well as inorganic ions were identified using GC-MS, LC-MS, HPLC and ion chromatography analyses, and their evolution during electrolysis was followed. Finally, based on this information, a plausible mineralization reaction pathway was proposed for three pharmaceuticals (HCT, TMD, OFL).

2. Material and methods

2.1. Chemicals

All chemicals used in this study were analytical grade and used as received without further purification. The pharmaceuticals HCT, TMD, Nad and OFL were supplied by Sigma Aldrich. Iron (II) sulfate heptahydrate (catalyst source, 99%) was purchased from Acros Organics. Sodium sulfate (Na_2SO_4) (supporting electrolyte), potassium sulfate (K_2SO_4), sodium perchlorate ($NaClO_4$), potassium phosphate monobasic, iron(II) perchlorate were supplied by Sigma-Aldrich, Merck, and Acros. Short-chain carboxylic acids (oxalic acid, oxamic acid, acetic acid and maleic acid were obtained from Acros, Fluka and Alfa Aesar. The pollutant solutions were prepared with ultrapure water obtained from a Millipore Milli-Q Simplicity 185 system with resistivity >18 MΩ cm at 25 °C. The pH of solutions was adjusted using analytical grade sulfuric acid (Acros). Organic solvents and other chemicals used were HPLC or analytic grade from Sigma-Aldrich, Fluka and Merck.

2.2. Electrochemical equipment

All the experiments were performed in an undivided cylindrical glass cell of 7 cm diameter and with a capacity of 250 mL at room temperature. The 230 mL solution was vigorously stirred by

a magnetic PTFE bar to have a good mass transport between the electrodes and compressed air was continuously bubbled into the cell through a silica frit. The air bubbling was started 5 min prior to electrolysis to ensure O_2 saturation in the solution. The electrochemical cell was equipped with a 3D carbon felt (18.0 cm × 5.0 cm × 0.5 cm, from Mersen, France), placed on the inner wall of the cell covering the total internal perimeter as the cathode and a 25-cm^2 BDD film on niobium support as the anode (from CONDIAS GmbH, Germany). A platinum anode with a similar area is used for a few experiments. CyberScan pH 1500 pH meter from Eutech Instruments was used to adjust the solution pH to 3.0 (well-known as the optimal value for electro-Fenton process (Kremer 2003; Brillas et al. 2009) using a 1 M H_2SO_4 or NaOH solution. A constant current, ranging between 50 and 1000 mA, was supplied with a Hameg HM8040 triple power DC supply.

2.3. Analytical methods and procedures

The concentration decay of pharmaceutical degradation experuments was monitored by HPLC using a Merck Lachrom Liquid chromatography equipped with a reverse phase column Purospher RP-18, 5 μm, 25 cm × 4.6 mm (i.d.) column and coupled with a diode array detector (DAD). Samples of 20 μL were injected in the column at 40°C. For the HCT, the detector was set at λ = 270 nm and the mobile phase composed of methanol / water 25:75 (v/v) was eluted at a flow rate of 0.5 mL min^{-1}. For TMD, the mobile phase was a mixture of methanol / phosphate buffer 40:60 (v/v) at a flowrate of 0.6 mL min^{-1}. The wavelength of detection was 228 nm. The phosphate buffer was composed of 3.5 g of potassium phosphate monobasic and 17.8 g of dipotassium hydrogen phosphate in 1 L of ultra-pure water and the pH was adjusted to 6.0 using orthophosphoric acid. For the nadolol, the mobile phase was composed of an acetate buffer and methanol (63/37 v/v) at 0.4 mL min^{-1}. The buffer was made of 0.1 M of sodium acetate and the pH adjusted to 6 by acetic acid. The wavelength of detection was 277

nm. Finally, the OFL was eluted by a mobile phase made of acetonitrile and acetate buffer 20/80 (v/v) at 0.5 mL min^{-1} and detected at 292 nm. The buffer was composed of 0.05 mol L^{-1} of citric acid and of 1 mol L^{-1} of ammonium acetate.

The short-chain carboxylic acids were identified and quantified by the same HPLC equipped with a Biorad column (9 µm, 250 mm × 4.6 mm) and the DAD detector was set at 220 nm. The mobile phase was a solution of H_2SO_4 at a concentration of 4 mM with a flow rate of 0.6 mL min^{-1}. Carboxylic acids were identified by comparison of their retention time with that of standard solutions and their quantification was achieved thanks to calibration curves.

Nitrate, nitrite, chloride, sulfate and fluoride ions released to the treated solutions were analyzed using a Dionex ICS-1000 Basic Ion Chromatography (IC) system equipped with a DS56 conductivity detector containing a cell heated at 35 °C using an Ion Pac AS4A-SC, 25 cm× 4 mm (i.d.), anion-exchange column, linked to an IonPac AG4A-SC, 5 cm × 4 mm (i.d.), column guard. The eluent was a mixture of 1.7 mM sodium bicarbonate ($NaHCO_3$) and 1.8 mM sodium carbonate (Na_2CO_3) at a flow rate of 1 mL min^{-1}. An ASRS-ULTRA II self-regenerating suppressor was used in order to improve the sensitivity of the detector. For ammonium ion detection, the same IC equipped with an IonPac CS12A, 25 cm × 4 mm (i.d.), cation-exchange column, linked to an IonPac CG12A, 5 cm × 4 mm (i.d.), column guard was used. Again, an electrochemical suppressor (CRS-ULTRA II) was employed, the. The eluent was a solution of 9.0 mM sulfuric acid at a flow rate of 1.0 mL min^{-1}. The volume of injections was 25 µL for the anions and the cations.

The mineralization degree of treated solutions was measured thanks to the total organic carbon (TOC) removal of the samples withdrawn from the treated solution at different electrolysis times. The TOC measurement was monitored by a Shimadzu VCSH TOC analyzer according to the 680 °C catalytic combustion method using platinum as catalyst. The injection volume was 50 µL. Reproducible TOC values with ± 2% accuracy were found using the non-purgeable

organic carbon method. The TOC abatement was calculated by dividing the TOC at time t by the TOC at the initial time.

From these data, the mineralization current efficiency (MCE) value for each trial was then estimated from Eqs. 23.

$$MCE(\%) = \frac{n\,F\,V\,(TOC(0)-TOC(t))}{4.32 * 10^7 m\,I\,t} * 100 \quad (23)$$

where TOC(0) –TOC(t) is the TOC decay (mg carbon L^{-1}), m is the number of carbon atoms of the molecule studied, t is the time of electrolysis (h), I is the applied current (A), V is the volume of the solution (L), 4.32 × 10^7 is a conversion factor to homogenize units and n is the number of electrons used to mineralize one molecule of pollutant into CO_2, H_2O and inorganic ions (NH_4^+, SO_4^{2-}, F^- and Cl^-) following the electrochemical combustion reaction as shown in Eqs. 24 a, b, c and d for HCT, TMD, Nad and OFL, respectively. The ion analysis showed that ammonium was formed dominantly (compared to nitrate), thus in the equations, were written considering ammonium as released nitrogen ion.

$$C_7H_8ClN_3O_4S_2 + 18H_2O \rightarrow 7CO_2 + 32H^+ + 2SO_4^{2-} + 3NH_4^+ + Cl^- + 30e^- \quad (24a)$$

$$C_{16}H_{25}NO_2 + 30H_2O \rightarrow 16CO_2 + 81H^+ + NH_4^+ + 82e^- \quad (24b)$$

$$C_{17}H_{27}NO_4 + 30H_2O \rightarrow 17CO_2 + NH_4^+ + 83H^+ + 84e^- \quad (24c)$$

$$C_{18}H_{20}FN_3O_4 + 32H_2O \rightarrow 18CO_2 + F^- + 3NH_4^+ + 72H^+ + 74e^- \quad (24d)$$

The energy consumed in kWh per g TOC removed was evaluated from Eq. 25.

$$EC\left(\frac{kWh}{gTOC}\right) = \frac{ECell*I*t}{(TOC(0)-TOC(t))*V} \quad (25)$$

GC-MS analyses were done by using a Thermo Scientific devise equipped with a TRACE 1300 gas chromatography coupled to an ISQ single quadrupole mass spectrophotometer operating in electron ionization mode at 70 eV. A 1 mM HCT and TMD solutions were electrolyzed during

10 min and 8 min respectively and then the 230 mL aqueous solutions were extracted two times with ethyl acetate and dichloromethane. Then the organic phase was dried over $MgSO_4$, filtered and concentrated to dryness with a rotary evaporator under vacuum. A few drops of ethyl acetate were added into the flask to dilute the residual solid phase and 3 µL of this solution were then injected into the GC-MS analyser through a TG-5Ms 0.25 mm, 30 m 0.25 mm (i.d.), column. The temperature of the injector and detector were 200 and 250°C, respectively. Helium was used as carrier gas at a flow rate of 1.5 mL min^{-1}. The temperature ramp was as following for the HCT: 40°C (held during 2 min), 10 °C min^{-1} to 280°C and 4 min at 280 °C and for the TMD: 100 °C during 1 min, 20 °C min^{-1} to 280 °C and kept at this temperature for 15 min. The mass spectra were identified by using Xcalibur datalibrary software for the aliphatic molecules and by analyzing the different mass spectrum for the aromatic compounds. For the aliphatic molecules, a derivatization procedure was used. 100 µL of the solution containing the solid phase diluted in ethyl acetate was added to 100 µL of BSTFA (N,O-bis-(trimethylsilyl)trifluoroacetamide), the final solution was put at 80°C for 1 h in an incubator. Then the mixture was cooled to room temperature and 3 µL were injected into the GC-MS.

LC-MS analysis were performed for the Nad and the OFL using an Hypersil Gold column (100 mm × 2.1 mm) 1.9 µ, at 40 °C and with a liquid flowrate of 0.2 mL min^{-1}. After drying the sample, the OFL was diluted in 1 mL of methanol / water 50/50 (v/v) and eluted by 0.1% formic acid / methanol 80/20 (v/v). Concerning the MS conditions, the ESI^+ (electrospray ionization) mode was used at 90 V. For the Nad, the evaporated solution was diluted in 1 mL of water and eluted by the same conditions. The ESI^+ mode was also used at 75 V.

When error bars are given on the graphs, they are calculated based on the standard deviation of the different experiments.

3. Results and Discussion

3.1. Influence of the operating parameters on the degradation kinetics

There are several parameters affecting the performance of the EF process during oxidation of organic pollutants. Among these parameters some are now well-known (Brillas et al. 2009; Oturan and Oturan 2018): solution pH (= 3.0), nature of the catalyst (Fe^{2+}), nature of electrolyte (Na_2SO_4). The temperature has a very little effect. However, for a given anode/cathode couple, the effect of two parameters: concentration of the catalyst (Fe^{2+}) and the value of applied current, should be studied to have optimal operating values for an effective treatment. The nature of the anode is also very important to have an efficient degradation.

3.1.1. Effect of the concentration of Fe^{2+}

The concentration of ferrous irons, used as catalyst, is one of the key parameters for an effective degradation of organic pollutants because it is directly linked to the formation of $^{\bullet}OH$ through Fenton's reaction (Eq. 19). To clarify the effect of catalyst concentration, experiments were done using 0.1 mM concentration of pharmaceuticals at 100 mA constant current. As shown in Figs. 12-15, rising the concentration of Fe^{+} from 0.05 mM to 0.1 mM (from 0.05 mM to 0.2 mM for the case of TMD, Fig. 13) increases the amount of $^{\bullet}OH$ formed and thus allows a quicker degradation of pharmaceuticals. However the concentrations above 0.1 mM Fe^{2+} for HCT, OFL and Nad and 0.2 mM for TMD lead to a decrease in oxidation kinetics that can be explained by the increase of the rate of the wasting reaction given in Eq. 26. Indeed, at high concentration of Fe^{2+}, this reaction can compete with oxidation of the pollutants for $^{\bullet}OH$ leading to a decrease in degradation kinetics (Panizza and Cerisola 2001; Dominguez et al. 2018b).

$$^{\bullet}OH + Fe^{2+} \rightarrow Fe^{3+} + OH^{-} \quad (26)$$

To evaluate quantitatively the effect of iron concentration on degradation rate of the pollutants, apparent rate constants of oxidation reaction were calculated assuming pseudo-first order reaction kinetics. Indeed, the experimental conditions being kept constant during the experiments, the formation rate of •OH/M(•OH) can be considered constant. On the other hand, the steady-state assumption can be applied to the concentration of hydroxyl radicals as they are very reactive species and cannot be accumulate in the medium (Sirés et al. 2007a; Brillas et al. 2009). Indeed the exponential decrease of the concentration in each case confirms this hypothesis. Accordingly, the value of apparent rate constant for oxidation of pharmaceuticals can be calculated from the slop of the straight lines obtained by plotting Ln (C/C_0) = f(t) as shown on the inset panels of the Figs. 12-15.

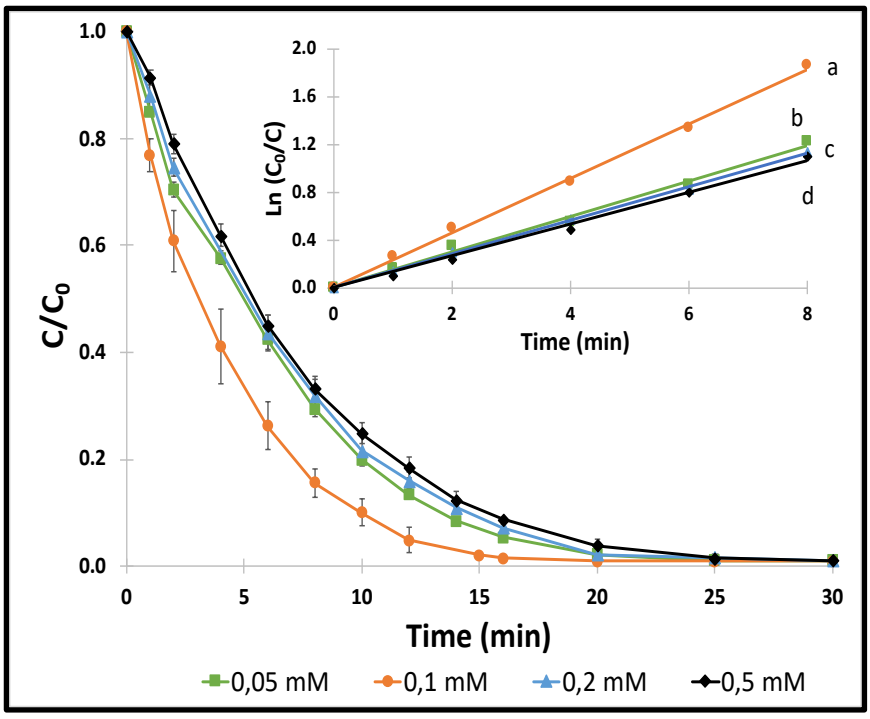

Fig. 12: Effect of catalyst (Fe^{2+}) concentration on the normalized HCT concentration decay kinetics at 100 mA constant current. $[HCT]_0$ = 0.1 mM, $[Na_2SO_4]_0$ = 0.05 M. a: y = 0.23x, R^2 = 0.998, b: y = 0.15x, R^2 = 0.993, c: y = 0.14x, R^2 = 0.999 and d: y = 0.13x, R^2 = 0.993.

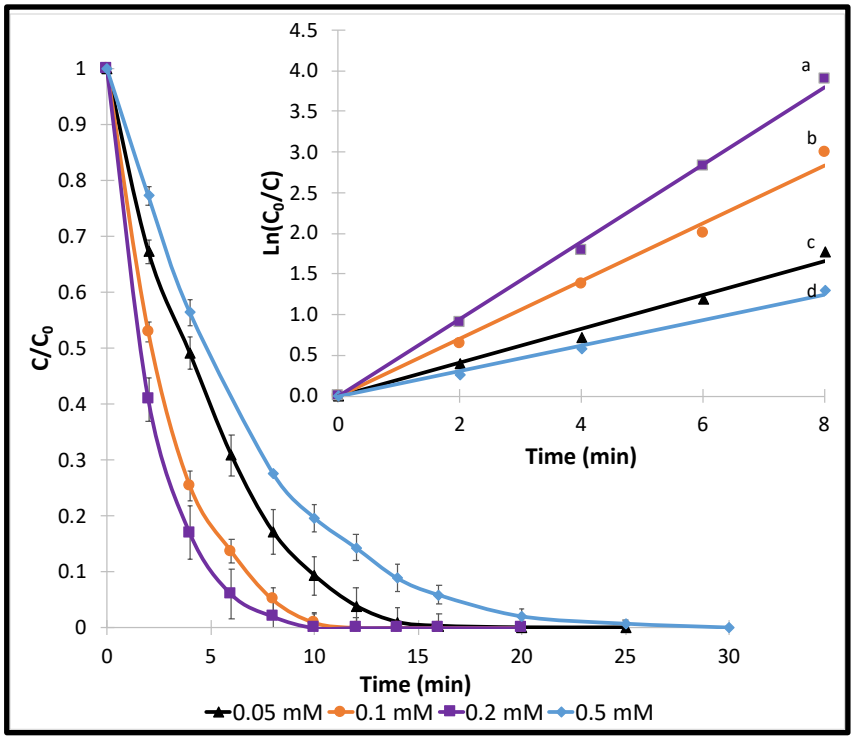

Fig. 13: Effect of catalyst (Fe^{2+}) concentration on the normalized TMD concentration decay kinetics at 100 mA constant current. $[TMD]_0$ = 0.1 mM, $[Na_2SO_4]_0$ = 0.05 M. a: y = 0.47x, R^2 = 0.997, b: y = 0.36x, R^2 = 0.990, c: y = 0.21x, R^2 = 0.984 and d: y = 0.16x, R^2 = 0.992.

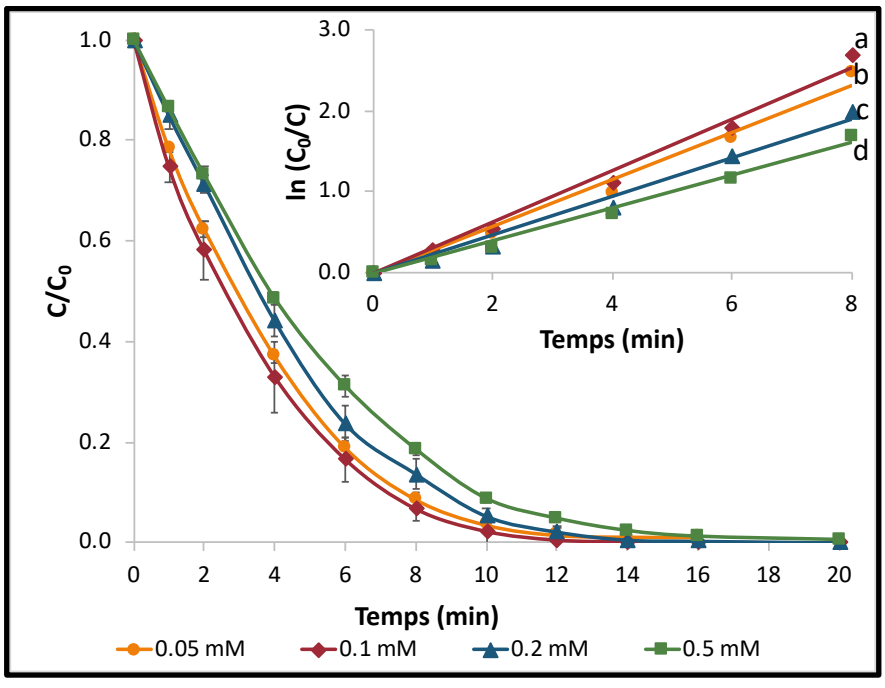

Fig. 14: Effect of catalyst (Fe^{2+}) concentration on the normalized OFL concentration decay kinetics at 100 mA constant current. $[OFL]_0$ = 0.1 mM, $[Na_2SO_4]_0$ = 0.05 M. a: y = 0.32x, R^2 = 0.9863, b: y = 0.29x, R^2 = 0.9853, c: y = 0.24x, R^2 = 0.9838 and d: y = 0.20x, R^2 = 0.9884.

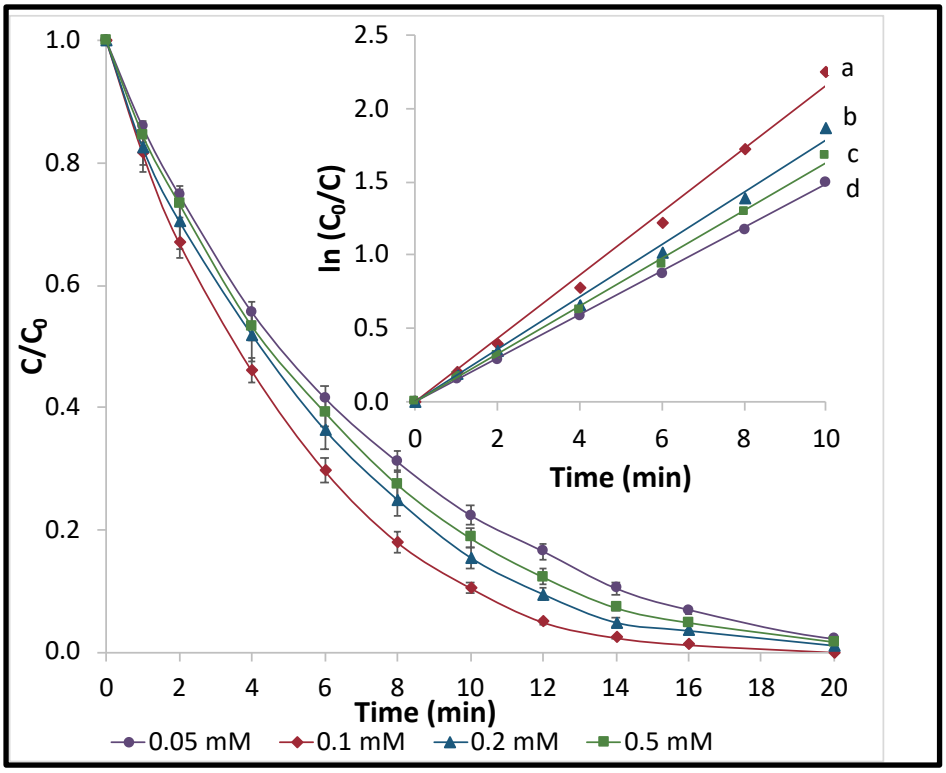

Fig. 15: Effect of catalyst (Fe^{2+}) concentration on the normalized Nad concentration decay kinetics at 100 mA constant current. $[Nad]_0$ = 0.1 mM, $[Na_2SO_4]_0$ = 0.05 M. a: y = 0.22x, R^2 = 0.9943, b: y = 0.18x, R^2 = 0.9945, c: y = 0.16x, R^2 = 0.9978 and d: y = 0.15x, R^2 = 0.9996.

3.1.2. Effect of the applied current on the degradation kinetics

The applied current is one of the most important parameters in EAOPs in general and in EF in particular for the degradation of organic pollutants. Figs. 16-19 illustrate the results obtained for currents ranged from 50 to 500 mA. For all the currents, the mass transfer is limiting the reaction. These results highlight that high current values promote the oxidative degradation kinetics of pharmaceutical under study due to the increase in the formation rate of the Fenton's reagent through the enhancement of electrochemical reactions (Eqs. 20-22) and therefore the amount of •OH/M(•OH) in the bulk solution (Eq. 19) and on the anode surface (Eq. 22). The production of high amount of •OH/M(•OH) leads to the high degradation rate of the organics (Ren et al. 2019). The results obtained in this study highlight the high efficiency of the EF treatment of the pharmaceuticals HCT, TMD, Nad and OFL solutions as these solutions were

completely oxidatively degraded in 15, 10, 12 and 10 min, respectively, at 500 mA constant current electrolysis. The apparent rate constants were also calculated for each current and pollutant. They were of 0.14, 0.19, 0.29 and 0.39 min^{-1} for 50, 100, 300 and 500 mA respectively for the HCT (Fig. 16) and of 0.70, 0.71 and 0.26 min^{-1} at 500 mA for TMD (Fig. 17), OFL (Fig. 18) and Nad (Fig. 19), respectively. For all the trend curves a good correlation coefficients were found proving the good accuracy of the pseudo first order reaction model. Nevertheless, the use of too high currents can promote side reactions such as H_2 evolution on the cathode or O_2 evolution on the anode (Zhang et al. 2007; Oturan and Oturan 2018). This behavior is visible as the rate constants do not increase proportionally to the applied current because of this enhancement of rate of side reactions with current, causing thus a loss in process efficiency. The increase of the current also promotes the formation of gas bubbles which decreases the conductivity of the solution and thus the process efficiency. Moreover, using a higher current increases electrical energy consumption and consequently process cost. Therefore, a good compromise has to be found between a suitable efficiency and a rational operating cost.

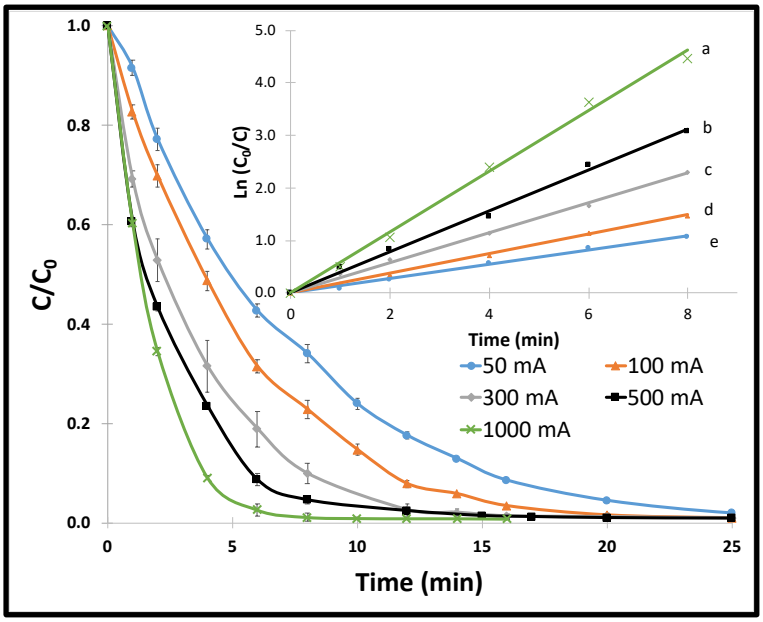

Fig. 16: Effect of current on degradation kinetics of 0.1 mM HCT in 0.05 M of Na_2SO_4 solution containing 0.1 mM Fe^{2+} (catalyst); a: y = 0.39x, R^2 = 0.994, b: y = 0.29x, R^2 = 0.996, c: y = 0.19x, R^2 = 0.999 and d: y = 0.14x, R^2 =0.996.

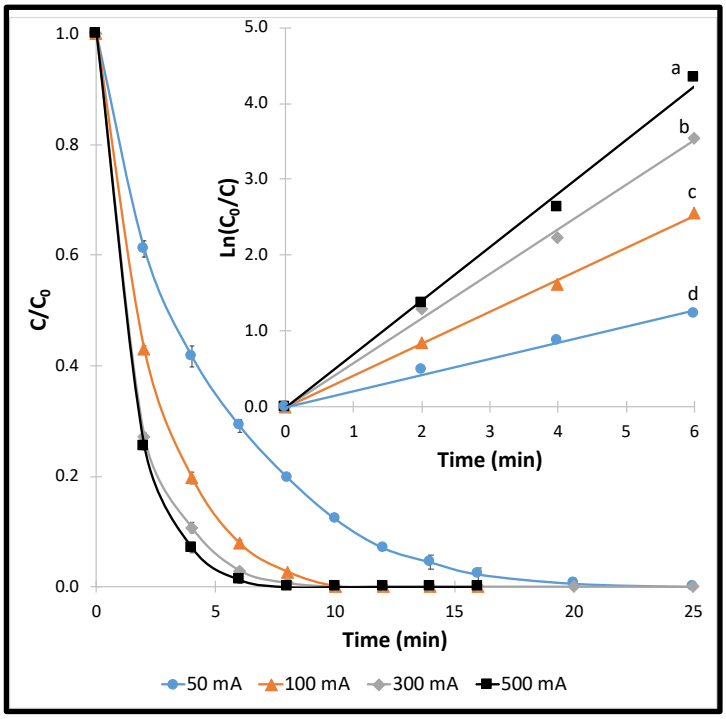

Fig. 17: Effect of current on degradation kinetics of 0.1 mM TMD in 0.05 M of Na_2SO_4 solution containing 0.2 mM Fe^{2+} (catalyst); a: y = 0.7x, R^2 = 0.995, b: y = 0.59x, R^2 = 0.995, c: y = 0.42x, R^2 = 0.998 and d: y = 0.21x, R^2 =0.991.

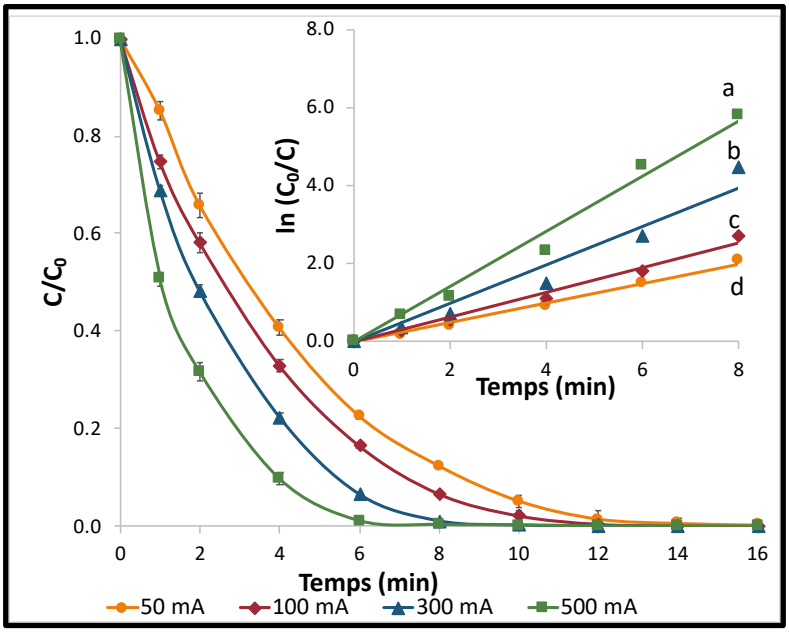

Fig. 18: Effect of current on degradation kinetics of 0.1 mM OFL in 0.05 M of Na_2SO_4 solution containing 0.1 mM Fe^{2+} (catalyst); a: y = 0.71x, R^2 = 0.985, b: y = 0.49x, R^2 = 0.956, c: y = 0.32x, R^2 = 0.986 and d: y = 0.25x, R^2 =0.990.

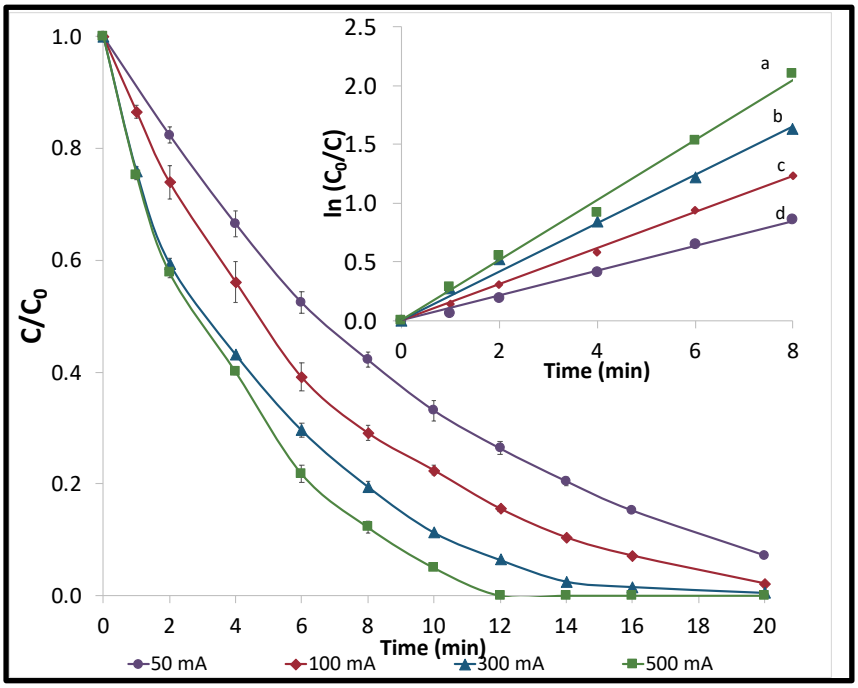

Fig. 19: Effect of current on degradation kinetics of 0.1 mM Nad in 0.05 M of Na_2SO_4 solution containing 0.1 mM Fe^{2+} (catalyst); a: y = 0.26x, R^2 = 0.994, b: y = 0.19x, R^2 = 0.986, c: y = 0.14x, R^2 = 0.998 and d: y = 0.11x, R^2 =0.997.

To consider the effect of the ions present in a real wastewater on the degradation of the HCT, a synthetic solution was prepared by adding different ions. The concentration of ions used were at the level of a real wastewater coming from an industrial production sites of antibiotics (Marcelino et al. 2016). Results are given in Fig. 20. There is a small decrease in the kinetic of degradation probably due to scavenging reactions with the added ions.

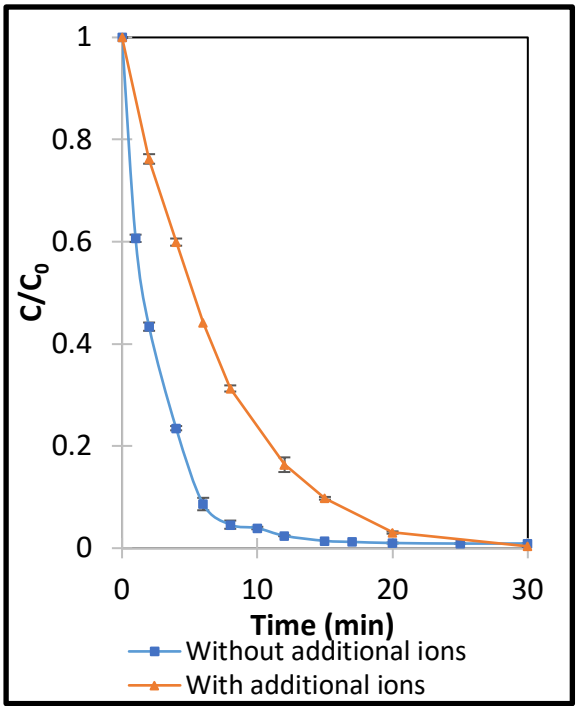

Fig. 20: Kinetic of degradation during the elimination of 0.1 mM HCT solution under 500 mA, 50 mM of Na_2SO_4 and 0.1 mM Fe^{2+} with and without additional inorganic ions. The additional compounds were 244 mg L^{-1} Na_2CO_3, 48 mg L^{-1} of Cl^-, 4 mg L^{-1} of PO_4^{3-}, 0.9 mg L^{-1} NO_2^- and 1.5 mg L^{-1} of NO_3^-.

3.2. Influence of the anode material on the degradation kinetics

The degradation of the Nad was also studied using a platinum anode. The Nad decay is represented in Fig. 21 for different current values. As for the BDD anode, the degradation efficiency is increasing with current until 500 mA. For 1000 mA, the kinetic curve is very similar to the one of 500 mA due to side and wasting reactions consuming the electrical energy and the hydroxyl radicals. The complete oxidation of Nad needs 40 min electrolysis at 300, 500 and 1000 mA which is much higher than for the degradation with the BDD being of 10, 12 and 20 min for 1000, 500 and 300 mA, respectively. This is due to the nature of anode material: BDD promotes the formation of high amounts of adsorbed hydroxyl radicals (due to its high O_2 evolution overpotential). Moreover, the BDD(•OH) is weakly sorbed on BDD surface enabling it to react easily with organics (Marselli et al. 2003) whereas the interaction is much stronger (chemisorption) in the case of Pt(•OH). Table 11 gives the value of the apparent rate

constants obtained for the mineralization process. As for the BDD anode, the apparent kinetics constants for Pt anode are not increasing proportionally to the current for the same reasons. The degradation constants for both Pt and BDD are quite similar in early electrolysis times (t < 8 min). Indeed, BDD(•OH) degrade and mineralize simultaneously whereas Pt(•OH) mostly degrade which result in a very similar degradation. This behavior was found in other already published reports for high currents (Guinea et al. 2008; El-Ghenymy et al. 2014; Sopaj et al. 2016).

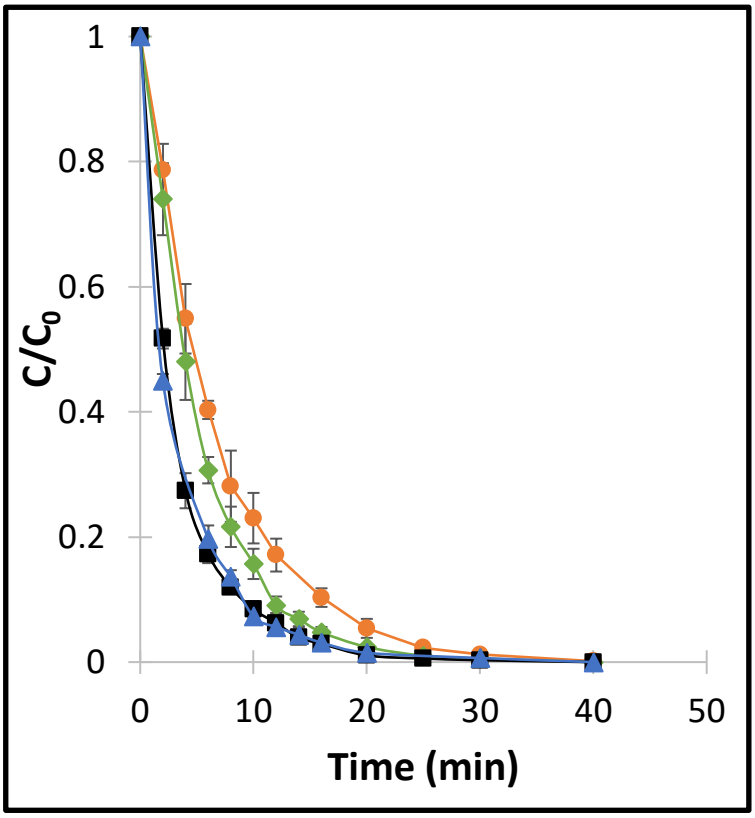

Fig. 21: Effect of current on decay of normalized concentration of Nad by electro-Fenton process with Pt anode. I (mA): 100 (●), 300 (◆), 500 (■) and 1000 (▲); [Na_2SO_4] = 50 mM; [Fe^{2+}] = 0.1 mM.

Table 11: Apparent rate constants (k_{app}) for Nad decay with BDD and Pt anode calculated based on the first 8 mins.

Anode	Current (A)	k_{app} (min^{-1})	Correlation coefficient
BDD	50	0.11	0.995
	100	0.15	0.998
	300	0.19	0.990
	500	0.26	0.995
	1000	0.3	0.988
Pt	100	0.15	0.994
	300	0.19	0.994
	500	0.26	0.962
	1000	0.28	0.980

3.3. Determination of the absolute rate constant for oxidation of four pharmaceuticals by hydroxyl radicals

The absolute (second order) rate constant of the oxidation of the pharmaceuticals under study by hydroxyl radicals was determined using the competition kinetics method following the Eq. 27 (Oturan et al. 2000). Benzoic acid (BA) was selected as the standard competitor since the rate constant for its oxidation by $^{\cdot}OH$ (k_{BA} = 4.3 x 10^9 M^{-1} s^{-1}) is well-known (Buxton et al. 1988).

$$\ln\left(\frac{[P]_0}{[P]}\right) = \frac{k_P}{k_{BA}} \times \ln\left(\frac{[BA]_0}{[BA]}\right) \quad (27)$$

with k_P and k_{BA} the absolute rate constant of the pollutant and BA respectively, $[P]_0$, the initial concentration in pollutant and $[P]$ the concentration of pollutant at t time. The concentrations are given in the same unity, mM usually.

To determine k_P, the electrolysis of equimolar concentration of the pharmaceutical under study and BA is performed under electro-Fenton conditions at 50 mA applied current. The decay in the concentration of both compounds was carried out over short electrolysis time and at lower current to avoid the interference of intermediate products. The determination of k_P was then done thanks to the slope of the regression line of Fig. 22 which was built following Eq. 27. The absolute rate constants were found to be: $(4.37 \pm 0.04) \times 10^9$, $(5.59 \pm 0.03) \times 10^9$, $(5.63 \pm 0.03) \times 10^9$ and $(5.55 \pm 0.05) \times 10^9$ M^{-1} s^{-1} for HCT, TMD, Nad and OFL, respectively. These values are very close and highlight the similar reactivity of the hydroxyl radicals towards four pharmaceutical selected.

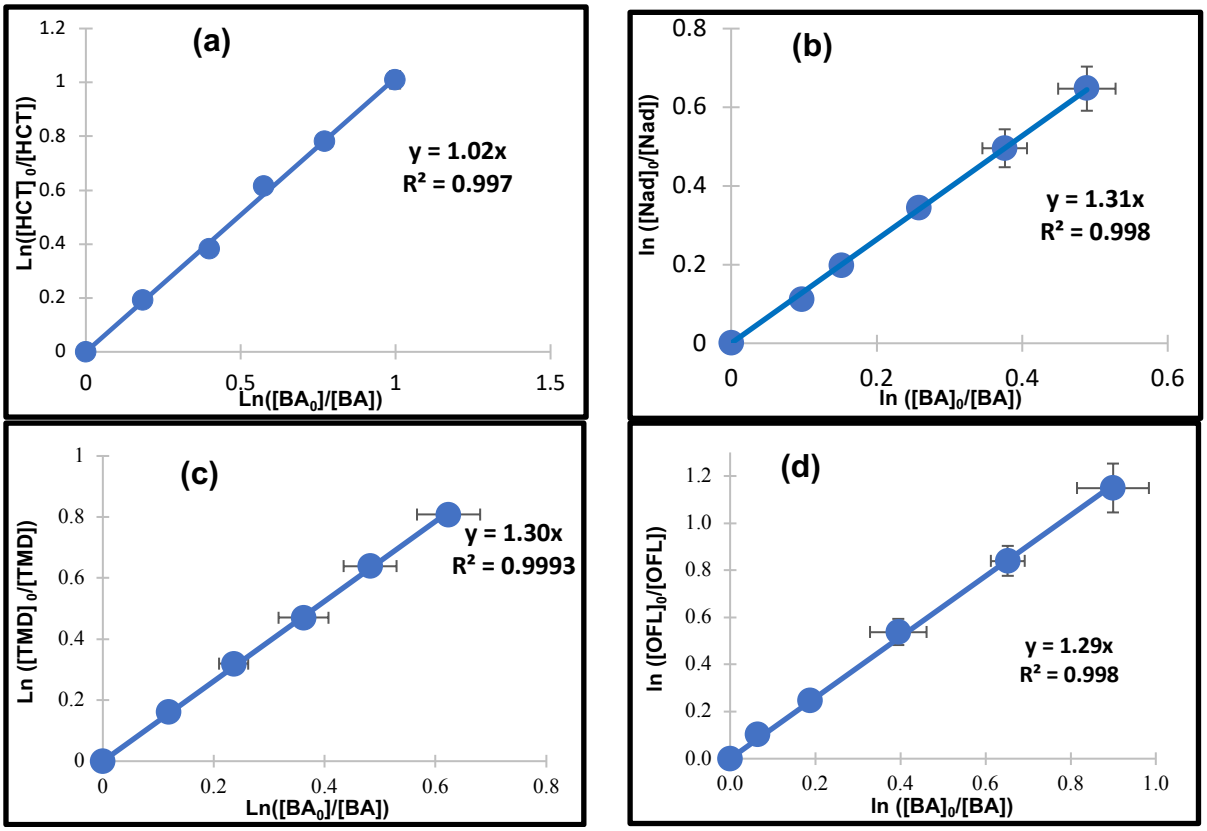

Fig. 22: Determination of the absolute second order rate constant for oxidation of pharmaceuticals HCT (a), Nad (b), TMD (c) and OFL (d) by hydroxyl radicals following Eq. 27. Experimental conditions: [HCT] = [Nab] = [TMD] = [OFL] = [BA] = 0.1 mM, $[Fe^{2+}]$ = 0.1 mM (0.2 in the case of TMD), $[Na_2SO_4]$ = 0.05 M, room temperature.

3.4. Mineralization of the pharmaceuticals

The mineralization of different pharmaceutical solutions was assessed by monitoring TOC measurements during treatment. The MCE and EC were then evaluated based on TOC removal data for different applied currents in order to find the better efficiency related to a lower cost. The nature of the anode was also considered by comparing the use of a BDD and Pt electrode. The measurements were carried out for currents ranging from 100 to 1000 mA.

3.4.1. Effect of the applied current on the mineralization of pharmaceutical solutions

As can be seen in Fig. 23, the TOC removal is faster at early treatment times and for high currents. Indeed the mineralization of 0.1 mM pharmaceuticals solutions lasts for 6 h for 300, 500 and 1000 mA, reaching TOC removal rates of 85%, 95%, 94% and 94% at 100 mA under same operating conditions, for HCT, TMD, Nad and OFL, respectively. Complete mineralization is attained at 500 and 1000 mA for all cases. However the increase in mineralization degree is not proportional to the applied current, particularly at high currents, as can be seen with the distance between the curves. The exponential decrease of TOC is due to the relatively easy degradation of the pharmaceuticals and their aromatic oxidation intermediates at early treatment times. Inversely, the mineralization efficiency becomes significantly slower at longer treatment times due to the formation of the aliphatic compounds such as carboxylic acids which are more resistant to hydroxyl radicals (Brillas et al. 2009; Oturan and Aaron 2014) and the decrease in the amount of organic matter in the solution (Brillas et al. 2009; Yang et al. 2019). This phenomenon is also illustrated by the MCE values representing the part of the current which mineralizes the pollutant. The MCE values are decreasing highlighting less mineralization efficiency for longer treatment times. The decrease in mineralization efficiency with higher currents is mainly due to the raise in the rate of side reactions, decreasing the oxidative ability of hydroxyl radicals towards organic contaminants. Among those reactions, the most occurring ones are the oxidation of BDD(•OH) (Eq. 28) and the wasting of •OH by H_2O_2 (Eq. 29) (Brillas et al. 2009; Oturan and Aaron 2014).

$$2\ M(^{\bullet}OH) \rightarrow 2\ M + O_2 + 2\ H^+ + 2\ e^- \quad (28)$$

$$H_2O_2 + {}^{\bullet}OH \rightarrow HO_2 + H_2O \quad (29)$$

The maximum MCE values are obtained for 100 mA (as expected) for 1 h of treatment, reaching 10, 12, 15 and 17% for HCT, TMD, Nad and OFL, respectively. The mineralization rates are between 5 and 10% for 300 mA and below 5% for 500 and 1000 mA, for all the four pharmaceuticals showing an important loss of energy. This low efficiency can be increased by using higher concentrations, for example. This was demonstrated by Brillas' group who degraded different concentrations of propranolol and could reach nearly 100% of MCE with 616 mg L^{-1} (Isarain-Chávez et al. 2010b) at the beginning of the treatment.

The evolution of EC during the treatment of 0.1 mM of pollutants by EF is presented in Fig. 24. This parameter is also growing with the current and the treatment time, as expected, since the same current value is applied along electrolysis with lower MCE over longer electrolysis times. The results show that EC maximum values are around 16, 12, 12 and 7 kWh $(g\ TOC)^{-1}$ for HCT, TMD, OFL and Nad, respectively, after 6 h electrolysis at 1000 mA. Considering the values of MCE and mineralization degree, the more efficient currents seem to be 300 mA and 500 mA for all the pharmaceuticals for a cost effective process. The mean EC values for those currents is around 2 kWh $(g\ TOC)^{-1}$.

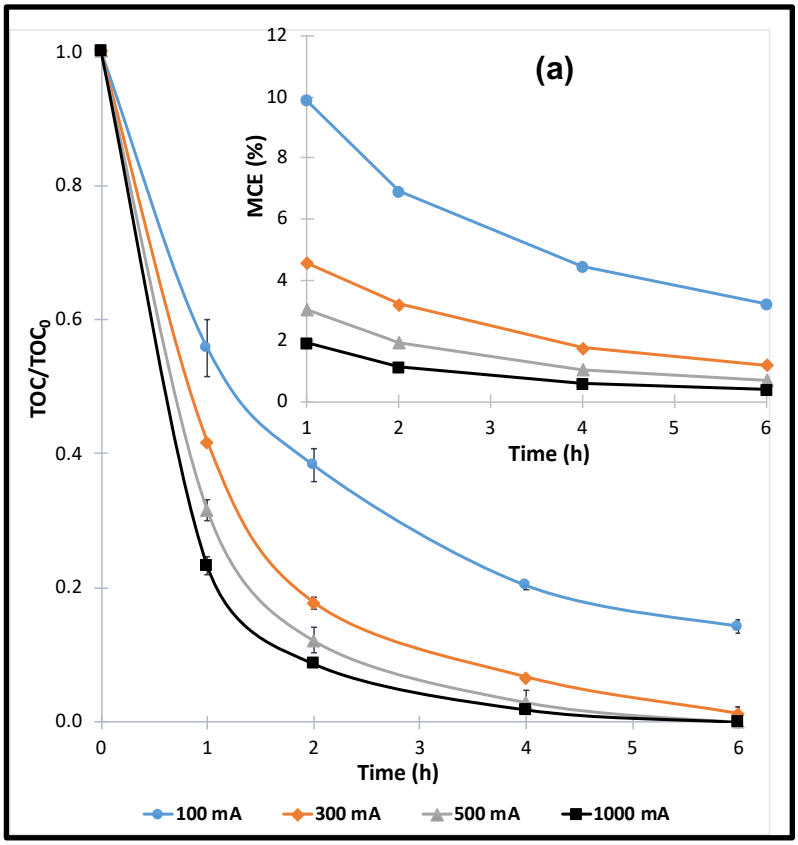
(a)
TOC/TOC0
Time (h)
MCE (%)
Time (h)
100 mA
300 mA
500 mA
1000 mA

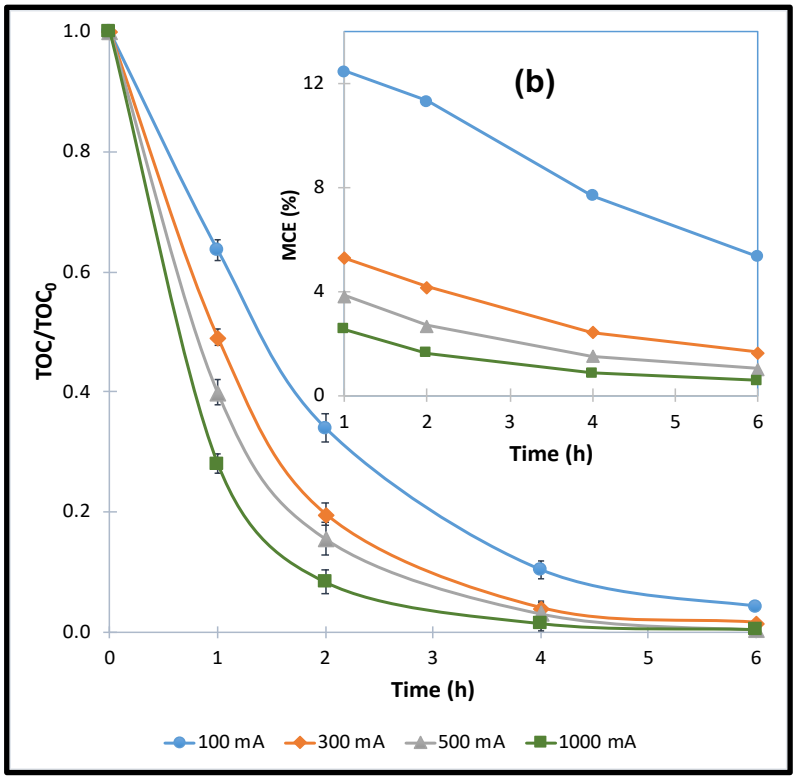
(b)
TOC/TOC0
Time (h)
MCE (%)
Time (h)
100 mA
300 mA
500 mA
1000 mA

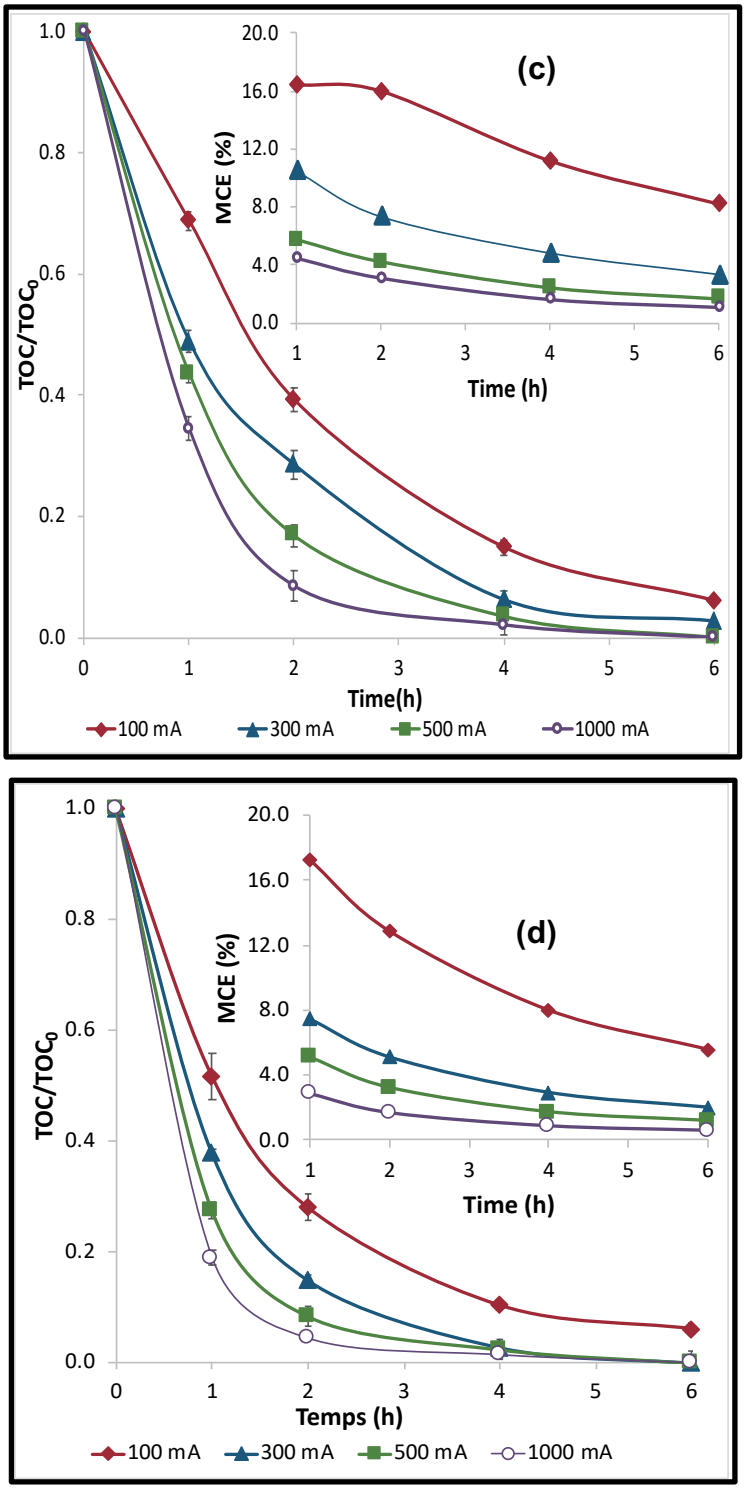

Fig. 23: Evolution of TOC decay and MCE (insert panel) as a function of time and current during treatment of 0.1 mM of HCT (corresponding to 8 mg L^{-1} initial TOC) (a), 0.1 mM of TMD (corresponding to 19.2 mg L^{-1} initial TOC) (b), 0.1 mM of Nad (corresponding to 20.1 mg L^{-1} initial TOC) (c) and 0.1 mM of OFL (corresponding to 22 mg L^{-1} initial TOC) (d) by electro-Fenton. Experimental conditions: [HCT] = [Nab] = [TMD] = [OFL] = 0.1 mM, [Fe^{2+}] = 0.1 mM (0.2 mM in the case of TMD), [Na_2SO_4] = 0.05 M, room temperature.

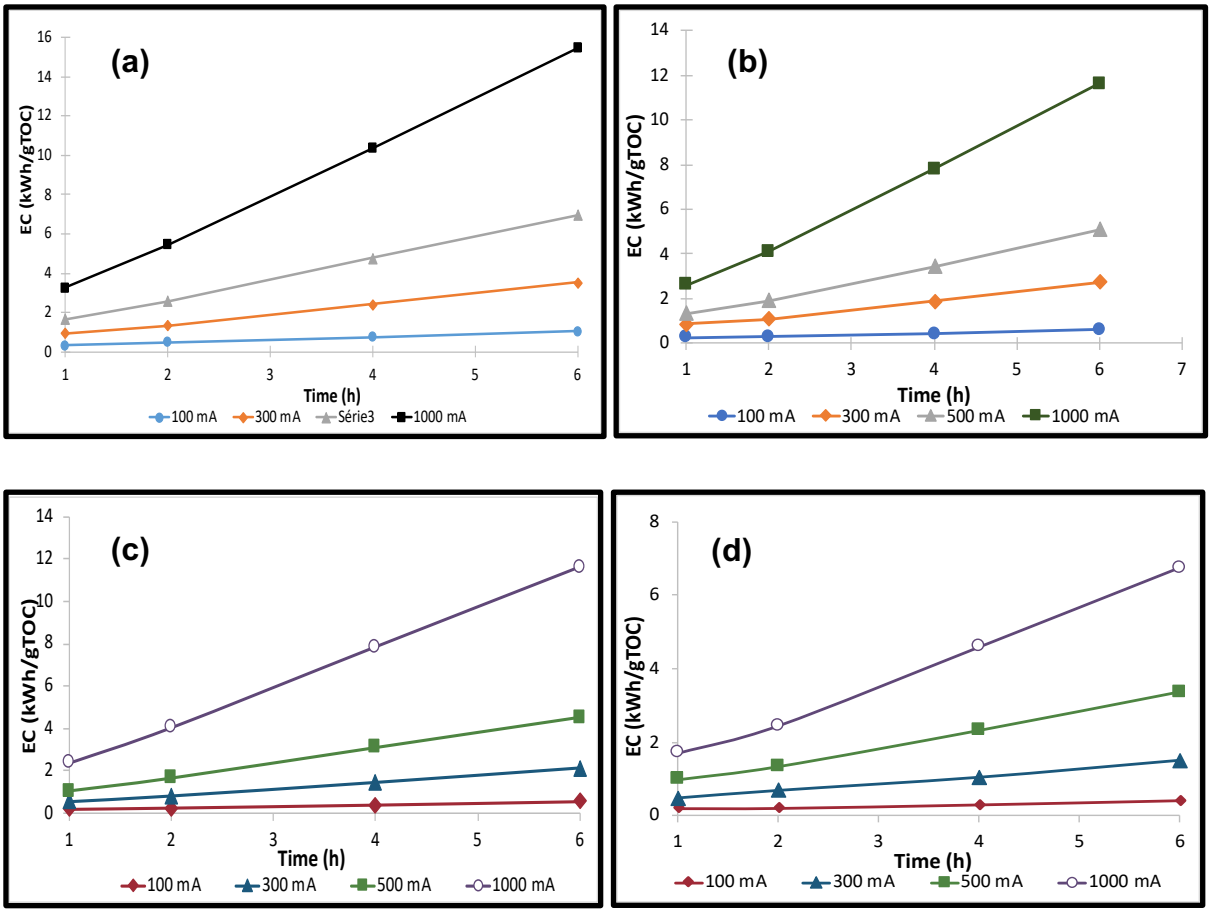

Fig. 24: Energy consumption (EC) for mineralization of pharmaceutical solutions: HCT (a), TMD (b), OFL (c) and Nad (d), calculated from Eq. 25, following TOC removal data of the Fig. 23, as a function of electrolysis time for different currents.

3.4.2. Influence of the anode material on the mineralization efficiency

The TOC decay was measured for both BDD and Pt anode under different currents ranging from 100 mA to 1000 mA and results are depicted on the Fig. 25. For the BDD anode, the TOC decay is increasing with the current intensity, reaching a total mineralization of the solution in 6 hours for both 500 and 1000 mA. The very similar trend between these two curves is due to waste reactions degrading BDD(•OH) or H_2O_2 for example (Eqs. 30-32) or to the generation of weaker oxidants such as $S_2O_8^{2-}$ or O_3 (Eq. 33 and 34) occurring at high currents (Panizza and Cerisola 2005; Guinea et al. 2008; Brillas et al. 2009; Oturan and Aaron 2014).

$$2\ BDD(^{\bullet}OH) \rightarrow 2\ BDD + O_2 + 2\ H^+ + 2\ e^- \quad (30)$$

$$H_2O_2 + {}^{\bullet}OH \rightarrow HO_2{}^{\bullet} + H_2O \quad (31)$$

$$2\ ({}^{\bullet}OH) \rightarrow H_2O_2 \quad (32)$$

$$2\ SO_4^{2-} \rightarrow S_2O_8^{2-} + 2\ e^- \quad (33)$$

$$3\ H_2O \rightarrow O_3 + 6\ H^+ + 6\ e^- \quad (34)$$

For the Pt anode, the increase of the current also results in higher mineralization rate until 300 mA. Higher currents increase the efficiency of side reactions that hinder the generation or favor the consumption of •OH/ Pt(•OH) (Eqs. 11 and 28). This decrease in efficiency happens at lower currents than for the BDD because the homogeneous •OH reacts with the iron (Eq. 26) at the same kinetic rate than homogeneous •OH with carboxylic acids and Pt(•OH) are less efficient than BDD(•OH) in the oxidation process. In other studies (Sopaj et al. 2016), this result was also obtained and they performed the anodic oxidation treatment to compare the role of •OH/ M(•OH). The difference of efficiency is explained by the predominant role of M(•OH) in the mineralization process compared to homogeneous •OH especially for long treatment times (6h) which enables the pollutant to reach the anode surface/diffusion layer. Thus as it was previously explained for the degradation, as BDD(•OH) are more formed and slightly adsorbed onto the anode surface their efficiency is much higher than Pt(•OH).

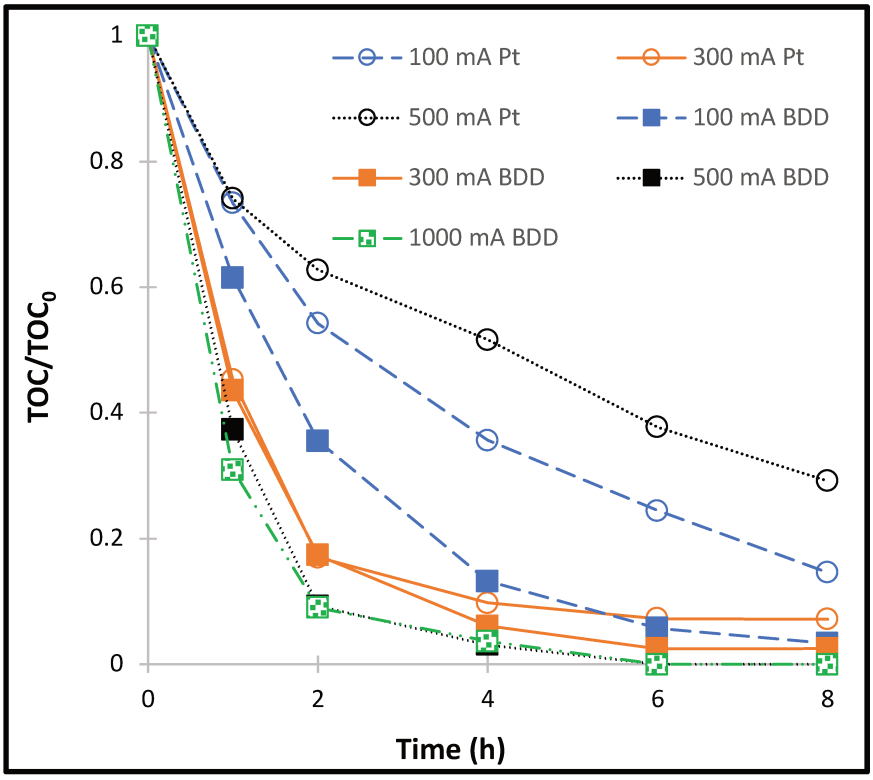

Fig. 25: Effect of current on normalized TOC removal of a 0.1 mM solution of Nad in 50 mM of Na_2SO_4 in EF process with BDD and Pt anodes in presence of 0.1 mM Fe^{2+} as catalyst.

3.4.3. Mineralization in conditions closer to real wastewaters

In order to analyze the applicability to a real wastewater, two experiments were carried out. First, a mixture of the four pharmaceuticals at 0.025 mM each was mineralized with different currents (Fig. 26). After 6 h treatment, the solution was entirely mineralized, thus the mixture of this four pharmaceuticals does not have a disrupting effect on the mineralization efficiency.

In the second experiments, some common ions were added to the mixture of four pharmaceuticals to observe their possible scavenging effects on the mineralization process in conditions closer to real wastewaters. Results are given in Fig. 27. No effect on the mineralization of the solution under study was found, as already reported by Marcelino et al. (2016).

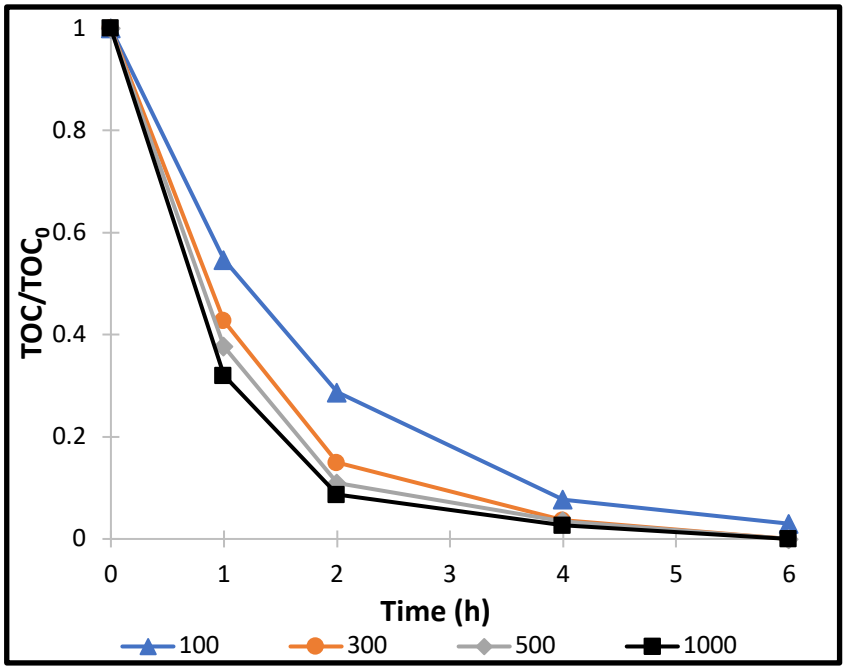

Fig. 26: Evolution of TOC decay as a function of time and applied current during treatment of a mixture of four pharmaceuticals (HCT + TMD + Nad + OFL) containing 0.025 mM of each by EF process of [Na_2SO_4] = 50 mM of [Fe^{2+}] = 0.1 mM.

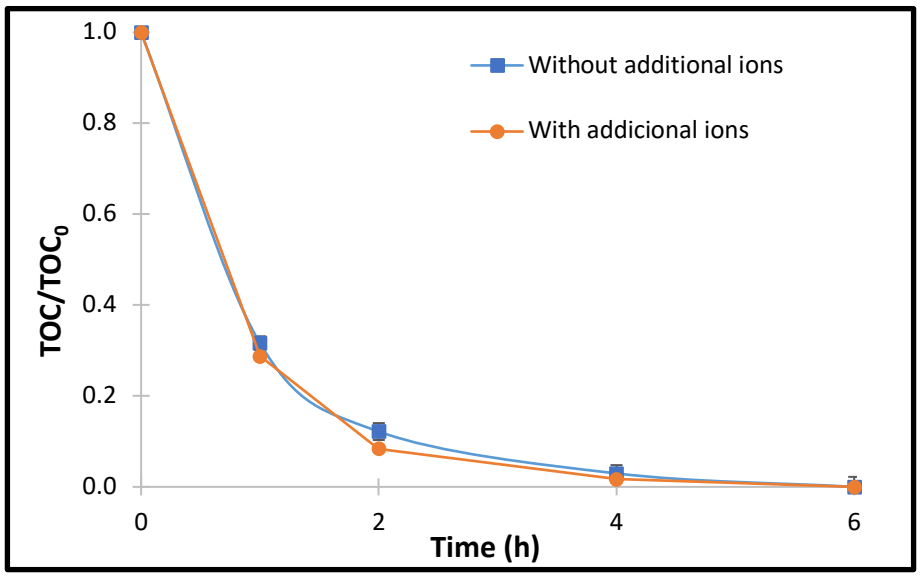

Fig. 27: TOC evolution during the mineralization of 0.1 mM HCT solution at 500 mA in 50 mM of Na_2SO_4 with and without additional ions using 0.1 mM Fe^{2+} as catalyst. The additional compounds were 244 mg L^{-1} Na_2CO_3, 48 mg L^{-1} of Cl^-, 4 mg L^{-1} of PO_4^{3-}, 0.9 mg L^{-1} of NO_2^- and 1.5 mg L^{-1} of NO_3^-.

3.4.4. Formation and Evolution of short chain carboxylic acids and mineral ions

The cleavage of aromatic/cyclic moieties of organic compounds under oxidative action of hydroxyl radicals is known to form aliphatic compounds that are further oxidized to carboxylic acids (Brillas et al. 2009; Dirany et al. 2012). In order to well understand the degradation of the organics, formed short-chain carboxylic acids during mineralization experiments were identified and their evolution was followed by HPLC using an ion-exclusion column. The evolution of the carboxylic acids created during the degradation process is presented in Figs. 28-31. For the HCT, oxamic, oxalic, maleic and acetic acids were detected and followed until 4 h of treatment. Maleic acid was completely degraded in 90 min, likely being transformed to oxalic and acetic acids which are more recalcitrant (Oturan et al. 2008b). Oxamic acid could be formed from the degradation of compounds containing an amino group (Garcia-Segura and Brillas 2011). The higher accumulation of oxalic (0.009 mM) and oxamic acid (0.0045 mM) after 1 h treatment can be explained by their recalcitrant behavior towards $^{\bullet}OH$/BDD($^{\bullet}OH$). For TMD, three carboxylic acids were identified: glyoxylic acid, oxalic acid and fumaric acid. The most important one was glyoxylic acid for which the concentration reached 0.07 mM after 1 h of treatment. The fumaric acid was accumulated in the solution only at trace level (around 10^{-5} mM); it was probably oxidized quickly into glyoxylic and/or oxalic acids. After 6 h of electrolysis, all the identified carboxylic acids were not anymore detectable in accordance with the very low value of TOC (section 3.4.) in these conditions. During the Nad degradation, oxalic, oxamic, acetic, glyoxylic and formic acids were formed. Glyoxylic disappeared after 1.5 h of EF treatment, possibly transformed into formic acid (Oturan et al. 2008b). Oxalic and oxamic acids were again found to be the more resistant; they could be detected until 4 h of EF treatment. For OFL, acetic, oxalic and oxamic acids were formed during the oxidation process

with a maximum concentration peak at about 1 h. Fumaric acid was detected in trace concentration. Then after 6 h they were all mineralized.

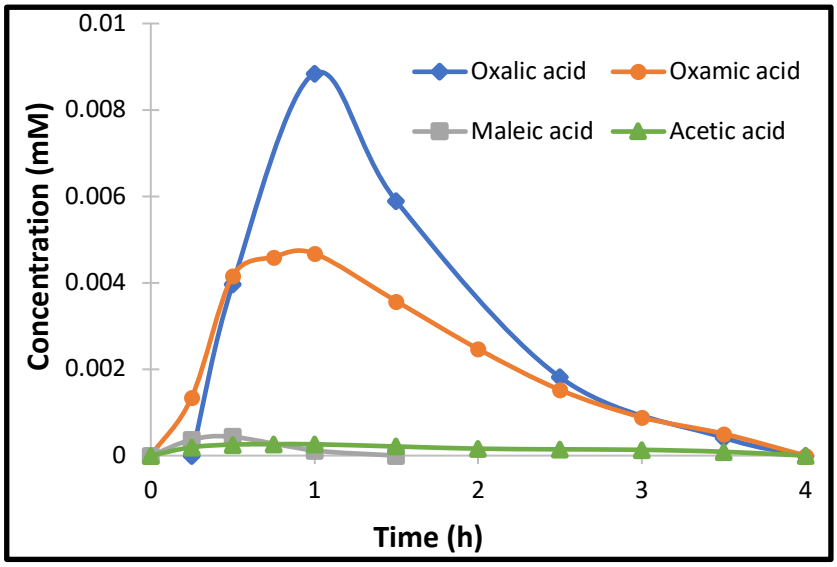

Fig. 28: Time-course of carboxylic acids during the electrolysis of 0.1 mM HCT at 500 mA constant current. $[Fe^{2+}]$ = 0.1 mM, $[Na_2SO_4]_0$ = 0.05 M, room temperature.

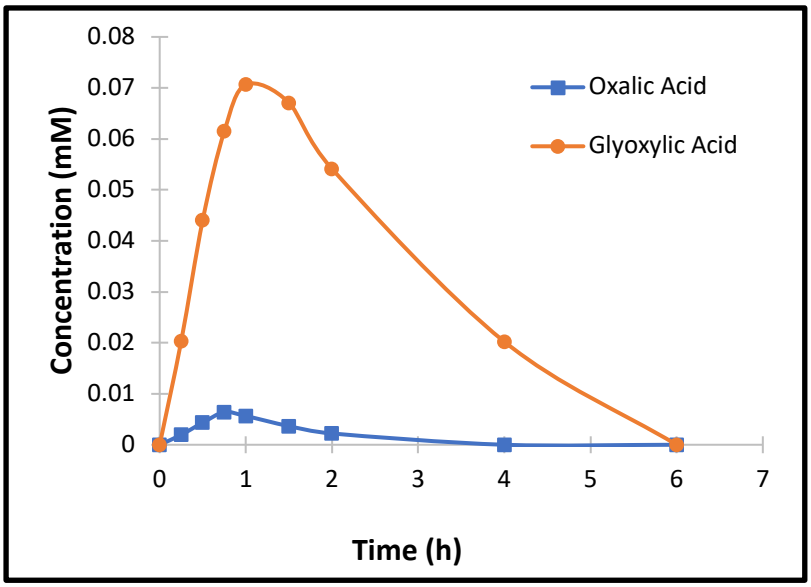

Fig. 29: Time-course of carboxylic acids during the electrolysis of 0.1 mM TMD at 500 mA and room temperature. $[Fe^{2+}]$ = 0.2 mM, $[Na_2SO_4]_0$ = 0.05 M.

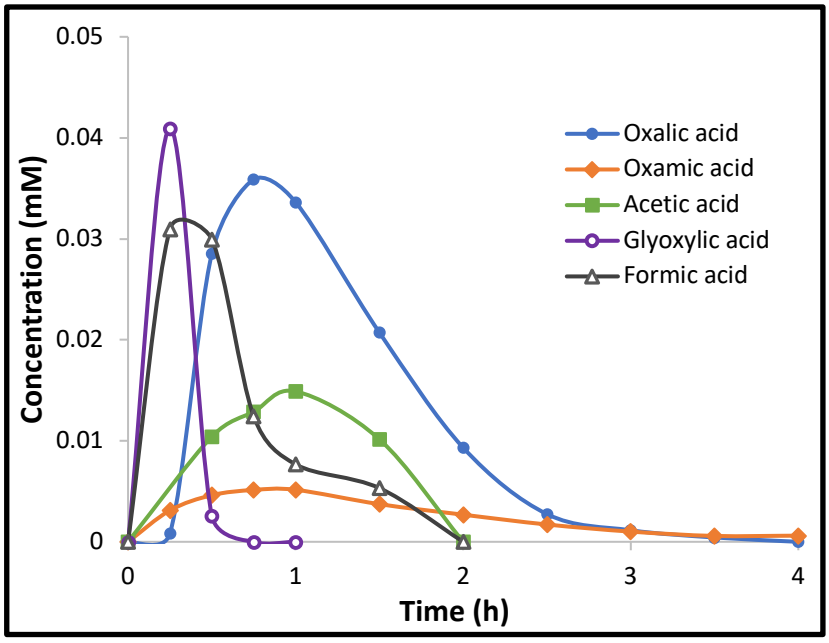

Fig. 30: Time-course of carboxylic acids during the electrolysis of 0.1 mM Nad at 500 mA and room temperature. $[Fe^{2+}]$ = 0.1 mM, $[Na_2SO_4]_0$ = 0.05 M, room temperature.

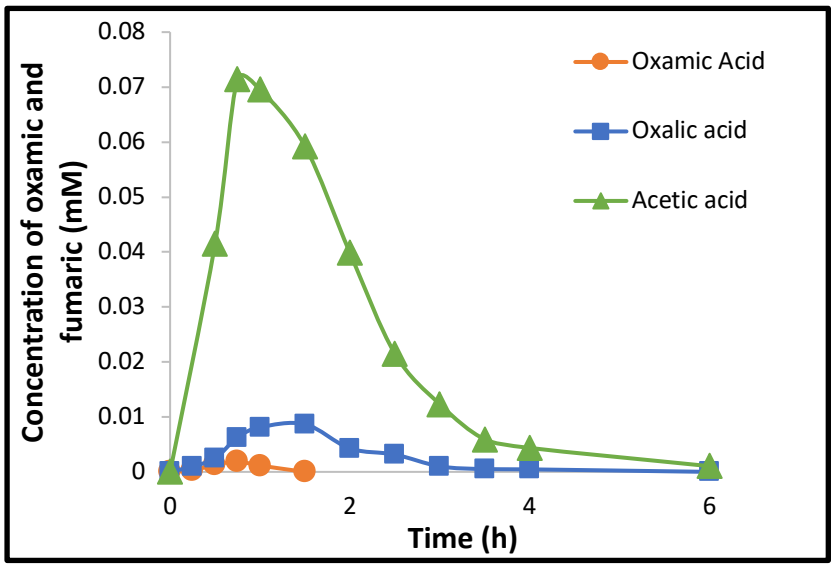

Fig. 31: Time-course of carboxylic acids formed during the electrolysis of 0.1 mM OFL at 500 mA constant current. $[Fe^{2+}]$ = 0.1 mM, $[Na_2SO_4]_0$ = 0.05 M, room temperature.

During the mineralization of organics, the heteroatoms present in the initial molecules are oxidized to their higher (often to the highest) oxidizing state and released to the solution as inorganic ions. Thus the evolution of inorganic ions formed during the mineralization of the pharmaceutical solutions was also followed by IC and results are depicted in Figs. 32-35. The

3 N atoms of the HCT and OFL molecules (0.1 mM) and the N atom of TMD and Nad were mineralized into NH_4^+ and NO_3^-. The presence of NO_2^- was not detected. After 4 or 6 h electrolysis, the largest amount of NH_4^+ was measured. In order to confirm this behavior, 1 mM solutions of NH_4^+ and NO_3^- were separately electrolyzed at different currents using K_2SO_4 as supporting electrolyte and 0.1 mM Fe^{2+} as catalyst and the results are detailed in the Fig 36. After 8 h treatment, the concentration of NH_4^+ was still equal to its initial value (1 mM) whereas NO_3^- was totally transformed into NH_4^+ (Fig. 36). These results confirm the data obtained during the mineralization of HCT and highlight the electro-reduction of NO_3^- into NH_4^+ taking the advantage of the large 3D surface of carbon-felt cathode. Similar results were already reported by Martin De Vidales et al. (2016) and Garcia-Segura et al. (2018).

The mineralization of the 2 S atoms of the HCT molecule was done with complete release of SO_4^{2-} ion (0.2 mM) into the solution after 2 h electrolysis confirming the rapid mineralization of entire S atoms. Concerning the Cl atom, the concentration of Cl^- reached 0.086 mM after 30 min treatment before starting to decrease gradually due to its oxidation at BDD anode to the chlorine gas Cl_2, which then reacts with water to form HClO (under EF condition of pH near 3). Chlorate and perchlorate can also be formed as the EF process is applied but those molecules could not be measured on the IC. This latter compound is an active chlorine specie that can contribute to the oxidation of HCT in the solution (Randazzo et al. 2011; Brito et al. 2015). Finally, the F atom of the OFL was completely released into F^- ion in 2 h of electro-Fenton treatment.

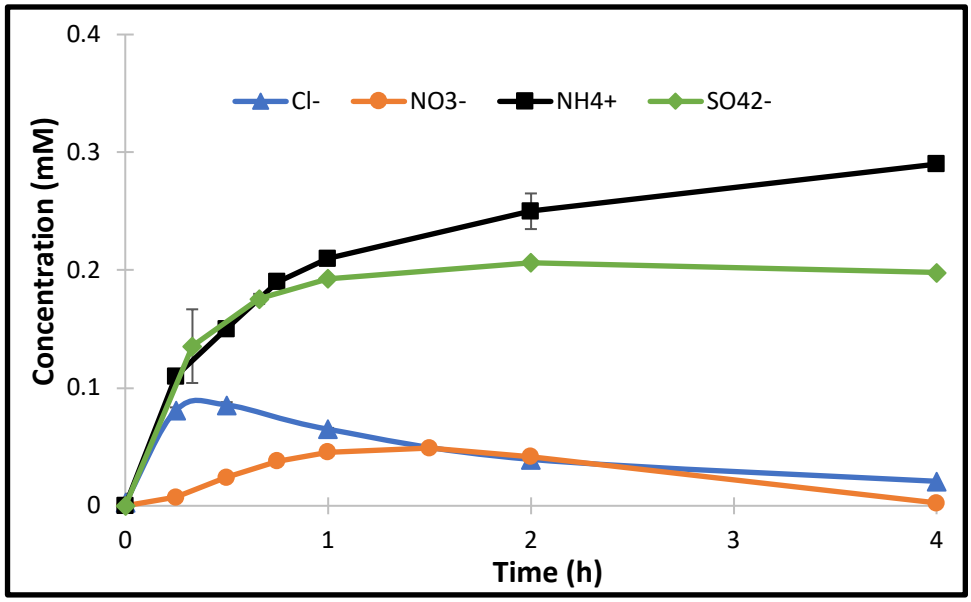

Fig. 32: Evolution of inorganic ions during the electrolysis of 0.1 mM HCT at 500 mA under conditions of Fig. 16. In the case of NH_4^+ and SO_4^{2-}, K_2SO_4 and $NaClO_4$ were used as supporting electrolyte respectively.

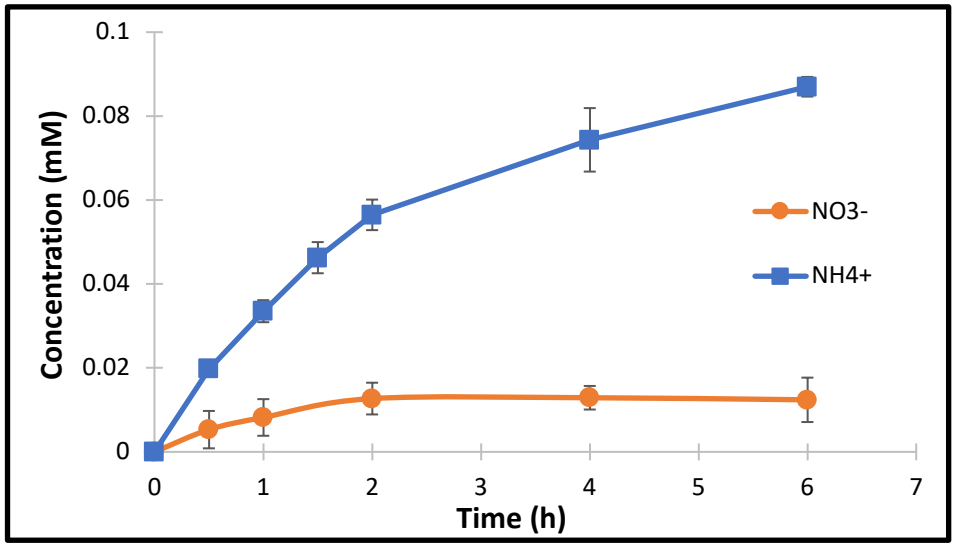

Fig. 33: Evolution of inorganic ions during the electrolysis of 0.1 mM TMD at 500 mA under conditions of Fig. 17. In the case of NH_4^+, K_2SO_4 was used as supporting electrolyte.

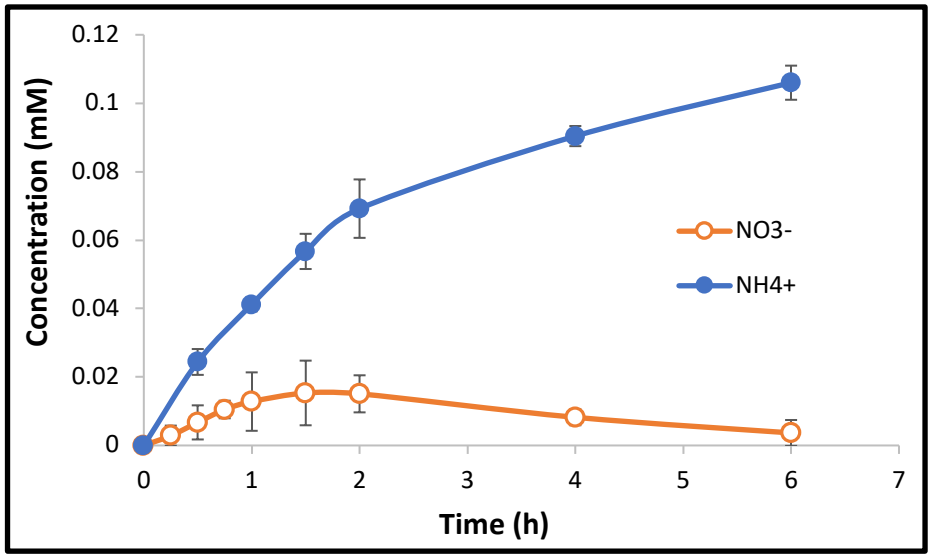

Fig. 34: Evolution of inorganic ions during the electrolysis of 0.1 mM Nad at 500 mA under conditions of Fig. 19. K_2SO_4 and $NaClO_4$ were used as supporting electrolyte, for NH_4^+ and SO_4^{2-}, respectively.

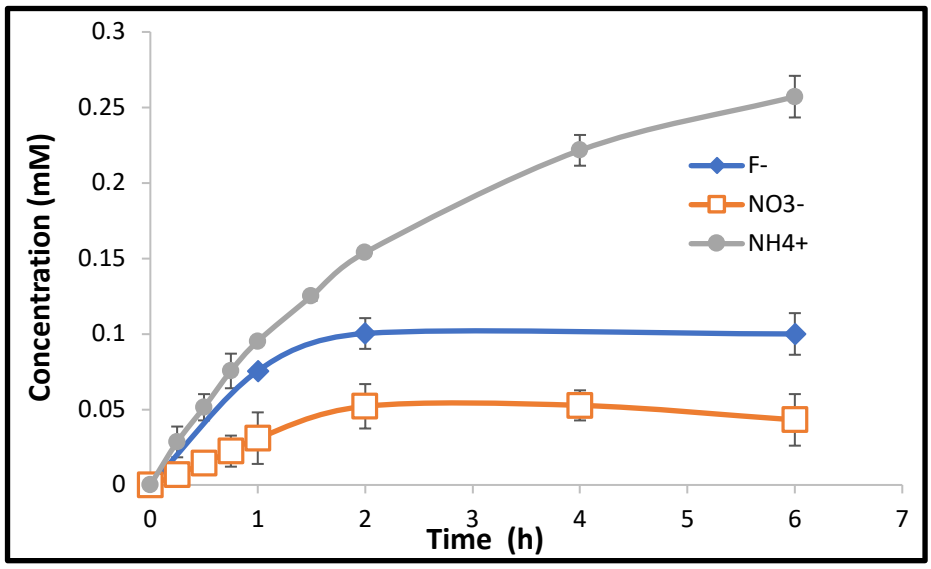

Fig. 34: Evolution of inorganic ions during the electrolysis of 0.1 mM OFL at 500 mA under conditions of Fig. 18. In the case of NH_4^+, K_2SO_4 was used as supporting electrolyte.

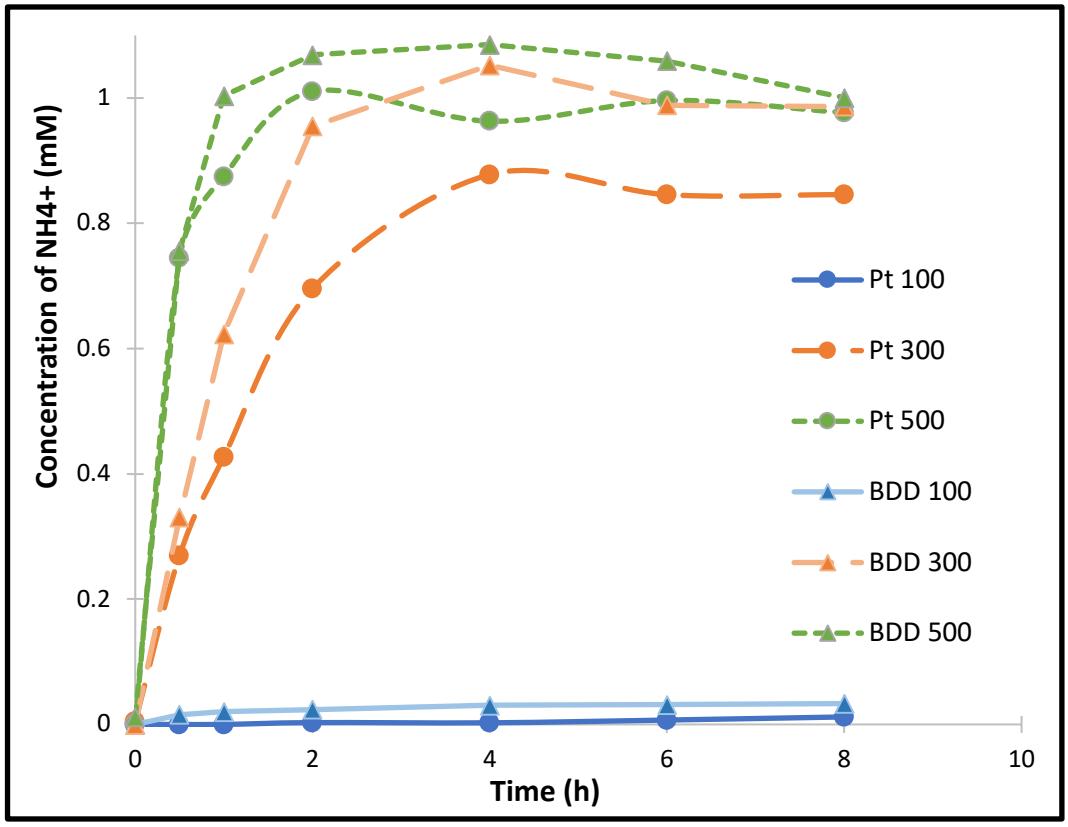

Fig. 36: Evolution of NH_4^+ concentration during EF treatment of 1 mM NO_3^- solution at different currents (mA) using BDD (▲) or Pt anodes (●).

3.5. Proposition mineralization pathway

It was not possible to identify the intermediates for Nad with the LC-MS analysis. Therefore the mineralization pathways were suggested for HCT, TMD and OFL based on GC-MS, LC-MS, ion-exclusion HPLC, ion chromatography analyses and TOC removal data.

3.5.1. Mineralization of HCT by hydroxyl radicals

In order to propose a mineralization pathway, the oxidation intermediates and the end-products were investigated. In addition to the identified short-chain carboxylic acids which constitute the last stage of the mineralization process and mineral ions as end-products, aromatic/cyclic intermediates formed during oxidation of HCT were also analyzed using GC-MS. These compounds were identified thanks to their molecular mass and fragmentations behavior (Annex

Table 3 and 4). Based on these data, a plausible mineralization pathway was proposed (Fig. 37). HCT (A) is first transformed into chlorothiazide which is possibly obtained by the double attack of hydroxyl radicals on the hydrogen linked to the nitrogen first and then on the hydrogen linked to the carbon connected to the nitrogen, as already reported by Borowska et al. (2016). This chlorothiazide is then whether hydrolyzed in acidic medium to give the product **B** or a substitution of $–NH_2$ group by –OH occurs to give product **C**. The intermediate **D** can be formed by simultaneous ipso-substitution of Cl (following an ipso attack of $^{\bullet}OH$ on –Cl position (Mousset et al. 2018)) and abstraction of H atom from -NH group linked to sulfonic acid group. The intermediates **B** and **C** were also reported by Borowska et al. (2016). The major pathway may be the formation of compound **C** as this peak is higher than that of **B** and **D**. The intermediate **E** can be formed from **B**, **C** or **D** following consecutive attacks of $^{\bullet}OH$ leading to the opening of N-N bond and desulfonation. Subsequent hydroxylation of **E** leads to the formation of compounds **F**, **G** and **H**. The quinone (**G** and **H**) are probably formed through previous formation of hydroquinones (that are not identified in this study probably because of their quick oxidation to quinone forms). Finally the compound **I** is formed from oxidation of the lateral group of **G**. These final polyhydroxylated compounds are not stable and undertake oxidative ring opening reactions to form carboxylic acids (compound **J** to **P**). The oxidation of these short-chain carboxylic acids by $^{\bullet}OH/M(^{\bullet}OH)$ constitutes the last stage of the mineralization, i.e., transformation to CO_2, H_2O and ammonium ion. The results obtained for the inorganic ions released are in accordance with the degradation pathway as ammonium ions are released after chlorine and sulfate ions.

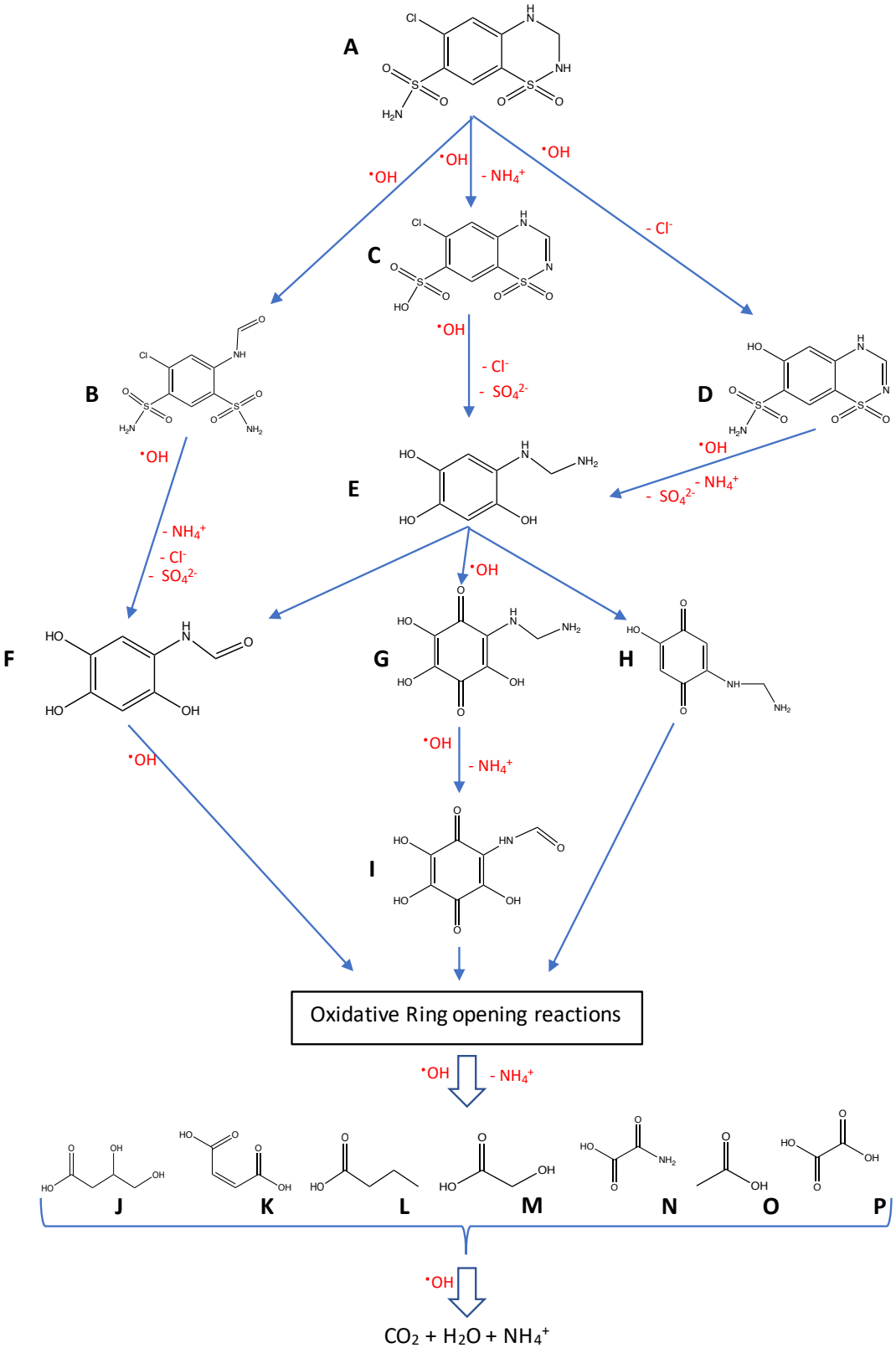

Fig.37: A plausible mineralization pathway for HCT by hydroxyl radicals based on the intermediate products identified using HPLC, IC and GC-MC analysis results.

3.5.2.. Mineralization pathway for oxidation of TMD by hydroxyl radicals

Gathering the results of sub-section 3.4.2. and the GC-MS results, it was possible to propose a degradation pathway for EF treatment of TMD (Fig. 38). Intermediates **B** to **G** were identified thanks to the fragmentation analysis of GC-MS spectrum, intermediates **H**, **I** and **J** were identified by ion-exclusion HPLC analysis. Two main routes can be established following paths from **A** to **G** or from **A** to **F**. In the first pathway, an O-demethylation associated with N-demethylations can transform TMD (**A**) into molecule **D**. These reactions were also reported during the degradation of TMD by ferrate and ozone (Zimmermann et al. 2012) and by electrochemical oxidation (Lütke Eversloh et al. 2015). The attack of hydroxyl radicals can also produce a dehydration of TMD producing intermediate **B** following an O-demethylation. This molecule is then degraded in product **E** by two N-demethylations. The further attack of hydroxyl radicals on the tertiary carbon of molecules **E** and **D** leads to the formation of molecule **G** by releasing ammonium ions (Giannakis et al. 2017; Lambropoulou et al. 2017). The second route starts with the N-demethylation of TMD and the hydroxylation of the aromatic cycle giving molecule **C** which is then followed by an O-demethylation to forms intermediate **F**. Finally oxidative ring opening reactions lead to the formation of carboxylic acids **H**, **I** and **J** (Fig. 38).

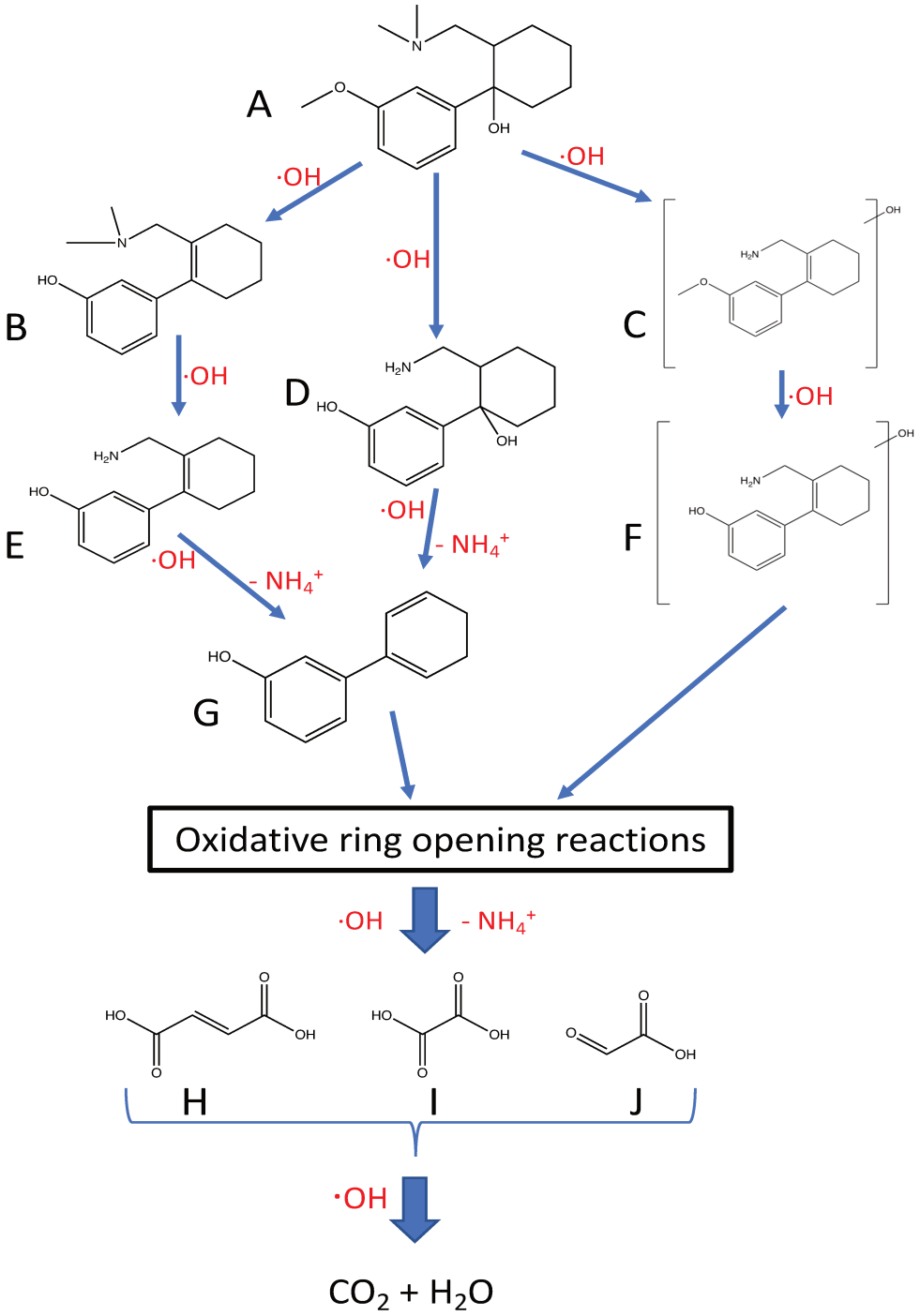

Fig 38: Degradation pathway for oxidation of TMT during electro-Fenton at 500 mA. [Na_2SO_4] = 50 mM, [Fe^{2+}] = 0.2.

3.5.3. Proposed mineralization pathway for oxidation of OFL by hydroxyl radicals

During the EF treatment of the OFL, four main routes of degradation could be identified thanks to HPLC and LC-MS analysis (Fig. 39). The structure modification happens at four different groups of the molecule; piperazinyl substituent, fluorine atom, quinolone moiety and to the cycle containing oxygen and azote atoms. Different degradation pathways of the OFL occurring during its oxidation under action of OH are depicted in Fig. 39. For the piperazinyl group, two types of degradation can occur: an α abstraction of H atom leading to the elimination of the methyl group to form intermediate **E** or a β abstraction where an hydrogen from the cycle is eliminated enabling the formation of molecules **C**, **D** and **G**. These types of degradation were already found during the degradation of levofloxacin by ozonation (Witte et al. 2009), during the photocatalytic treatment of ofloxacin (Vasquez and Hapeshi 2013) and during the degradation of ciprofloxacin by ozonation (Dewitte et al. 2008). Further oxidation by hydroxyl radicals on the piperazinyl substituent can lead to the formation of molecules **H** and **I** (Hapeshi et al. 2013; Pi et al. 2014). Finally the whole piperazinyl can be replaced by an hydroxyl group as in molecules **B** and **F**. Concerning the fluorine atom, it can be released in the solution as F^- by an ipso attack of the hydroxyl radicals (Michael et al. 2013; Mousset et al. 2018). The quinolone can be transformed, by the loss of C_3O, in a carboxylic group as in molecule **E** (Michael et al. 2013) or in an enone group as in molecule **A** and **G** (Vasquez and Hapeshi 2013; Pi et al. 2014; Yahya et al. 2014). Finally, the cycle containing the oxygen and the azote can loss C_2 (molecule **C**) or C_3 (molecule **D**, **G** and **I**), this was also found for the ozonation treatment of the OFL (Tay and Madehi 2015).

At the end of the degradation after oxidative ring opening reactions, three carboxylic acids could be identified (**J, K, L**).

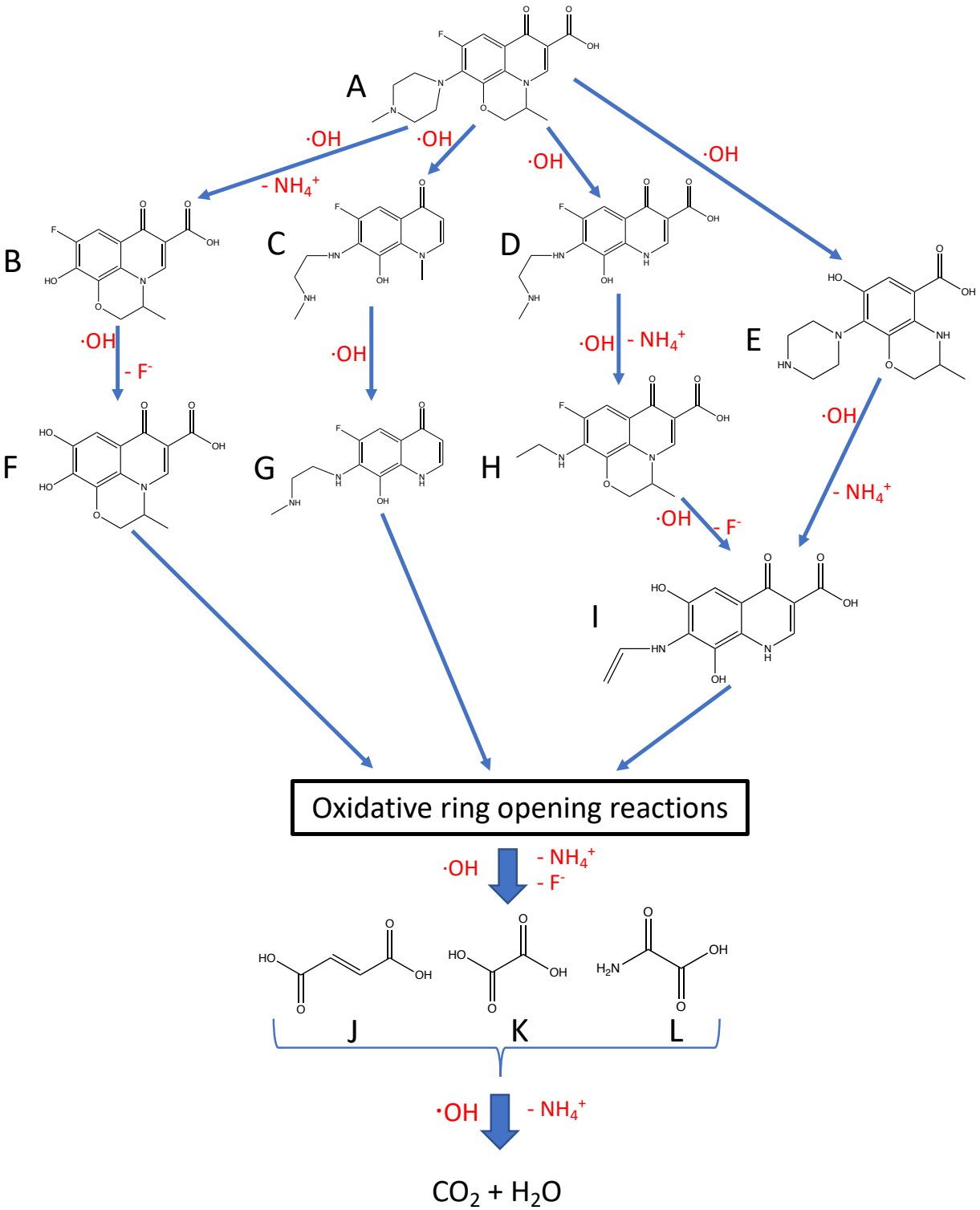

Fig 39: Degradation pathway during the electrolysis at 500 mA of OFL, 50 mM of Na_2SO_4 as the supporting electrolyte at 0.1 mM iron (II).

3.5. Conclusions

The results and discussion done above show that the pharmaceutical solutions under study were efficiently treated reaching high mineralization rates by EF process under the best operating conditions: catalyst (Fe^{2+}) concentration of 0.1 mM except for TMD (0.2 mM), and currents between 300 and 500 mA in 0.05 M Na_2SO_4 as supporting electrolyte. The absolute rate constants for oxidation of HCT, TMD, Nad and OFL by hydroxyl radicals were also determined using the competition kinetics method and found to be $(4.37 \pm 0.04) \times 10^9$, $(5.59 \pm 0.03) \times 10^9$, $(5.63 \pm 0.03) \times 10^9$ and $(5.55 \pm 0.05) \times 10^9$ M^{-1} s^{-1} respectively. The complete mineralization of 0.1 mM of all the pollutant solutions was reached at 6 h treatment. Finally, this study ends by proposing a plausible mineralization pathway of the three pharmaceuticals (HCT, TMD and OFL) by hydroxyl radical generated in EF process. These results illustrate the non-selectivity of the hydroxyl radicals, being able to eliminate nearly any organic compounds. The EF treatment is steel at scale up stage. Some pilots were built and successfully tested which suggest the possible use of this process at pre-industrial scale. This point will be discussed in next chapter. The idea would be to implement this system at the exit of industrial companies as the treatment is more efficient when the pollutant concentration is higher.

References:

Antonopoulou M, Konstantinou I (2016) Photocatalytic degradation and mineralization of tramadol pharmaceutical in aqueous TiO2 suspensions: evaluation of kinetics, mechanisms and ecotoxicity. Appl Catal A Gen 515:136–143. doi: 10.1016/j.apcata.2016.02.005

Ayoub K, van Hullebusch ED, Cassir M, Bermond A (2010) Application of advanced oxidation processes for TNT removal: A review. J Hazard Mater 178:10–28. doi: http://dx.doi.org/10.1016/j.jhazmat.2010.02.042

Bellakhal N, Oturan MA, Oturan N, Dachraoui M (2006) Olive Oil Mill Wastewater Treatment by the electro-Fenton Process. Environ Chem 3:345–349.

Borowska E, Bourgin M, Hollender J, et al (2016) Oxidation of cetirizine, fexofenadine and hydrochlorothiazide during ozonation: Kinetics and formation of transformation products. Water Res 94:350–362. doi: 10.1016/j.watres.2016.02.020

Bouissou-Schurtz C, Houeto P, Guerbet M, et al (2014) Ecological risk assessment of the presence of pharmaceutical residues in a French national water survey. Regul Toxicol Pharmacol 69:296–303. doi: 10.1016/j.yrtph.2014.04.006

Boxall ABA (2004) The environmental side effects of medication. EMBO Rep 5:1110–1116. doi: 10.1038/sj.embor.7400307

Brillas E, Sirés I, Oturan MA (2009) Electro-fenton process and related electrochemical technologies based on fenton's reaction chemistry. Chem Rev 109:6570–6631. doi: 10.1021/cr900136g

Brito C do N, de Araújo DM, Martínez-Huitle CA, Rodrigo MA (2015) Understanding active chlorine species production using boron doped diamond films with lower and higher sp3/sp2 ratio. Electrochem commun 55:34–38. doi: https://doi.org/10.1016/j.elecom.2015.03.013

Buxton G V, Greenstock CL, Helman WP, Ross AB (1988) Critical review of rate constants for reactions of hydrated electrons, hydrogen atoms and hydroxyl radicals (.OH/.O-) in aqueous solution. J Phys Chem Ref Data 17:513–886. doi: 10.1063/1.555805

Changotra R, Rajput H, Dhir A (2017) Natural soil mediated photo Fenton-like processes in treatment of pharmaceuticals : batch and continuous approach. Chemosphere 188:345–353. doi: 10.1016/j.chemosphere.2017.09.016

Dewitte B, Dewulf JO, Links C (2008) Ozonation of ciprofloxacin in water: HRMS identification of reaction products and pathways. Environ Sci Technol 42:4889–4895.

Dirany A, Sirés I, Oturan N, et al (2012) Electrochemical treatment of the antibiotic sulfachloropyridazine: kinetics, reaction pathways, and toxicity evolution. Environ Sci Technol 46:4074–4082. doi: 10.1021/es204621q

Dominguez CM, Oturan N, Romero A, et al (2018) Optimization of electro-Fenton process for effective degradation of organochlorine pesticide lindane. Catal Today 313:196–202. doi: https://doi.org/10.1016/j.cattod.2017.10.028

El-Ghenymy A, Rodríguez RM, Brillas E, et al (2014) Electro-Fenton degradation of the antibiotic sulfanilamide with Pt/carbon-felt and BDD/carbon-felt cells. Kinetics, reaction intermediates, and toxicity assessment. Environ Sci Pollut Res 21:8368–8378. doi: 10.1007/s11356-014-2773-3

Faouzi M, Cañizares P, Gadri A, et al (2006) Advanced oxidation processes for the treatment of wastes polluted with azoic dyes. Electrochim Acta 52:325–331. doi: http://dx.doi.org/10.1016/j.electacta.2006.05.011

Fernández C, González-Doncel M, Pro J, et al (2010) Occurrence of pharmaceutically active compounds in surface waters of the henares-jarama-tajo river system (madrid, spain) and

a potential risk characterization. Sci. Total Environ. 408:543–551.
Gabet-Giraud V, Miège C, Choubert JM, et al (2010) Occurrence and removal of estrogens and beta blockers by various processes in wastewater treatment plants. Sci Total Environ 408:4257–4269. doi: 10.1016/j.scitotenv.2010.05.023
Garcia-Segura S, Brillas E (2011) Mineralization of the recalcitrant oxalic and oxamic acids by electrochemical advanced oxidation processes using a boron-doped diamond anode. Water Res 45:2975–2984. doi: http://dx.doi.org/10.1016/j.watres.2011.03.017
Garcia-Segura S, Lanzarini-Lopes M, Hristovski K, Westerhoff P (2018) Electrocatalytic reduction of nitrate: fundamentals to full-scale water treatment applications. Appl Catal B Environ 236:546–568. doi: https://doi.org/10.1016/j.apcatb.2018.05.041
Ghalwa NA, Abu-Shawish HM, Zaggout FR, et al (2014) Electrochemical degradation of tramadol hydrochloride: novel use of potentiometric carbon paste electrodes as a tracer. Arab J Chem 7:708–714. doi: 10.1016/j.arabjc.2010.12.007
Giannakis S, Hendaoui I, Jovic M, et al (2017) Solar photo-Fenton and UV / H 2 O 2 processes against the antidepressant Venlafaxine in urban wastewaters and human urine . Intermediates formation and biodegradability assessment. Chem Eng J 308:492–504. doi: 10.1016/j.cej.2016.09.084
Guinea E, Arias C, Cabot PL, et al (2008) Mineralization of salicylic acid in acidic aqueous medium by electrochemical advanced oxidation processes using platinum and boron-doped diamond as anode and cathodically generated hydrogen peroxide. Water Res 42:499–511. doi: 10.1016/j.watres.2007.07.046
Hapeshi E, Fotiou I, Fatta-kassinos D (2013) Sonophotocatalytic treatment of ofloxacin in secondary treated effluent and elucidation of its transformation products. Chem Eng J 224:96–105. doi: 10.1016/j.cej.2012.11.048
Hummel D, Loffler D, Fink G, Ternes TA (2006) Simultaneous determination of psychoactive drugs and their metabolites in aqueous matrices by liquid chromatography mass spectrometry. Environ Sci Technol 40:7321–7328.
Isarain-Chávez E, Rodríguez RM, Garrido JA, et al (2010) Degradation of the beta-blocker propranolol by electrochemical advanced oxidation processes based on Fenton's reaction chemistry using a boron-doped diamond anode. Electrochim Acta 56:215–221. doi: 10.1016/j.electacta.2010.08.097
Jones OAH, Voulvoulis N, Lester JN (2005) Human pharmaceuticals in wastewater treatment processes. Crit Rev Environ Sci Technol 35:401–427. doi: 10.1080/10643380590956966
Kabdasli I, Olmez-Hanci T, Akgun G, Tunay O (2019) Assessment of pollution profile ans wastewater control alternatives of a pharmaceutical industry. Fresenius Environ Bull 28:516–522.
Khetan KS, Collins JT (2007) Human pharmaceuticals in the aquatic environment : a challenge to green chemistry human pharmaceuticals in the aquatic environment : a challenge to green chemistry. Chem Rev 107:2319–2364. doi: 10.1021/cr020441w
Kremer ML (2003) The Fenton Reaction. Dependence of the Rate on pH. J Phys Chem A 107:1734–1741. doi: 10.1021/jp020654p
Küster A, Adler N (2014) Pharmaceuticals in the environment : scientific evidence of risks and its regulation. R Soc Publ. doi: 10.1098/rstb.2013.0587
Lambropoulou D, Evgenidou E, Saliverou V, et al (2017) Degradation of venlafaxine using TiO 2 / UV process : kinetic studies, RSM optimization, identification of transformation products and toxicity evaluation. J Hazard Mater 323:513–526. doi: 10.1016/j.jhazmat.2016.04.074
Lindsey ME, Meyer M, Thurman EM (2001) Analysis of trace levels of sulfonamide and tetracycline antimicrobials in groundwater and surface water using solid-phase extraction and liquid chromatography/mass spectrometry. Anal Chem 73:4640–4646.

Luo Y, Guo W, Ngo HH, et al (2014) A review on the occurrence of micropollutants in the aquatic environment and their fate and removal during wastewater treatment. Sci Total Environ 473–474:619–641. doi: 10.1016/j.scitotenv.2013.12.065
Lütke Eversloh C, Schulz M, Wagner M, Ternes TA (2015) Electrochemical oxidation of tramadol in low-salinity reverse osmosis concentrates using boron-doped diamond anodes. Water Res 72:293–304. doi: 10.1016/j.watres.2014.12.021
Marcelino RBP, Andrade LN, Starling MCVM, et al (2016) Evaluation of aerobic and anaerobic biodegradability and toxicity assessment of real pharmaceutical wastewater from industrial production of antibiotics. Brazilian J Chem Eng 33:445–452.
Margot J, Rossi L, Barry DA, Holliger C (2015) A review of the fate of micropollutants in wastewater treatment plants. WIREs Water 2:457–487. doi: 10.1002/wat2.1090
Marselli B, Garcia-Gomez J, Michaud P-A, et al (2003) Electrogeneration of hydroxyl radicals on boron-doped diamond electrodes. J Electrochem Soc 150:D79–D83. doi: 10.1149/1.1553790
Martin De Vidales MJ, Millan M, Saez C, et al (2016) What happens to inorganic nitrogen species during conductive diamond electrochemical oxidation of real wastewater? Electrochem commun 67:65–68. doi: 10.1016/j.elecom.2016.03.014
Mendoza A, Aceña J, Pérez S, et al (2015) Pharmaceuticals and iodinated contrast media in a hospital wastewater: a case study to analyse their presence and characterise their environmental risk and hazard. Environ Res 140:225–241. doi: 10.1016/j.envres.2015.04.003
Michael I, Hapeshi E, Aceña J, et al (2013) Light-induced catalytic transformation of ofloxacin by solar Fenton in various water matrices at a pilot plant: mineralization and characterization of major intermediate products. Sci Total Environ 462:39–48. doi: 10.1016/j.scitotenv.2013.04.054
Mousset E, Oturan N, Oturan MA (2018) An unprecedented route of OH radical reactivity evidenced by an electrocatalytical process: Ipso-substitution with perhalogenocarbon compounds. Appl Catal B Environ 226:135–146. doi: https://doi.org/10.1016/j.apcatb.2017.12.028
Mousset E, Wang Z, Hammaker J, Lefebvre O (2016) Physico-chemical properties of pristine graphene and its performance as electrode material for electro-Fenton treatment of wastewater. Electrochim Acta 214:217–230. doi: 10.1016/j.electacta.2016.08.002
Nidheesh P V., Gandhimathi R (2012) Trends in electro-Fenton process for water and wastewater treatment: an overview. Desalination 299:1–15. doi: 10.1016/j.desal.2012.05.011
Oturan MA, Aaron J-J (2014) Advanced oxidation processes in water/wastewater treatment: principles and applications. A Review. Crit Rev Environ Sci Technol 44:2577–2641. doi: 10.1080/10643389.2013.829765
Oturan MA, Peiroten J, Chartrin P, Acher AJ (2000) Complete destruction of p-Nitrophenol in aqueous medium by electro-fenton method. Environ Sci Technol 34:3474–3479. doi: 10.1021/es990901b
Oturan MA, Pimentel M, Oturan N, Sirés I (2008) Reaction sequence for the mineralization of the short-chain carboxylic acids usually formed upon cleavage of aromatics during electrochemical Fenton treatment. Electrochim Acta 54:173–182. doi: https://doi.org/10.1016/j.electacta.2008.08.012
Oturan N, Brillas E, Oturan MA (2012) Unprecedented total mineralization of atrazine and cyanuric acid by anodic oxidation and electro-Fenton with a boron-doped diamond anode. Environ Chem Lett 10:165–170. doi: 10.1007/s10311-011-0337-z
Oturan N, Oturan MA (2018) Electro-Fenton process : background , new developments and applications. In: Martínez-Huitle CA, Rodrigo MA, Scialdone O (eds) Electrochemical

Water Treatment Methods. Elsevier, pp 1–32
Özcan A, Şahin Y, Oturan MA (2013) Complete removal of the insecticide azinphos-methyl from water by the electro-Fenton method – A kinetic and mechanistic study. Water Res 47:1470–1479. doi: http://dx.doi.org/10.1016/j.watres.2012.12.016
Panizza M, Cerisola G (2005) Application of diamond electrodes to electrochemical processes. Electrochim Acta 51:191–199. doi: 10.1016/j.electacta.2005.04.023
Panizza M, Cerisola G (2009) Direct and mediated anodic oxidation of organic pollutants. Chem Rev 109:6541–6569. doi: 10.1021/cr9001319
Panizza M, Cerisola G (2001) Removal of organic pollutants from industrial wastewater by electrogenerated Fenton's reagent. Water Res 35:3987–3992. doi: 10.1016/S0043-1354(01)00135-X
Pi Y, Feng J, Sun J, Song M (2014) Oxidation of ofloxacin by Oxone/Co2+: identification of reaction products and pathways. Environ Sci Pollut Res 3031–3040. doi: 10.1007/s11356-013-2220-x
Pulicharla R, Kumar R, Kaur S, et al (2015) Toxicity of chlortetracycline and its metal complexes to model microorganisms in wastewater sludge. Sci Total Environ 532:669–675. doi: 10.1016/j.scitotenv.2015.05.140
Randazzo S, Scialdone O, Brillas E, Sirés I (2011) Comparative electrochemical treatments of two chlorinated aliphatic hydrocarbons. Time course of the main reaction by-products. J Hazard Mater 192:1555–1564. doi: http://dx.doi.org/10.1016/j.jhazmat.2011.06.075
Ren G, Zhou M, Su P, et al (2019) Simultaneous sulfadiazines degradation and disinfection from municipal secondary effluent by a flow-through electro-Fenton process with graphene-modified cathode. J Hazard Mater 368:830–839. doi: https://doi.org/10.1016/j.jhazmat.2019.01.109
Rodrigo MA, Cañizares P, Sánchez-Carretero A, Sáez C (2010) Use of conductive-diamond electrochemical oxidation for wastewater treatment. Catal Today 151:173–177. doi: https://doi.org/10.1016/j.cattod.2010.01.058
Rúa-Gómez PC, Püttmann W (2012) Impact of wastewater treatment plant discharge of lidocaine, tramadol, venlafaxine and their metabolites on the quality of surface waters and groundwater. J Environ Monit 14:1391–1399. doi: 10.1039/c2em10950f
Rúa-Gómez PC, Püttmann W (2013) Degradation of lidocaine, tramadol, venlafaxine and the metabolites O-desmethyltramadol and O-desmethylvenlafaxine in surface waters. Chemosphere 90:1952–1959. doi: 10.1016/j.chemosphere.2012.10.039
Sirés I, Brillas E (2012) Remediation of water pollution caused by pharmaceutical residues based on electrochemical separation and degradation technologies: a review. Environ Int 40:212–229. doi: 10.1016/j.envint.2011.07.012
Sirés I, Brillas E, Oturan MA, et al (2014) Electrochemical advanced oxidation processes: today and tomorrow. A review. Environ Sci Pollut Res 21:8336–8367. doi: 10.1007/s11356-014-2783-1
Sirés I, Garrido JA, Rodríguez RM, et al (2007) Catalytic behavior of the Fe3+/Fe2+ system in the electro-Fenton degradation of the antimicrobial chlorophene. Appl Catal B Environ 72:382–394. doi: 10.1016/j.apcatb.2006.11.016
Sopaj F, Oturan N, Pinson J, et al (2016) Effect of the anode materials on the efficiency of the electro-Fenton process for the mineralization of the antibiotic sulfamethazine. Appl Catal B Environ 199:331–341. doi: 10.1016/j.apcatb.2016.06.035
Tay KS, Madehi N (2015) Ozonation of ofloxacin in water: by-products, degradation pathway and ecotoxicity assessment. Sci Total Environ 520:23–31. doi: https://doi.org/10.1016/j.scitotenv.2015.03.033
Vasquez MI, Hapeshi E (2013) Biodegradation potential of ofloxacin and its resulting transformation products during photolytic and photocatalytic treatment. Environ Sci

Pollut Res 1302–1309. doi: 10.1007/s11356-012-1096-5
Vergili I, Kaya Y, Gönder ZB, et al (2019) Occurence and prioritization of pharmaceutical active compounds in domestic / municipal wastewater treatment plants. Bull Environ Contam Toxicol 102:252–258. doi: 10.1007/s00128-019-02550-z
Verlicchi P, Galletti A, Petrovic M, BarcelÓ D (2010) Hospital effluents as a source of emerging pollutants: An overview of micropollutants and sustainable treatment options. J Hydrol 389:416–428. doi: 10.1016/j.jhydrol.2010.06.005
Witte B De, Langenhove H Van, Hemelsoet K, et al (2009) Chemosphere Levofloxacin ozonation in water : rate determining process parameters and reaction pathway elucidation. Chemosphere 76:683–689. doi: 10.1016/j.chemosphere.2009.03.048
Yahya MS, Oturan N, El Kacemi K, et al (2014) Oxidative degradation study on antimicrobial agent ciprofloxacin by electro-fenton process: Kinetics and oxidation products. Chemosphere 117:447–454. doi: 10.1016/j.chemosphere.2014.08.016
Yang W, Zhou M, Oturan N, et al (2019) Electrocatalytic destruction of pharmaceutical imatinib by electro-Fenton process with graphene-based cathode.
Yu Y, Huang F, He Y, et al (2019) Heterogeneous fenton-like degradation of o floxacin over sludge derived carbon as catalysts : mechanism and performance. Sci Total Environ 654:942–947. doi: 10.1016/j.scitotenv.2018.11.156
Zhang H, Fei C, Zhang D, Tang F (2007) Degradation of 4-nitrophenol in aqueous medium by electro-Fenton method. J Hazard Mater 145:227–232. doi: 10.1016/j.jhazmat.2006.11.016
Zimmermann SG, Schmukat A, Schulz M, et al (2012) Kinetic and mechanistic investigations of the oxidation of tramadol by ferrate and ozone. Environ Sci Technol 46:876–884. doi: 10.1021/es203348q

CHAPTER 3

Study on the efficiency of a new pilot scale continuous reactor for wastewater treatment by electrochemical advanced oxidation processes: influence of operating conditions and focus on hydrodynamics

1. Introduction

Electrochemical advanced oxidation processes (EAOPs) such as anodic oxidation (AO) and electro-Fenton (EF) are promising technologies to eliminate persistent and harmful organic pollutants from the environment (Iniesta et al. 2001; Hupert et al. 2003; Brillas et al. 2009). EAOPs produce strong oxidants, such as hydroxyl radicals which are able to degrade in a non-specific way nearly any type of pollutants as they are the strongest oxidants after fluorine (E^0 = 2.8 V *vs* SHE in acidic medium) (Eq. 8). EAOPs are able to achieve both degradation and mineralization of a large range of organic pollutants and effluents such as landfill leachate (Oturan et al. 2015; Zhou et al. 2016), pesticides (Rodrigo et al. 2014b; Dominguez et al. 2018a), dyes (Alcocer et al. 2018; Nidheesh et al. 2018) or pharmaceuticals (García-Montoya et al. 2015). The efficiency of these processes mainly depends on electrode materials, configuration of the electrochemical device, operating conditions, etc. (Monteil et al. 2018). Boron-doped diamond (BDD) is a particularly interesting anode material as it has a strong ability for oxidation of organic compounds and a long lifetime (Panizza et al. 2001; Actis et al. 2008; Cañizares et al. 2008; Brillas et al. 2009; Wei et al. 2011). BDD has a high overvoltage of oxygen evolution reaction allowing a large window for generation at its surface weakly adsorbed hydroxyl radicals.

The influence of the different operating parameters on the efficiency of these processes is now well-known and understood thanks to studies performed at lab-scale in batch conditions. The current, the concentration of pollutant or the concentration of the catalyst (mainly Fe^{2+} ion) were studied in order to optimize the kinetics of degradation at the lower cost. Besides, several studies have identified the mineralization pathways of various pollutants (Sirés et al. 2010; Dirany et al. 2012; Loaiza-Ambuludi et al. 2013; Bocos et al. 2016b; Dominguez et al. 2018a; Ganiyu et al. 2018), and sometimes the toxicity of the resulting solution was assessed (Oturan et al. 2008c; Dirany et al. 2012). The challenge is now to scale up the process in order to move

towards industrialization for removal of recalcitrant organic pollutants from water. Particularly, the development of continuous flow reactors is required in order to overcome the traditional limitations of conventional batch reactors for the treatment of large flow of effluents (Liang et al. 2008; Basha et al. 2012; Ling et al. 2015; Pillai and Gupta 2015; Rahmani et al. 2016; Pillai and Gupta 2017; Borzyszkowska and Espinoza-montero 2018).

A first step in scaling up is to move from lab-scale batch studies to the development of engineered pilot-scale continuous reactors. At this scale, only few studies have analyzed the influence of operating parameters such as current and catalyst concentration on the performance of the reactor (El-Ghenymy et al. 2013a; Olvera-vargas et al. 2015; Ren et al. 2016). Few studies have considered the influence of hydrodynamic conditions in the reactor, which becomes a key parameter for this kind of application. For instance, the link between the hydrodynamic and the degradation of phenol was examined by Polcaro et al. (2007) and Saravanathamizhan et al. (2008). The reactor had a simple hydrodynamic configuration, which was represented by a continuous-stirred tank reactor (CSTR) (Polcaro et al. 2007) or by a CSTR with a bypass, active and dead zones with exchange flow between the active and the dead zone (Saravanathamizhan et al. 2008). In another study, a continuous multi-cell reactor was implemented and the model of a plug flow reactor was found to describe accurately this system (Ling et al. 2015). However, there is a real need to go further in the analysis of the link between hydrodynamics and the efficiency of the continuous reactors since hydrodynamics governs the characteristic times of mixing and the retention time of pollutants in the reactor. The hydrodynamic behavior of pilot scale continuous reactors is in general more complex than lab scale reactors that follow CSTR behavior. Some behavioral deviations from ideal reactors may appear such as the presence of dead and recirculation zones or short circuit that affect the global efficiency of the process. There is thus a need to perfectly know the influence of the operational parameters such as flow

rate, reactor configuration or aeration on the hydrodynamic behavior of the reactor in order to optimize its efficiency.

In this context, the present work focuses on a new pilot-scale reactor operating in continuous mode. Hydrochlorothiazide (HCT), a diuretic, was chosen as a model pollutant as (i) it could be found in effluents from hospitals (Mendoza et al. 2015), (ii) it is hardly removed by wastewater treatment plants (Margot et al. 2015), (iii) its occurrence in surface water has been evidenced (Bouissou-Schurtz et al. 2014) and (iv) it is harmful toward the environment (Fernández et al. 2010). First, an empirical design of experiments (DOE) approach was used to identify the most critical operating parameters for the efficiency of the process such as current density, iron concentration, flow rate and the reactor configuration with the number of electrodes and the distance between them. Secondly, the influence of flow rate and reactor configuration on the efficiency of hydrodynamics was studied in depth and linked with the efficiency of the process. Finally, a hydrodynamic retention time distribution (RTD) model was developed and combined for the first time with a kinetic model in order to describe the mineralization of pollutants by EAOPs in such new pilot scale continuous reactor.

2. Materials and methods

2.1. Chemicals

The pharmaceutical HCT ($C_7H_8ClN_3O_4S_2$, purity >99%) and sodium sulfate (Na_2SO_4), the supporting electrolyte, were purchased from Sigma Aldrich. HCT solutions were prepared with ultrapure water obtained from a Millipore Milli-Q Simplicity 185 system with resistivity >18 MΩ cm at 25 °C. The pH of the solutions was adjusted using analytical grade sulfuric acid or sodium hydroxide (Acros). Organic solvents and other chemicals used were HPLC or analytic grade from Sigma-Aldrich, Fluka and Merck.

2.2. Electrochemical equipment

The electrochemical reactor made of plexiglass was equipped with two different configurations. In the first configuration, the reactor is composed of 7 anodes and 7 cathodes separated by 4 cm each other (Fig. 40), in the second one it is composed of 14 anodes and 14 cathodes separated by 2 cm each other. Anodes are made of BDD film on niobium support (from CONDIAS GmbH) of 30 cm^2 and cathodes are made of 3D carbon felt (from Mersen, France) of 30 cm^2. Two peristatic pumps FH100 were used to control the flow throughout the reactor at flow rates of 20.4, 42.5, 85.0, 127.5 and 170.0 mL min^{-1}. Air supply was provided by a fine bubble diffuser (Fig. 40) and controlled by an air flowmeter. To assess the influence of the airflow, two airflows were tested (0.2 and 0.6 L min^{-1}) without changing the other operating conditions. The results were very similar for oxidative degradation of HCT and for the mineralization of its solution. Thus, it was decided to work with airflow of 0.2 L min^{-1} in all experiments. The solutions to be degraded contain 0.1 mM of HCT, 50 mM of Na_2SO_4 and the pH is adjusted to 3 with 1 M of sulfuric acid. A constant current was delivered by a Microlab power supply to the electrodes mounted in parallel.

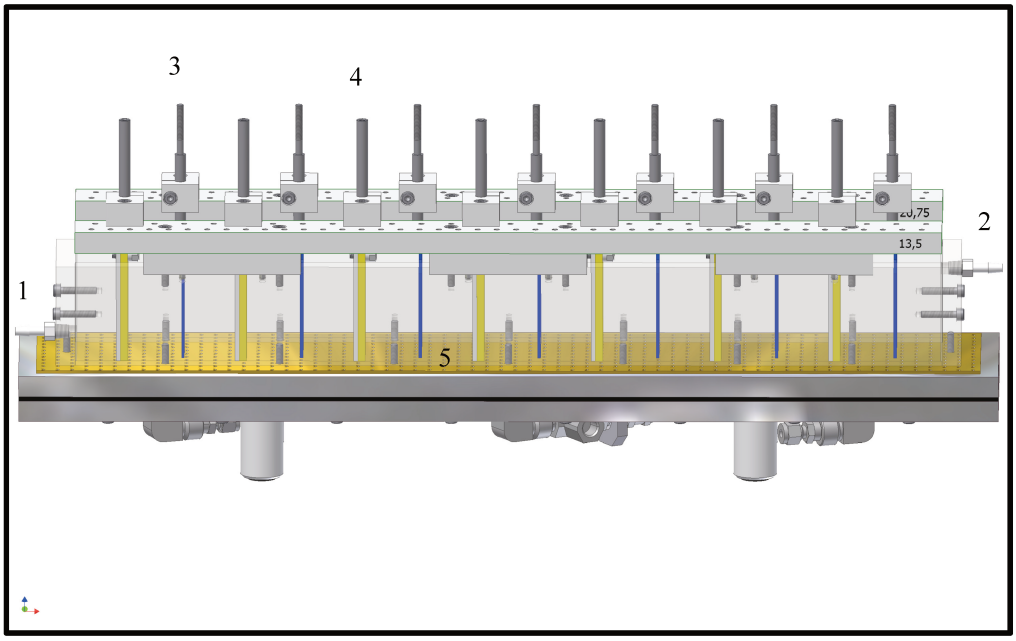

Fig. 40: Schematic representation of the lab scale pilot in the configuration with 14 electrodes done with the software Solidworks, 1: inlet, 2: outlet, 3: BDD anode, 4: carbon felt cathode and 5 air inlet.

2.3. HCT degradation and mineralization

The HCT concentration is measured to determine the decay of HCT concentration when the steady state is reached. All experiments are at least performed in duplicate.

The degradation study was monitored by an HPLC analyzer (Merck Lachrom Liquid chromatography) equipped with a L-2310 pump and a reverse phase (Pursopher RP-18), 5 µm, 25 cm × 4.6 mm (i.d.) column and coupled with a L-7455 photo-diode array detector. The eluent conditions were: 95/5 water/methanol at a liquid flow rate of 0.25 mL min^{-1} and the UV detector was set at 270 nm. Samples of 20 µL were injected in the column at 40°C.

The mineralization of HCT solutions was determined by the measure of the total organic carbon (TOC) using a Shimadzu VCSH TOC analyzer according to the catalytic combustion method at 680 °C. Reproducible TOC values with ± 2% accuracy were found using the non-purgeable organic carbon method. The mineralization rate (%) was calculated thanks to Eq. 35.

$$\%\, Mineralization = \frac{TOC_0 - TOC_f}{TOC_0} \quad (35)$$

where TOC_0 is the the TOC at the beginning of the experiment and TOC_f, the TOC at steady state. For both mineralization and degradation, the quasi steady state was reached after 3 residence times (Annex Fig. 1). The modelling of the kinetic was performed by the software Aquasim® (Reichert 1998).

2.4. Mineralization current efficiency (MCE) and energy consumption (EC)

The EC was determined to evaluate the operating cost of the process. The EC formula (Brillas et al. 2009) was modified to fit the continuous mode is given in Eq. 36.

$$EC(kWh/gTOC) = \frac{E*I}{(TOC_0 - TOC_f)*D*3600} \quad (36)$$

with *E*, the cell voltage (V), *I* the current (A) and *D* the flow rate in L s^{-1}.

The MCE was used to estimate the efficiency of the reactor in the treatment of the HCT solution. The MCE usual formula (Brillas et al. 2009) was modified in order to be consistent with the continuous mode (Eq. 37).

$$MCE(\%) = \frac{n\,F\,(TOC_0 0 - TOC_f)}{M\,m\,I\,D} * 100 \quad (37)$$

where m is the number of carbon atoms of HCT (7), M is the molar mass of the carbon (12 000 mg mol^{-1}) and n is the number of electrons used to mineralize one molecule of HCT following the Eq. 38 assuming that N atoms of HCT were mainly converted to NH_4^+.

$$C_7H_8ClN_3O_4S_2 + 18\ H_2O \rightarrow 7\ CO_2 + 32\ H^+ + 2\ SO_4^{2-} + 3\ NH_4^+ + Cl^- + 30\ e^- \quad (38)$$

2.5. Design of experiments (DOE)

To have an empirical overview of the influence of selected operating parameters on the degradation, the mineralization, the EC and the MCE during the EF and the AO treatments, the Doehlert experimental design was applied. This method requires the selection of input

parameters of interest. The liquid flow rate was chosen as it is an important parameter for continuous process, since it governs the hydraulic retention time in the reactor. The current and the catalyst (Fe^{2+}) concentration were added as they are key parameters in electrochemical processes. The Doehlert matrix for three parameters consists of 13 experiments. For each parameter (Ui), different values were tested according to the Doehlert matrix (Table 12) between a maximum and a minimum level chosen according to lab scale studies. Table 13 gives the minimum and maximum level for each parameter and its coded value (Xi) according to the following equation (Eq. 39).

$$Xi = \left(\frac{Ui - Ui0}{\Delta Ui}\right) \alpha i \quad (39)$$

with Ui_0, the central value for Ui, ΔUi, the gap between the highest and the lowest value for Ui and αi, equal to 1, $\frac{\sqrt{3}}{2}$ and $\frac{\sqrt{6}}{3}$ for α1, α2 and α3 respectively.

Table 12: Experimental variables and Doehlert matrix

	Experimental variables			Doehlert Matrix		
	U_1	U_2	U_3	X_1	X_2	X_3
1	33.3	95.2	0.13	1	0	0
2	3.3	95.2	0.13	-1	0	0
3	25.8	170.0	0.13	0.5	0.866	0
4	10.8	20.4	0.13	-0.5	-0.866	0
5	25.8	20.4	0.13	0.5	-0.866	0
6	10.8	170.0	0.13	-0.5	0.866	0
7	25.8	120.7	0.25	0.5	0.287	0.816
8	10.8	69.7	0	-0.5	-0.287	-0.816
9	25.8	69.7	0	0.5	-0.287	-0.816
10	18.4	144.5	0	0	0.577	-0.816
11	10.8	120.7	0.25	-0.5	0.287	0.816
12	18.4	45.9	0.25	0	-0.577	0.816
13	18.4	95.2	0.13	0	0	0

Table 13: Extremum values for each parameter

Variables	Maximum Ui	Minimum Ui	Maximum Xi	Minimum Xi
Current (A) 1	33.3	3.3	1	-1
Flow rate (mL min^{-1}) 2	170	20.4	0.866	-0.866
Fe^{2+} concentration (mM) 3	0.25	0	0.816	-0.816

The response function (Y) is a second order polynomial function expressed by Eq. 40:

$$Y = bo + b_1X_1 + b_2X_2 + b_3X_3 + b_{11}X_{11}^2 + b_{22}X_{22}^2 + b_{33}X_{33}^2 + b_{12}X_1X_2 + b_{13}X_1X_3 + b_{23}X_2X_3 \quad (40)$$

with b_i and b_{ii} the coefficients of the model. The software Nemrod® was used to estimate the different coefficients.

2.6. Retention time distribution (RTD)

RTD experiments were performed by the tracer method (Viva and Brunazzi 2009). When the reactor was entirely filled and the flow stable, a salt tracer (6 mL of 233 g L^{-1} of KCl) was injected at the entrance of the reactor by a syringe of 10 mL. The conductivity of the tracer leaving the reactor was measured. After each acquisition the reactor was emptied and ultrapure water was used to clean it.

The theoretical residence time (τ) is defined thanks to the volume of the reactor and the flow rate (Eq. 41) and represents the theoretical mean time to flow through the reactor.

$$\tau = V/Q \quad (41)$$

with τ in min, V the volume of the reactor (mL) and Q the flow rate (mL min^{-1}).

To model the RTD functions a dimensionless time is convenient; it is defined by the time divided by the theoretical retention time (Eq. 42).

$$\theta = t / \tau \quad (42)$$

with t, the time (min) and τ the theoretical residence time (min).

The residence time distribution function (E) gives the age distribution frequency of fluid elements leaving the reactor (Eq. 43).

$$E(\theta) = C(\theta)/C_0 \quad (43)$$

with θ, the dimensionless time, $C(\theta)$, the tracer concentration at the exit of the reactor at time θ and C_0, the tracer concentration obtained if all the injected mass was diluted into the volume of the reactor (1.7 L). C_0 (concentration of the tracer) is equal to $1.1 * 10^{-2}$ M. Thanks to the shape

of the RTD curves the reactor modelling can be identified. The mean residence time is then obtained thanks to the following equation (Eq. 44).

$$Ts = \frac{\int_0^1 \theta\, E(\theta) d\theta}{\int_0^1 E(\theta) d\theta} \quad (44)$$

2.7. Mathematical tools

To compare the model results with experimental measurements the index of agreement (IOA) (Eq. 45) was used (Mousset et al. 2016; Trellu et al. 2016b).

$$\mathrm{IoA} = 1 - \frac{\sum_{i=1}^{K} (y_i - z_i)^2}{\sum_{i=1}^{K} (|z_i - y_M| + |y_i - y_M|)^2} \quad (45)$$

where K is the number of observed values, y_i is a numerically simulated value, z_i is the corresponding experimentally observed value, y_M is the average of the numerically simulated values.

The correlation coefficient was calculated by Eq. 46.

$$\mathrm{R} = \sum_{i=1}^{P} [(xi - xm) * (yi - ym)] \,/\, \left(\sqrt{\left(\sum_{i=1}^{P} [(xi - xm)\text{^}2]\right)} * \sqrt{\sum_{i=1}^{P} [(yi - ym)\text{^}2]}\right) \quad (46)$$

with R, the correlation coefficient, xi, an experimental point, xm, the mean of the experimental points, yi, a theoretical point, ym, the mean of the theoretical points and P the number of points.

3. Results and discussion

3.1. Influence of operating parameters and configuration on the reactor efficiencies

To identify the relative influence of different operating parameters on the degradation of HCT and mineralization of its solution, and therefore on the MCE and EC, a DOE method was applied. Three parameters were considered: i) the current density, ii) the flow rate and iii) the catalyst (Fe^{2+}) concentration. The 14-electrode configuration was used in this part. The thirteen different experiments and their results are detailed in Table 14. With regard to the oxidative degradation of HCT, a complete degradation was observed for several conditions and thus the model could not be applied. However, it was evidenced that the current was by far the most important parameter for the degradation efficiency of the reactor. This is in accordance with batch experiments (Ellouze et al. 2017). Additionally, other experiments have been performed in order to compare two reactor configurations.

Table 14: Mineralization and degradation rate, MCE and EC obtained for different experiments

Experiment	Mineralization rate (%)	Degradation rate (%)	MCE (%)	EC (kWh (g TOC)$^{-1}$)
1	25.5	100	2.06	6.13
2	5.2	23	4.19	1.01
3	9.7	67	1.79	6.08
4	45.1	97	2.54	2.86
5	82	100	2.33	4.56
6	7.3	30	2.58	2.71
7	17.1	100	1.85	6.05
8	13.9	54	2.85	2.66
9	27.8	100	1.97	5.98
10	7.4	68	1.55	6.16
11	11.7	56	2.84	2.59
12	37.8	100	2.20	4.30
13	14.8	91.5	1.70	5.40

3.1.1. Mineralization, EC and MCE

Unlike the degradation, the mineralization fitted well with the polynomial model. The different coefficients estimated are given in Fig. 41a. A correlation coefficient of 0.972 and an adjusted one of 0.9 were obtained with these coefficients values thanks to Nemrod® software.

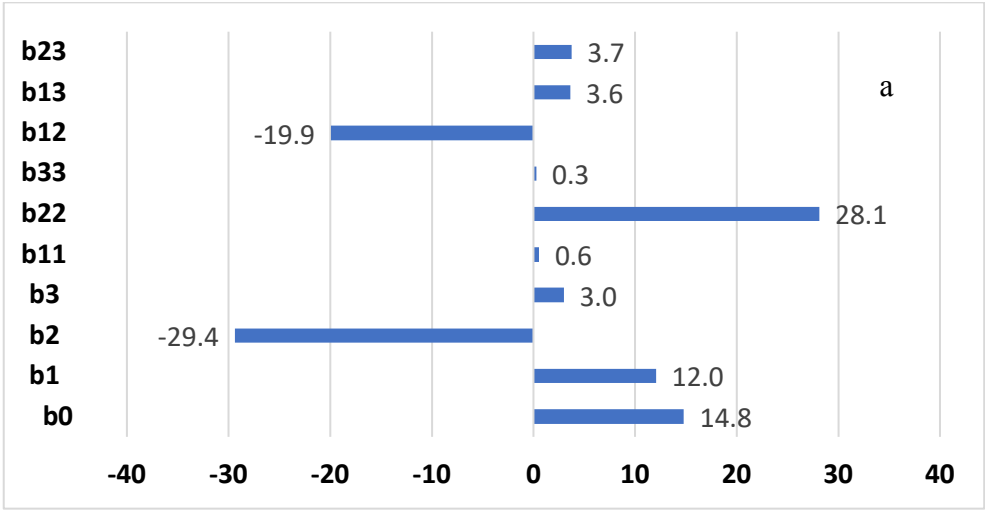

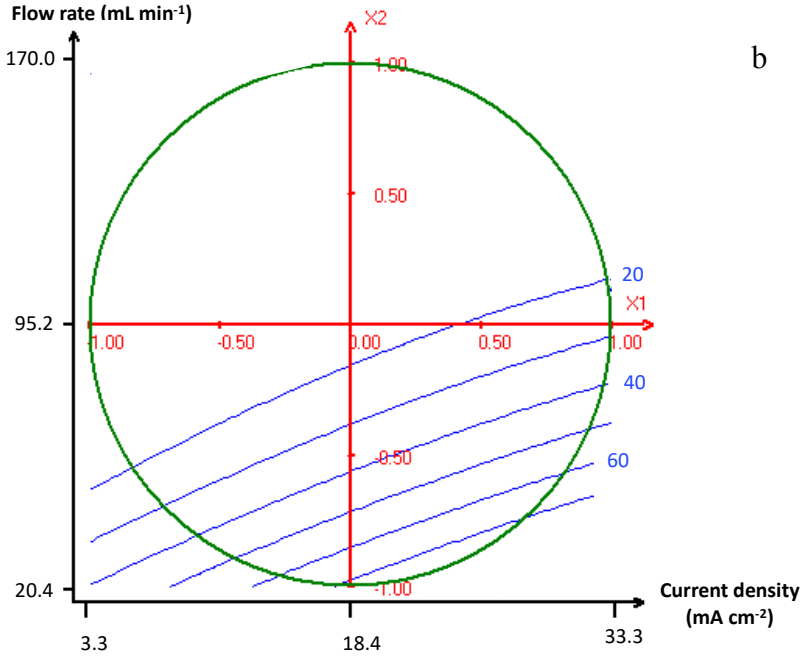

Fig. 41: Coefficients of the polynomial function (a) and (b) contour plots versus the liquid flow rate (mL min^{-1}) and the current density (mA cm^{-2}) obtained from the Doelhert matrix for the mineralization rate of HCT.

In the range of operating parameters selected, from the coefficient values obtained it appears that the most important parameter was the flow rate (X_2) followed by the current ($|b_2| > |b_1| > |b_3|$). The catalyst concentration appears to have much less influence on the mineralization than the two other operational parameters. This suggests that AO is the main process influencing mineralization. Although EF is generally more efficient than AO for degradation, the mineralization efficiency differs little (Guinea et al. 2010; Feng et al. 2014). This point will be discussed deeply in a next sub-section.

The positive sign of b_1 and b_3 means that the mineralization rate will increase by increasing the catalyst concentration and the current. This fact was expected as by increasing the current more hydroxyl radicals are formed and the increase in catalyst concentration (in a certain range) promotes the Fenton reaction. The minus sign of the coefficient b_2 means that to increase the mineralization rate, the flow rate has to be reduced; this is due to the longer treatment time inside the reactor. The important absolute value of coefficient b_{12} means that the current and the flow rate are connected and govern mainly the efficiency of the mineralization process. The minus sign indicates that those two parameters work in the opposite way, one brings a positive effect while the other plays a negative effect on the mineralization. This is consistent with the sign of the coefficient b_1 and b_2 which are opposite. Thus, for a better mineralization rate, the current should increase and the flow rate decrease. This behavior was verified by analyzing the results of run 4 to 8 (Annex Table 1). It can be observed that the higher is the flow rate, the lower is the mineralization. This result can be explained by the lower contact time of the solution with hydroxyl radicals. The effect of the current was also verified with run 9-11 (Annex

Table 1) since an increase of the current from 10 to 22 mA cm^{-2} leads to an increase of the mineralization rate from 50% to 76%.

Thanks to the polynomial function Y, it is possible to predict the mineralization rates in the area defined by the upper and lower values of each parameter. Indeed, by replacing all the coded values: X_1 (current), X_2 (flow rate) and X_3 (Fe^{2+} concentration) in Eq. 46, the mineralization rate (Y) can be estimated. This can be illustrated by contour plots. Fig. 41b illustrates the flow rate versus the current at a given catalyst concentration at the center of its range (X_3=0). For instance, the line blue 40 corresponds to the "iso-mineralization rate" of 40% representing all the conditions of flow rates and currents where the mineralization rate is of 40% at a defined Fe^{2+} concentration of 0.13 mM.

Fig. 42 illustrates the contour plots for MCE and EC. In Fig. 42a and Fig. 42b, one isocurve represents all the conditions of flow rates and currents at Fe^{2+} concentration of 0.13 mM where the EC and the MCE have respectively a defined value.

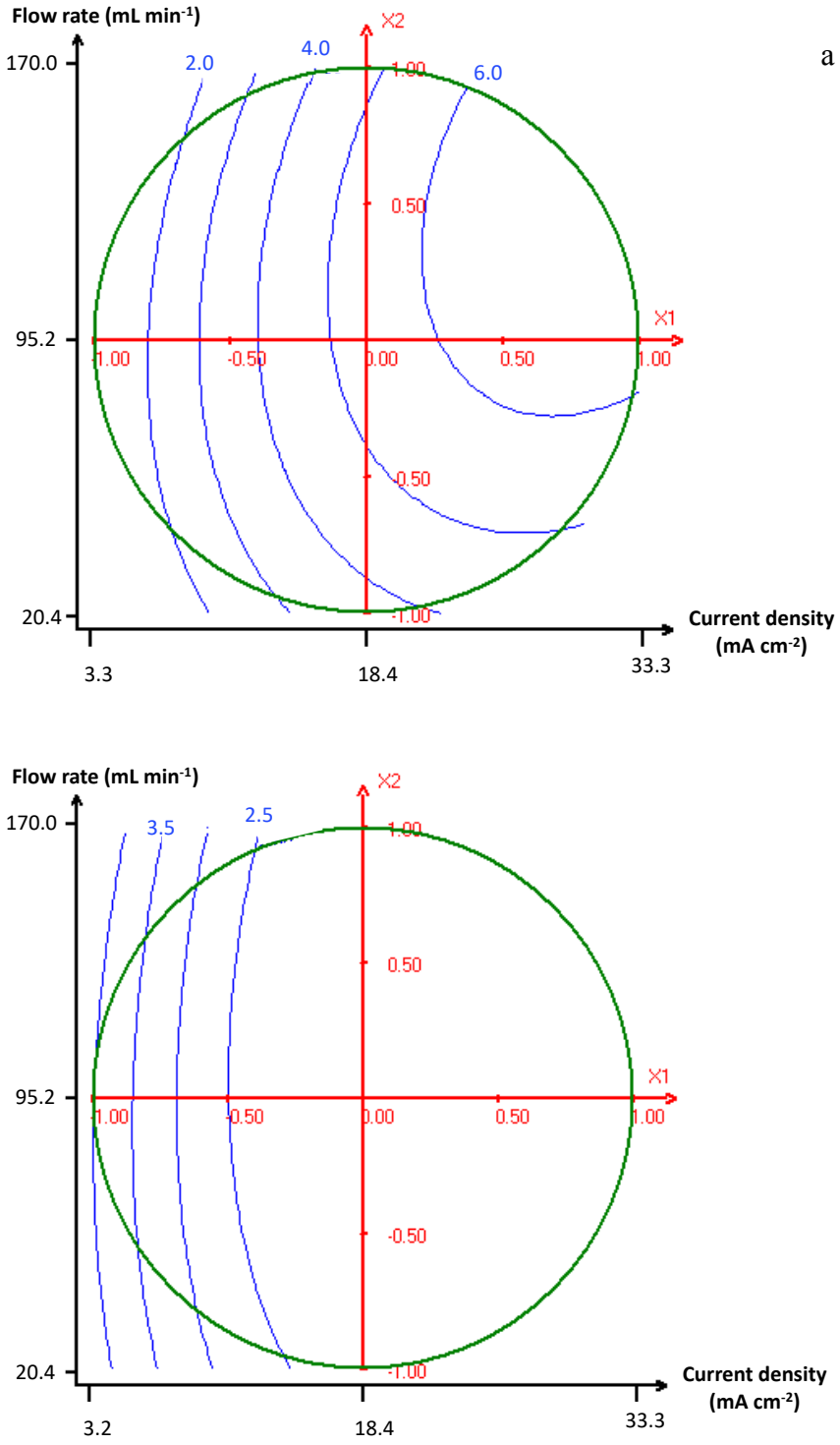

Fig. 42: Contour plots of the EC in kWh $(gTOC)^{-1}$ (a) and MCE in % (b) versus the liquid flow rate (mL min^{-1}) and the current density (mA cm^{-2}).

For both MCE and EC, the current is the most important operating parameter ($|b_1| > |b_2|$) as illustrated in Fig.42 where the iso-curves are parallels to the flow rate axis. Here also the catalyst

concentration has nearly no impact. The lower is the current, the higher is the MCE and the lower is the EC. This opposite influence of the high currents can be explained by scavenging reactions that occur at higher current intensity, for example water oxidation at the anode and H_2 evolution at the cathode (Zhang et al. 2007). Finally, a compromise between a high degradation and an acceptable EC and MCE has to be chosen. In other terms, a good balance for the current and flow rate is required.

Finally, this process is really advantageous compared to more conventional processes because of its high mineralization power allowing high mineralization rate. For example, 97% of the initial TOC value could be removed under 47.6 mA cm^{-2} current, flow rate of 20.4 mL min^{-1}, 0.2 L min^{-1} of air flow rate and 50 mM of Na_2SO_4. This process is much more efficient than an activated sludge treatment were only 30% of HCT is in general eliminated in conventional wastewater treatment plants (Margot et al. 2015). It seems also to be more efficient than O_3 treatment where only 80% of the solution is mineralized (Rosal and Agüera 2008). However, even if this process is very efficient compared to the conventional methods, some energy is wasted in side reactions as can be seen with the MCE values of Fig. 42b. Thus a compromise should be reached between high efficiency and cost effective process. Therefore the combination of electro-Fenton with a biological treatment can constitute a promising option. The goal of such a coupling being to transform the non-biodegradable compounds into biodegradable species in a first stage by electro-Fenton, and then apply a biodegradation step to reach high mineralization degrees.

3.1.2. Influence of the configuration on the mineralization rate and EC

To deeper understand the interactions between reactor configuration and operational parameters, two configurations were tested: the first with 14 electrodes and a gap of 4 cm

between electrodes and the second with 28 electrodes and a distance of 2 cm between electrodes.

Table 15: Influence of the configuration on the mineralization rate at steady state. 0.1 mM of HCT, 50 mM of Na_2SO_4 and 0.2 $L.min^{-1}$ of air were used for all the experiments.

Run	Flow rate ($mL\ min^{-1}$)	Current (A)	Current density ($mA\ cm^{-2}$)	Configuration	Mineralization (%)
1	20.4	2.55	12	14	55
2	20.4	2.55	6	28	66
3	20.4	5.1	12	28	81

The mineralization of the solution was tested for both configurations with different currents or with similar currents but different current densities. For the same total applied current, the mineralization is higher for the 28-electrode system (by comparing Run 1 and 2 of the Table 15). This can be explained by the low extent of side reactions at low current densities, thus the applied current is less wasted in the system allowing better mineralization rate. For the same current per cell, the mineralization is much higher with this 28 electrodes system (around 30% of increases by comparing Run 1 and 3). This confirms that the most important parameter is the contact time between the solution and the electrodes which was already highlighted by the importance of the flow rate.

The operating cost (EC) was also considered for both configurations. Fig. 43 depicts the results obtained. As can be seen from this figure, the 28-electrode configuration is more cost effective as for the same current density per branch the EC is always higher for the 14-electrode configuration.

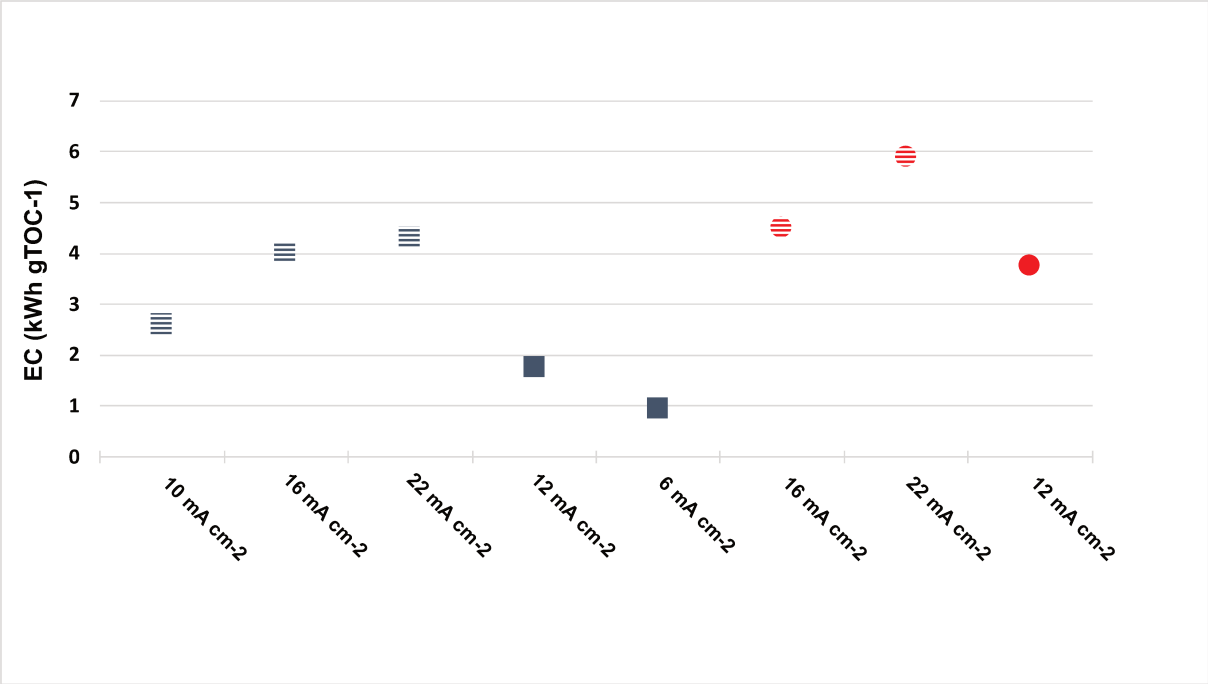

Fig. 43: EC for different configurations, different flow rates and different current densities under 0.2 L min^{-1} of air. Circles correspond to the 14-electrode and squares to the 28-electrode configurations, full points to a flow rate of 20.4 mL min^{-1} and stripe dots to a flow rate of 42.5 mL min^{-1}.

To conclude, the best operating parameter is clearly the flow rate for the mineralization and the current density for both the EC and the MCE values. The impact of the Fe^{2+} (catalyst) concentration is difficult to analyze; it seems to have a very little effect on the mineralization efficiency in the 14-electrode system. The gap between the electrodes (4 cm) could explain this difference, as preventing the regeneration of iron due to the limiting mass transfer of ferric ion to the cathode (Zhang et al. 2006). Thus the 28-electrode configuration was tested and only a small increase in the mineralization rate was observed. However, the ratio between the total cathode surface and the total anode surface is largely smaller than that used in most batch studies which leads to a lower Fe^{2+} and H_2O_2 relative production at the cathode, promoting rather AO compared to EF. In our batch experiments, the cathode covers all the inner surface of the electrochemical cell ($S_{cathode}/V_{solution}$ = 0.9 cm^{-1}) whereas in the pilot this ratio is much lower ($S_{cathode}/V_{solution}$ = 0.25 cm^{-1}). Moreover, this low surface ratio associated to the continuous flow in the reactor could also promote the oxidation of Fe^{2+} and H_2O_2 at the anode

compared to other studies. Adding a cathode on the floor or sides of the reactor directly linked to the air bubbling to promote H_2O_2 production could constitute a solution to this issue.

The role of the configuration is very important as it drastically influences the mineralization rate and the cost of the process. The comparison between the two configurations leads to the following statement: for both point of view, the 28-electrode configuration is better, with shorter distance between the electrodes and higher active surface area.

This part has demonstrated that the flow rate and the configuration play an important role on the EC and the mineralization rate. Thus, as they are closely associated to the path followed by the pollutants in the reactor, a deeper analysis of the hydrodynamics in the reactor was carried out.

3.2. Hydrodynamics

3.2.1. RTD curves

RTD curves were drawn in order to identify the variation of flow pattern in the reactor and to choose the most suitable model to characterize the pilot. Fig. 44 shows the RTD curves obtained for the system containing 28 electrodes at different flow rates. The equivalent chart for 14-electrode configuration is given in Annex Fig. 2. The parabolic shape of the curves shows that there is no by-pass or short-circuit in the reactor. One can observe that the higher is the flow rate, the thinner is the peak and the smaller is the area of the peak. The lower slope at the end of the curves highlights the presence of stagnant zones (Haoran et al. 2013). For both 14- and 28-electrode configurations, it can be observed similar shapes. Thus, the same model is applied for both configurations, as described below.

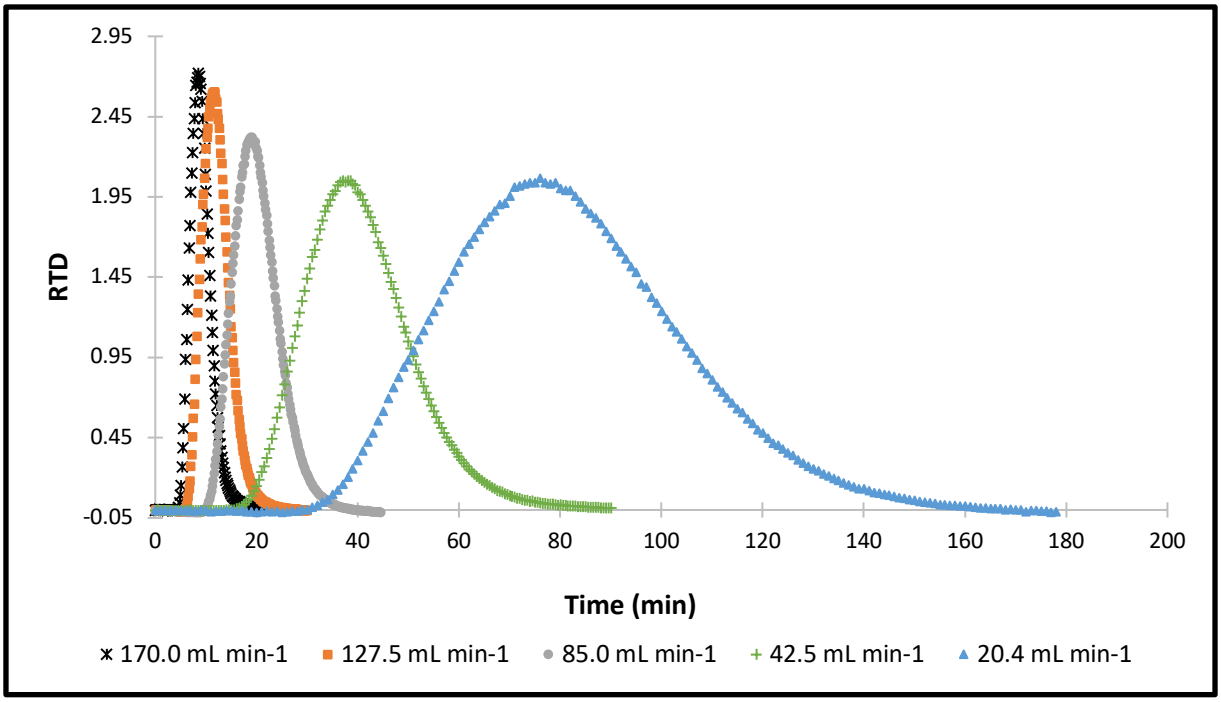

Fig. 44: RTD functions plotted against the time for different flow rates under 0.2 mL min^{-1} of air with 28-electrode configuration.

The mean retention time (Ts) can be estimated as the time when half of the area of the curve is reached. As the peaks are quite symmetric the mean retention times can be read on the curve at the top of each peak. Table 16 compares the theoretical retention time (τ) with the Ts for the two configurations at different flow rates. The τ is higher than Ts, which is a characteristic phenomenon observed when dead volumes are present in the reactor. Furthermore, Ts for 28-electrode configuration is longer than Ts for 14-electrode configuration because of additional troublemakers in the 28-electrode system that lengthen the flow path inside the reactor (Annex Fig. 4).

Table 16: Residence time (τ) and mean residence time (Ts) for different flow rates with 14- and 28-electrode configurations.

Q (mL min^{-1})	20.4	42.5	85.0	127.5	170.0
τ (min)	83	40	20	13	10
Ts (28-elect) (min)	78	38	19	12	9
Ts (14-elect) (min)	66	34	18	11	-

Because of the symmetric aspect of the curves and the presence of dead volumes, the model of continuously stirred tank reactors in series with dead volumes was selected and compared to the classical plug flow model. The CSTR model was also proposed as the vertical bubbling enable to realize an efficient mixing of the solution.

3.2.2. Model

In order to confirm this hypothesis, the experimental were compared to the CSTR in series model. The RTD ($E(\theta)$) for the CSTR model is given by the Eq. 47.

$$E(\theta) = \frac{1}{mN} * \frac{N\text{^}2}{(N-1)!} * \ \theta\text{^}(N-1) \ * \exp\left(-\frac{N\theta}{m}\right) \quad (47)$$

with m, the fraction of active volume, and N the number of continuously stirred tank reactors. When N approaches 1, the reactor is similar to a CSTR and when N approaches infinity, the model is approaching a plug flow. Both m and N were estimated thanks to the Excel solver. In order to check the strength of the model, different initial parameter (N and m) were taken and the correlation coefficient was calculated by Eq. 11. All the correlation coefficients were over 0.9928 (Table 18) which confirms the suitability for the model.

This CSTR in series model was then compared to the plug flow model describe by Eq. 48.

$$E(t) = \frac{1}{2 * Ts} * \sqrt{\frac{Pe}{\pi}} * e^{-\frac{Pe\left(1-\frac{t}{Ts}\right)^2}{4}} \quad (48)$$

with Pe the Peclet number representing the proportion of convective flow compared to diffusive flow. The plug flow model is known to be well representing a system when the Pe number is over 100. Both Ts and Pe were estimated thanks to Excel solver with the RTD curves. The different parameters were calculated for the 28-electrode configuration. Ts, Pe and the correlation coefficient are given in Table 17 for all the flow rates.

Table 17: Mean residence time Ts, Pe number and the correlation coefficient for different flow rates with 28 electrodes.

Q (mL min^{-1})	20.4	42.5	85.0	127.5	170.0
Pe	36	43	55	58	65
Ts (min)	78	38	18	13	9
R^2	0.982	0.973	0.978	0.987	0.985

The Pe numbers grow with higher flow rates, which mean that the flow is being more convective for higher flow rates. Meanwhile the Pe numbers are below 100 meaning that the plug flow model is not relevant, even more as the more accurate flow rates are the lower ones. The correlation coefficient for the CSTR model (Table 18) are closer to 1 than for the plug flow model (Table 17) which is also in favor of the mixed tank reactors. Thus the CSTR model in series with dead volumes will be used to study the reactor (Annex Fig. 3).

Table 18: Correlation coefficients for the two configurations at different flow rates for the CSTR in series model.

Flow rate ($mL.min^{-1}$)	20.4	42.5	85	127	170
14 electrodes	0.9928	0.9988	0.9995	0.9995	-
28 electrodes	0.9995	0.9994	0.9994	0.9992	0.9988

3.2.3. Experimental parameters (N and m)

As flow rate is directly related to the RTD, the relation between this parameter and the number of CSTR as well as the fraction of active volume was studied in order to characterize the reactor for both configurations (Fig. 45).

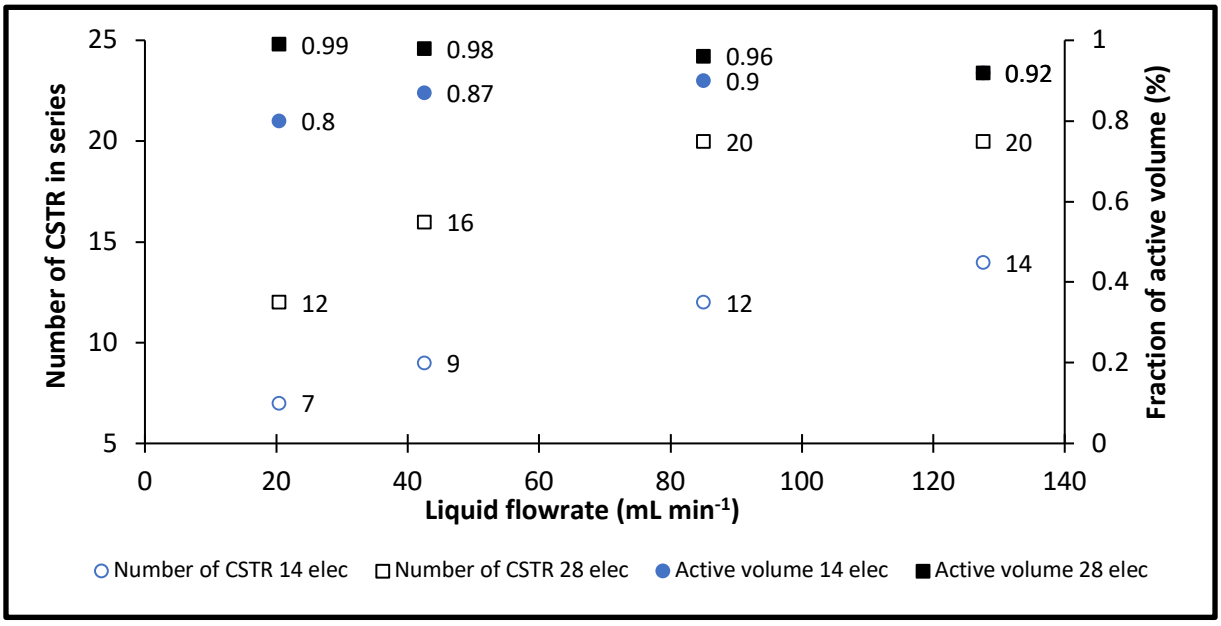

Fig. 45: Number of continuously stirred reactors in series (N) and fraction of active volume (m) plotted against the liquid flow rate, under 0.2 mL min^{-1} of air with 14- and 28-electrode configurations.

As shown in Fig. 45, for the 14-electrode system, the fraction of active volume is increasing with the liquid flow rate, being of 80% at 20.4 mL min^{-1} and of 92% at 128 mL min^{-1}. In the reactor the mixing and the shear rate are due to: (i) the flow rate in the reactor and the contact

with the obstacles (electrodes) and (ii) the air flow of small bubbles from the air diffuser. Thus by increasing the liquid flow rates, the liquid velocity is increasing and the turbulence around the electrodes is also increasing leading to a better mixing and thus to lower dead zones and stagnant zones in the reactor at high flow rate. Higher liquid flow rate enhances the mixing between active and dead zones resulting in the activation of a portion of the volume of the stagnant zone (Saravanathamizhan et al. 2008; Djoudi et al. 2012). For the 28-electrode system, the fraction of active volume is nearly the same for all the flow rates and is higher than that obtained for the 14-electrode system. The difference between the two configurations can be explained by the larger number of electrodes which increases the turbulence in the reactor leading to a lower dead volume (Djoudi et al. 2012). However, at the highest flow rate (127.5 mL min^{-1}), the fraction of active volume is the same for both configurations due to the high velocity promoting a better mixing in the reactor.

The number of CSTR in series increases with the liquid flow rate for both configurations (Fig 45). At low flow rate, the reactor approaches a few continuously stirred tank reactors behavior and by increasing the flow rate it tends to a plug flow reactor (Yuan et al. 2004; Furman et al. 2005; Saravanathamizhan et al. 2008; Xiao-chang et al. 2008; Djoudi et al. 2012). The slope inflection at high flow rate highlights that the effect of the increase in the flow rate on the number of CSTR is lower in these conditions. The number of CSTR in series is higher for the configuration with 28-electrode configuration than for the configuration with 14 electrodes, whatever the liquid flow rate. This means that by increasing the number of electrodes, the hydrodynamic behavior tends more towards a plug flow reactor. This observation is logical since by increasing the number of electrodes, the number of “reactors perfectly mixed” is increased due to more complex water flow provided by the series of baffles (electrodes) under which the wastewater is forced to flow.

Another parameter, the air flow rate, was tested since it is an important characteristic of the hydrodynamics of the pilot. Two flow rates were chosen: 0.2 and 1 L min^{-1} and the number of CSTR in series and the fraction of active volume were considered (Fig.46). The increase of the aeration rate decreases the number of CSTR being of 4, 6, 9 and 11 reactors for 20.4, 42.5, 85 and 127.5 mL min^{-1}, respectively. The lower number of reactors is due to a better mixing produced by the aeration which makes the system tend toward the CSTR model.

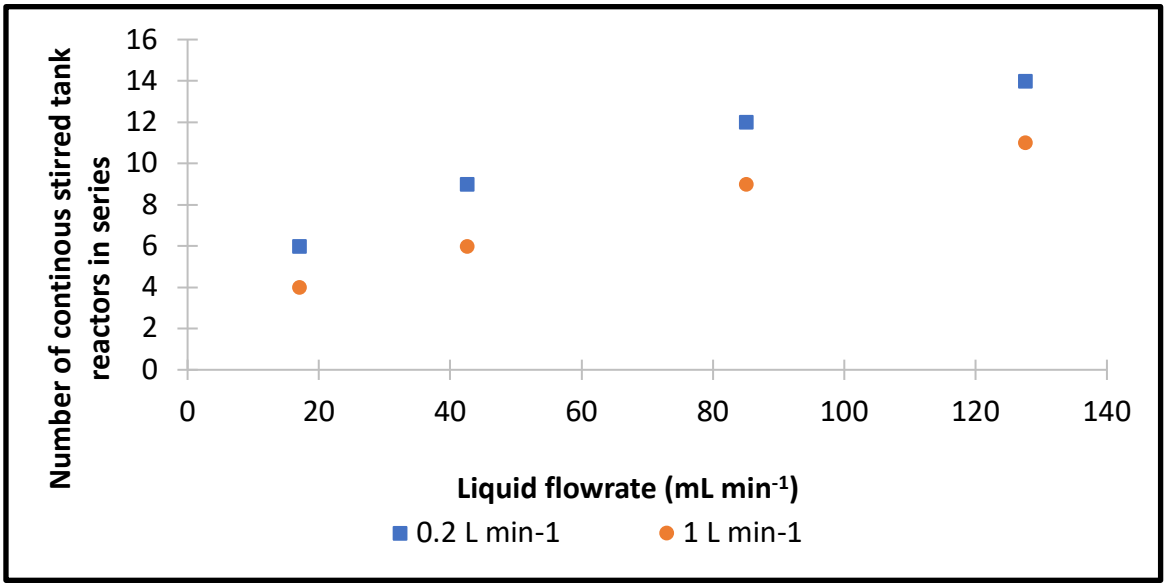

Fig. 46: Number of continuously stirred reactors in series (N) plotted against the liquid flow rate, under 0.2 L min^{-1} and 1 L min^{-1} of air with 14 electrodes.

Concerning the fraction of active volume (Fig. 47), no real difference was observed between 0.2 L min^{-1} and 1 L min^{-1}. Higher air flow rates were tested (5 and 8 L min^{-1}) but the introduction of high air flow lead to high gas retention that decreased the liquid volume in the reactor. This volume could not be estimated properly due to the high gas retention in the reactor and therefore these results were not considered. This parameter still need to be optimized since it could significantly affect the production of H_2O_2. A compromise should be found: a too low air flow rate will lead to a poor efficiency of the electro-Fenton whereas a too high flow rate could lead to high gas retention which is likely to increase the electrical resistance of the solution.

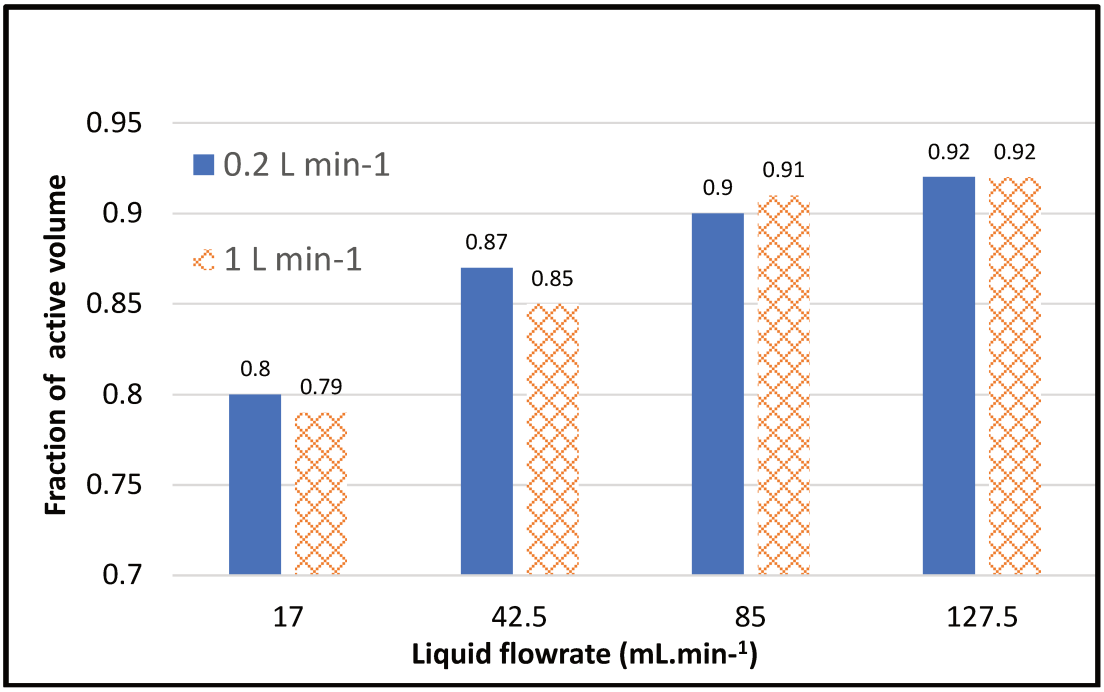

Fig. 47: Fraction of active volume plotted against the liquid flow rate, under 0.2 L min^{-1} and 1 L min^{-1} of air with 14 electrodes.

To conclude, the 28-electrode configuration is also better in terms of hydrodynamic as the presence of more electrodes promotes a better mixing inside the reactor. This configuration is well-described by the CSTR in series with dead volumes model.

3.3. Mineralization and modelling

The model developed in this section considered both the hydrodynamic model and the electrochemical mineralization using a well-known kinetic model (Panizza et al. 2001; Michaud 2002; Lan et al. 2018; Mousset et al. 2019a). The 28-electrode configuration was used.

3.3.1. Kinetic model

The following assumptions are made for the development of the model: i) the pollutant is degraded at the surface of the BDD anode by AO, ii) mediated oxidation is not taken into

account to simplify the model, and iii) the temperature and the volume of the reactor are considered constant, as observed experimentally (Mousset et al. 2019a).

Two different behaviors can be observed depending on whether the reaction is limited by mass transport or charge transfer reaction. The limiting current density (J_{lim}) has to be calculated according to Eq. 49 and compared to the applied current density (J_{app}) in order to know in which regime the reactor is operating (Eq. 50).

$$Jlim = nFKC \quad (49)$$

$$Japp = I / A \quad (50)$$

where n is the number of electrons to mineralize the pollutant (Eq. 38), F is the Faraday constant equal to 96500 C mol^{-1}, K is an overall mass transfer coefficient (m s^{-1}), C is the concentration of carbon (mmol L^{-1}), I is the current (A), A is the anode surface (m^2) and J the current density in A m^{-2}.

When $J_{app} < J_{lim}$, the system is controlled by the current and when $J_{lim} > J_{app}$ then the system is operating under mass transfer control. The expression of the anodic oxidation rate r_{ao} is given by the Eqs. 51 and 52 (Panizza et al. 2001; Michaud 2002; Lan et al. 2018; Mousset et al. 2019a).

If $J_{app} < J_{lim}$ then, $r_{ao} = KAC^0/V$ (51)

If $J_{app} > J_{lim}$, then $r_{ao} = KAC/V$ (52)

where C^0 is the initial concentration of carbon (0.7 mM), V is the volume of the reactors (m^3) and r_{ao} in mmol L^{-1} s^{-1}. For the pilot J_{app} is equal to 166 A m^{-2} (0.5/0.003) for each CSTR. As K is gathering all the transfer system it is strongly linked to the flow rate. Thus values of K were estimated using the software Aquasim® (Annex Table 2) for all the different flow rates. These values are in the same order of magnitude (10^{-5}) which is a common value. For all the flow rates, $J_{app} > J_{lim}$, so it can be assumed that the pilot is operating under mass transport control (Eq. 52). Mass balance can be written assuming that only an AO is occurring (Eq. 53).

$$\frac{dC}{dt} = Q * \frac{Ce-Cs}{V} - \frac{K\,AC}{V} \quad (53)$$

where Q is the liquid flow rate ($m^3\ s^{-1}$), Ce is the concentration of carbon entering the reactor (mM) and Cs is the concentration exiting the reactor (mM).

As the reactor is operating in continuous mode, a steady state is reached after around 3 Ts. At steady state Eq. 53 can be simplified in Eq. 54.

$$0 = Q * \frac{Ce-Cs}{V} - \frac{K\,AC}{V} \quad (54)$$

Thanks to the hydrodynamic study (section 3.2), the reactor can be modeled by p CSTR in series with dead zones where no mineralization occurs. Eq. 54 can be applied for every CSTR and for the p^{th} reactor the concentration at its exit is given by Eq. 55. This equation was used to calculate the concentration at the exit of every CSTR at steady state.

$$Cp = \frac{Q^p * Ce}{(Q+K*A)^p} \quad (55)$$

3.3.2. Comparison between the experimental values and the model

Experiments were carried out to measure the carbon mineralization in the steady state at three different points of the pilot under 0.2 L min^{-1} of air and in the configuration with 28 electrodes. Position 1 is considered to be around the second CSTR, position 2 is the middle of the reactor and position 3 is the exit of the reactor (Fig. 48).

Fig. 48: Schematic representation of the pilot in the configuration with 28 electrodes with the position of sampling

Table 19: IOA for different flow rates

Q (mL min^{-1})	20.4	42.5	85.0	127.5
IOA	0.9994	0.9992	0.988	0.984

The model was drawn and the value of the concentration for each CSTR was calculated in the steady state. The model was then challenged to the experimental points and the results are given in Fig. 49. The experimental values and the model are following the same trend. In order to validate the model, the IOA was calculated. The different values are given in Table 19.

All the IOA values are higher than 0.984. Thus, the model is able to describe the degradation for different positions in the reactor at steady state. By the use of a numerical model, more complex kinetic models could be implemented. Thanks to this model (3.4.1.) it is possible to optimize an "electrochemical plug flow" reactor having the higher mineralization rate with the smaller mean retention time. As an example more than 90 % of the solution is mineralized with the 20.4 mL min^{-1} flow rate thus using a lower flow rate (mean residence time) will consume more energy for nearly the same result. For a different approach, when only a certain part of the solution needs to be mineralized (for a combined treatment for instance) then thanks to this model, the flow rate and hydrodynamic can be estimated to minimize the energy consumption. The operating cost can also be decreased by tempting to apply a different J_{app} in all the "perfectly mixed reactors" close to J_{lim} to maximize the MCE. This is possible by controlling the current (J_{app}) or to fix aeration, flow rates, configurations to adjust it to J_{lim}. To a larger extent this study can enable to design reactors and optimize their performances.

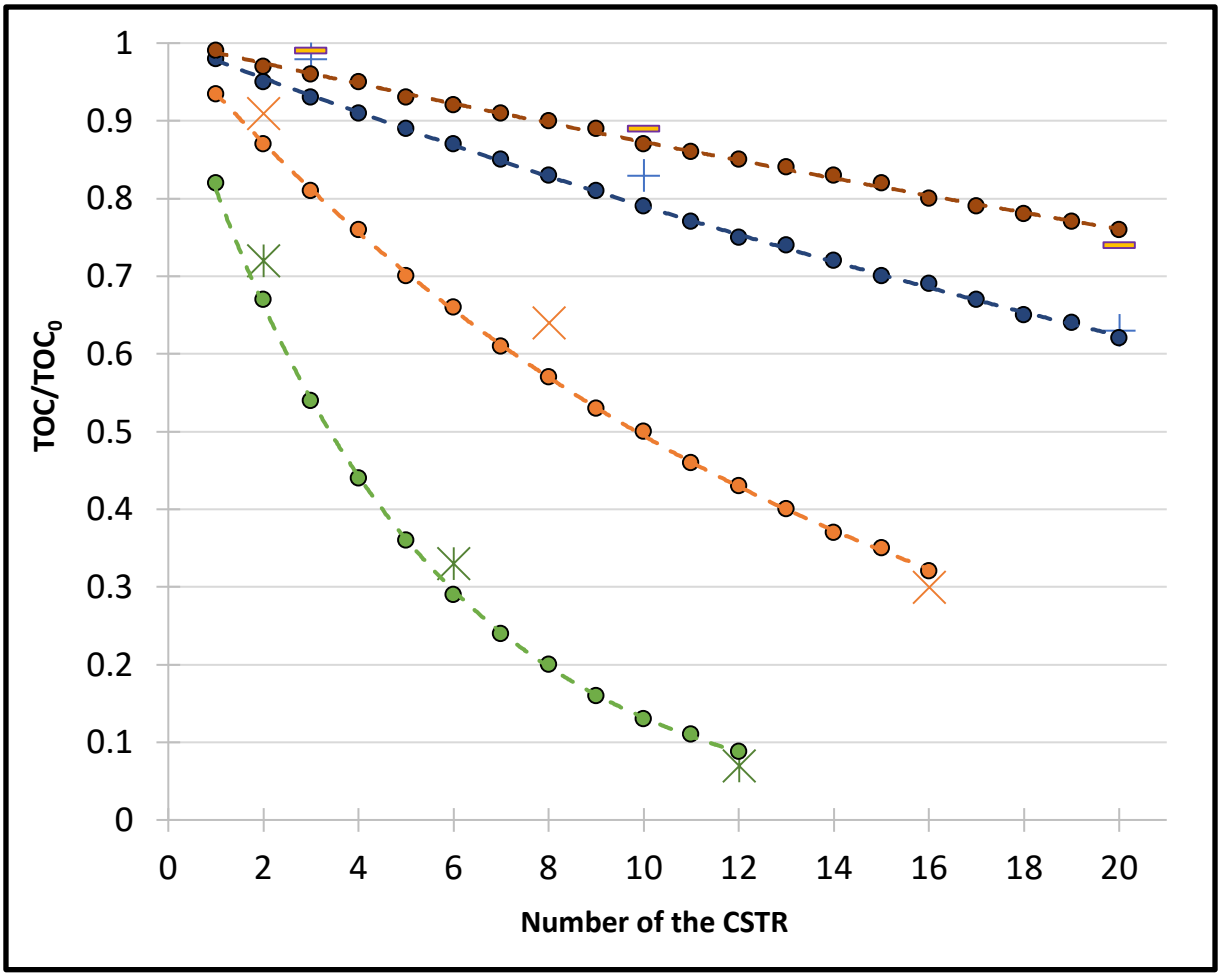

Fig. 49: Experimental TOC of the solution (Exp) and TOC calculated by the model (Mod) plotted against the number of the CSTR, under 0.2 L min^{-1} of air with 28 electrodes, 7 A for different flow rates. The circles represent the model, the cross with 3 branches and two branches represent the experimental points at 20.4 and 42.5 mL min^{-1}§ respectively. The + and – symbols represent flow rates of 85.0 and 127.5 mL min^{-1} , respectively.

However, this model has some limitations: i) the model used is a first stage analyze and does not reflect all the reactions occurring in the solution (see section 3.4.1), ii) the aeration may have a role to play in the hydrodynamics of the reactor but this aspect is not taken into account, iii) only the steady state is considered as the calculations could be simplified but an overall understanding of the process may be interesting.

4. Conclusion

In this study, a DOE was first carried out in order to find the more important parameters regarding the mineralization rate, the MCE and the EC for mineralization of HCT aqueous solution. It was shown that the flow rate was more impacting on the mineralization rate whereas the current was more important for the EC and the MCE. The lower was the flow rate, the higher was the mineralization rate due to the longer treatment time. Some deeper experiments were then carried out to evidence the effect of the reactor configuration on the mineralization efficiency and the operating cost. The 28-electrode configuration was found to be better than the 14-electrode configuration, the former promoting the mixing with more troublemakers and having a longer flow path.

To better understand the important role of the flow rate and the configuration, an hydrodynamic study was performed. RTD curves were obtained and compared to the CSTR in series with dead zones and to the plug flow models. These CSTRs suited better with the RTD curves thus, this model was chosen to model the reactor. With this model, the number of CSTR, the active volume and the mean retention time were studied for different flow rates and configurations. The hydrodynamic study confirms the DOE: the 28-electrode configuration had a lower dead volume thanks to the better mixing and a lower EC. Low flow rates approached a perfectly mixed tank reactor with high mean residence time.

Finally, a mathematical model for the mineralization of HCT solution was established, combining a pseudo first order kinetic of mineralization with the hydrodynamic model. This model was compared to experimental points and a good IOA was calculated demonstrating the good suitability of this model.

This is the first time that a model was developed combining both hydrodynamics and kinetic to describe an electrochemical pilot. This study enables to predict for this type of reactor the % of

mineralization for the more accurate mean residence time and the best electrode configurations. Several applications of this model can be offered: having the best % of mineralization but also in order to perform a combined treatment, to find the best conditions to reach a given % of mineralization (length of the reactor, configuration, flow rate, current) at the lowest cost. Eventually, to a larger extent, the mathematical model can be implemented in order to consider the mediated oxidation, the role of the aeration, etc. to perfectly model the pilot and control the process paving the way for the scale-up of the treatment.

References:

Actis P, Denoyelle A, Boukherroub R, Szunerits S (2008) Influence of the surface termination on the electrochemical properties of boron-doped diamond (BDD) interfaces. Electrochem commun 10:402–406. doi: 10.1016/j.elecom.2007.12.032

Alcocer S, Picos A, Uribe AR, et al (2018) Comparative study for degradation of industrial dyes by electrochemical advanced oxidation processes with BDD anode in a laboratory stirred tank reactor. Chemosphere 205:682–689. doi: 10.1016/j.chemosphere.2018.04.155

Basha CA, Sendhil J, Selvakumar K V, et al (2012) Electrochemical degradation of textile dyeing industry ef fl uent in batch and flow reactor systems. Desalination 285:188–197. doi: 10.1016/j.desal.2011.09.054

Bocos E, Oturan N, Sanromán MÁ, Oturan MA (2016) Elimination of radiocontrast agent diatrizoic acid from water by electrochemical advanced oxidation : Kinetics study , mechanism and mineralization pathway. JEAC 772:1–8. doi: 10.1016/j.jelechem.2016.04.011

Borzyszkowska AF, Espinoza-montero PJ (2018) Electrochemical degradation of 5-FU using a flow reactor with BDD electrode : comparison of two electrochemical systems. Chemosphere 201:816–825. doi: 10.1016/j.chemosphere.2018.03.050

Bouissou-Schurtz C, Houeto P, Guerbet M, et al (2014) Ecological risk assessment of the presence of pharmaceutical residues in a French national water survey. Regul Toxicol Pharmacol 69:296–303. doi: 10.1016/j.yrtph.2014.04.006

Brillas E, Sirés I, Oturan MA (2009) Electro-fenton process and related electrochemical technologies based on fenton's reaction chemistry. Chem Rev 109:6570–6631. doi: 10.1021/cr900136g

Cañizares P, Beteta A, Sáez C, et al (2008) Conductive-Diamond Electrochemical-Oxidation in the treatment of effluents from door-manufacturing factories. J Environ Eng Manag 18:183–191.

Dirany A, Sirés I, Oturan N, et al (2012) Electrochemical treatment of the antibiotic sulfachloropyridazine: kinetics, reaction pathways, and toxicity evolution. Environ Sci Technol 46:4074–4082. doi: 10.1021/es204621q

Djoudi W, Aissani-benissad F, Ozil P (2012) Flow modeling in electrochemical tubular reactor containing volumetric electrode : application to copper cementation. Chem Eng Res Des 90:1582–1589. doi: 10.1016/j.cherd.2012.02.003

Dominguez CM, Oturan N, Romero A, et al (2018) Removal of lindane wastes by advanced electrochemical oxidation. Chemosphere 202:400–409. doi: 10.1016/j.chemosphere.2018.03.124

El-Ghenymy A, Cabot PL, Centellas F, et al (2013) Mineralization of sulfanilamide by electro-Fenton and solar photoelectro-Fenton in a pre-pilot plant with a Pt/air-diffusion cell. Chemosphere 91:1324–1331. doi: 10.1016/j.chemosphere.2013.03.005

Ellouze S, Kessemtini S, Clematis D, et al (2017) Application of Doehlert design to the electro-Fenton treatment of bismarck brown Y. J Electroanal Chem 799:34–39. doi: 10.1016/j.jelechem.2017.05.042

Feng L, Oturan N, van Hullebusch ED, et al (2014) Degradation of anti-inflammatory drug ketoprofen by electro-oxidation: Comparison of electro-Fenton and anodic oxidation processes. Environ Sci Pollut Res 21:8406–8416. doi: 10.1007/s11356-014-2774-2

Fernández C, González-Doncel M, Pro J, et al (2010) Occurrence of pharmaceutically active compounds in surface waters of the henares-jarama-tajo river system (madrid, spain) and a potential risk characterization. Sci. Total Environ. 408:543–551.

Furman L, Leclerc JP, Stegowski Z (2005) Tracer investigation of a packed column under

variable flow. Chem Eng Sci 60:3043–3048. doi: 10.1016/j.ces.2004.12.024
Ganiyu SO, Huong Le TX, Bechelany M, et al (2018) Electrochemical mineralization of sulfamethoxazole over wide pH range using FeII FeIII LDH modified carbon felt cathode: degradation pathway, toxicity and reusability of the modified cathode. Chem Eng J 350:844–855. doi: 10.1016/j.cej.2018.04.141
García-Montoya MF, Gutiérrez-Granados S, Alatorre-Ordaz A, et al (2015) Application of electrochemical/BDD process for the treatment wastewater effluents containing pharmaceutical compounds. J Ind Eng Chem 31:238–243. doi: 10.1016/j.jiec.2015.06.030
Guinea E, Garrido JA, Rodríguez RM, et al (2010) Degradation of the fluoroquinolone enrofloxacin by electrochemical advanced oxidation processes based on hydrogen peroxide electrogeneration. Electrochim Acta 55:2101–2115. doi: 10.1016/j.electacta.2009.11.040
Haoran P, Valérie L, Etienne P, Gilles H (2013) The influence of porous structure and biofilm on the hydrodynamics of two types of trickle filters. Chem Eng J 231:163–171. doi: 10.1016/j.cej.2013.06.115
Hupert M, Muck A, Wang J, et al (2003) Conductive diamond thin-films in electrochemistry. Diam Relat Mater 12:1940–1949. doi: 10.1016/S0925-9635
Iniesta J, Michaud PA, Panizza M, et al (2001) Electrochemical oxidation of phenol at boron-doped diamond electrode. Electrochim Acta 46:3573–3578.
Lan Y, Coetsier C, Causserand C, Groenen Serrano K (2018) An experimental and modelling study of the electrochemical oxidation of pharmaceuticals using a boron-doped diamond anode. Chem Eng J 333:486–494. doi: 10.1016/j.cej.2017.09.164
Liang W, Qu J, Wang K, et al (2008) Electrochemical degradation of cyanobacterial toxin microcystin-LR using Ti/RuO2 electrodes in a continuous tubular reactor. Environ Eng Sci 25:635–642. doi: 10.1089/ees.2006.0273
Ling Y, Xu H, Chen X (2015) Continuous multi-cell electrochemical reactor for pollutant oxidation. Chem Eng Sci 122:630–636. doi: 10.1016/j.ces.2014.10.031
Loaiza-Ambuludi S, Panizza M, Oturan N, et al (2013) Electro-Fenton degradation of anti-inflammatory drug ibuprofen in hydroorganic medium. J Electroanal Chem 702:31–36. doi: 10.1016/j.jelechem.2013.05.006
Margot J, Rossi L, Barry DA, Holliger C (2015) A review of the fate of micropollutants in wastewater treatment plants. WIREs Water 2:457–487. doi: 10.1002/wat2.1090
Mendoza A, Aceña J, Pérez S, et al (2015) Pharmaceuticals and iodinated contrast media in a hospital wastewater: a case study to analyse their presence and characterise their environmental risk and hazard. Environ Res 140:225–241. doi: 10.1016/j.envres.2015.04.003
Michaud PA (2002) Comportement anodique du diamant synthetique dopé au bore.
Monteil H, Péchaud Y, Oturan N, Oturan MA (2018) A review on efficiency and cost effectiveness of electro- and bio-electro-Fenton processes: application to the treatment of pharmaceutical pollutants in water. Chem Eng J. doi: https://doi.org/10.1016/j.cej.2018.07.179
Mousset E, Pechaud Y, Oturan N, Oturan MA (2019) Charge transfer/mass transport competition in advanced hybrid electrocatalytic wastewater treatment: development of a new current efficiency relation. Appl Catal B Environ 240:102–111. doi: 10.1016/j.apcatb.2018.08.055
Mousset E, Wang Z, Hammaker J, Lefebvre O (2016) Physico-chemical properties of pristine graphene and its performance as electrode material for electro-Fenton treatment of wastewater. Electrochim Acta 214:217–230. doi: 10.1016/j.electacta.2016.08.002
Nidheesh P V, Zhou M, Oturan MA (2018) An overview on the removal of synthetic dyes

from water by electrochemical advanced oxidation processes. Chemosphere 197:210–227. doi: https://doi.org/10.1016/j.chemosphere.2017.12.195
Olvera-vargas H, Oturan N, Oturan MA, Brillas E (2015) Electro-Fenton and solar photoelectro-Fenton treatments of the pharmaceutical ranitidine in pre-pilot flow plant scale. Sep Purif Technol 146:127–135. doi: 10.1016/j.seppur.2015.03.046
Oturan N, Trajkovska S, Oturan MA, et al (2008) Study of the toxicity of diuron and its metabolites formed in aqueous medium during application of the electrochemical advanced oxidation process "electro-Fenton." Chemosphere 73:1550–1556. doi: 10.1016/j.chemosphere.2008.07.082
Oturan N, van Hullebusch ED, Zhang H, et al (2015) Occurrence and removal of organic micropollutants in landfill leachates treated by electrochemical advanced oxidation processes. Environ Sci Technol 49:12187–12196. doi: 10.1021/acs.est.5b02809
Panizza M, Michaud P a., Cerisola G, Comninellis C (2001) Anodic oxidation of 2-naphthol at boron-doped diamond electrodes. J Electroanal Chem 507:206–214. doi: 10.1016/S0022-0728(01)00398-9
Pillai IMS, Gupta AK (2015) Batch and continuous flow anodic oxidation of 2 , 4-dinitrophenol : modeling , degradation pathway and toxicity. JEAC 756:108–117. doi: 10.1016/j.jelechem.2015.08.020
Pillai IMS, Gupta AK (2017) Performance analysis of a continuous serpentine flow reactor for electrochemical oxidation of synthetic and real textile wastewater : energy consumption , mass transfer coef fi cient and economic analysis. J Environ Manage 193:524–531. doi: 10.1016/j.jenvman.2017.02.046
Polcaro AM, Vacca A, Mascia M, et al (2007) Characterization of a stirred tank electrochemical cell for water disinfection processes. Electrochim Acta 52:2595–2602. doi: 10.1016/j.electacta.2006.09.015
Rahmani AR, Godini K, Nematollahi D, et al (2016) Degradation of azo dye C.I. acid red 18 using an eco-friendly and continuous electrochemical process. Korean J Chem Eng 33:532–538. doi: 10.1007/s11814-015-0175-y
Reichert P (1998) Computer program for the identification and simulation of aquatic system.
Ren G, Zhou M, Liu M, et al (2016) A novel vertical-flow electro-Fenton reactor for organic wastewater treatment. Chem Eng J 298:55–67. doi: 10.1016/j.cej.2016.04.011
Rodrigo MA, Oturan N, Oturan MA (2014) Electrochemically assisted remediation of pesticides in soils and water: a review. Chem Rev 114:8720–8745. doi: 10.1021/cr500077e
Rosal ARR, Agüera JAPMMA (2008) Ozone-Based Technologies in water and wastewater treatment.
Saravanathamizhan R, Paranthaman R, Balasubramanian N, Basha CA (2008) Residence time distribution in continuous stirred tank electrochemical reactor. Chem Eng J 142:209–216. doi: 10.1016/j.cej.2008.02.017
Sirés I, Oturan N, Oturan MA (2010) Electrochemical degradation of beta-blockers. Studies on single and multicomponent synthetic aqueous solutions. Water Res 44:3109–3120. doi: 10.1016/j.watres.2010.03.005
Trellu C, Péchaud Y, Oturan N, et al (2016) Comparative study on the removal of humic acids from drinking water by anodic oxidation and electro-Fenton processes: mineralization efficiency and modelling. Appl Catal B Environ 194:32–41. doi: 10.1016/j.apcatb.2016.04.039
Viva A, Brunazzi E (2009) The influence of modular structure on the hydrodynamics of catalytic structured packings for reactive separation processes. AIDIC Conf Ser 9:345–353.
Wei J, Zhu X, Ni J (2011) Electrochemical oxidation of phenol at boron-doped diamond

electrode in pulse current mode. Electrochim Acta 56:5310–5315. doi: 10.1016/j.electacta.2011.04.006
Xiao-chang CAO, Ting-an Z, Qiu-yue Z (2008) Computational simulation of fluid dynamics in a tubular stirred reactor. Trans Nonferrous Met Soc China 19:489–495. doi: 10.1016/S1003-6326(08)60301-5
Yuan Y, Han M, Wang D, Jin Y (2004) Liquid phase residence time distribution for a two-phase countercurrent flow in a packed column with a novel internal. Chem Eng Process 43:1469–1474. doi: 10.1016/j.cep.2004.01.007
Zhang H, Fei C, Zhang D, Tang F (2007) Degradation of 4-nitrophenol in aqueous medium by electro-Fenton method. J Hazard Mater 145:227–232. doi: 10.1016/j.jhazmat.2006.11.016
Zhang H, Zhang D, Zhou J (2006) Removal of COD from landfill leachate by electro-Fenton method. J Hazard Mater 135:106–111. doi: 10.1016/j.jhazmat.2005.11.025
Zhou B, Yu Z, Wei Q, et al (2016) Electrochemical oxidation of biological pretreated and membrane separated landfill leachate concentrates on boron doped diamond anode. Appl Surf Sci 377:406–415. doi: 10.1016/j.apsusc.2016.03.045

CHAPTER 4

Electrochemical advanced oxidation processes combined with a biological treatment for wastewater treatment: a deep understanding on the influence of operating conditions and global efficiency.

1. Introduction

In our today's life pharmaceuticals are highly consumed especially to treat diseases or to prevent them. Once being used, they enter the environment mostly by human and animal excretion and discharge of polluted effluents coming from pharmaceutical industries, domestic and hospital effluents (Duong et al. 2008; Kümmerer 2009b). Their occurrence in the environment is due to the lack of efficiency of the existing treatment in wastewater treatment plant (WWTP) mostly based on a biological elimination (Stackelberg et al. 2007).

Several treatment techniques are used to eliminate the organic micro-pollutants; some of them are based on the transfer of the pollutant from one phase to another one like physico-chemicals techniques such as adsorption (Rivera-utrilla et al. 2013) and membrane technologies (Göbel et al. 2007). Others are directly eliminating the pharmaceutical such as advanced oxidation processes (AOPs) (Klavarioti et al. 2009; Oturan and Aaron 2014). AOPs are based on the formation of strong oxidants such as hydroxyl radicals, the second strongest oxidant after fluorine, able to eliminate nearly any type of organic molecules (Brillas et al. 2009; Sirés and Brillas 2012). Among the AOPs, electrochemical advanced oxidation processes such as electro-Fenton (EF) or anodic oxidation (AO) are commonly used as they are i) very efficient to remove organic pollutants from water, ii) environmentally friendly and iii) easy to set up (Panizza and Cerisola 2001; Brillas et al. 2009; Sirés et al. 2014; Olvera-Vargas et al. 2018). For these treatments, the operating conditions and the nature of the anode are important parameters that significantly influence the efficiency of the treatment. Among anodes, boron doped diamond (BDD) and platine (Pt) are often used. BDD is used because of i) its high oxidation efficiency, ii) its high current efficiency and iii) its long lifetime (Actis et al. 2008; Brillas et al. 2009; Wei et al. 2011; Oturan et al. 2012; Sopaj et al. 2016). Comparatively, Pt is less efficient as its oxidation power is lower compared to BDD (Panizza and Cerisola 2005; Rodrigo et al. 2010).

BDD mineralizes quickly the organics without enabling the formation of a lot of intermediates whereas the Pt enables to accumulate intermediates such as carboxylic acids (CAs).

One of the most important drawback of EAOPs is the relatively high operating cost in the case of long treatment times. To overcome this disadvantage, the combination of an EAOP and a biological treatment to decrease the operating costs while keeping a good mineralization rate has been proposed (Ganzenko et al. 2017; Monteil et al. 2018). Two different treatment modes can then be employed, weather beginning by the biological treatment when the effluents contain high concentration of biodegradable products or starting with the EAOP when the solution is not biodegradable (Oller et al. 2011; Ganzenko et al. 2014; Olvera-Vargas et al. 2016a; Monteil et al. 2018). Some studies investigated the effect of such a combined treatment on the elimination of pharmaceuticals at lab scale and highlighted that this combination can be very effective (Ferrag-Siagh et al. 2013; Ferrag-Siagh et al. 2014; Mansour et al. 2014; Mansour et al. 2015a; Mansour et al. 2015b; Olvera-Vargas et al. 2016a; Olvera-Vargas et al. 2016b; Ganzenko et al. 2017; Roshini et al. 2017; Zaghdoudi et al. 2017; Aboudalle et al. 2018). However, a key step in the process control of this type of coupling is to better understand how the operating conditions applied on the EAOP will influence the efficiency of the biological treatment.

In this context, this chapter aims at trying to explain why some conditions are more interesting based on the nature of the anode (BDD or Pt) and on the impact of the parent pollutants and the by-products. The diuretic hydrochlorothiazide (HCT) was chosen as the model pollutant for this study as i) it is hardly eliminated by wastewater treatment plants (Margot et al. 2015), ii) it was found in surface water (Bouissou-Schurtz et al. 2014) and iii) it is toxic to the environment (Fernández et al. 2010). The EF and AO treatments of this compound with a pilot scale reactor were investigated in a previous chapter (Chapter 3). The first part of this chapter will focus on the interest of performing a combined process showing the inadequacy of a biological treatment

alone and the possibility to decrease the operating costs. Some specific conditions are required to efficiently perform this combined treatment. The second part deals with identifying them. Finally, the third part uses the specific conditions found previously to obtain a good mineralization rate.

2. Material and methods

2.1. Chemicals

All chemicals used in this study were analytical grade and used as received without further purification. The pharmaceutical HCT ($C_7H_8ClN_3O_4S_2$, purity > 99%) was supplied by Sigma Aldrich. Iron (II) sulfate heptahydrate (catalyst source, 99%) was purchased from Acros Organics. Sodium sulfate (Na_2SO_4) (supporting electrolyte) was supplied from Sigma-Aldrich. $MgSO_4$ (Chimie-Plus Laboratoire), $Cacl_2$ $2H_2O$ (Merck), $FeCl_3$ (Sigma Aldrich), NH_4Cl (Merck), Na_2HPO_4 (Acros), K_2HPO_4 (VWR) and KH_2PO_4 (Acros) were used as nutrients or buffer for the biological treatment. Short-chain CAs (oxalic, oxamic, acetic and maleic acids were obtained from Acros, Fluka and Alfa Aesar. Solutions were prepared with osmosis water equipment purchased from Cloup which keeps conductivity below 20 $\mu S\ cm^{-1}$. The pH of solutions was adjusted using analytical grade sulfuric acid (Acros) and sodium hydroxide (Fluka). Organic solvents used were HPLC or analytic grade from Sigma-Aldrich, Fluka and Merck.

2.2. Electrochemical treatment

HCT solutions were prepared at different concentrations in 50 mM of sodium sulfate (as electrolyte) and the solution pH is adjusted to 3.0 by a CyberScan 1500 from Eutech Instruments and a 1 M H_2SO_4 solution. In the case of the AO oxidation the solutions were left

as stated above for the EF treatment, 0.1 mM of ferrous iron was added to the solution, a usual concentration for the EF degradation.

2.2.1. Batch treatment

The different batch experiments were performed in an open undivided cylindrical cell of 250 mL. The electrochemical cell was composed of whether a BDD or Pt anode and a carbon felt cathode. The anodes had around 30 cm^2 surface area. BDD was purchased from CONDIAS GmbH in Germany. The cathode was a 3D structure measuring 18 * 5.0 * 0.5 cm^3; it was placed on the inner wall of the cell covering the total internal perimeter. It was purchased from Mersen (France). The solutions were stirred with a magnetic bar. The degradation and the mineralization of the synthetic effluent were performed under current-controlled conditions using a Hameg HM8040 triple power DC supply. Continuous saturation of O_2 was ensured by bubbling air starting 10 min before starting the electrolysis.

2.2.2. Treatment with electrochemical pilot

The electrochemical pilot is made of plexiglass and has a capacity of 1.7 L (Fig. 50). The reactor is composed of 14 anodes and 14 cathodes separated by 2 cm. Anodes are made of BDD film on niobium support (from CONDIAS GmbH) of 30 cm^2 and cathodes are made of 3D carbon felt of 30 cm^2 (from Mersen). Two peristatic pumps FH100 drive the flow throughout the reactor. Aeration was set at 0.2 L min^{-1} provided from the whole surface of the bottom of the reactor and is adjusted by an air flowmeter. A constant current was delivered by a Microlab power supply to the electrodes mounted in parallel.

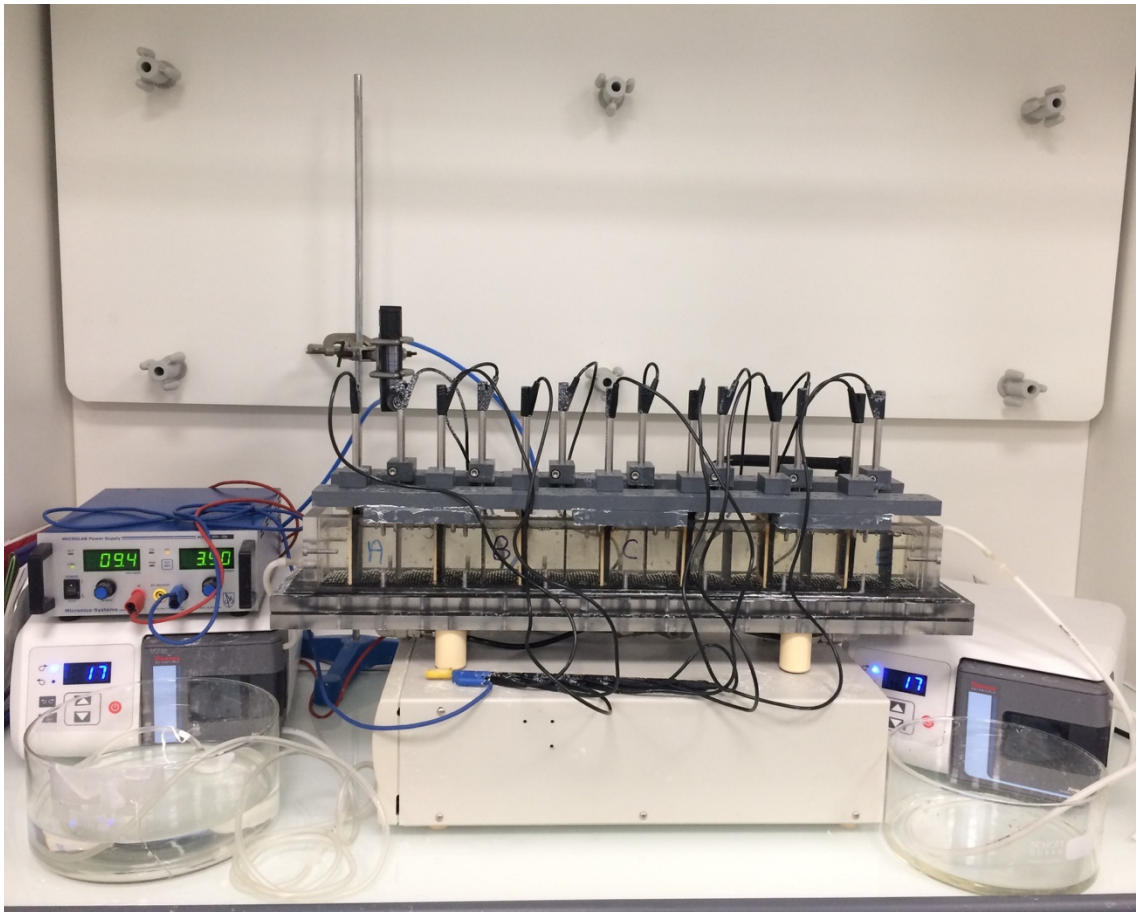

Fig. 50: The pilot reactor of 1.7 L and the whole set up.

2.3. Biological treatment

Three inoculums were used for the biodegradation assays. The first one was taken from an activated sludge reactor from the WWTP from Jablines. The second inoculum was taken from the mixed liquor of an aerobic biofilter from the WWTP Saint-Thibault des Vignes (named biofilters). The last inoculum used was a sample of µ-organisms already acclimated to the pollutant and to the CAs from a previous treatment (named selected µ-organisms). The µ-organisms were centrifuged, washed with tap water and then added to a new solution.

The initial volatile suspended solid (VSS) concentration was measured for every sample and a dilution factor was calculated to reach an initial concentration of VSS of 0.01 gVSS L^{-1} for each

biodegradation test. This low value was chosen to avoid TOC measure disruption with soluble organic matter coming from biomass.

The biodegradation tests were performed in an erlenmeyer flask of 500 mL closed with cotton to enable gas exchange but prevent contamination. The biological reactor was operated as follows: pH adjustment with 1 M Na_2SO_4 and 1 M NaOH to keep the pH in the range 6.5-7.5; mechanical stirring using a rotative plate at 122 RPM (revolution per minute) provided by Merck and room temperature (22 ± 3) °C. Different nutrients compositions were tested especially with different N concentrations (5 to 20 mg L^{-1}) and no effect was observed between experiments, meaning that nutrients were not limiting. From these observations the following concentrations were applied: 18.75 mg L^{-1} of NH_4Cl (corresponding to 5 mg L^{-1} $N\text{-}NH_4$), 36.5 mg L^{-1} of $Cacl_2$ 2 H_2O, 0.26 mg L^{-1} $FeCl_3$ 6 H_2O and 11 mg L^{-1} of $MgSO_4$. The phosphate buffer used was composed of 334 mg L^{-1} of Na_2HPO_4, 85 mg L^{-1} of KH_2PO_4 and 208 mg L^{-1} of K_2HPO_4 (Rodier et al. 2009).

Experiments with and without external addition of air were also performed and no difference was observed since oxygen was in excess, thus no external aeration was applied. The effect of the addition of sodium sulfite to eliminate the residual hydrogen peroxide was tested on the bacteria and no effect was found thus 5 mL of a 0.5 M sodium sulfite solution was added for all the biodegradation tests.

A bio-adsorption study was carried out to confirm that the degradation was due to a real elimination and not to the transfer of the pollutant to another phase. After 5 min, 1 h, 2 h and 6 h samples were taken of the HCT mixed with the bacteria and its concentration remained constant, meaning that adsorption was negligible.

2.4. Analytical methods

Before each analytical measure the solution was filtered through a 0.2 μm filter made of PTFE (polytetrafluoroethylene). When error bars are given on the graphs, they are calculated based on the standard deviation of the different experiments.

2.4.1. HPLC analysis

HCT and its aromatic degradation intermediates were followed and measured by using an uHPLC equipped with a Hypersil Gold column (100 mm * 2.1 mm), 1.9 μ and coupled with a diode array detector (DAD). The temperature of the column was set at 40°C. The injection volumes were of 5 μL. The mobile phase was composed of water/methanol (95:5) both containing 1% of acetic acid at 0.08 mL min^{-1}. The wavelength of detection was set at 270 nm.

Oxamic, maleic, acetic and oxalic acids were identified and quantified by a Merck Lachrom Liquid chromatograph equipped with a Bio-Rad Aminex 5 μm, 25 cm × 4.6 mm (i.d.) column and coupled with a DAD. The mobile phase was H_2SO_4 at 4 mM at a flowrate of 0.6 mL min^{-1}. The detector was set at 220 nm. A calibration curve was performed for each detected acid. Experiments were carried out using a total concentration of CAs of 250 mg C L^{-1} with 6.5, 3.35, 0.075 and 0.075 mM of oxalic, oxamic, maleic and acetic acid respectively (concentrations are proportional to the one of chapter 2).

2.4.2. TOC analysis

The mineralization of the solution was followed by measuring the total organic carbon (TOC) of treated solutions using a Shimadzu VCSH TOC analyzer. 2 drops of 1 M H_2SO_4 were added to each sample of 5 mL to acidify the solution in order to eliminate mineral carbon such as

carbonates. Reproducible values with ± 2% accuracy were detected. The injection volumes were of 50 µL.

2.4.3. Liquid chromatography (LC) – mass spectroscopy (MS) analysis

LC-MS analyses were performed to identify Aromatic intermediates (AIs) formed during the AO treatment of the HCT. The same Hypersil Gold column at 40°C and a liquid flowrate of 0.2 mL min^{-1} were used. After extracting from the treated solution with ethyl acetate, the sample was completely dried under vacuum. Then it was diluted in 1 mL of methanol / water 50/50 (v/v) and eluted by 0.1% formic acid / methanol 90/10 (v/v) solution. Concerning the mass conditions, the ESI (electrospray ionization) mode was used at 90 V.

3. Results and discussion

3.1. Interests of combining EAOPs and a biological treatment

To analyze the interest of combining AO or EF with a biological treatment, each treatment was first studied alone.

3.1.1. Inefficiency of a biological treatment alone in the case of persistent organics

An experiment was carried out in batch reactor to assess the ability of µ-organisms to eliminate the HCT without pre-treatment using an EAOP. Fig. 51 shows the concentration dynamics of HCT during one month in the biological reactor. The HCT concentration remained stable, highlighting the inability of the µ-organisms from WWTP to eliminate HCT despite the great microbial diversity of the inoculum. This result is in agreement with the low mean percentage

of elimination of this molecule (30%) in wastewater treatment plants in Europe and United States (Margot et al. 2015).

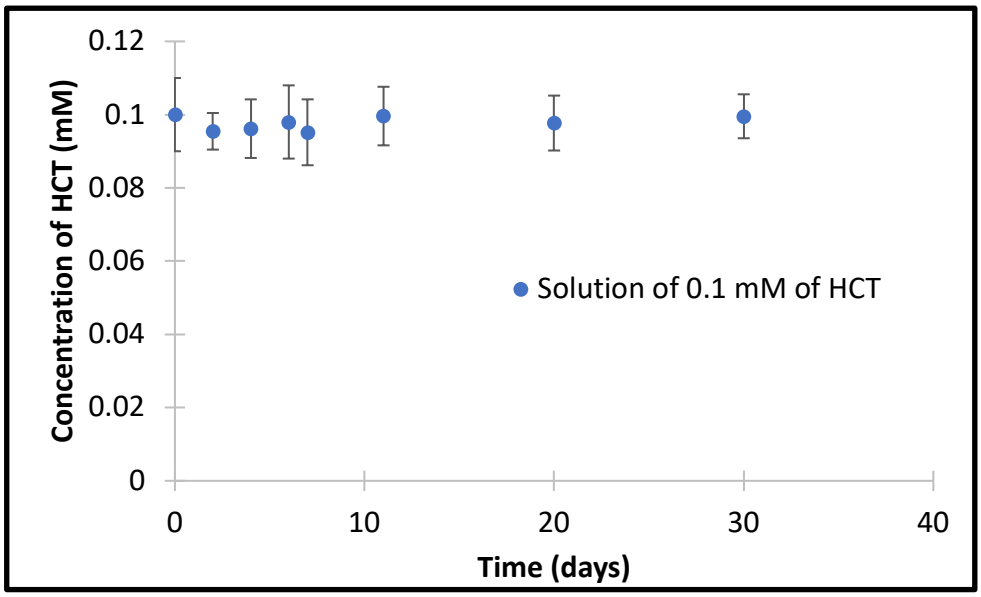

Fig. 51: Evolution of HCT concentration as a function of time for 0.1 mM HCT solution mixed with 0.1 gVSS L^{-1} of activated sludge.

3.1.2. AO to mineralize a HCT solution

The mineralization of 0.1 mM HCT solution was performed in the pilot-scale reactor by AO in the continuous mode. Results of the mineralization rate for different currents are given in Fig. 52. As already studied in chapter 3, it was possible to observe that the mineralization rate at the pilot output depends on the operating conditions and can reach high mineralization rates.

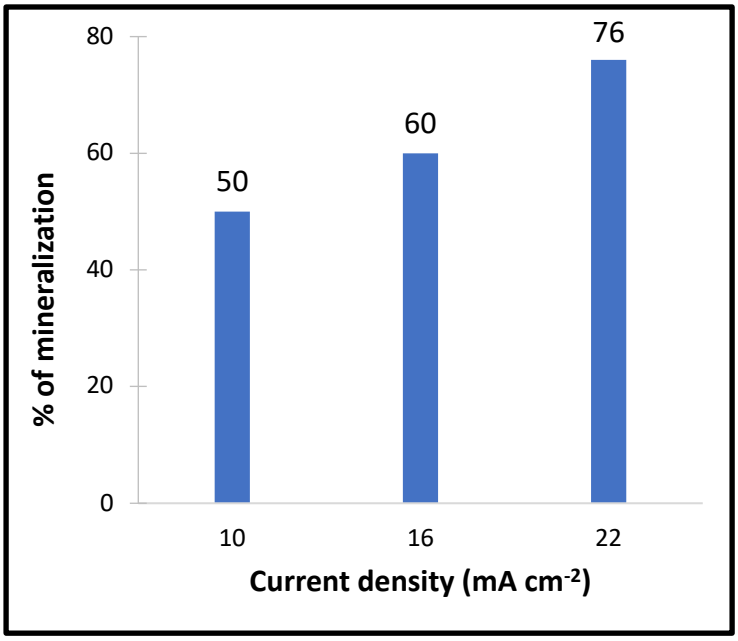

Fig. 52: % of mineralization at steady state during the AO treatment of a 0.1 mM HCT solution in 50 mM Na_2SO_4, 0.2 L min^{-1} of air and 42.5 mL min^{-1} for different currents and with a mean residence time of 36 min in the pilot reactor of Fig. 50.

3.1.3. Electro-chemical pre-treatment followed by a biological post-treatment

Biological treatment alone appeared inefficient whereas AO is really efficient but with an EC that increases with treatment time (chapter 2). In order to get a cost effective treatment, the feasibility of the combination of an EAOP and biological treatment was assessed. To evaluate the cost of the energy saved, the price (P) for the treatment of 1 m^3 of 0.1 mM HCT solution in the pilot reactor was estimated according to the Eq. 56.

$$P = U * I * 10^{-3} * h * 0.1461 \quad (56)$$

with P in euros, U the voltage (in Volt), I the current (in Ampere), h, the time of treatment (in h) and 0.1461 the mean price of the French kWh in 2019 in euro.

The cost of electrical energy obtained for different mineralization rates are given in Fig. 53. For a similar flow rate, by reducing the mineralization from 76 to 60% and from 76 to 50%, the electrical cost could be divided by 1.5 and 3 respectively. To reach the same mineralization rate

it is then necessary to mineralize the residual solution with a biological treatment to reach the same global mineralization efficiency.

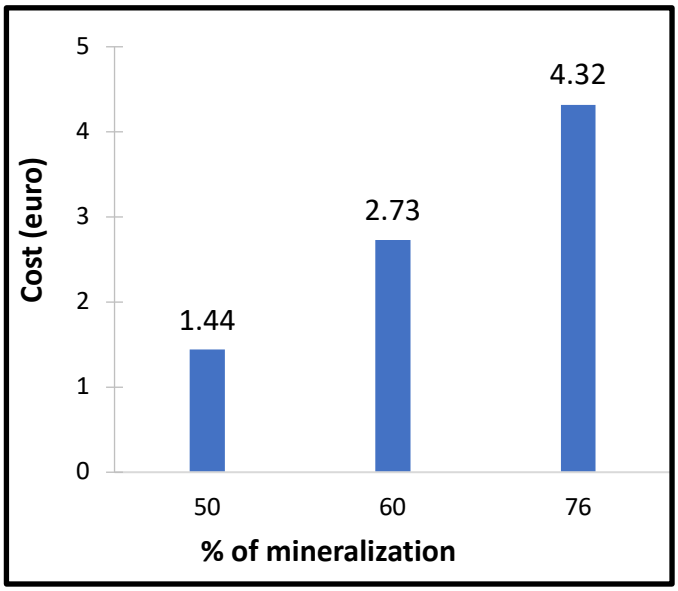

Fig. 53: Cost for the AO treatment described in Fig. 52, using 6, 7 and 8 V to mineralize 50, 60 and 70% of the 0.1 mM HCT solution, respectively.

Some combined treatments were then performed in order to assess the efficiency of such system by varying the operational conditions. For most of them the biomass was not able to mineralize the electrochemically pre-treated solution. However, for one operational condition some information could be extracted. In this study, a solution of 0.84 mM of HCT (62 mgC L^{-1}) was treated by AO in the pilot at a flow rate of 20.4 mL min^{-1} (with mean residence time of 82 min) under 24 mA cm^{-2} constant current density and effluents were collected after 15 (A), 30 (B), 45 (C) and 120 (D) min. A biological batch experiment was then performed with 0.01 gVSS L^{-1} of activated sludge mixed with 250 mL of the treated solutions. After the electrochemical pre-treatment, HCT was totally degraded for all conditions except for the condition A where 27% of HCT was still remaining in the solution. The results of the combined treatment concerning the total mineralization rate are given in Fig. 54.

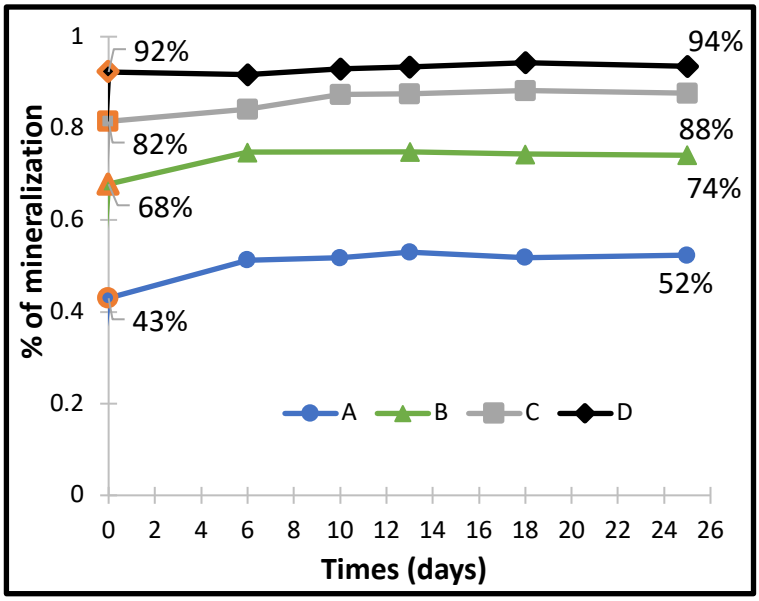

Fig. 54: Evolution of mineralization of 0.1 mM HCT solution during the combined treatment of 0.01 gVSS L^{-1} of activated sludge.

Whatever the experimental conditions, only a small part was mineralized by the biological treatment: respectively 9, 7, 7 and 2% for conditions A, B, C and D. These results highlight that the solutions are certainly composed by molecules very low biodegradable even by an inoculum with a large microbial diversity. This was confirmed by an analysis of the more concentrated intermediates during the biological treatment. Indeed, thanks to the uHPLC analysis, the peak area of these AIs was found to remain stable highlighting their non-biodegradability by the µ-organisms. Then, by using LC-MS analysis, their structure were found and confirmed that these molecules were still containing aromatic groups difficultly degraded by µ-organisms (Table 20). Thus, the biodegradable fraction is certainly composed by smaller molecules and especially CAs, known to be biodegradable (Ganzenko et al. 2017). For condition D, the low biodegradation rate could also be linked to the very low carbon concentration remaining in the solution after the electrochemical treatment (5 mgC L^{-1}), organic carbon certainly becoming limiting for the µ-organisms.

In this part, it was demonstrated that combining an electrochemical treatment with a biological degradation could reduce the operating costs. However, the conditions applied in this part for the AO treatment cannot lead to an efficient biological degradation probably due to the presence of AIs. Thus, next section will focus on finding the best operating conditions to provide biodegradable compounds and eliminate the non-biodegradable species.

Table 20: Structure of AIs identified by LC-MS during the treatment of a concentrated solution of HCT (0.42 mM) by AO.

Name	Structure
6-hydroxy-4*H*-benzo[*e*][1,2,4]thiadiazine-7-sulfonamide 1,1-dioxide	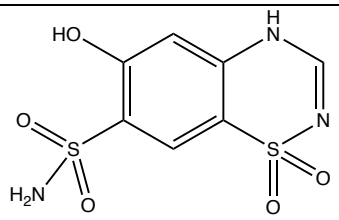
4-chloro-2-formamido-5-sulfamoylbenzenesulfonic acid	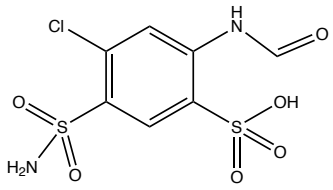
4-amino-6-chlorobenzene-1,3-disulfonamide	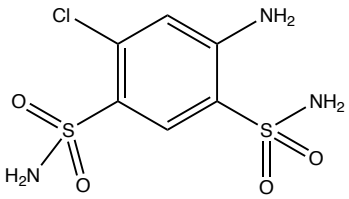
6-chloro-4*H*-benzo[*e*][1,2,4]thiadiazine-7-sulfonamide 1,1-dioxide	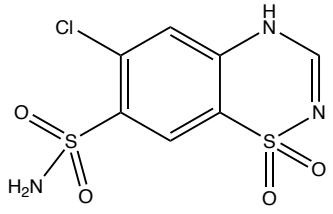

3.2. Evaluation of the biodegradability of specific intermediates formed during the AO treatment of HCT

3.2.1. Can the CAs formed during the AO be mineralized by biological treatment?

Four CAs were formed during the degradation of HCT in batch reactor according to a previous study of our group (Monteil et al. 2019 and chapter 2 of this work). Based on this observation, these 4 molecules were chosen as model of CAs and their relative concentrations were kept as already detected (Table 21).

Table 21: Structure and concentration of CAs used in the study in biodegradation experiments.

Name	Molecule	Concentration (mM)
Oxalic Acid	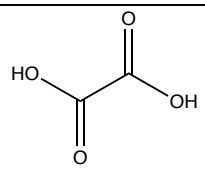	6.5
Oxamic Acid	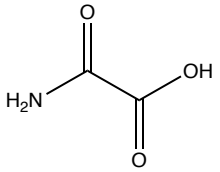	3.35
Maleic Acid	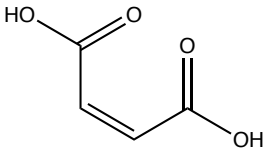	0.075
Acetic Acid	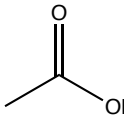	0.075

Three experiments were carried out using 250 mgC L^{-1} with 0.01 gVSS L^{-1} of inoculum. For experiments 1, 2 and 3 (Fig. 55), the inoculums were respectively activated sludge, biofilters and selected µ-organisms.

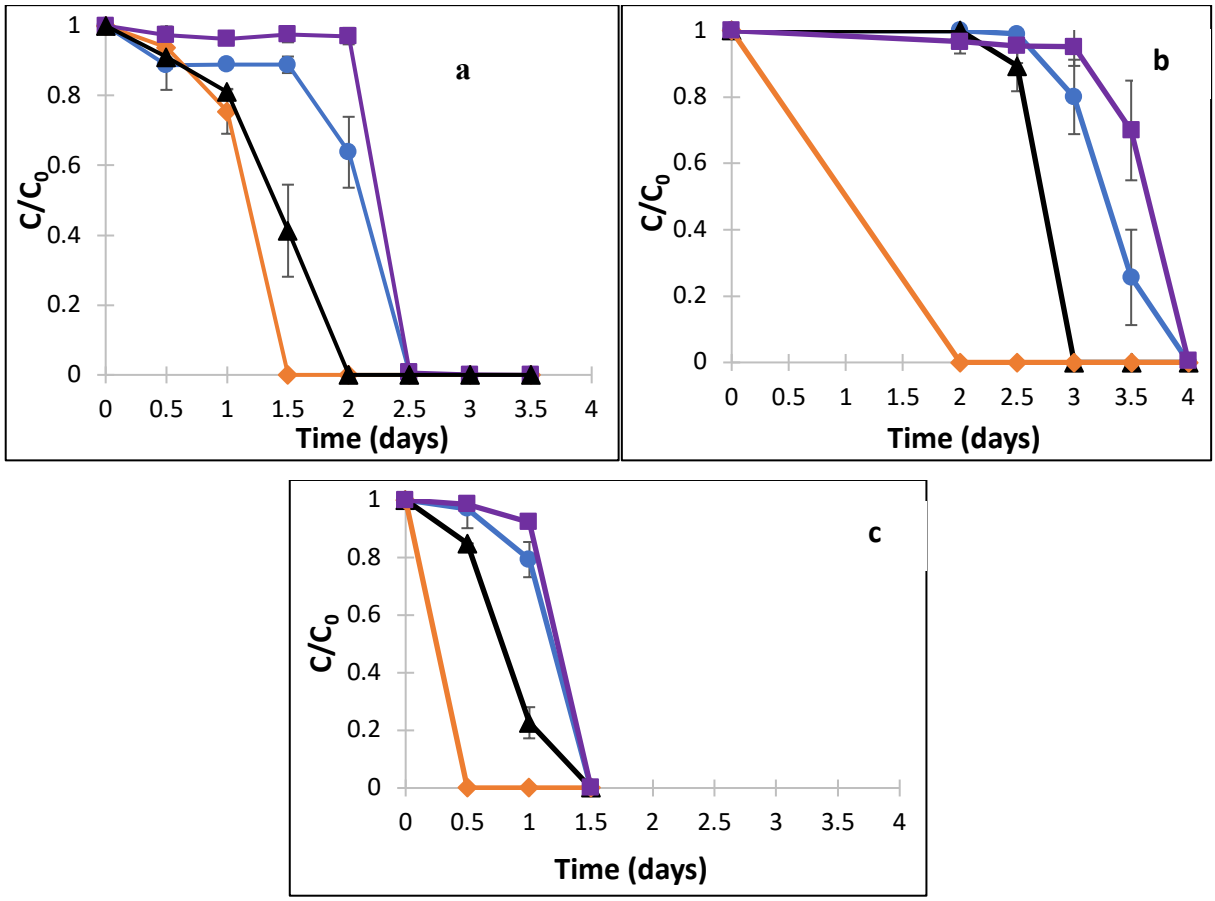

Fig. 55: CAs degraded by a) activated sludge inoculum b) biofilters inoculum c) the µ-organisms previously selected from biofilters. Oxamic acid (■), oxalic acid (●), acetic acid (▲), maleic acid (◆).

According to Fig. 55, all the CAs were successfully mineralized for all the inoculum by the biological treatments after a lag phase. The TOC was measured at the end of the experiments; with a value closed to 0 for all the experiments highlighting a total mineralization of the CAs. For all the experiments, the CAs were sequentially degraded in the same order: first the maleic acid, then the acetic acid followed by the oxalic acid and finally the oxamic acid. The maleic acid is certainly transformed into smaller molecules thus, this molecule may not be mineralized first. Concerning the difference between the oxamic and the oxalic, it can be supposed that it is due to the amine function. The degradation rate was almost zero for the oxamic, oxalic and

maleic acid during their lag phase. The degradation rate using the treatment with activated sludge biomass as inoculum was quicker than the mixed liquor from the biofilters but slower than the bacteria from the selected biofilters. Indeed, when bacteria are pre-selected, the concentration of active bacteria for these CAs is higher and the µ-organisms are already acclimated to the chemical conditions reducing significantly the lag phase resulting in a faster degradation kinetics. However, even with this pre-selection, the sequential degradation is still present with the maleic acid degraded first (0.5 day) and the oxamic acid the last.

The sequential degradation can be linked to the carbon catabolite repression which is an important regulatory mechanism for µ-organisms. It allows µ-organisms to preferentially use easily metabolizable carbon sources over relatively less favorable carbon source. For instance this phenomenon is illustrated by diauxic growth during which bacteria assimilate firstly energy-efficient and rapidly metabolizable sugars (glucose) for which they already have the enzymes then less-favored carbohydrates for which they need to synthesize the enzymes (Loomis Jr. and Magasanik 1967).

This sequential degradation of the CAs has not yet been studied whereas it can be very important in the case of a continuous treatment where only the most degradable acids would be eliminated if a continuously stirred tank reactor (CSTR) reactor was used. To face this problem, a reactor with a plug flow behavior could be used; the most easily degradable CAs being degraded in the first layers of the reactors and the less degradable ones in the last layers of the reactor.

3.2.3. Inhibiting effect of the pollutant and of the AIs on the biological degradation

To clarify the inhibiting effect of the HCT and of its AIs, three experimental conditions were compared: (i) the solution of 250 mgC L^{-1} of CAs alone, (ii) the solution of 250 mgC L^{-1} of CAs mixed with a solution of 0.42 mM of HCT and, (iii) the solution of 250 mgC L^{-1} of CAs

with a pre-treated solution containing AIs and a residual HCT concentration of 0.015 mM. Fig. 56 depicts the degradation of maleic acid (Fig 56a), acetic acid (Fig 56b), oxalic acid (Fig 56c), and oxamic acid (Fig 56d). As can be seen in Fig.56, the CAs are degraded in the same order as in sub-section 3.2.1: first the maleic acid, then the acetic, oxalic and finally oxamic acids were degraded. For all the CAs, the solution containing only the CAs is degraded first and as expected the curve are very similar to the experiment of sub-section 3.2.1. Then, the solution containing the CAs and the AI is mineralized. The degradation of the solution with the HCT and the CAs requires a longer treatment time which is composed of two parts: (i) an accommodation time and (ii) a degradation period. For instance, for the oxamic acid (Fig 56d), the accommodation time is of 2, 3 and 4 days for the CAs alone, the CAs and the AI, and the CAs and the HCT, respectively, whereas the degradation period is of 0.5 and 1.5 days for the CAs alone and for the CAs and the HCT, respectively. The accommodation time and the degradation time are longer with the AIs and the HCT than the solution of CAs alone, showing that the presence of HCT and its AIs, at least temporarily, slows down the activity of the µ-organisms. This behavior is also verified in Fig 56b and 56c for oxalic and acetic acids, respectively. For the maleic acid (Fig 56a), it is harder to observe the difference between the curves as this acid is very quickly degraded; shorter interval of sampling should have been taken to identify it. In a continuous treatment, the acclimation time is not important as the µ-organisms would already be selected for the different CAs; however the kinetic of degradation is very important in order to eliminate the CAs during the mean residence time. As the kinetics of degradation is longer with the AIs and the HCT in the solution, it is essential to eliminate them or at least to reduce significantly their concentration in order to have an efficient biotreatment on the biodegradable part of the solution (CAs).

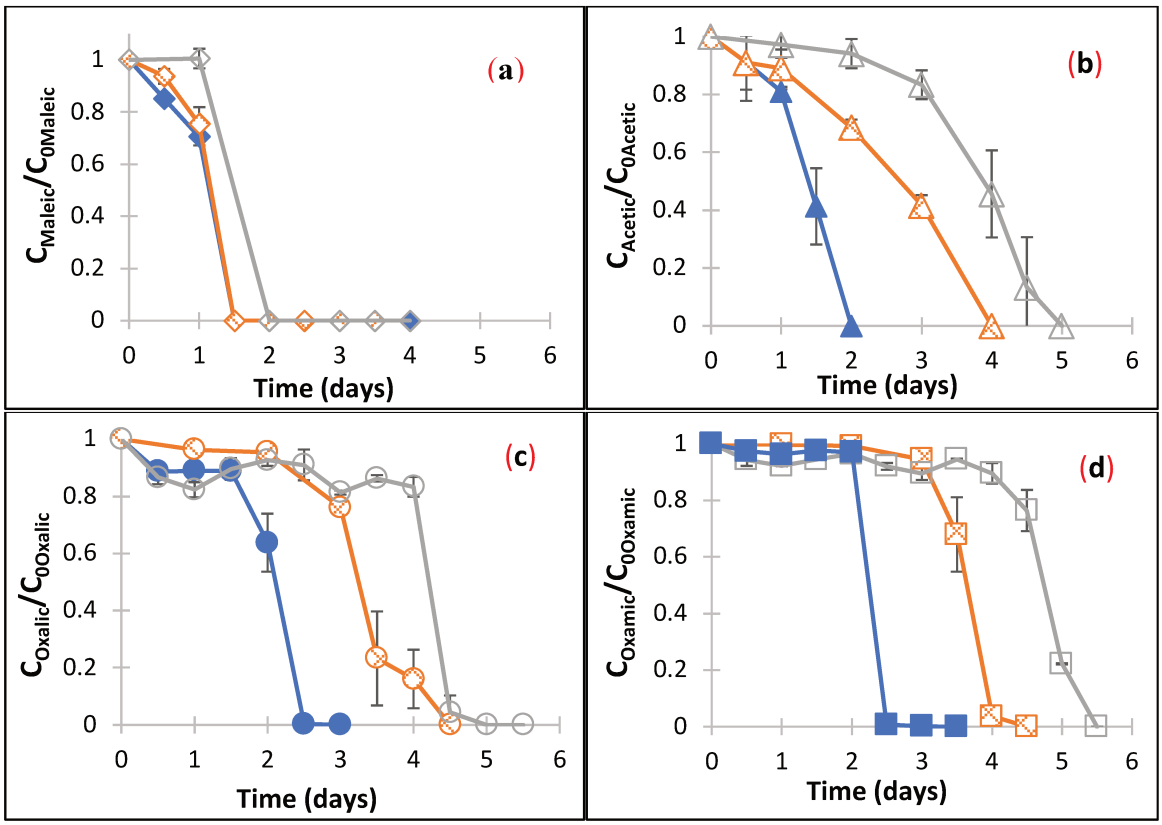

Fig. 56: Degradation of maleic (a), acetic (b), oxalic (c) and oxamic acids (d) during a biological treatment with 0.01 gVSS L^{-1} of activated sludge mixed with the four CAs(●) and with a solution of CAs and HCT (○) or a solution of CAs with HCT and AIs (⊗) .

Supplementary experiments were carried out to assess the toxicity of AIs at different concentrations. The solution of AIs without dilution or diluted 2 and 5 times was mixed with 250 mgC L^{-1} of CAs and 0.01 gVSS L^{-1} of selected inoculum. Again, the degradation of each CA was followed (Fig. 57). The CAs were still degraded in a sequential way and in the same order as in subsection 3.2.1. The overall degradation, considering the lag phase and the phase of degradation, was completed first for the solution containing only the CAs, then for the solution with the AIs diluted by 5 (D5), followed by the solution with the AIs diluted by 2 (D2) and finally for the solution without dilution (D0). This behavior was observed for all the CAs. The lag time was visible only for two CAs: for the oxamic (Fig. 57c) and the oxalic acids (Fig 57d). This can be explained by the inoculum used as discussed previously since in these

experiments, pre-selected biomass was used. For the oxalic acid, the lag time was of 0.5, 1, 2 and 3 d for the solution CAs, D5, D2 and D0, respectively. The degradation phase was also longer for all the CAs with the addition of the solution of AI. This means that the microbial activity during the degradation phase was also reduced and this decrease increased with the AI concentrations. For the acetic acid (Fig. 58), the slope of the kinetic curves was 0.67, 0.5, 0.33 and 0.25 d^{-1} for CAs, D5, D2 and D0, respectively. This inhibiting effect can be modelled by a classical Monod inhibition model by considering an [AI] concentration of 1 for D0 (Eq. 57).

$$k = k_{max} \frac{K_I}{K_I + [AI]} \quad (57)$$

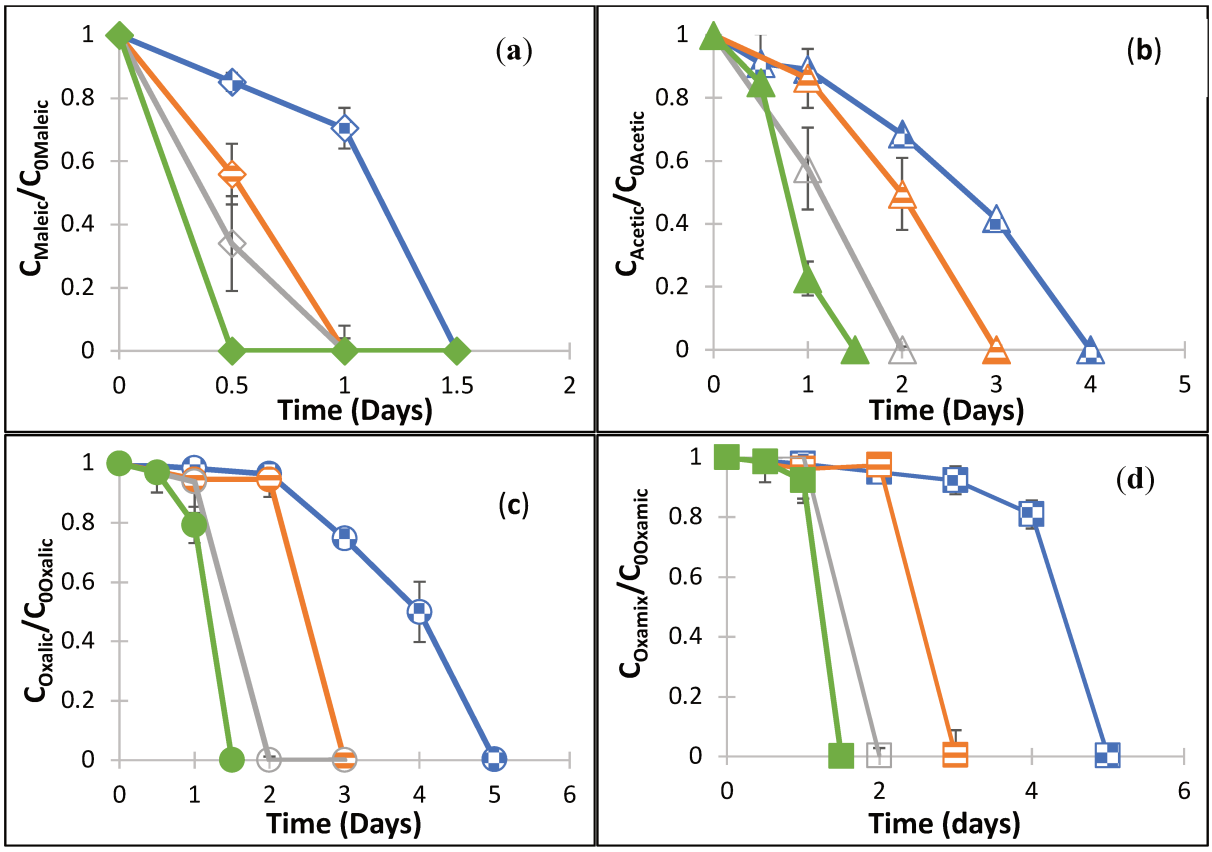

Fig. 57: Degradation of Maleic (a), acetic (b), oxalic (c) and oxamic acid (d) during a biological treatment with 0.01 gVSS.L^{-1} of selected biofilters mixed with the four CAs ●, and the HCT and AIs solution (CAs and HCT and AIs) ◓, or the HCT and AIs solution diluted by 2 ⊖, or the HCT and AIs solution diluted by 5 ○.

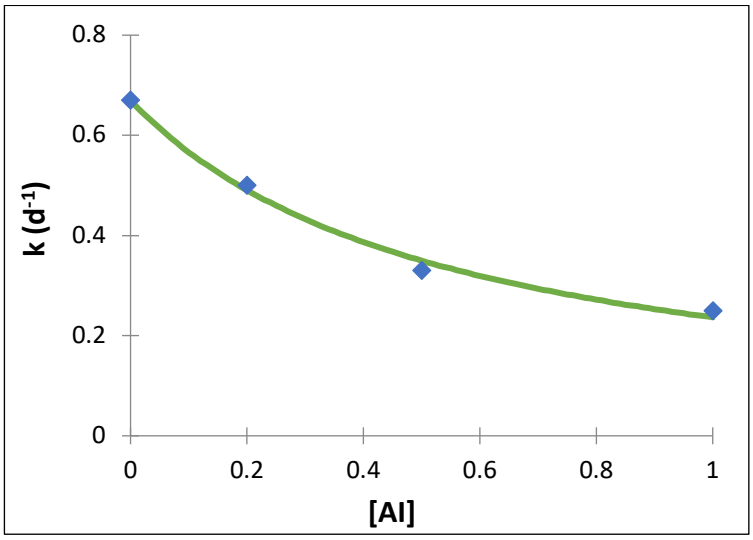

Fig. 58: Influence of the dilution of the pre-treated solution on the degradation kinetic of the acetic acid.

This model and the results obtained highlight that the lower is the concentration of AIs the quicker is the degradation rate after the lag phase. The development of these inhibition models could help to optimize the operational conditions of the electrochemical treatment, the possible dilution and help to predict the performance of the combination of treatment. However more experiments need to be performed to achieve this objective. For condition D5, for the acetic acid, the acclimation phase was similar to that of the CAs alone and the degradation kinetic was only 25% lower than for CAs. A maximum concentration of no or little inhibition could then be defined for the intermediates of Table 20 thanks to their peak area on the uHPLC.

3.3. Application of appropriate operating conditions to optimize the combined treatment

The main objective of this section is to use the lessons learned from the previous sections to select optimal conditions for the electrochemical treatment in order to optimize the efficiency

of the combined treatment. The experiment were performed at lab scale first as the operating conditions are easier to handle and then they will be carried out in the pilot reactor.

3.3.1. Experiments with BDD anodes

3.3.1.1. Finding good operating conditions at lab scale for an efficient combined treatment

The pilot reactor is composed of BDD electrodes that are very efficient to eliminate pollutants as they are non-active anodes (Martínez-Huitle et al. 2015; Nidheesh et al. 2019). They enable to form adsorbed hydroxyl radicals M(•OH) on the surface of the anode material. M(•OH) are very powerful oxidants and efficient to eliminate organic compounds (Panizza and Cerisola 2009). This high efficiency has to be controlled for the combined process in order to only convert the mother pollutant to biodegradable intermediates and to limit as much possible its mineralization. Thus a very low current was applied (30 mA) to degrade 230 mL of a 0.2 mM HCT solution. The AIs and the CAs were followed over time and the objective was to stop the treatment when the concentration of CAs was maximal with the lowest concentration of AIs and with a reasonable amount of carbon in the solution. However, even at a very low current it was not possible to eliminate all the intermediates while keeping a high value of TOC. The reaction was thus stopped after 2.5 h when the HCT was completely degraded. At this time, the final TOC value was 11.2 mgC L^{-1}. The concentration of AIs were below the concentrations found in sub-section 3.2.3 for the condition D5, meaning that their concentration were not influencing too much the microbial activity. The TOC value was followed during the post-biological treatment and the results are depicted in Fig. 59. 28% of the initial TOC was mineralized during the AO treatment. The following biological treatment was slow during the three first days corresponding to an acclimation phase, then an exponential increase lasted from day 5 to day 10 and finally a stabilization phase was observed until the end of the experiment. The residual carbon (5.4 mgC L^{-1}) at the end of the biodegradation corresponds to the non-

biodegradable part which was not converted into biodegradable carbon by the AO. 38% of initial solution were mineralized by the biological treatment enabling to globally mineralize 66%. This combined treatment was thus successful as the mineralization was mainly due to the biological treatment enabling to save energy. Thus these operating conditions to eliminate the HCT and the AIs and form CAs were successful and they were adapted to the pilot. To achieve higher mineralization rates, another step of electrochemical and biological treatments on the remaining solution could be considered. In view of a combination of continuous electrochemical and biological treatments, a recirculation loop at the inlet of the electrochemical treatment could be considered.

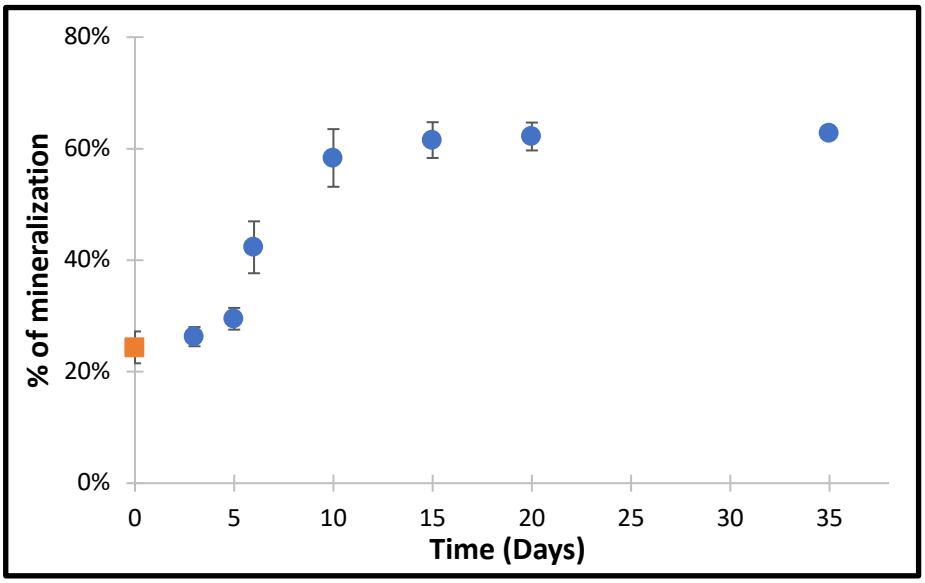

Fig. 59: Combined treatment of 230 mL a 0.2 mM HCT solution at 30 mA and 2.5 h followed by a post biological treatment using activated sludge with 0.01 gVSS L^{-1} of µ-organisms. The squared point corresponds to the electrochemical treatment and the dot points to the biological mineralization.

3.3.1.2. Finding good operating conditions for pilot scale for an efficient combined treatment

In the same way than in the previous section, the objective was to avoid mineralization and to promote the degradation of HCT and of AIs by applying a very low current density. However

as the pilot reactor works in the continuous mode, the flow rate constitutes also a key factor and its value has to be chosen carefully. As discussed in the previous chapter, a low flow rate encourages a high level of mineralization whereas a high flow rate leads to mean retention time lower than the degradation of the pollutant. Based on the results obtained in chapter 3, it was chosen to use an intermediate flow rate of 42.5 mL min^{-1}. Three experiments were carried out with three different current densities in order to reach different mineralization rates: 4.0, 8.6 and 16.2 mA cm^{-2} to mineralize 40, 50 and 60% of the solution, respectively. During these experiments the CAs, the main AIs, the mother pollutant and the TOC were followed. Table 22 gives the results obtained for the three runs. As expressed in this table, three different mineralization rates were obtained: 40, 47 and 60% for run 1, 2 and 3, respectively. In order to choose the best operating conditions, three characteristics were compared: (i) the total amount of CAs, (ii) the concentration of the more concentrated AI and (iii) the percentage of elimination of the HCT. Concerning the degradation of HCT, run 2 and 3 attained more than 99% of removal whereas run 1 reached only 91%. The total concentration of CAs was of 0.017, 0.018 and 0.031 mM of C for run 1, 2 and 3 respectively. Finally, only run 3 attained the concentrations of AIs below the maximum value defined in sub-section 3.2.3 meaning that in run 1 and 2, the biodegradation could be affected by the presence of these AIs. Based on those criteria, the operating conditions of run 3 were selected as the best ones.

Table 22: Results for the different experiments

Run	1	2	3
% of mineralization	**40**	**47**	**60**
Oxalic acid (mM)	*0.0037*	*0.0050*	*0.011*
Oxamic acid (mM)	*0.0015*	*0.0026*	*0.0037*
Maleic acid (mM)	*0.0012*	*0.00057*	*0.00025*
Acetic acid (mM)	*0.0010*	*0.00045*	*0.00031*
Total CAs (mMC)	**0.017**	**0.018**	**0.031**
Intermediates below the level	**No**	**No**	**Yes**
% of HCT eliminated	91	> 99	> 99

3.3.2. Finding good operating conditions with Platine electrode at batch scale

To find the optimal operating conditions for a combined treatment a suitable anode is required. As it was demonstrated previously, the BDD anode is very efficient to mineralize a solution but its very high mineralization power makes the process uncontrollable. Thus, to choose a more suitable anode the process has to be well understood. In the case of active metal anode, the adsorbed hydroxyl radicals formed by oxidation of water (Eq. 58) can lead to the formation of high state oxide by oxygen transfer reaction (Eq. 59). This high state oxide performs a selective oxidation of organic compounds contrarily to the non-active anode (such as BDD) where the adsorbed hydroxyl radicals are able to non-selectively mineralized the solution which results in complete combustion of organics to CO_2. Thus an active anode is more suitable for a selective oxidation of the pollutant. Pt was chosen as it is a common active electrode.

$$MO + H_2O \rightarrow MO(^{\cdot}OH) + H^+ + e^- \quad (58)$$

$$MO(^{\cdot}OH) \rightarrow MO + H^{+} + e^{-} \quad (59)$$

As an example, oxalic acid and formic acid could not be mineralized by the EF treatment with Pt anode of 2.5 L of a ranitidine solution at 112.6 mg L^{-1} concentration (Olvera-Vargas et al. 2015c). Based on this example, an EF treatment was applied in order to form the maximum amount of CAs. Again, the concentration of CAs, the AIs and the mineralization rate were followed during the process. After 1 h, all the intermediates were degraded with mineralization rate of only 35% and the total CA concentration of 6.3 mgC L^{-1} in the solution. The CAs concentration was 3 times higher compared to the AO using BDD anode highlighting the better suitability of the use of a Pt electrode. Fig. 60 describes the results obtained for the combined treatment. In the same way as the experiments with BDD anode, an acclimation phase was observed but it was much shorter. Then, an exponential phase was observed until day 9 followed by a stabilization of the mineralization rate. The biological treatment mineralized 50% of the initial TOC reaching an overall mineralization degree of nearly 85% with a residual TOC of 2.3 mgC L^{-1}. So, to oxidize selectively the pollutants and to perform an efficient combined treatment, the use of Pt anode seems more appropriate. However, Pt being highly expensive, (even than BDD), a relatively chipper anode should be selected for a scale up at industrial level. In this frame, DSA or sub-stoichiometric TiO_2 anodes can then be proposed for an industrial scale as they are relatively cheaper active anodes. At short term, the combined treatment should be tested with DSA or sub-stoichiometric TiO_2 anodes to perform the EF or AO in the pilot reactor before combining with biodegradation.

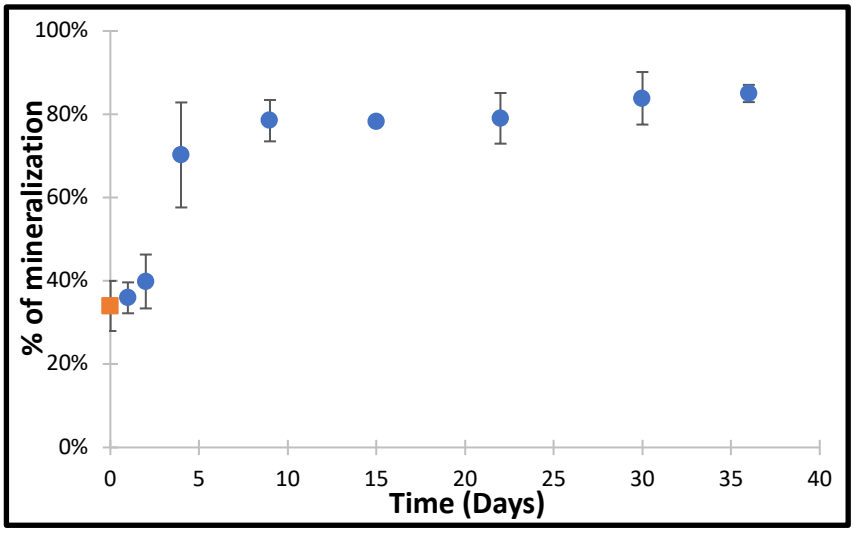

Fig. 60: Combined treatment of 230 mL of a 0.2 mM HCT solution. Biodegradation of electro-Fenton pre-treated solution at 100 mA during 1 h using Pt anode under following operating conditions: : [Na_2SO_4] = 50 mM, [Fe^{2+}] = 0.1 mM, pH 3 and room temperature. Biological treatment was performed using activated sludge and 0.01 gVSS L^{-1} of µ-organisms. The squared point corresponds to the electrochemical treatment and the circle points to the biological mineralization.

4. Conclusions

This chapter demonstrates the clear interest of a combined treatment between an EAOP and biological treatment to significantly improve the performance of biological treatment and to reduce the cost of the electrochemical treatment alone. The biological treatment alone was not able to degrade the solution of HCT. It was also demonstrated that the operating cost could be divided by 3 while using the pilot in the case of a pre-treatment of 1 m^3 HCT solution followed by a biodegradation step.

Two experiments were carried out to understand to disrupting effect of the AIs and the HCT during the degradation of four biodegradable CAs: oxalic, oxamic, maleic and acetic acids. The presence in the solution of the HCT and the AI inhibit the µ-organisms' activity by increasing the acclimation time and decreasing the degradation kinetic of CAs under study. A different lag phase and degradation kinetic could be identified for these CAs. The maleic acid was

mineralized first followed by the acetic and oxalic acids. The oxamic acid required the longest treatment time. Different dilutions of the AIs and HCT solution were realized to measure their inhibiting effect on the mineralization of CAs. This inhibition can be modelled by a Monod inhibition model highlighting that the inhibition depends on the concentration of HCT and AIs for the acetic acid. The results obtained showed that for the dilution by 5, the concentration of AIs and HCT was not disrupting significantly the biodegradation. Thus, to perform an efficient combined treatment, it was evidenced that some specific conditions for the electrochemical treatment should be applied with the aim of i) degrading the pollutant HCT while reaching a low mineralization degree, ii) reducing the AI concentration and iii) promoting the formation of the biodegradable compounds like CAs.

Finally the combined treatment at lab scale was tested in the conditions described previously. As BDD anode was used a low current was applied to minimize the mineralization and promote the formation of CAs. The combined treatment was successful as 66% of the solution was mineralized including 38% by the biotreatment. The same strategy was then applied to the pilot with three conditions tested, the best condition was a current of 6.8 A corresponding to a current density of 16.2 mA cm^{-2}, a flow rate of 42.5 mL min^{-1} leading to 60% mineralization before the biological treatment.

In order to favor the formation of CAs and a low mineralization rate of the solution, a pre-treatment with electro-Fenton using a Pt electrode as an active anode was performed. With this anode, a mineralization degree of 85% was attained, including 50% of TOC removal by bio-treatment which implies a drastic reduction in the operating costs. To conclude, combining an electrochemical treatment with a biodegradation seems to be a very efficient way to reduce the operating costs. However, some specific conditions should be applied and the use of an active anode could give even better results. Research should be done on this last aspect.

References:

Aboudalle A, Djelal H, Fourcade F, et al (2018) Metronidazole removal by means of a combined system coupling an electro- Fenton process and a conventional biological treatment : by-products monitoring and performance enhancement. J Hazard Mater 359:85–95. doi: 10.1016/j.jhazmat.2018.07.006

Actis P, Denoyelle A, Boukherroub R, Szunerits S (2008) Influence of the surface termination on the electrochemical properties of boron-doped diamond (BDD) interfaces. Electrochem commun 10:402–406. doi: 10.1016/j.elecom.2007.12.032

Bouissou-Schurtz C, Houeto P, Guerbet M, et al (2014) Ecological risk assessment of the presence of pharmaceutical residues in a French national water survey. Regul Toxicol Pharmacol 69:296–303. doi: 10.1016/j.yrtph.2014.04.006

Brillas E, Sirés I, Oturan MA (2009) Electro-fenton process and related electrochemical technologies based on fenton's reaction chemistry. Chem Rev 109:6570–6631. doi: 10.1021/cr900136g

Duong H, Pham N, Nguyen H, et al (2008) Occurrence , fate and antibiotic resistance of fluoroquinolone antibacterials in hospital wastewaters in Hanoi, Vietnam. Chemosphere 72:968–973. doi: 10.1016/j.chemosphere.2008.03.009

Fernández C, González-Doncel M, Pro J, et al (2010) Occurrence of pharmaceutically active compounds in surface waters of the henares-jarama-tajo river system (madrid, spain) and a potential risk characterization. Sci. Total Environ. 408:543–551.

Ferrag-Siagh F, Fourcade F, Soutrel I, et al (2013) Tetracycline degradation and mineralization by the coupling of an electro-Fenton pretreatment and a biological process. J Chem Technol Biotechnol 88:1380–1386. doi: 10.1002/jctb.3990

Ferrag-Siagh F, Fourcade F, Soutrel I, et al (2014) Electro-Fenton pretreatment for the improvement of tylosin biodegradability. Environ Sci Pollut Res 21:8534–8542. doi: 10.1007/s11356-014-2771-5

Ganzenko O, Huguenot D, van Hullebusch ED, et al (2014) Electrochemical advanced oxidation and biological processes for wastewater treatment: a review of the combined approaches. Environ Sci Pollut Res 21:8493–8524. doi: 10.1007/s11356-014-2770-6

Ganzenko O, Trellu C, Papirio S, et al (2017) Bioelectro-Fenton: evaluation of a combined biological—advanced oxidation treatment for pharmaceutical wastewater. Environ Sci Pollut Res 1–10. doi: 10.1007/s11356-017-8450-6

Göbel A, Mcardell CS, Joss A, et al (2007) Fate of sulfonamides, macrolides, and trimethoprim in different wastewater treatment technologies. Sci Total Environ 372:361–371. doi: 10.1016/j.scitotenv.2006.07.039

Klavarioti M, Mantzavinos D, Kassinos D (2009) Removal of residual pharmaceuticals from aqueous systems by advanced oxidation processes. Environ Int 35:402–417. doi: http://dx.doi.org/10.1016/j.envint.2008.07.009

Kümmerer K (2009) The presence of pharmaceuticals in the environment due to human use - present knowledge and future challenges. J Environ Manage 90:2354–2366. doi: 10.1016/j.jenvman.2009.01.023

Loomis Jr WF, Magasanik B (1967) Glucose-lactose diauxie in Escherichia coli. J Bacteriol 93:1397–1401.

Mansour D, Fourcade F, Huguet S, et al (2014) Improvement of the activated sludge treatment by its combination with electro Fenton for the mineralization of sulfamethazine. Int Biodeterior Biodegrad 88:29–36. doi: 10.1016/j.ibiod.2013.11.016

Mansour D, Fourcade F, Soutrel I, et al (2015a) Mineralization of synthetic and industrial pharmaceutical effluent containing trimethoprim by combining electro-Fenton and

activated sludge treatment. J Taiwan Inst Chem Eng 53:58–67. doi: 10.1016/j.jtice.2015.02.022
Mansour D, Fourcade F, Soutrel I, et al (2015b) Relevance of a combined process coupling electro-Fenton and biological treatment for the remediation of sulfamethazine solutions - Application to an industrial pharmaceutical effluent. Comptes Rendus Chim 18:39–44. doi: 10.1016/j.crci.2014.05.005
Margot J, Rossi L, Barry DA, Holliger C (2015) A review of the fate of micropollutants in wastewater treatment plants. WIREs Water 2:457–487. doi: 10.1002/wat2.1090
Martínez-Huitle CA, Rodrigo MA, Sirés I, Scialdone O (2015) Single and coupled electrochemical processes and reactors for the abatement of organic water pollutants: a critical review. Chem Rev 115:13362–13407. doi: 10.1021/acs.chemrev.5b00361
Monteil H, Oturan N, Péchaud Y, Oturan MA (2019) Efficient removal of diuretic hydrochlorothiazide from water by electro-Fenton process using BDD anode: a kinetic and degradation pathway study.
Monteil H, Péchaud Y, Oturan N, Oturan MA (2018) A review on efficiency and cost effectiveness of electro- and bio-electro-Fenton processes: application to the treatment of pharmaceutical pollutants in water. Chem Eng J. doi: https://doi.org/10.1016/j.cej.2018.07.179
Nidheesh P V, Divyapriya G, Oturan N, et al (2019) Environmental applications of boron-doped diamond electrodes: 1. Applications in water and wastewater treatment. ChemElectrocem 2124–2142. doi: 10.1002/celc.201801876
Oller I, Malato S, Sánchez-Pérez JA (2011) Combination of Advanced Oxidation Processes and biological treatments for wastewater decontamination: a review. Sci Total Environ 409:4141–4166. doi: 10.1016/j.scitotenv.2010.08.061
Olvera-Vargas H, Cocerva T, Oturan N, et al (2016a) Bioelectro-Fenton: a sustainable integrated process for removal of organic pollutants from water: application to mineralization of metoprolol. J Hazard Mater 319:13–23. doi: 10.1016/j.jhazmat.2015.12.010
Olvera-Vargas H, Oturan N, Buisson D, Oturan MA (2016b) A coupled bio-EF process for mineralization of the pharmaceuticals furosemide and ranitidine: feasibility assessment. Chemosphere 155:606–613. doi: 10.1016/j.chemosphere.2016.04.091
Olvera-Vargas H, Oturan N, Oturan MA, Brillas E (2015) Electro-Fenton and solar photoelectro-Fenton treatments of the pharmaceutical ranitidine in pre-pilot flow plant scale. Sep Purif Technol 146:127–135. doi: 10.1016/j.seppur.2015.03.046
Olvera-Vargas H, Trellu C, Oturan N, Oturan MA (2018) Bio-electro-Fenton: A New Combined Process – Principles and Applications BT - Electro-Fenton Process: New Trends and Scale-Up. In: Zhou M, Oturan MA, Sirés I (eds). Springer Singapore, Singapore, pp 29–56
Oturan MA, Aaron J-J (2014) Advanced oxidation processes in water/wastewater treatment: principles and applications. A Review. Crit Rev Environ Sci Technol 44:2577–2641. doi: 10.1080/10643389.2013.829765
Oturan N, Brillas E, Oturan MA (2012) Unprecedented total mineralization of atrazine and cyanuric acid by anodic oxidation and electro-Fenton with a boron-doped diamond anode. Environ Chem Lett 10:165–170. doi: 10.1007/s10311-011-0337-z
Panizza M, Cerisola G (2005) Application of diamond electrodes to electrochemical processes. Electrochim Acta 51:191–199. doi: 10.1016/j.electacta.2005.04.023
Panizza M, Cerisola G (2001) Removal of organic pollutants from industrial wastewater by electrogenerated Fenton's reagent. Water Res 35:3987–3992. doi: 10.1016/S0043-1354(01)00135-X
Panizza M, Cerisola G (2009) Direct and mediated anodic oxidation of organic pollutants.

Chem Rev 109:6541–6569. doi: 10.1021/cr9001319
Rivera-utrilla J, Sánchez-polo M, Ferro-garcía MÁ, Prados-joya G (2013) Pharmaceuticals as emerging contaminants and their removal from water. A review. Chemosphere 93:1268–1287. doi: 10.1016/j.chemosphere.2013.07.059
Rodier J, Legube B, Merlet N (2009) Analyse de l'eau, Dunot.
Rodrigo MA, Cañizares P, Sánchez-Carretero A, Sáez C (2010) Use of conductive-diamond electrochemical oxidation for wastewater treatment. Catal Today 151:173–177. doi: https://doi.org/10.1016/j.cattod.2010.01.058
Roshini PS, Gandhimathi R, Ramesh ST, Nidheesh P V (2017) Combined electro-Fenton and biological processes for the treatment of industrial textile effluent : mineralization and toxicity analysis. J Hazard Toxic Radioact Waste. doi: 10.1061/(ASCE)HZ.2153-5515.0000370.
Sirés I, Brillas E (2012) Remediation of water pollution caused by pharmaceutical residues based on electrochemical separation and degradation technologies: a review. Environ Int 40:212–229. doi: 10.1016/j.envint.2011.07.012
Sirés I, Brillas E, Oturan MA, et al (2014) Electrochemical advanced oxidation processes: today and tomorrow. A review. Environ Sci Pollut Res 21:8336–8367. doi: 10.1007/s11356-014-2783-1
Sopaj F, Oturan N, Pinson J, et al (2016) Effect of the anode materials on the efficiency of the electro-Fenton process for the mineralization of the antibiotic sulfamethazine. Appl Catal B Environ 199:331–341. doi: 10.1016/j.apcatb.2016.06.035
Stackelberg PE, Gibs J, Furlong ET, et al (2007) Efficiency of conventional drinking-water-treatment processes in removal of pharmaceuticals and other organic compounds. 377:255–272. doi: 10.1016/j.scitotenv.2007.01.095
Wei J, Zhu X, Ni J (2011) Electrochemical oxidation of phenol at boron-doped diamond electrode in pulse current mode. Electrochim Acta 56:5310–5315. doi: 10.1016/j.electacta.2011.04.006
Zaghdoudi M, Fourcade F, Soutrel I, et al (2017) Direct and indirect electrochemical reduction prior to a biological treatment for dimetridazole removal. J Hazard Mater 335:10–17. doi: 10.1016/j.jhazmat.2017.04.028

CONCLUSIONS AND PERSPECTIVES

This thesis presents a way of treating pharmaceuticals from wastewaters. First electrochemical advanced oxidation processes experiments were performed at lab scale to understand the different operating parameters then the process was scale-up and experiments were carried out in a pilot reactor. Then based on these results, a model was designed to describe the mineralization rate in the reactor. Finally to reduce the operating costs, the electrochemical process was combined with a biological treatment.

EF treatment of the different molecules

The oxidative degradation and mineralization of four pharmaceuticals, namely hydrochlorothiazide (HCT), tramadol (TMD), Nadolol (Nad) and ofloxacin (OFL), by electro-Fenton (EF) were deeply studied in this work. The impact of two operating parameters (the catalyst concentration and the current) was considered for the four pollutants. For all of them increasing the Fe^{2+} concentration from 0.05 to 0.1 mM (or 0.2 mM for TMD) increased the kinetic of oxidation of 0.1 min^{-1} as an average among the four pollutants. However a higher concentration slowed down the oxidation due to side reactions. A similar behavior was identified for the current. The absolute rate constant for the oxidation of the different molecules was determined using the competition kinetics method and found to be of $(4.37 \pm 0.04) \times 10^9$ M^{-1} s^{-1}, $(5.59 \pm 0.03) \times 10^9$ M^{-1} s^{-1}, $(5.63 \pm 0.03) \times 10^9$ M^{-1} s^{-1} and $(5.55 \pm 0.05) \times 10^9$ M^{-1} s^{-1} for HCT, TMD, Nad and OFL respectively. The mineralization of these molecules was also successfully performed as after 6 h of EF all the solutions were totally mineralized. Thus the EF treatment was able to successfully eliminate the HCT, Nad, TMD and OFL with similar kinetic of degradation and totally mineralized the pharmaceutical solutions highlighting the non-selectivity of the hydroxyl radicals and their ability to treat pharmaceuticals.

Scale-up of the experiment

Once the EF at lab scale was well understood and the best operating parameters found in batch, a pilot was designed and built to assess the efficiency of the process at larger scale and in the continuous mode to be closer to real conditions. Different choices were made during construction of the lab scale pilot presented in this thesis work: (i) the configuration and the size of the electrodes, (ii) the aeration supply and (iii) the manner to plug the electrodes weather in series or in parallel.

(i) We have decided to design a "plug flow reactor" by putting a stack of electrodes weather than bigger sized electrodes as the use of bigger electrodes produces a non-uniform repartition of the current on the electrode surface which reduces the yield. A reasonable number of electrode-pairs was chosen (7 or 14 anodes) in order to study different parameters influencing the treatment efficiency and energy consumption. The electrodes were placed alternately (cathode-anode-cathode...) in order to make the flow run between the electrodes to increase the contact time between the molecules and the electrodes.

(ii) The air supply had two objectives: to provide O_2 gas to the cathode to form H_2O_2 and to increase the mixing between two electrodes. A rubber layer with small sized holes was put on the bottom of the reactor and compressed air was blown under the pilot. This system is used in biological wastewater treatment plants and provides small sized gas bubbles ($d < 2$ mm) which favor the oxygen mass transfer to the cathode and the mixing.

(iii) Finally the way of plugging the electrodes was considered. When BDD electrodes are used, a too high current can damage them. Using a parallel plugging enables to have

a higher amount in each brunch of the circuit which is not possible in series as the current is not divided. Thus the electrodes were plugged in parallel.

The study of the pilot was carried out in three parts, first a DOE (design of experiments) was performed in order to analyze the performance of the reactor and define the more impacting parameters. Then, to understand the flowing in the reactor, an hydrodynamic study was performed. Finally, a model coupling hydrodynamics and mineralization kinetics was developed using the results of the two previous points.

DOE

The DOE had two objectives: first identifying the more impacting operational parameter and then to have an overview of the ability of the reactor to degrade and mineralize the selected pharmaceuticals. The current density, the flow rate and the catalyst (Fe^{2+}) concentration were chosen based on the lab scale results (chapter 2) and on the literature. For the mineralization rate, the flow rate was the more impacting parameter with a coefficient 2.5 and 10 times higher than the coefficient for the current and the catalyst concentration respectively. The Fe^{2+} concentration appeared to have nearly any effect. This latter can be explained by the size of the cathode: at batch scale, the cathode covers all the inner surface of the electrochemical cell ($S_{cathode}/V_{solution}$ = 0.9) (chapter 2) whereas in the pilot, this ratio is significantly lower ($S_{cathode}/V_{solution}$ = 0.25) which implies less production of H_2O_2 and thus less EF efficiency. A solution could be to add a carbon felt layer on the floor and on the sides of the pilot to produce higher amounts of hydrogen peroxide. Nevertheless there could be a worst repartition of current with this addition of cathode thus, this will need to be tested.

To evaluate the operating cost, the DOE was also performed for the EC. The current was found to be divided by two when the configuration was changed from 14 electrodes to 28 electrodes

which favors this second configuration. Two configurations were tested but this pilot gives the opportunity to try closer distance between electrodes. Thus by reducing the gap between the electrodes, the electrical resistance could be reduced and could make the pilot even more cost effective.

This pilot was proved to be very efficient, able to reach nearly total mineralization rate, thus to make it even more efficient an hydrodynamic study was carried out, aiming at identifying the role of the flow rate in the mineralization process and in the flowing.

Hydrodynamic study of the pilot

It is one of the first time that the impact of the hydrodynamic have been considered in an electrochemical reactor performing EF and AO. The first step in this part was to model the flowing by a Retention Time Distribution (RTD) study. Whatever the experimental conditions the model of several perfectly mixed tank reactor in series with a dead volume mimicked the experimental RTD curves. Two operational parameters were analyzed with this model: the configuration of the electrodes and the flow rate. For all the conditions tested, the dead volume was less than 20 % which shows that the mixing inside the reactor was good and it was even better for the 28-electrode configuration. Concerning the flow rate, the lower it was the more the reactor tends to a low number of perfectly mixed tank reactors the higher is the mean retention time which enables a longer contact time between the organics and the hydroxyl radicals.

Model of the mineralization

A new model was developed by combining the hydrodynamic and the pseudo first order kinetic for the mineralization of the solution. The model is able to describe the mineralization for

different positions in the reactor at steady state. Thanks to this model it is possible to optimize an "electrochemical plug flow" reactor depending on the treatment objectives: having the highest mineralization rate, performing a combined treatment, reaching a setpoint value, … To improve this study, an overall characterization of the role of the aeration should be performed related to the mineralization process and the hydrodynamic study as it plays a very important role in the production of H_2O_2 and on the mixing. Estimating the value of constant K (by considering the gas-liquid transfer, the mass transfer, the troublemakers impact, the flow rate, etc.) will be a very important point to consider for further research. Indeed, it will enable to save energy by having J_{app} close to J_{lim} which maximizes the MCE. J_{lim} can also be reached by putting the adequate distance between the electrodes which will optimize the EC and to keep J_{app} close to J_{lim} during the entire treatment different currents could be applied to fit with the concentration decrease. The mathematical model will have to consider the aeration but also other chemical reactions such as mediated oxidations to perfectly model the pilot and pave the way for an industrialization of the process. In addition, to evaluate possible disrupting effects, experiments on real wastewaters are needed especially the effect of the water hardness should be tested.

This pilot is very reliable as no clogging nor leak were seen during the two years of experimentation. It is particularly interesting to treat effluents with high or moderate concentrations of pollutants and small particles as it increases the mass transfer and the conductivity of the solution and thus the MCE (Ledezma Estrada et al. 2012). For effluents with low concentration of pollutants the use of reactive membranes or micro-reactors (Mousset et al. 2019b) should be used to reduce the mass transfer limitation but required a solution without particles to avoid fouling or clogging. Nevertheless, the use of our pilot is also possible with a pre-concentration step by means of active carbon (El Kateb et al. 2019), for example, or by improving the mass transfer with the optimization of the mixing or by reducing the loss of

energy by reducing the gap between the electrodes. Thus this pilot seems to be a promising solution to treat wastewater effluents.

To sum-up:

* The scale up of the EF and the AO was shown to be very successful by demonstrating a very high efficiency.

* The importance of the flow rate and the configuration were clearly identified thanks to the hydrodynamic study and the DOE.

* A model was designed enabling to optimize the operating conditions to reach a given mineralization rate.

Combined treatment

The chapter 4 demonstrated the clear opportunities of a combined treatment for two main reasons: first, because of the incapacity of the µ-organisms to degrade the HCT, used as a model pollutant, and secondly, because of the drastic reduction in operating costs provided by this combined treatment. Indeed, to treat 1 m^3 solution of pollutant with the use of the pilot followed by a biodegradation, the operating costs could be divided by three.

To perform an efficient treatment, it was evidenced that some specific conditions for the electrochemical treatment should be applied: the aim was to degrade the pharmaceutical pollutant, reduce the aromatic intermediates concentration and promote the formation of the biodegradable compounds. The presence in the solution of the active substance and the aromatic intermediates (AIs) disrupt the µ-organisms' activity by lengthening the lag phase and by decreasing the kinetic of degradation, promoting a sequential degradation. For the lag phase a continuous treatment could solve the problem as the µ-organisms would be selected and will thus be able to metabolize the biodegradable compounds, mainly the carboxylic acids (CAs). For the kinetic of degradation there could be a problem as only the more biodegradable

compounds could be degraded during their residence time in the biological reactor. In order to face this problem a reactor working as a plug flow could be used. Indeed, in the first sections the more biodegradable compounds would be degraded and then in further sections the less biodegradable compounds would be eliminated as being the only carbon sources for the μ-organisms.

Finally these operating conditions were tested with the combined treatment at lab scale in batch as the operating parameters are easier to control in order to degrade the pollutant and the AIs and form a maximum of biodegradable compounds (CAs,..). As BDD anodes constituted the pilot, a BDD anode was selected to perform the combined treatment at lab scale in order to find good operating conditions. As BDD anode is a very powerful anode, a low current can be applied to minimize the mineralization to allow the solution to have enough carbon for the μ-organisms. The combined treatment was successful as 66% of the solution was mineralized and 38% by the biotreatment.

The same strategy was then applied to the pilot with three conditions tested. The best one was able to form CAs at higher concentrations and degrade more AIs. During this experiment a current of 6.8 A was applied and a flow rate of 42.5 mL min^{-1} leading to 60% of mineralization on the electrochemical pre-treatment was used. Only three conditions could be tested because of the lack of time, but a deeper analysis would be very interesting such as realizing a DOE using at least the flow rate and the current as parameters and by measuring the amount of CAs, AI, mother pollutant and the TOC value.

In order to form more CAs and to mineralize less the solution, a treatment with a Pt electrode was performed as it is active less powerful anode. With the Pt electrode, 85% of the solution was mineralized including 50% by the biotreatment which implies a drastic reduction in the operating costs. However, Pt electrode is very expensive thus in the aim of industrialization a cheaper active anode should be used and therefore DSA or sub-stoichiometric TiO_2 anodes can

be proposed. To predict the efficiency of the combined treatment it would be interesting to developpe kinetic models such as the Monod one used to describe the degradation of the acetic acid.

Summary of the perspectives

The perspectives of this thesis work would mostly be concentrated on the decrease of the costs which are at the moment the real problem of the method. The different axes are:

- The use of concentrated solutions in order to have better MCE% and to decrease the wasting of energy. Two options were proposed whether to concentrate diluted solution on activated carbon, for example, or to perform the electrochemical treatment directly at the exit of a pharmaceutical production unit or directly on an industrial organic wastewater.
- The use of cheaper active anodes, such as DSA or sub-stoichiometric TiO_2 anodes, at pilot scale and with the combined treatment.
- To deeper the hydrodynamic study by considering the role of aeration, the calculation of the global transfer K to better model the pilot and optimize its performance.
- To identify the effect of gathering the electrodes to reach J_{lim} and to evaluate the impact of the iron with higher cathode surface.
- To complexify the mathematical model to consider other chemical reactions and the aeration.
- To developpe mathematical models for the biological reactions of the post-treatment.

References:

El Kateb M, Trellu C, Darwich A, et al (2019) Electrochemical advanced oxidation processes using novel electrode materials for mineralization and biodegradability enhancement of nanofiltration concentrate of landfill leachates. Water Res 162:446–455. doi: https://doi.org/10.1016/j.watres.2019.07.005

Ledezma Estrada A, Li YY, Wang A (2012) Biodegradability enhancement of wastewater containing cefalexin by means of the electro-Fenton oxidation process. J Hazard Mater 227–228:41–48. doi: 10.1016/j.jhazmat.2012.04.079

Mousset E, Puce M, Pons M-N (2019) Advanced electro-oxidation with boron-doped diamond for acetaminophen removal from real wastewater in a microfluidic reactor: kinetics and mass-transfer studies. ChemElectroChem 6:2908–2916. doi: 10.1002/celc.201900182

Scientific communications:

Publications:

- **A review:** Monteil H, Péchaud Y, Oturan N, Oturan MA (2018) *A review on efficiency and cost effectiveness of electro- and bio-electro-Fenton processes: application to the treatment of pharmaceutical pollutants in water*. Chem Eng J. doi: https://doi.org/10.1016/j.cej.2018.07.179

- **An article:** Monteil H, Péchaud Y, Oturan N, Oturan MA (2019) *Efficient removal of diuretic hydrochlorothiazide from water by electro-Fenton process using BDD anode: a kinetic and degradation pathway study*. Environmental Chemistry, doi: https://doi.org/10.1071/EN19121

3 more articles will be submitted soon:

- Monteil H, Oturan N, Péchaud Y, Oturan MA, *Electro-Fenton treatment of the widely used analgesic tramadol using BDD anode: a kinetic, energetic and degradation pathway study.* Chemosphere

- Monteil H, Péchaud Y, Trellu C, Oturan N, Oturan MA, *Efficiency of a new pilot scale continuous reactor for wastewater treatment by electrochemical advanced oxidation processes: influence of operating conditions and focus on hydrodynamics,* Chem. Eng. J.

- Monteil H, Péchaud Y, Oturan N, Oturan MA, *Electrochemical advanced oxidation processes combined with a biological treatment for wastewater treatment: a deep understanding on the influence of operating conditions and global efficiency*, Water Research.

Posters:

- Monteil H, Péchaud Y, Oturan N, Oturan MA, *Traitement multi-échelles d'un polluant pharmaceutique par procédé électro-Fenton* during the J3P conference in Nancy : Procédés électrochimiques avancés pour le traitement des eaux.

- Monteil H, Péchaud Y, Oturan N, Oturan MA, *Traitement de résidus de médicaments par oxydation avancée électro-Fenton*, during the JIE 2018 conference in Poitiers: Journées informations eaux and communication in the proceeding of conference.

Mobility in Chile :

1 month in the university of Santiago in Chili with the Ecos-Sud project n°: C17E05. The project in the LEQMA was to study, with a 10 L pilot reactor, the combined treatment: solar photoelectro-Fenton process. This process was applied to the treatment of 5 pharmaceuticals. This method of treatment was presented in Toledo for the 25th Topical Meeting of the International Society of Electrochemistry, *Elimination of pharmaceutical pollutants of emerging concerns by solar photoelectro-Fenton*, Ricardo Salazar, Sebastián Bugueño, Carla Toledo-Neira, Hélène Monteil

Annexes

Annex Table 1: Influence of t the configuration on the mineralization rate at steady state. 0.1 mM of HCT, 50 mM of Na_2SO_4 and 0.2 L.min^{-1} of air were used for all the experiments.

Run	Flow rate (mL min^{-1})	Current density (A)	Configuration	Mineralization (%)
4	20.4	16.6	14	61
5	28.9	16.6	14	48
6	42.5	16.6	14	36
7	85.0	16.6	14	14
8	170.0	16.6	14	9
9	42.5	10.0	28	50
10	42.5	16.2	28	60
11	42.5	22.4	28	76
12	42.5	16.2	14	37

Annex Table 2: K for different flow rates

Q (mL min^{-1})	20.4	42.5	85.0	127.5
K (m s^{-1})	2.52*10^{-5}	1.62*10^{-5}	1.44*10^{-5}	1.01*10^{-5}

Annex Table 3: Compounds found using the following conditions: 1 mM hydrochlorothiazide, 1 mM Fe, 10 min of electrolysis, extraction with dichloromethane and ethyl acetate.

Name	Molecule	Fragmentation	Identification letter
N-(5-chloro-2,4-disulfamoylphenyl)formamide	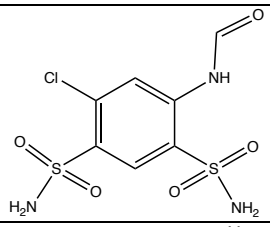	73, 313,75, 132, 55, 69, 189, 206,285	B
6-chloro-4*H*-benzo[*e*][1,2,4]thiadiazine-7-sulfonic acid 1,1-dioxide	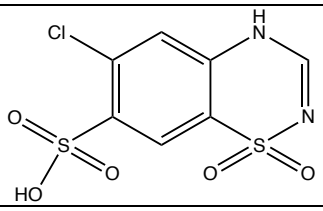	294, 199, 296, 93, 141, 213, 201, 279	C
6-hydroxy-4*H*-benzo[*e*][1,2,4]thiadiazine-7-sulfonamide 1,1-dioxide	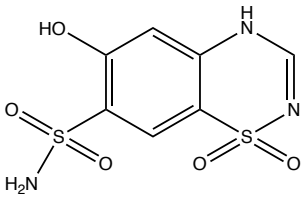	125, 77, 201, 277, 157, 175	D
5-hydrazineylbenzene-1,2,4-triol	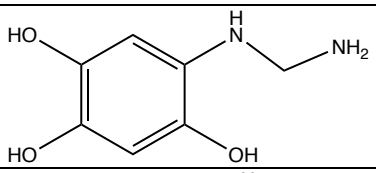	77, 141, 170	E
N-(2,4,5-trihydroxyphenyl)formamide	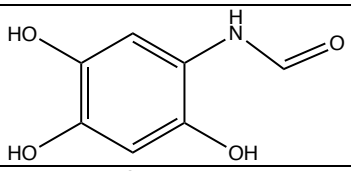	109, 151, 69, 85, 57, 67 169,	F
2-((aminomethyl)amino)-3,5,6-trihydroxycyclohexa-2,5-diene-1,4-dione	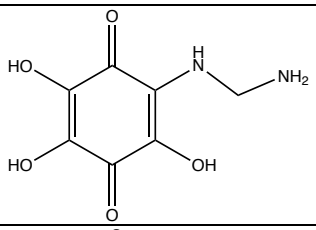	73, 60, 57, 55, 71, 85, 129, 69, 157, 115,171, 200	G
2-((aminomethyl)amino)-5-hydroxycyclohexa-2,5-diene-1,4-dione	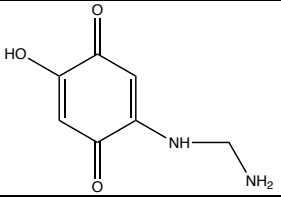	59, 71, 57, 55, 73, 77, 105, 112, 133 168	H
N-(2,4,5-trihydroxy-3,6-dioxocyclohexa-1,4-dien-1-yl)formamide	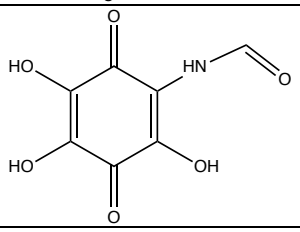	71, 73, 55, 153, 57,69, 60, 199, 170, 99	I

Annex Table 4: Aliphatic compound found using the following conditions: 1 mM hydrochlorothiazide, 1 mM Fe, 10 min of electrolysis, extraction with dichloromethane and ethyl acetate, derivatization (BSTFA).

Name	Molecule (without sillilation)	Fragmentation	Probability (%)	Retention time (min)	Letter identification
Butyric acid	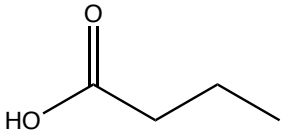	75, 145, 73, 146, 117	72	4.55	L
2-hydroxyacetic acid	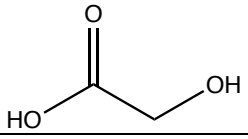	147, 73, 66, 148, 77	67	6.13	M
3,4-dihydroxybutanoic acid	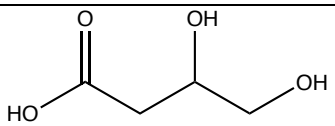	73, 147, 233, 189, 231	69	9.55	J

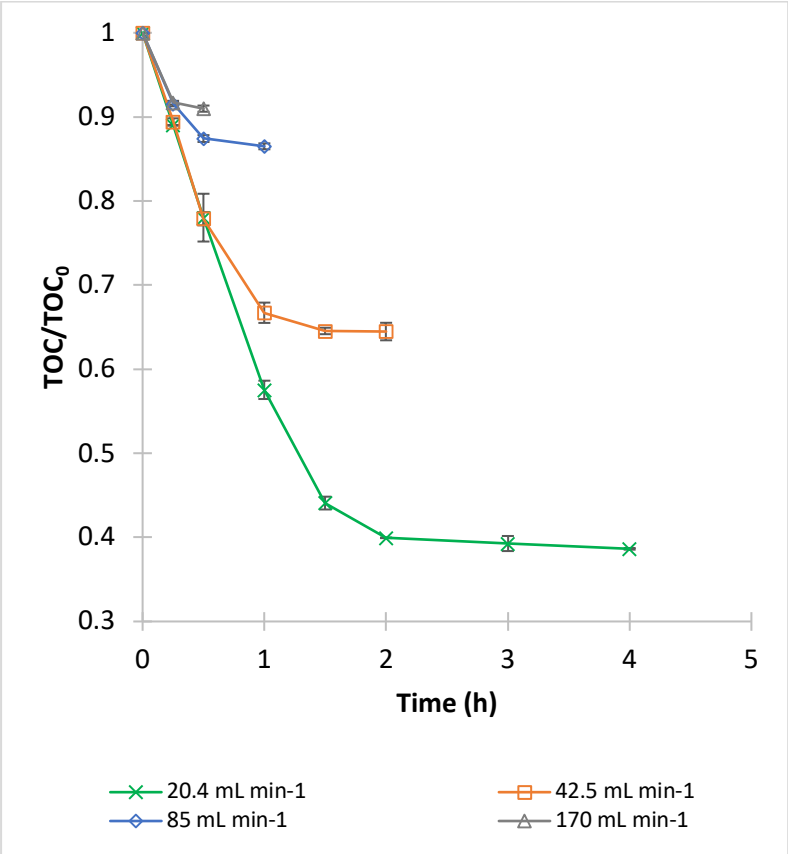

Annex Fig. 1: TOC/TOC_0 plotted against the time, under 0.2 mL min^{-1} of air and 3.A with 14 electrodes, 0.1 mM of HCT and 50 mM of Na_2SO_4 for different liquid flow rates.

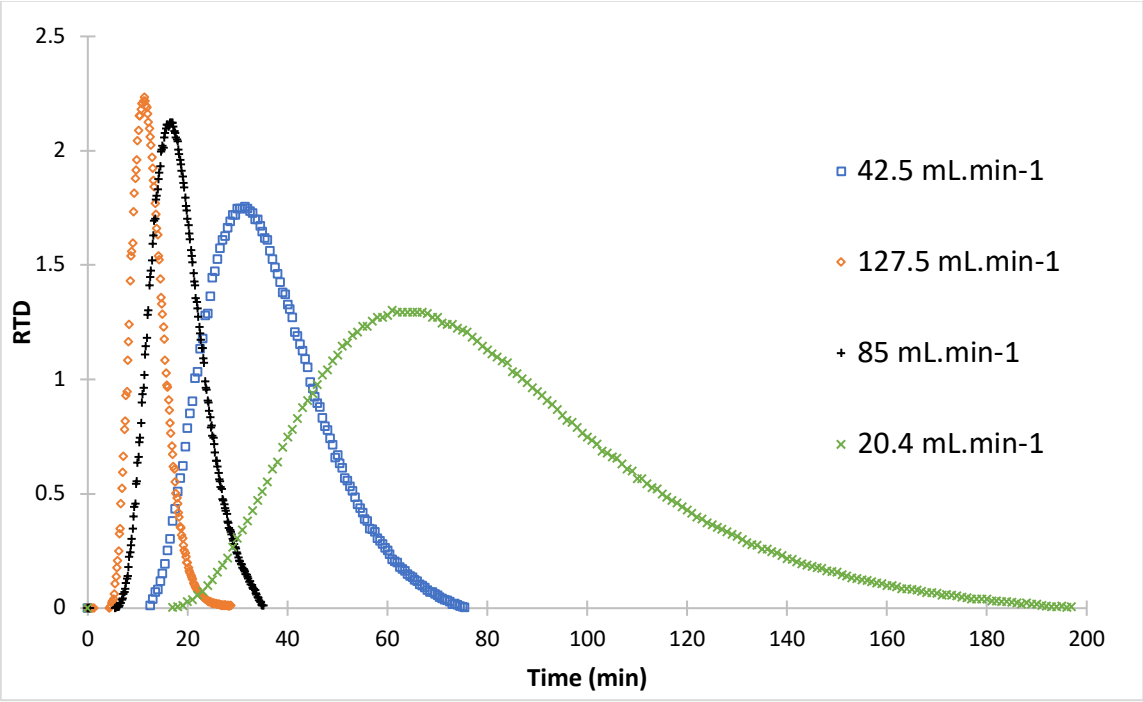

Annex Fig. 2: RTD functions plotted against the time for different flow rates under 0.2 mL min^{-1} of air with 14 electrodes

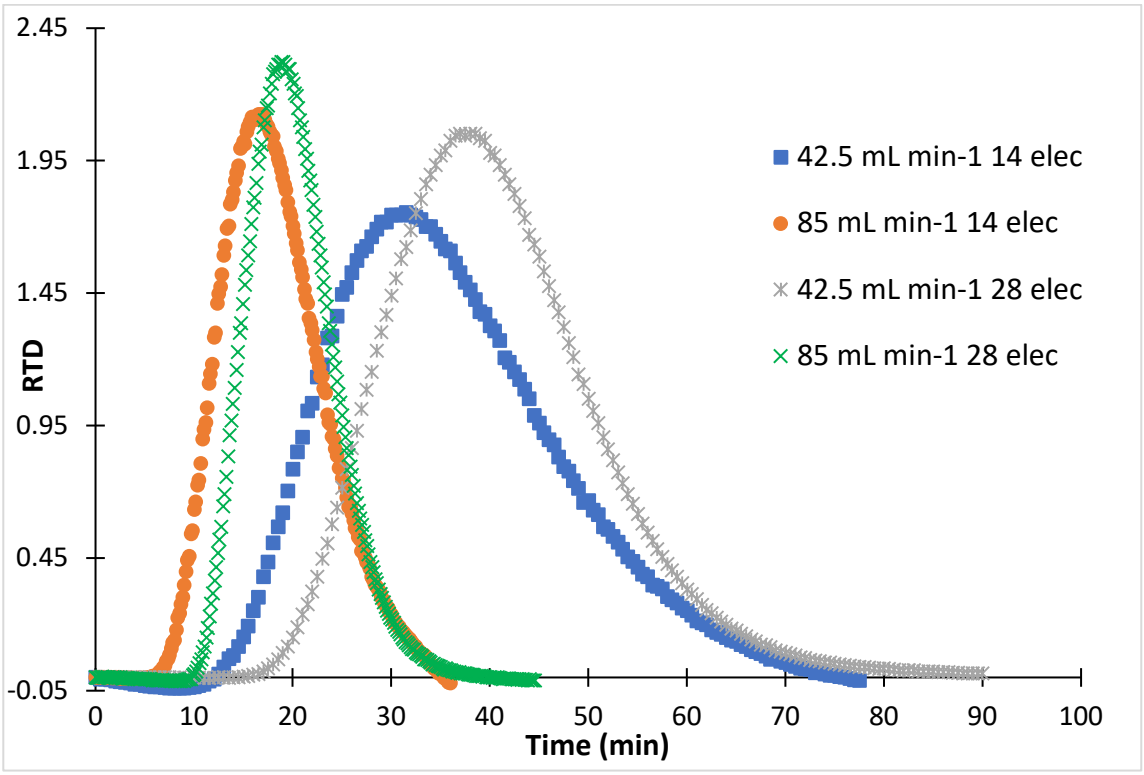

Annex Fig. 3: RTD curves plotted against the time, under 0.2 L min^{-1} of air, 42.5 and 85 mL min^{-1} with 14 and 28 electrodes

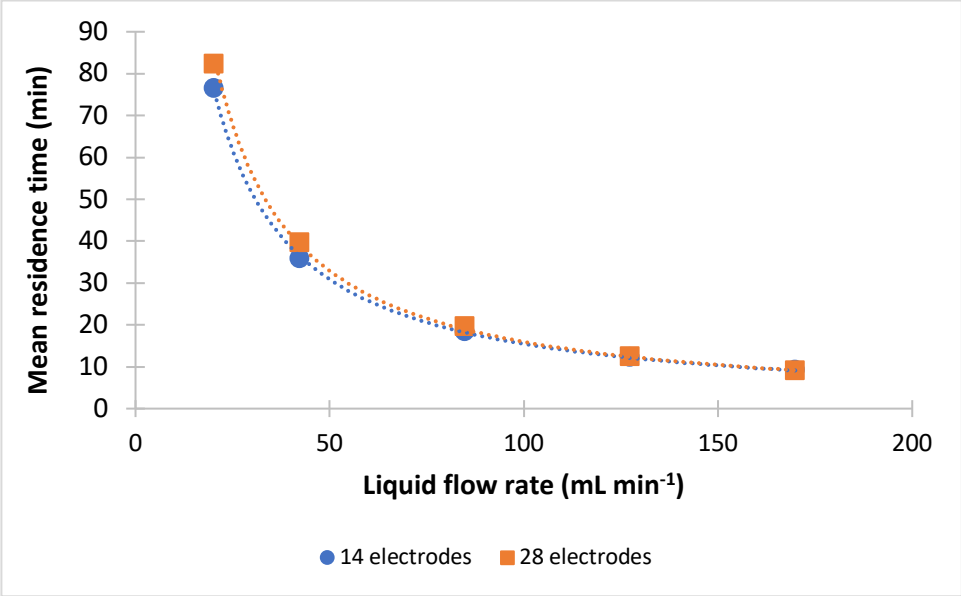

Annex Fig. 4: Mean retention time (Ts) plotted against the liquid flow rate, under 0.2 L min^{-1} of air with 14 electrodes and 28 electrodes.